THE ELECTRICAL CONDUCTIVITY OF SOME HYDROUS AND ANHYDROUS MOLTEN SILICATES AS A FUNCTION OF TEMPERATURE AND PRESSURE

by

John Satherley

A thesis

submitted for the degree of Doctor of Philosophy

in Chemistry

at

Victoria University of Wellington

November 1983

ABSTRACT

This thesis is concerned with the measurement and interpretation of electrical conductivity in molten silicates. Physicochemical properties and structural models of silica and silicates are reviewed first, to give a general picture of their behaviour. Electrical conductivity was measured as a function of temperature, pressure and water composition. To make these measurements an internally heated pressure vessel, designed to operate at temperatures up to 1200°C and pressures up to 5 kbars was constructed. Conductivity measurements were made on the following anhydrous and hydrous silicate melts: SiO_2/Na_2O 60/40, 65/35, 75/25, 78/22 mol%; $SiO_2/Na_2O/CaO$ 72/24/4 mol%; Mt. Erebus lava; SiO_2/Na_2O 78/22 mol% + ~5 wt% H_2O and Mt. Erebus lava + ~4 wt% H_2O in the temperature range 850-1000°C and the pressure range 0-1.3 kbar. Arrhenius temperature and pressure dependencies on conductivity were observed. The pressure coefficient of conductivity was zero for the anhydrous melts well above T_g but small and positive for the hydrous silicates. Water caused ~40% reduction in conductivity when added to a melt which was accounted for in terms of the mixed alkali effect. Conductivity isobars for the hydrous silicates passed through a maximum as a function of increasing temperature. The conductivity behaviour as a function of temperature and pressure is analogous to that observed in partially ionised liquids and is intrepretated in an identical way. The range of operation of a piezoelectric α-quartz crystal viscometer was extended to allow measurement of viscosity as a function of temperature.

VICTORIA UNIVERSITY OF WELLINGTON

ACKNOWLEDGEMENTS

I wish to express my gratitude to my supervisor, Dr Stuart Smedley, for his guidance, encouragement and helpful discussions throughout the course of this work. Special thanks are due to Mr Cliff Snell for his invaluable technical assistance in the construction of the experimental equipment and for checking the technical details in Chapter III. I would also like to acknowledge technical assistance from other University technicians: Mr Ernie Millington and staff of the University Workshops for their machining work and advice on technical matters, Mr Lawrie Morton for constructing the electronic equipment to operate the high temperature furnace inside the pressure vessel, Mr Cliff Taylor and Mr Ian Crighton for glassblowing work, Mr John Casey for the photographic work contained herein, and Mr Ken Palmer for electron microprobe analyses of silicate glass samples.

I am grateful to Mr Paul Anderson for drawing Figure 3.1 and giving advice and help on the graphic work contained herein. I wish to thank the Computing Services Centre staff for their assistance with the manuscript preparation. A special thank you to Mrs Alida Sewell who willingly undertook the arduous task of reading the manuscript and correcting my spelling, punctuation and grammatical mistakes. The thesis is much improved as a result of her work.

I gratefully acknowledge financial support from the Department of Scientific and Industrial Research on contract SIR: UV/6/13: GS.

Thank you to everyone who has assisted me in any way, especially my mother, Keith and Alida Sewell, and my past and present flatmates who have all encouraged and supported me in lots of different ways throughout the course of this work.

Finally, I would like to thank 'I.H.P.V. Hubert', although not always well behaved, nevertheless in the end 'he' made it all possible.

CONTENTS

LIST OF FIGURES

LIST OF TABLES

LIST OF PLATES

GLOSSARY OF SYMBOLS

A	Cross sectional area of a conductor
a	Radius of quartz crystals
a_i	Activity of component i
C	Capacitance
C_m	Capacitance load on the gauge crystal
c_i	Concentration of ion i
D_i	Diffusion coefficient of component i
E	Electric field
E_η	Activation energy of viscosity
E_D	Activation energy of diffusion
E_κ	Activation energy of conductivity
e	Charge on a proton
F	Faraday's constant
F_i	Force exerted on ion by a gradient of chemical potiential
f_{xy}	Shear force in x-direction with velocity gradient in y-direction
G	Conductance
G_c	Conductance corrected for leads resistance
h	Planck's constant
I	Ion-oxygen attraction
J_i	Flux of species i
k	Henry's law constant
M_i	Gram formula weight of component i

m	Mass of quartz crystals and rod
N	Transformer ratio
N_A	Avogadro's number
n	An integer
P	Pressure
Q^{-1}	Mechanical damping
q	Electric charge
R	Electrical resistance
r	Ionic radius
r_+	Cation radius
r_-	Anion radius
T	Temperature
T_b	Boiling temperature
T_g	Glass transition temperature
T_m	Melting temperature
T_{max}	Temperature of conductivity maximum
T_o	Ideal glass transition temperature
t	Time
t_i	Transport number of ion i
u_i	Electric mobility of ion i
V	Volume
ΔV	Electrical potiential difference
V^*	Activation volume
V_a	Hard core volume
V_d	Drive voltage
$V_{d,1}$	Drive voltage at period 1
$V_{d,2}$	Drive voltage at period 2

$V_{d,r}$	Drive voltage at resonance
V_f	Free volume
V_g	Gauage voltage
V_m	Molar volume
V_o	Volume at T_o
ΔV_κ	Activation volume of conduction
v	Velocity of ions in an elctrolyte
v_i	Partial molar volume of component i
X_i	Mole fraction of component i
z	Charge on an ion
α	Linear coefficient of thermal expansion
β_s	Adiabatic compressibility
β_T	Isothermal compressibility
γ	Surface tension
ε	Relative permittivity
ζ_o	Interaction potiential constant in equation (2.48)
η_s	Shear viscosity
η^*	Complex viscosity of an elasticoviscous fluid
κ	Conductivity
λ	Wavelength
Λ	Molar conductivity
μ_i	Chemical potiential of component i
ρ	Density
τ	Period of vibration
τ_1	Period at drive voltage $V_{d,1}$
τ_2	Period at drive voltage $V_{d,2}$
ω	Radial frequency

Chapter I

INTRODUCTION

The earth's crust and mantle are composed predominatly of silicates. This predominance arises because silica can combine with or dissolve the oxides of 9/10 of the elements. Due to their abundance and importance in extractive metallurgy and the glass and ceramic industries, silicates are some of the most widely studied materials. Recently molten silicates have become the focus of study in disciplines examining igneous processes. Any knowledge of the variation of properties such as viscosity with pressure, volume or temperature provides insight into the nature of the melt and its rheological behaviour. This is of importance in understanding and predicting magma behaviour in the asethenosphere, the region between the earth's crust and upper mantle, where the temperature and pressure regime is such that molten or partial molten phases are present. Physical chemists are interested in the physicochemical properties of high temperature liquids. Transport property data gives information about kinetic processes such as crystallisation; the size and number of charge carriers and the size of flow units. From this data structural information can be inferred. Questions of structure are important in silicates because there exists a whole range of anionic groups from a giant three-dimensional molecule in pure silica to discrete SiO_4^{4-} anions jostling randomly in molten orthosilicates.

Of special interest, particularly to geophysicists, is the effect of H_2O and pressure on transport properties. The presence of H_2O in a magma causes it to push its way, due to the pressure differential, to the earth's surface. Water has been found to have a profound effect on molten silicates, causing (1) a lowering of the liquidus temperature and (2) a decrease in viscosity. The latter has important implications in predicting the time taken for a magma to move from deep in the earth's crust to the surface and the time taken for crystal settling and other igneous processes. Pressure dependence on transport properties have been only recently examined and no clear picture has emerged of its effect, although, in some silicate compositions viscosity has a negative pressure dependence. These findings are only qualitative and quantitative studies are only just beginning. Further, most of the work reported is for complex silicate systems from which structural conclusions cannot be drawn. To obtain quantitative data from which structural information can be obtained, simple silicate systems need to be studied systematically over wide temperature and pressure ranges. Careful studies of this type, in the 1950's, on molten binary silicates, measuring electrical conductance and electrolysis products established the ionic nature of these liquids. Further systematic studies of this sort ought to be initiated to elucidate the structural effects of H_2O on silicate melts.

The main reason for the lack of quantitative data is the experimental problems associated with high temperature and pressure research on silicate liquids. Apparatus must be able to withstand temperatures of the order of 1200°C and pressures of 5 kbar. Another major difficulty is

the requirement that the container to hold the molten silicate sample be sealed to allow variable concentrations of water, from dry to saturated. Under such conditions the melt is extremely corrosive, which severely restricts the type of materials available from which to construct the container. In the case of electrical conductance studies a high temperature electrode insulator is required which is inert with respect to molten silicate.

In response to this lack of experimental data, and the general importance of this information, and not withstanding the experimental problems, the Chemistry Department of Victoria University of Wellington in conjunction with the Department of Scientific and Industrial Research have initiated a project to study viscosity, electrical conductivity and P.V.T. relations in hydrous and anhydrous silicates as a function of temperature and pressure. Since the partial pressure of water is so high at magmatic temperatures all experimental apparatus must be contained within an internally heated pressure vessel. The sample container must be made from noble metals and high purity alumina to withstand the corrosive liquids. Work on this project already carried out includes: (1) Developing a viscometer to operate inside a pressure vessel. This is a viscometer which utilises the piezoelectric properties of α-quartz crystals and has been satisfactorily tested at room temperature (1). (2) Completing a feasibility study for using this viscometer as a function of temperature (2) and (3) Designing an internally heated pressure vessel to withstand 5 kbar and provide a temperature controlled hot-zone of 1200°C (2).

The aims of the present study have been: (1) To assemble the internally heated pressure vessel and the ancillary equipment to operate it. (2) To design and construct an electrical conductance cell. (3) To test the internally heated pressure vessel facility by making electrical conductance measurements on hydrous and anhydrous molten silicates as a function of temperature and pressure and (4) To extend the range of operation of the viscometer to higher temperatures. Conductance was measured initially because it is the easiest transport property to measure; it can be measured precisely and it provides information about factors controlling the kinetics of mass transport. The silicate systems examined in this work are as follows: Binary SiO_2/Na_2O melts in the composition range 22-40 mol% Na_2O, a ternary $SiO_2/Na_2O/CaO$ 72/24/4 mol% melt, Mount Erebus lava, hydrous SiO_2/Na_2O 78/22 mol% melt and hydrous Mount Erebus lava. Conductance data on SiO_2/Na_2O binary silicates at one atmosphere are available. Na_2O is a network breaker and is present in most naturally occurring silicates. It is of interest to determine the effect of pressure and water on the melt conductivity. CaO is also a network breaker, although its network breaking tendency is not as great as for Na_2O, and is also an important constituent of natural systems. However, in binary SiO_2/CaO melts the liquidus temperature at the eutectic composition is too high for the present experimental equipment (the maximum experimental temperature was limited to 1000°C) and therefore the ternary $SiO_2/Na_2O/CaO$ system is considered. When the effect of Na_2O on SiO_2 is known the effect of CaO in the ternary system can be inferred. The conductivity of molten Mount Erebus lava has not been measured. It is an interesting lava, in that it has an unusually

high concentration of Na_2O giving it a relatively low liquidus temperature and a high fluidity. The low liquidus temperature made it possible for study in the present work as an example of a naturally occurring silicate system, and with dissolved water, an example of a simulated magma. This initial study enables the effects of pressure on conductance for a range of silicates to be assessed and the effects of H_2O, and Na^+ and Ca^{2+} cations on the conductance to be better understood.

Unfortunately the number of results is limited due to the time required to construct a new cell after each experimental run and the time required in assembling the delicate internal parts of the pressure vessel. Removal of the glass from the cell without damaging it proved almost impossible. Experimental measurements on these liquids are extremely difficult to obtain.

The thesis begins, chapter II, with a review of the physicochemical properties of molten silica and silicates. Structural models which have been proposed to account for these physicochemical properties are also reviewed. Chapter III describes the construction of the internally heated pressure vessel facility. Experimental techniques involved in measuring electrical conductance and viscosity at high temperatures and pressures are also described. The conductivity results are presented in Chapter IV and discussed in Chapter V.

Chapter II

THE PHYSICOCHEMICAL PROPERTIES OF MOLTEN SILICATES

In this chapter the equilibrium and non-equilibrium properties of molten silica and silicates are reviewed. Structural models of molten silicates relevant to the present study are also reviewed.

2.1 EQUILIBRIUM PROPERTIES OF LIQUID SILICA AND SILICATES

2.1.1 Equilibrium Properties of Silica

2.1.1.1 Crystalline Silica

Table 2.1 lists various equilibrium properties of the crystalline forms of silica; vitreous and liquid silica are included for comparison. Silica is found in three crystalline forms: quartz, tridymite and cristobalite. Quartz and cristobalite each have a high and low temperature modification whereas tridymite has three modifications (3). These modifications involve changes of both symmetry and density (Table 2.1). There are two types of transformations between the various modifications of silica. Displacive transformations, such as the inversion between high and low forms, result in displacement or change in bond direction but do not involve breaking existing bonds between Si and O atoms. Reconstructive transformations, in contrast, involve rupture of existing bond networks and subsequent reformation of new ones. The conversion from quartz to tridymite is an example of a reconstructive transformation.

TABLE 2.1

Equilibrium Properties of Crystalline, Vitreous and Liquid Silica

	α-Quartz	β-Quartz	β-Tridymite	β-Cristobalite	Vitreous	Liquid
T_g /°C					1200	
T_m /°C		1550	1703	1713	~1500	
Heat of fusion /kcalmol^{-1}	2.04			2.1		
T_b /°C						2230
Transition temp /°C	573[a]	867[b]	1470[c]			
Heat of transition / cal g^{-1}	2.50[a]	200[b]	70[a]	200[a]		
Heat capacity / cal g^{-1}(100°)$^{-1}$	0.166	0.189	0.113		0.185	
Lattice constant a /Å	4.9127	5.01	5.03	7.11		
Lattice constant c /Å	5.4046	5.47	8.22			
Expansivity /(°C)$^{-1}$					5.4x10^{-7}	~10^{-6}
Si-O distance /Å	1.61	1.55		1.541	1.62	
Si-O-Si angle /°	142	145		152	146	
Molar volumes /cm^{3}mol^{-1}	22.7	24.0		27.3	27.2	27.96
Density /g cm^{-3}	2.65	2.53	2.26	2.21	2.195	2.094
Mohs Hardness	7				5.5	
Tensile strength /kg cm^2	1210				43872	
Velocity sound /m s^{-1}	5870				5730	
Dielectric constant	4.55				3.810	
Refractive index 5893A	1.5442		1.4773	1.484[d]	1.4584	
Compressibility / cm^{2}dyn^{-1}x10^{-12}	2.65				3	

[a]Transition α-β; [b]Transition β-quartz to β-tridymite
[c]Transition β-tridymite to β-cristobalte; [d]For α modification

Data from reference (3).

Low or α-quartz is enantiomorphic and is stable to 573°C. Above this temperature α-quartz converts to β-quartz which has a more regular lattice structure and is non-piezoelectric. At 867°C a more substantial change occurs; SiO_4 tetrahedra are rearranged to form β-tridymite(ρ = 2.30 gcm^{-3} compared to 2.65 gcm^{-3} for quartz). A second major change occurs at 1470°C giving β-cristobalite (ρ = 2.27 gcm^{-3}) which melts at 1713°C to a colourless liquid of high viscosity.

In crystalline silica, and indeed in all silicates with the exception of stishovite, silicon atoms are always tetrahedrally bonded to four oxygen atoms producing a three dimensional lattice structure. Stishovite, one of the high pressure forms of silica (the other is coesite), has six O atoms surrounding each Si atom. The SiO_4 tetrahedron is the basic building unit of all silicates. Bond lengths and angles change slightly (Table 2.1) depending on the crystalline environment but otherwise the tetrahedra remain unchanged. The different forms of silica arise because the tetrahedra can add together in a variety of ways. In the presence of interstitial cations and anions the number of crystalline structures increases dramatically since the bonding patterns of the tetrahedra are increased. This is illustrated, for example, by the wide variety of naturally occurring silicate minerals. Since the Si-O bonds are strong, covalent and network producing, giving rise to many different crystalline forms, it may be expected that some of the structural characteristics of the crystalline forms will be preserved in the liquid state. In fact the silicate anions postulated (4) to exist in liquid silicates are similar to those in crystalline silicates.

2.1.1.2 Liquid Silica

Table 2.2 compares equilibrium properties of liquid silica with two other similar liquids: GeO_2 and BeF_2, a typical molten salt, NaCl and water. SiO_2, GeO_2, and BeF_2, together with $ZnCl_2$, B_2O_3 and P_2O_5 are the most notable examples of network liquids; that is, liquids with a disordered three-dimensional continuous network held together by strong covalent M-X (X = O, Cl, F) bonds. The most characteristic features of network liquids are their one atmosphere non-equilibrium properties at their melting temperatures (section 2.2.5). Both GeO_2 and BeF_2 have similar crystalline structures to SiO_2 and their structures in the vitreous and liquid states are also similar to SiO_2. Molten sodium chloride is a typical ionic liquid, that is, electrical conduction in this liquid arises from the movement of cations and anions. It is a high temperature liquid like the network liquids and its equilibrium properties are relatively similar (Table 2.2) to the network liquids, apart from its surface tension which is a factor of two and three less than BeF_2 and SiO_2, respectively. However, the non-equilibrium properties of NaCl are dissimilar to network liquids (section 2.2.5). It has been argued by several authors (12), (13) that liquid SiO_2 and H_2O, although existing as liquids in different temperature regimes, have many physicochemical features in common. Further, their crystalline structures are similar. SiO_2 (14) is believed to pass through a density maximum analogously to water and both have negative pressure coefficients of viscosity (15). Their solvating properties are similar; both undergo dramatic structural alterations when salts or metal oxides are added to water and silica, respectively. These changes are reflected

TABLE 2.2

Equilibrium Properties of Liquids: SiO_2, GeO_2, BeF_2, NaCl and H_2O

	SiO_2	GeO_2	BeF_2	NaCl	H_2O
T_m /°C	1713	1115	552	801	0
T_b /°C	2230		~1159	1465	
T_g /°C	1200	~537	319		
dT_g/dP /°C kbar^{-1}	40				
Density (crystal) /g cm^{-3}	2.21	4.28		2.165	
Density (glass) /g cm^{-3}	2.158	3.667	1.968		
Density (at ~T_m) /g cm^{-3}	2.094[a]	3.465	1.96	1.56	0.99987
	2.072[b]				
	2.057[c]				
	2.045[d]				
	1.929[e]				
Molar Vol. (at T_m) /cm^3	27.96	30.19	23.73	37.46	18
Expansivity /(°C)$^{-1}$	5x10^{-6}	4x10^{-4}	3.5x10^{-4}	3.9x10^{-4}	2.57x10^{-4}
Isothermal compressibility /Pa^{-1}	8.5x10^{-11}			4.0x10^{-10}	4.57x10^{-10}
Surface tension (~T_m) /dyne cm^{-1}	307	259	200	98	71.97

[a]1935°C; [b]2048°C; [c]2114°C; [d]2165°C; [e]2322°C

Data from references (5), (6), (7), (8), (9), (10) and (11).

particularly in their transport property behaviour. The comparisons of these similar and diverse liquids with liquid silica aids in the process of characterising the type of liquid that is produced when silica is fused and when metal oxides are added to it.

The first interesting point to note in Table 2.2 is the relatively large temperature range in which the liquid phase exists for all the liquids except H_2O. The latter is due to weak hydrogen bonding whereas the former have strong covalent and electrostatic bonding in the cases of the network liquids and NaCl, respectively. Water molecules are easily formed by breaking the weak hydrogen bonds and thus water boils at low temperatures. The network liquids, however, are like giant molecules; high thermal energy is required to break off small entities and thus they have very high boiling temperatures.

Network liquids, unlike NaCl and H_2O, invariably form glasses when cooled below their normal freezing temperatures. Glasses arise when the rate of cooling is greater than the rate at which entities in a liquid can reorientate themselves into a crystal lattice; a 'frozen liquid' results. Although viscosity indicates the 'frozen liquid' is solid-like, X-rays studies show that the structure is characteristic of the liquid state; it lacks long range periodicity. Supercooled liquid silica forms a glass of very low expansion coefficient (Table 2.2) which softens at ~1500°C and has a glass transition temperature, T_g (the temperature at which viscosity reaches 10^{12} Pa s), of ~1200°C. T_g depends on the pressure at the time of glass formation; it increases by ~40°C per kbar for silica.

Bacon et al. (5) have made the only direct density measurements on molten silica. Their results are shown in Table 2.2. The expansivity coefficient calculated from this data gives a value of $\sim 1 \times 10^{-4} (^{\circ}C)^{-1}$ which is much greater than vitreous silica ($\sim 5.4 \times 10^{-7} (^{\circ}C)^{-1}$). The expansivity coefficient obtained from Bacon's data is similar to that for the other liquids in Table 2.2. However, some recent calculations by Richet et al. (16) to determine the heat capacity of silica at constant volume, C_v, have shown that the expansivity may be closer to 10^{-6} to $10^{-7} (^{\circ}C)^{-1}$ which is slightly greater than amorphous silica. If the lower value is the correct one then it adds support to the view that the structures of glassy and liquid silica are very similar (17). However, more direct measurements are required to establish this.

Molten silica is one of the least compressible fluids (Table 2.2). There is a dispute in the literature about the magnitude of the compressibility. Bockris and Kojonen (18) and Bloom and Bockris (19) assumed that the adiabatic compressibility of liquid silica was equal to the compressibility of vitreous silica, $\sim 1 \times 10^{-11}$ Pa^{-1}. Baidov and Kunin (20), have measured the ultrasonic velocity in liquid silica and have calculated the adiabatic compressibility to be $\sim 1 \times 10^{-11}$ Pa^{-1}. However, recent measurements of isothermal compressibility on molten silica by Bucaro and Dardy (21) show the value to be $\sim 8.5 \times 10^{-11}$ Pa^{-1} and Laberge et al. (22) have determined the adiabatic compressibility and found it to be $\sim 7 \times 10^{-11}$ Pa^{-1}. Both these values are close to the adiabatic compressibilities of binary alkali silicates (18) and much greater than vitreous silica. Fray (23) has calculated the difference between the isothermal and the adiabatic compressibility for silica and it is

equal to $\sim 0.3 \times 10^{-11}$ Pa^{-1}, which is negligible. These recent measurements suggest differences between the liquid and glassy states which contradicts the above conclusion based on expansion coefficients. Further measurements of of the compressibility of molten silica are required.

The surface tension, γ, of a liquid is a measure of the binding forces between the constituents in the liquid and it also provides information concerning the work done in forming a hole in a liquid. γ varies considerably depending on the type of liquid. For example, the surface tension of molecular liquids and liquid metals is, respectively, approximately a factor of 10 less than, and an order of magnitude greater than that for molten silica (11). Surface tension of the network liquids in Table 2.2 are all of the same order of magnitude whereas molten NaCl is about 1/3 that of molten silica and water about 1/4. Unlike most liquids the temperature coefficient of surface tension of many network oxides is positive. Mackenzie (24) has suggested two possible reasons for this anomaly: (1) a preferred orientation of SiO_4 tetrahedra occurring in the surface layer, and (2) dissociation or changes in coordination number with increasing temperature. Kingery (9) claims, from a comparison of the calculated surface entropy and the measured values of $d\gamma/dT$, that (1) can only be a minor contribution to the observed positive coefficient and that the major contribution arises from a decreasing degree of association with increasing temperature.

2.1.2 Effect of Metal Oxides and Volatile Components on the Equilibrium Properties of Liquid Silica

2.1.2.1 Binary and Ternary Silicates

The addition of a metal oxide to molten silica causes remarkable changes to the equilibrium properties. Phenomena associated with melting show the most dramatic changes. Table 2.3 shows the melting point of a selection of binary silicates at their eutectic points, arranged according to groups on the periodic table. Figure 2.1 is part of the binary soda-silica phase diagram. It shows the effect of increasing amounts of soda on the melting point of silica. The addition of ~25 mol% soda cause a 900°C reduction in the melting point of silica. The addition of a third component to a eutectic mixture generally lowers the melting temperature still further although only by a small amount compared to the the effect of the first component. A metal oxide also lowers the glass transition temperature and a third component has a similar effect on T_g as on the melting temperature. Both T_m and T_g increase as pressure increases. There is very little data on the effect of pressure on melting points. Boettcher et al. (27), have recently determined the fusion curves of albite ($NaAlSi_3O_8$) and diopside ($CaMgSi_2O_6$) to 30 kbar. The temperature of the onset of melting is increased by 250°C and 330°C for albite and diopside, respectively, on application of 30 kbar. Silicates of three or more components frequently melt incongruently, i.e. there is partial melting. This phenomena becomes even more pronounced in magmatic liquids.

Numerous measurements have been made on the density of binary and ternary silicates, (28), (29), (30), (31), (32), (33), (34), (35), (36). Molar volumes and partial molar volumes can be calculated from density data.

TABLE 2.3

Melting temperatures of a selection of binary silicates at their eutectic points

Metal Oxide	T_m(Metal Oxide) /°C	T_m(Eutectic) /°C	Composition at Eutectic /mol% MO
Group Ia Oxides			
Li_2O	>1700	1024	45
Na_2O	s1275	~790	25
K_2O	d350	~740	33
Group IIa Oxides			
BeO	2530	1670	5
MgO	2852	1543	35
CaO	2614	1436	37
SrO	2420	1358	45
BaO	1918	1370	47
Group IIIb Oxides			
B_2O_3	450	1498	2-5
Al_2O_3	2072	1592	5
Group IVb Oxides			
GeO_2	1115	990	96
PbO	886	715	84
Group IVa Oxides			
TiO_2	1840	1550	10
ZrO_2	~2700	1675	12
Group VIIa Oxides			
MnO	1781	1251	62
Group VIII Oxides			
FeO	1369	1180	75
CoO	1800	1382	56

Data from reference (25)

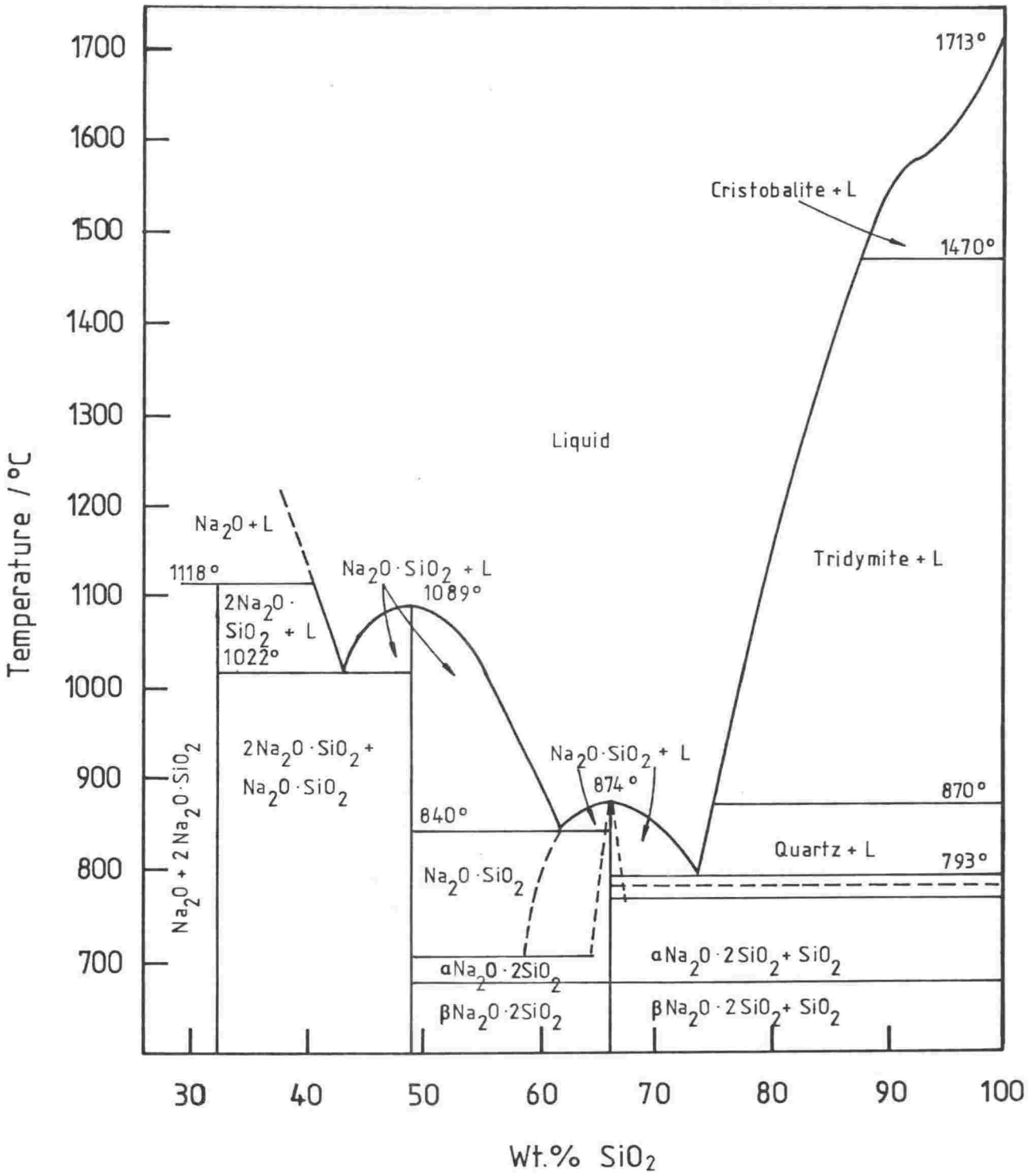

Figure 2.1— Phase diagram of the binary SiO_2/Na_2O system (26).

Figures 2.2 and 2.3 show the molar volumes of alkali and alkaline earth binary silicate melts. The addition of a metal oxide causes substantial changes, both positive and negative, to the molar volume of silica. Figure 2.4 shows the expansivities of the alkali silicates plotted against mol% alkali oxide; expansion is almost zero till about ~12 mol% alkali oxide is reached. Substantial structural changes have been postulated to occur in this region (29). When the expansivity of both the alkali and alkaline earth metal binary silicates are plotted against 'ion-oxygen attraction' all the points lie on the same line (Figure 2.5). This has been explained in the following way (30). In a silicate of composition such that the anions are relatively large in comparison with the cations, the expansivity would be expected to be due largely to the change in the equilibrium cation-oxygen separation, a_o; $a = \text{const.}\ da_o/dT$. If the ionic contribution to the heat capacity and the exponent of the repulsive energy term are assumed to be approximately constant, then it may be shown that $a = \text{const.}/I$, where I is the 'ion-oxygen attraction' and is equal to $2z_+/a_o^2$.

Bottinga and Weill (37) and Bottinga et al. (38) assembled all the available density data on molten silicates to derive an equation for the density as a function of composition. This equation was based on the observation that the partial molar volumes of all components in silicate liquids are independent of chemical composition in the range 0.4 to 0.8 mole fraction of SiO_2. The density, ρ, may be expressed as

$$\rho = \sum_i X_i M_i / X_i v_i$$

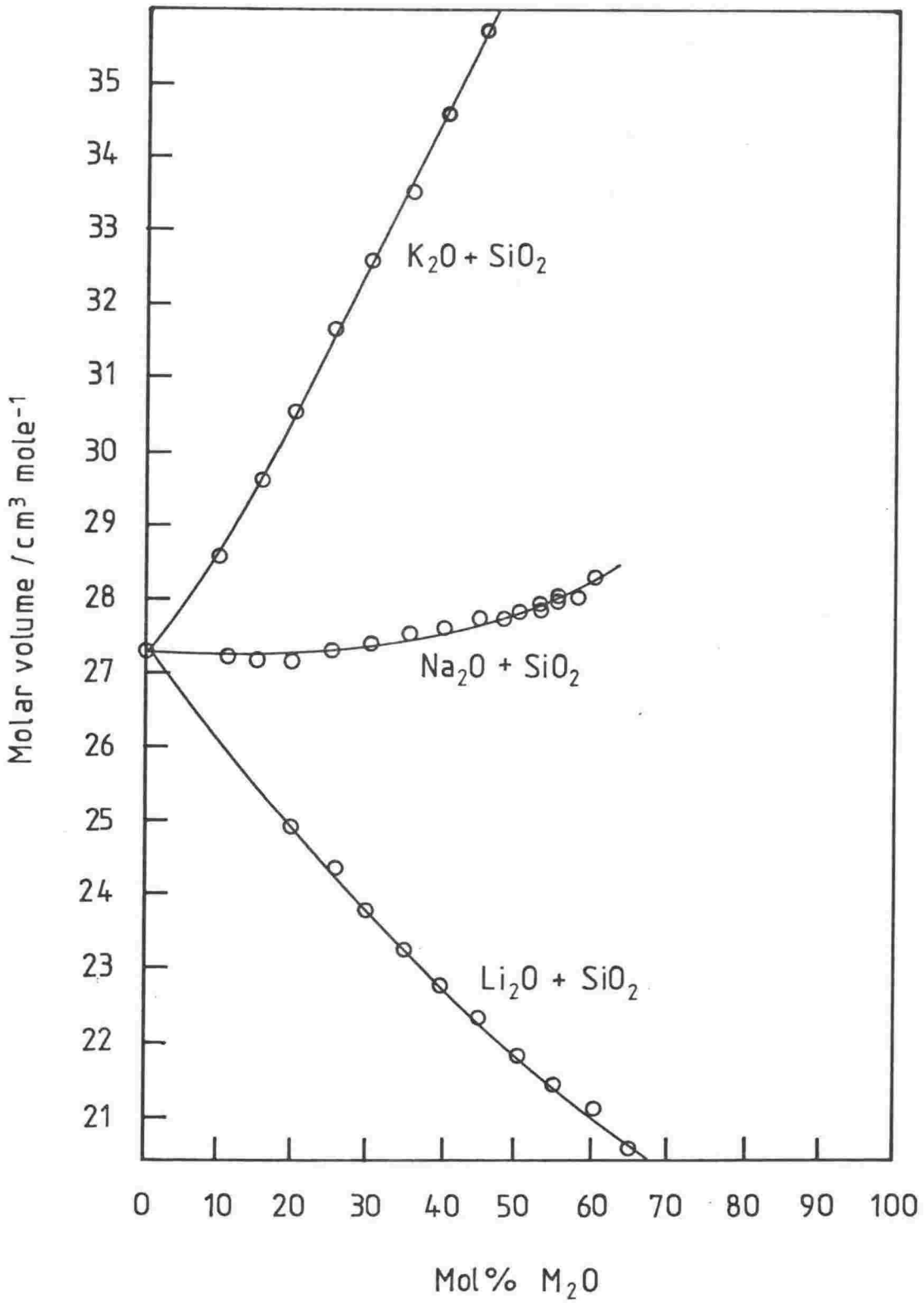

Figure 2.2—Molar volume at 1400°C as a function of mol% M_2O (29).

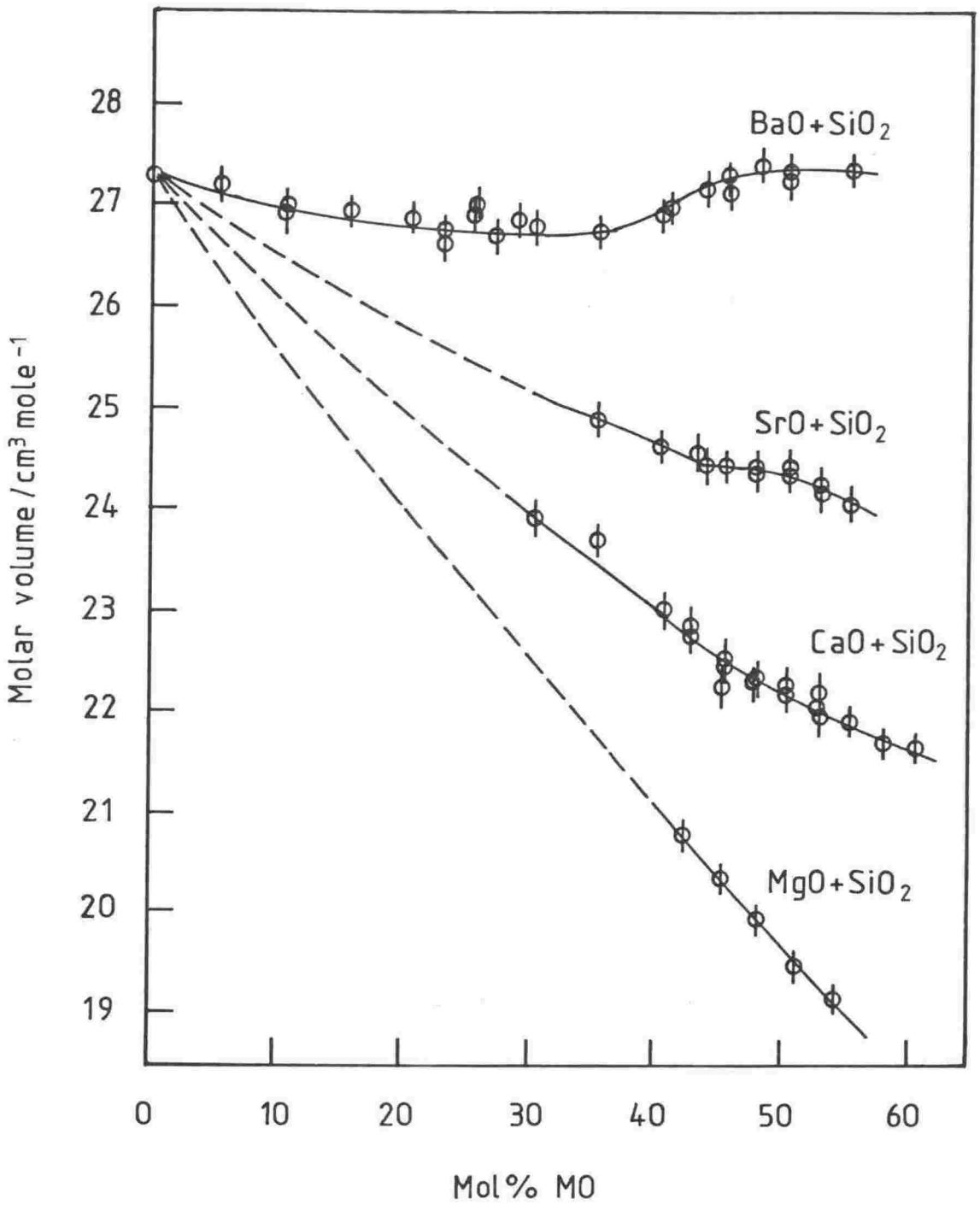

Figure 2.3—Molar volume at 1700°C as a function of mol% MO (30).

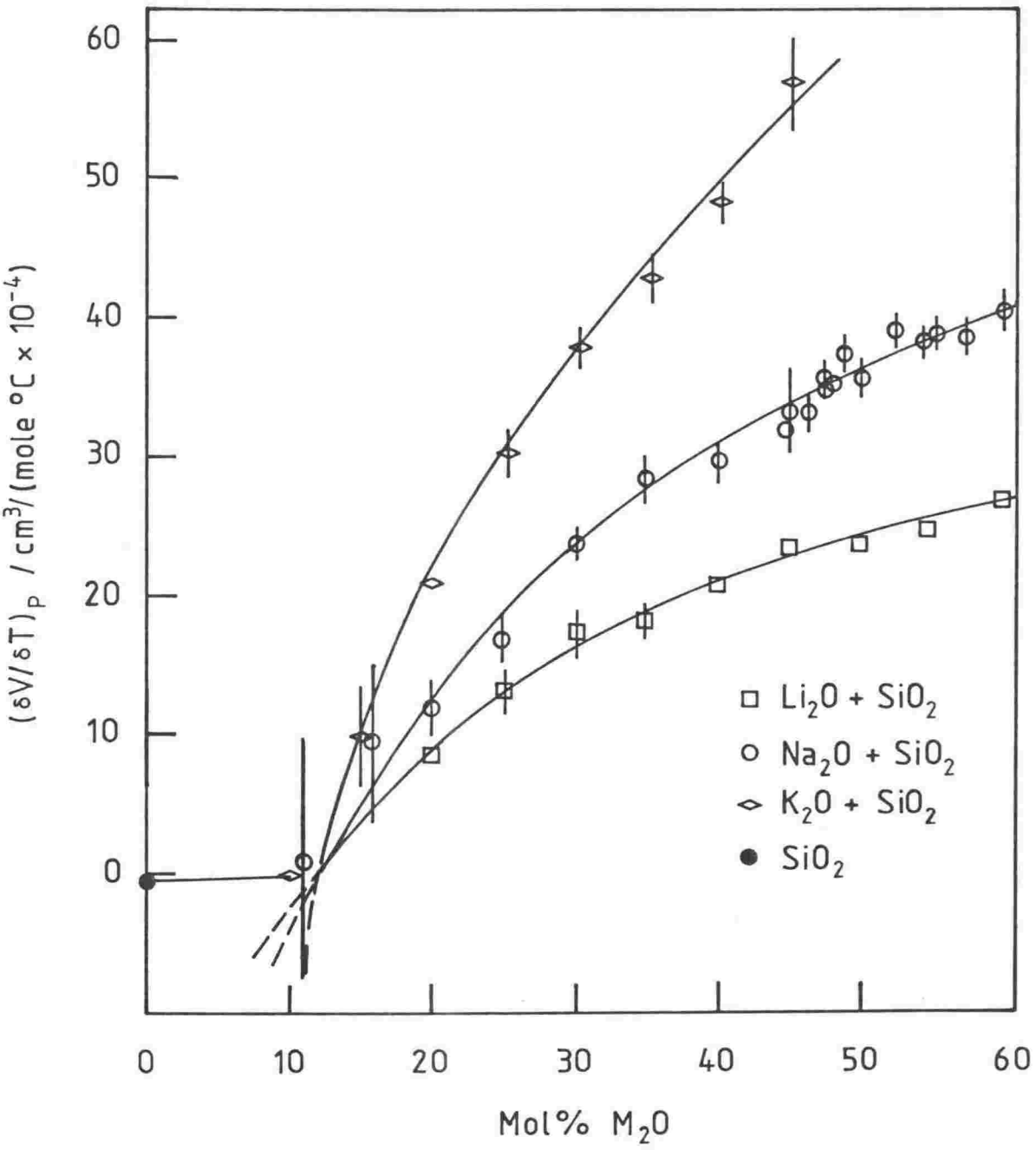

Figure 2.4—Expansion of molten alkali silicates as a function of mol% M_2O (29).

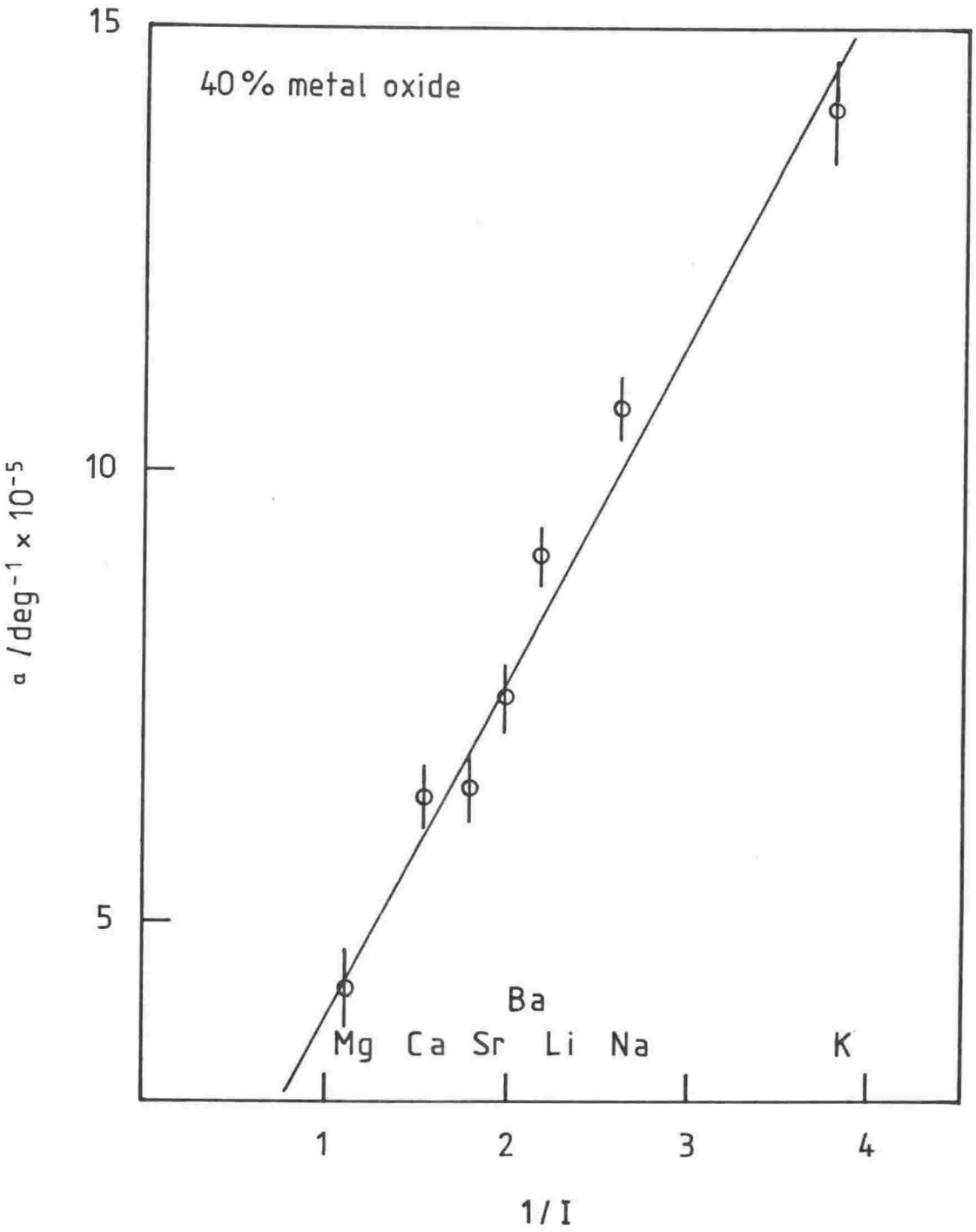

Figure 2.5—Expansivity at 40 mol% metal oxide as a function of "ion-oxygen attraction", I (30).

where X_i is the mole fraction of component i, v_i its partial molar volume and M_i its gram formula weight. More recent measurements by Aksay and Pask (36) have shown that the partial molar volume of alumina in a binary silica-alumina melt is composition dependent even within the above restricted composition range of silica. Consequently, Bottinga et al. (38) have derived a new equation for density which incorporates the partial molar volume dependence on alumina.

The binary and ternary silicates, unlike silica, have relatively large changes in volume on melting from a glass to a liquid. These changes can be ~10-20% (17).

Adiabatic compressibility of alkali oxide binary silicates have been measured by Bloom and Bockris (19), Bockris and Kojonen (18), Baidov and Kunin (20) and Laberge et al. (22). Results from these systems are shown in Figure 2.6. The melts become more compressible at higher temperatures and for initial concentrations of metal oxide; further metal oxide may cause an increase or decrease in the compressibility depending on the particular metal oxide. Figure 2.6 shows that there are inflexions in the compressibility isotherms in the ~(10-35) mol% metal oxide. This was taken as supporting evidence for the 'iceberg' model of silicate structure. The 'iceberg' model predicts that there would be little change in the compressibility in the region (10-33) mol% metal oxide.

Surface tension results are shown in Figure 2.7. King (39) found that the surface tension of most silicates (with the exception of K_2O-SiO_2) increased with increasing metal oxide content. King also noted that there was a direct relationship, first observed by Dietzel (40), between

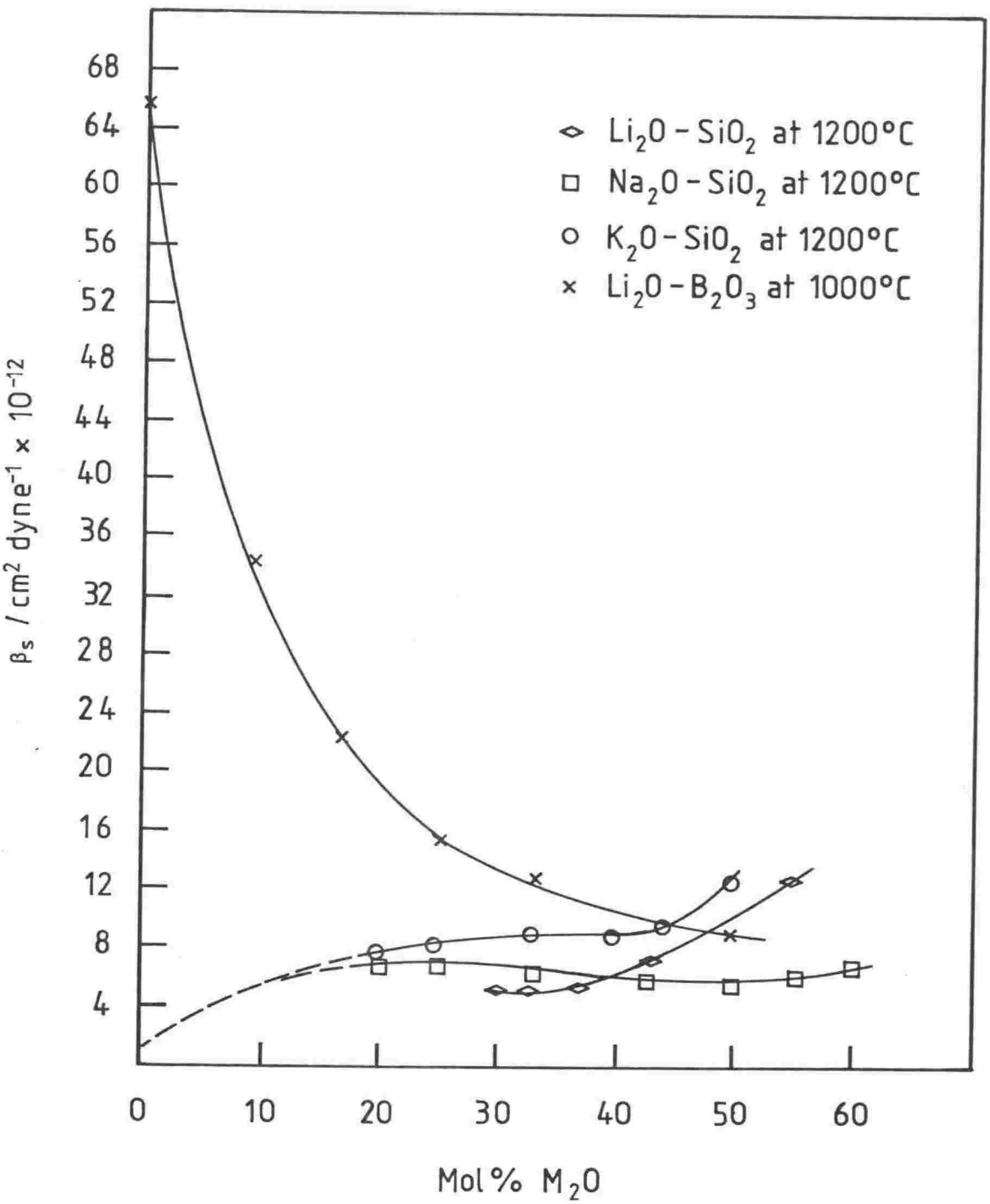

Figure 2.6—Adiabatic compressibility at 1200 °C as a function of M_2O composition (18).

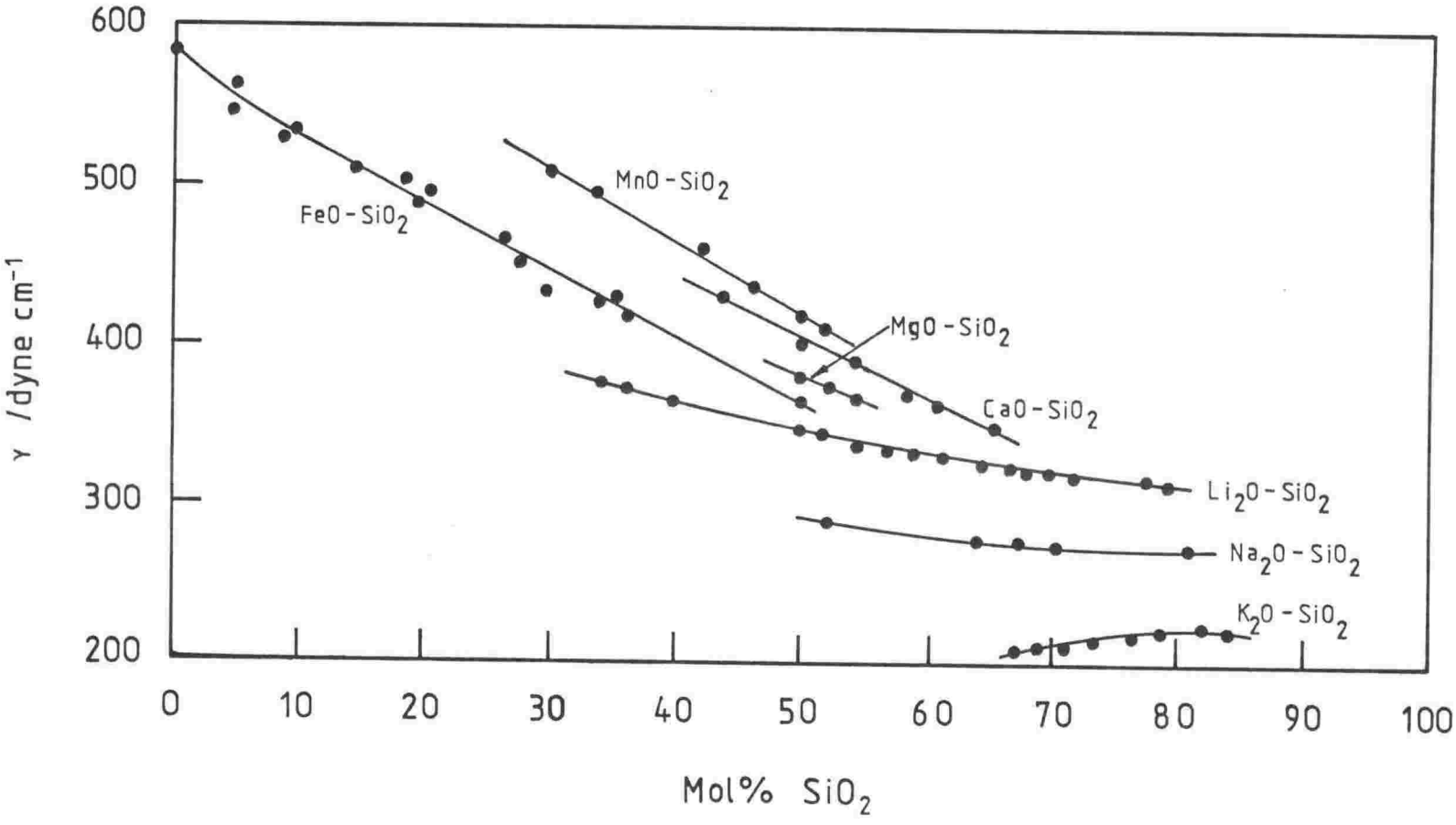

Figure 2.7—Surface tension of some binary silicates as a function of SiO_2 composition (39).

r/z, the ratio of ionic radius to valency of the cation, and F, the increase of surface tension produced in a glass by the addition of unit per cent by weight of a given oxide. A further interesting finding is that the surface tension increases with increasing temperature. King has shown that the surface tension temperature coefficient is a linear function of z/r, which includes the cations: K^+, Na^+, Li^+, Ca^{2+}, Mn^{2+}, Fe^{2+} and Mg^{2+}. The positive temperature coefficient becomes more positive as z/r increases and thus more abnormal. Why this abnormal behaviour should occur is not well understood (39).

2.1.2.2 Multicomponent and Naturally Occurring Silicates

The majority of studies reported in the geological literature on equilibrium properties of silicates are concerned with melting phenomena and phase relationships. Thermodynamic properties of multicomponent silicates have been measured by Carmichael et al. (41) along with numerous other workers. Four of the more interesting properties: density, compressibility, partial molar volume and surface tension will be discussed here briefly.

Fujii and Kushiro (42) have measured the density of an olivine tholeiite melt as a function of pressure. At pressures less than ~15 kbar the melt is more compressible than the corresponding glass. Beyond 15 kbar the reverse is the case. The isothermal compressibility of the melt calculated from this data is $\sim 6 \times 10^{-11}$ Pa^{-1} which is comparable to the adiabatic compressibilities of binary alkali metal oxide silicates (18)

Nelson and Carmichael (43), have measured the density of 21 silicate liquids over a temperature range 1000°C to 1600°C and over the following composition ranges with each component in mol%: SiO_2 (35-79%), TiO_2 (4-36%), Al_2O_3 (5-25%), FeO (11-41%), MgO (7-28%), CaO (7-35%), Na_2O (5-50%), and K_2O (4-20%). These compositions cover the upper range observed in magmas for each oxide. These authors have combined their results with additional data from the literature and have derived partial molar volumes for the above components at five different temperatures. No compositional dependence of partial molar volume was detected within experimental uncertainty. This finding is consistent with the results on binary and ternary silicates by Tomlinson et al. (30) and Riebling (32), (33). Nelson and Carmichael concluded that the lack of partial molar volume dependence on composition was consistent with the density equation proposed by Bottinga and Weill (37). However, Aksay and Pask (36) found that in binary SiO_2-Al_2O_3 melts the partial molar volumes of Al_2O_3 were composition dependent. This finding prompted Bottinga et al. (38) to revise their equation for calculating the density of alumino-silicate melts.

There are two published papers on the surface tension of natural silicate melts. In order to understand the complex eruptive behaviour of magmatic melts it is necessary to evaluate the closely related effects of surface tension and the rates of nucleation and growth of bubbles. Murase and McBirney (44) measured the surface tension of four igneous melts: a tholeiitic and an alkali-olivine basalt, an andesite, and a rhyolite as well as a synthetic lunar melt. They found that surface tension is directly proportional to temperature between 1000°C and

1450°C and covers a range of 0.25-0.425 Nm^{-1}. The temperature coefficients are all positive apart from the alkali-olivine basalt which has a negative coefficient. No satisfactory explanation was given for this anomaly. Walker and Mullins (45) have measured the surface tension of four lava compositions (limburgite to andesite) from 1200 to 1500°C. The magnitude of γ was in the range 0.35-0.37 Nm^{-1} and was similar to Murase and McBirney's data only at 1200°C. The results were less temperature sensitive than those of Murase and McBirney (44) and all the results had positive temperature coefficients. The linear relationship between the temperature coefficient $d\gamma/dT$ plotted against z/r, found by King (39) for binary silicates, appears to extend to complex melts. Plots of $d\gamma/dT$ versus z/r for 1^+ and 2^+ cations lie on three lines: disilicates, metasilicates and orthosilicates depending on the cation environment.

2.1.2.3 Hydrous Silicates

The study of hydrous silicates has been concentrated almost exclusively on the acquisition of melting relations and solubility data. Surface tension (46), the effect of oxygen fugacity (47), (48) and the solubility of volatiles (49), (50) other than water have also been measured.

Melting point depressions caused by the addition of water have been found to be analogous to the depressions arising from the addition of metal oxides. A relationship has been found between the solubility and partial pressure of water. There have been a number of attempts to elucidate the dissolution of water in silicate melts.

SiO_2-H_2O

Kennedy et al. (51) have determined the phase relations between silica and water as a function of temperature and pressure (Figure 2.8). Their work agrees well with earlier measurements by Tuttle and England (52), who determined only part of the phase diagram. The addition of H_2O depresses the melting point of silica in an analogous way to metal oxides. A critical end point for the univariant equilibrium curve was found at 1080°C and 9.7 kbar. At this point the composition is approximately 75 wt% SiO_2 to 25 wt% H_2O and the melting point of silica is depressed by ~600°C.

The solubility of water in molten silica has been found to depend on the square root of the partial pressure of water, from very low pressures < 1 bar to pressures ~10 kbar (53). Bedford noted that the solubility is not very temperature sensitive in the region 700-1500°C. The solubility dependence on the square root of the partial pressure of water has been taken to be consistent with the following reaction (54), (55):

$$H_2O + \text{-Si-O-Si-} \longrightarrow \text{-Si-OH HO-Si-}$$

which is analogous to the reaction of metal oxides with silica.

Binary and Ternary Silicates Containing Water

The melting temperatures of binary and ternary silicates are depressed by the addition of water. However, compositional variations controlling the extent of depression can only be qualitatively explained at present. The most complete set of data on melting relations that exist is for albite determined by Shimada (56) (Figure 2.9). This Figure

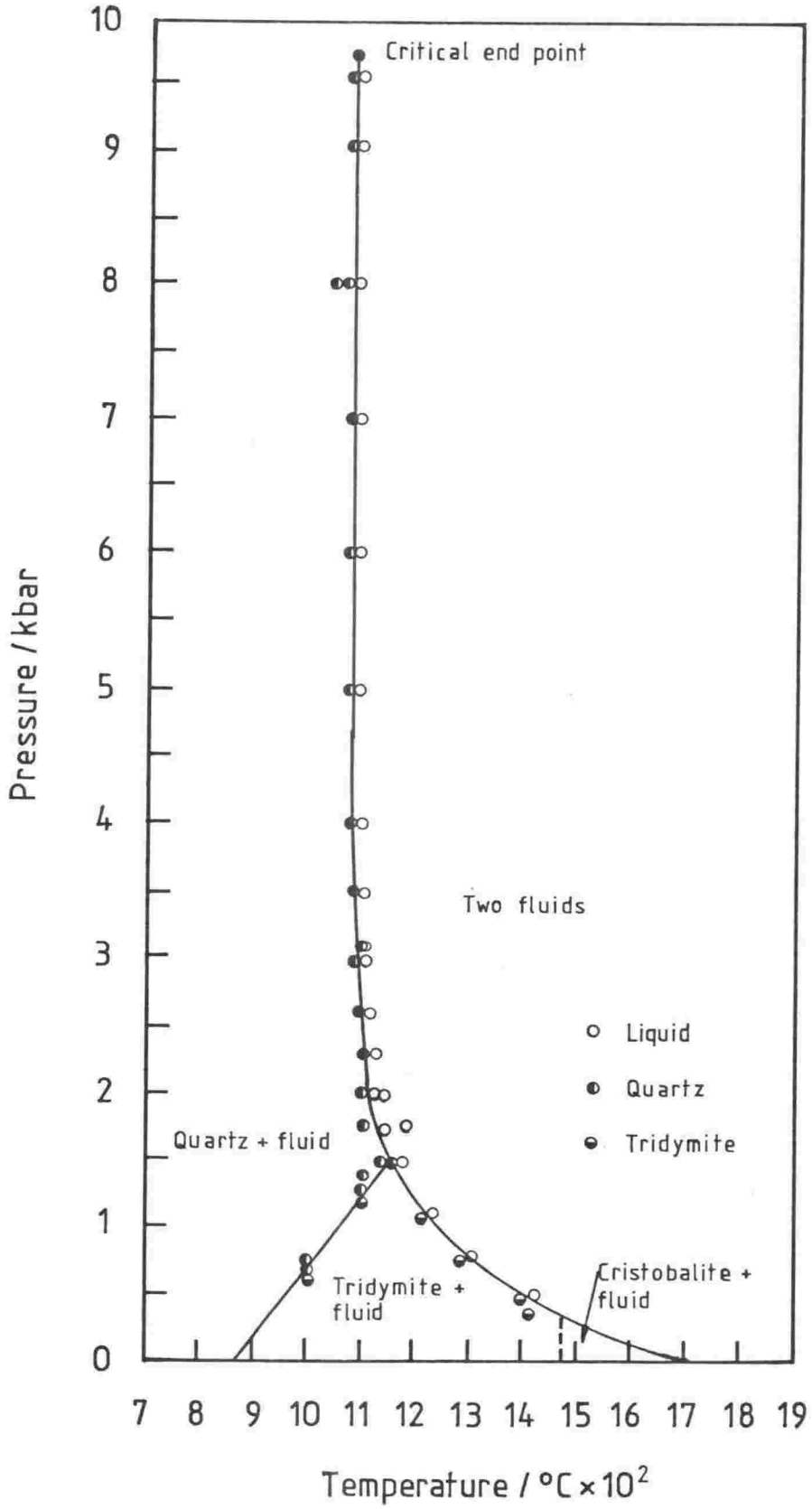

Figure 2.8—Melting relations of SiO_2 in equilibrium with H_2O as a function of pressure (51).

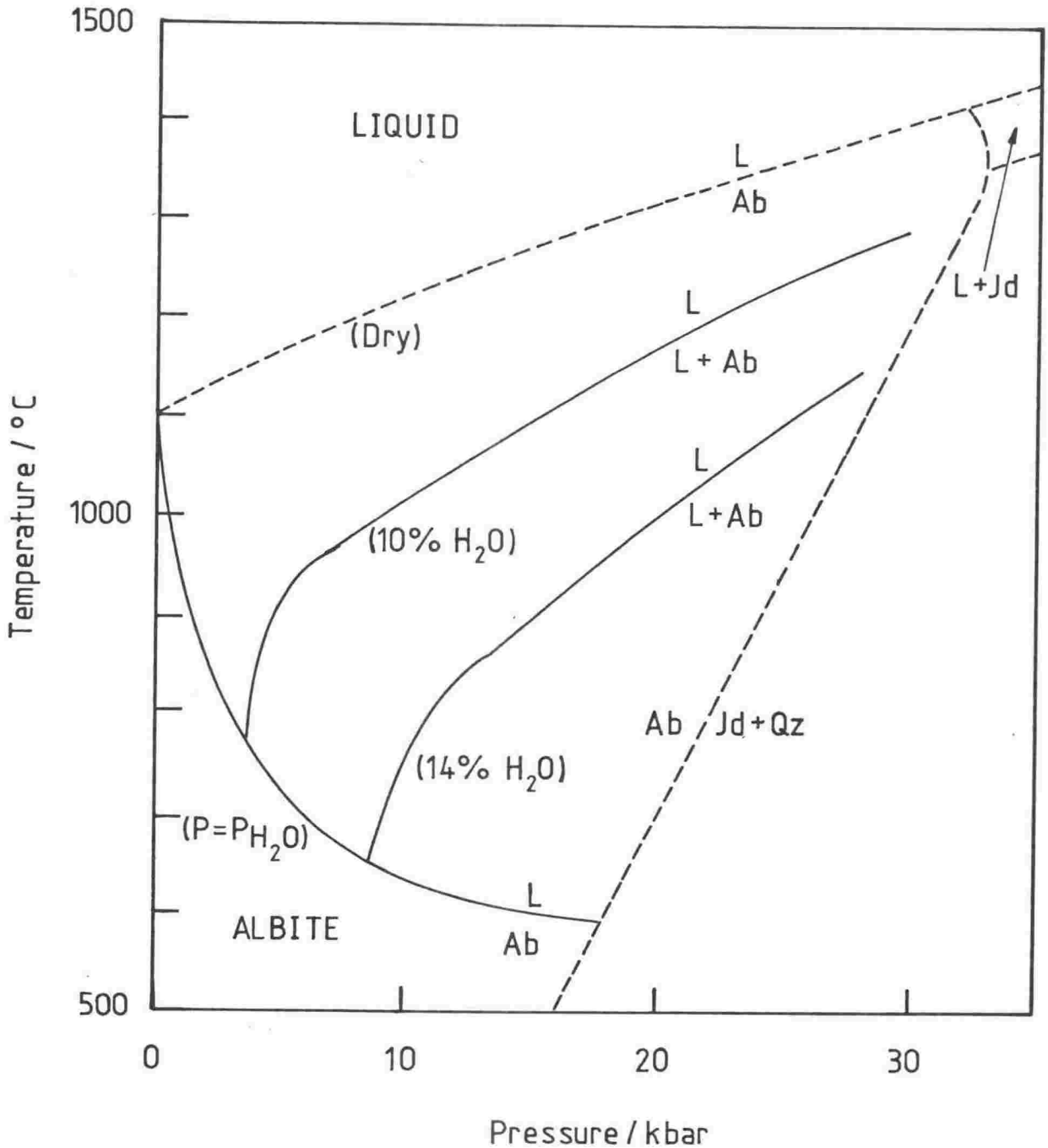

Figure 2.9—Effect of water on the melting of albite at high pressures. The broken curves show the melting curve and the curve of the transformation of albite to jadeite plus quartz under dry conditions (56).

shows that the melting point for anhydrous crystalline albite increases as pressure increases at the rate of ~10°C(kbar)$^{-1}$. When albite is subjected to water pressure the melting temperature drops ~400°C on applying 5 kbar pressure. Further increases in pressure do not lower the melting temperature as rapidly; the curve quickly flattens out. The melting point depression is not as large as for silica. If, however, a specific quantity of water is sealed, with albite, into a capsule and the temperature and pressure are both raised then the melting temperature initially drops as the saturation curve is followed but as pressure is increased still further the melt becomes undersaturated and the melting temperature begins to increase as for the dry silicate.

Orlova (57) determined the solubility of water in an albite melt at 945°C and 1125°C and pressures of 1000 and 4000 atmospheres. His results show that the content of water (s) in glasses, subsequent to quenching, expressed in wt% is proportional to the square root of water pressure. Kadik and Lebedev (58) found 18 wt% water could be dissolved in an albite melt at 10 kbar and 1300°C.

Walsh et al. (59), Tomlinson (54) and Russell (60) have each measured the solubility of water in various binary silicate melts and have found the solubility to depend on the square root of the partial pressure of water. Moulson and Roberts (61) confirmed this relationship for silica glass. Uys and King (62) as well as Kurkjian and Russell (55) examined the effect of alkali oxide on the solubility of water. The former workers found that the solubility of water is not appreciably effected by the 'basicity' of the silicate melt until the orthosilicate composition is approached, where the water solubility increases as

alkali oxide increases. This phenomenon occurs for those silicates in which the cation has a small ion-oxygen attraction, for example, Li^+ and Ca^+. These cations also form relatively stable hydroxides. The water solubility decreases for those cations with strong ion-oxygen attraction, for example, Fe^{2+}, Co^{2+} and Zn^{2+}. These cations tend to form less stable hydroxides. Temperature appears to have little influence on water solubility. The heat of solution of the water is therefore nearly zero, indicating strong bonding within the melt. The latter workers measured the effect of basicity on water solubility in alkali silicates in the compostion range 15 to 45 mol% alkali oxide. They found a minimum in the water content at about 25 mol% alkali. This was interpreted in terms of two different solution mechanisms: On the high silica side the reaction was as already described above and on the high alkali side

$$-\overset{|}{\underset{|}{Si}}-ONa \quad NaO-\overset{|}{\underset{|}{Si}}- + H_2O_{(g)} \longrightarrow -\overset{|}{\underset{|}{Si}}-O-\overset{|}{\underset{|}{Si}}- + 2Na^+ + 2OH^-$$

where the water is acting as a polymersing agent. It would seem that depending on the composition of the silicate, water may act as either a polymerising or depolymerising agent (62).

Carbon dioxide dissolves in silicate melts according to the equilibrium reaction (63):

$$CO_2 + O^{2-} \rightleftharpoons CO_3^{2-}$$

Equilibrium will shift to the right with increasing basicity. Carbon dioxide has been found to participate in a melt as only a polymerising agent (64). The addition of the volatiles water and carbon dioxide to

silicate melts undoubtedly changes the solubilities of other components and therefore the distribution of the cations.

Burnham and Davis have published two papers on the system albite-water (65), (66) dealing with P-V-T relations and other thermodynamic variables and phase relationships.

Naturally Occurring Silicates Containing Water

The effect of water on the melting relations of molten minerals is of great interest to researchers studying the asthenosphere. Consequently numerous studies exist in the geological literature (67), (68), (69), (70), (71), (72), (73). This work has shown that water causes a similar reduction in the melting point as for binary and ternary silicates. Many studies have been reported on the solubility of water and carbon dioxide in magmatic liquids (74), (75), (76), (77), (78), (79). One of the most informative of these is one by Scarfe (77). Based on the observation that the viscosity of magmas with ultrabasic composition is relatively low and thus less polymerised than, say, basaltic melts at the same temperature and pressure and that water acts as a depolymersing agent, Scarfe measured the solubility in three types of magmas to test the hypothesis that ultrabasic magmas dissolve less water than basic or acidic magmas. The composition of the three magmas studied by Scarfe is given in Table 2.4. Figure 2.10 shows the solubility results. Water solubility increases with water pressure for all compositions. Melts of ultrabasic composition a and b dissolve significantly less water than basaltic melts at the same temperatures and pressures, confirming Scarfe's hypothesis. He also observes that acidic melts dissolve even more water than basic melts.

TABLE 2.4

Composition of Magmas studied by Scarfe

Oxide	a[1]	b	c
SiO_2	42.17	46.60	53.24
TiO_2	2.59	1.40	0.96
Al_2O_3	12.70	11.80	15.00
Fe_2O_3	7.08	3.19	2.98
FeO	5.87	8.47	7.04
MnO	0.25	0.19	0.18
MgO	7.17	14.70	6.26
CaO	12.80	11.20	10.60
Na_2O	3.40	1.73	2.64
K_2O	1.92	0.13	0.87
H_2O^+	3.88	1.29	1.39
H_2O^-	1.12	0.35	0.43
P_2O_5	0.57	0.11	0.12

a - Olivine melanephelinite.

b - Picritic rock.

c - Tholeiite.

[1]Compositions in weight %.

Table from reference (77).

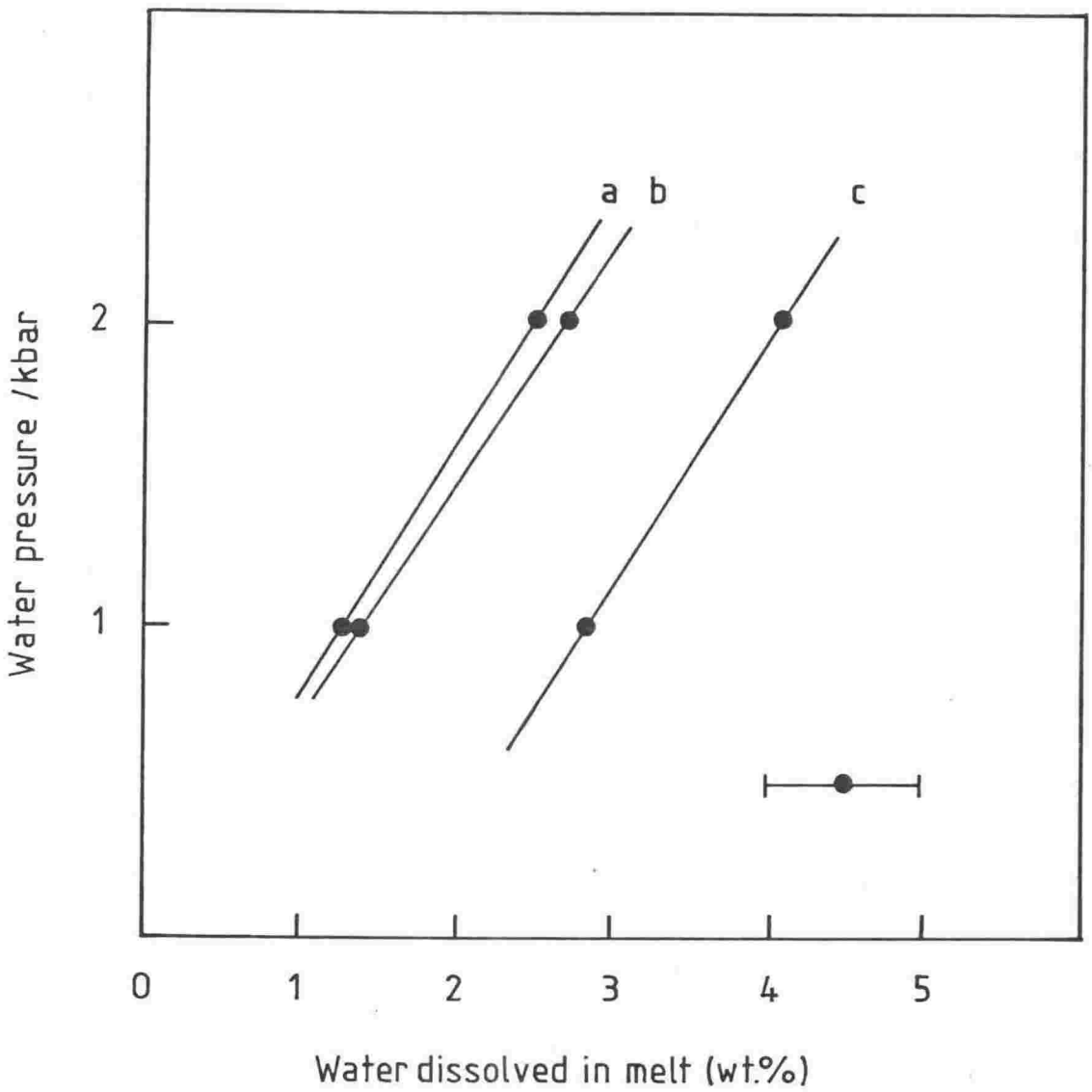

Figure 2.10—Water solubilities at 1350°C for melts of basaltic and ultrabasaltic composition. a-olivine melanephelinite; b-picrite; c-tholeiite, see Table 2.4 for the composition of these melts. Horizontal bar shows uncertainty in the measurements (77).

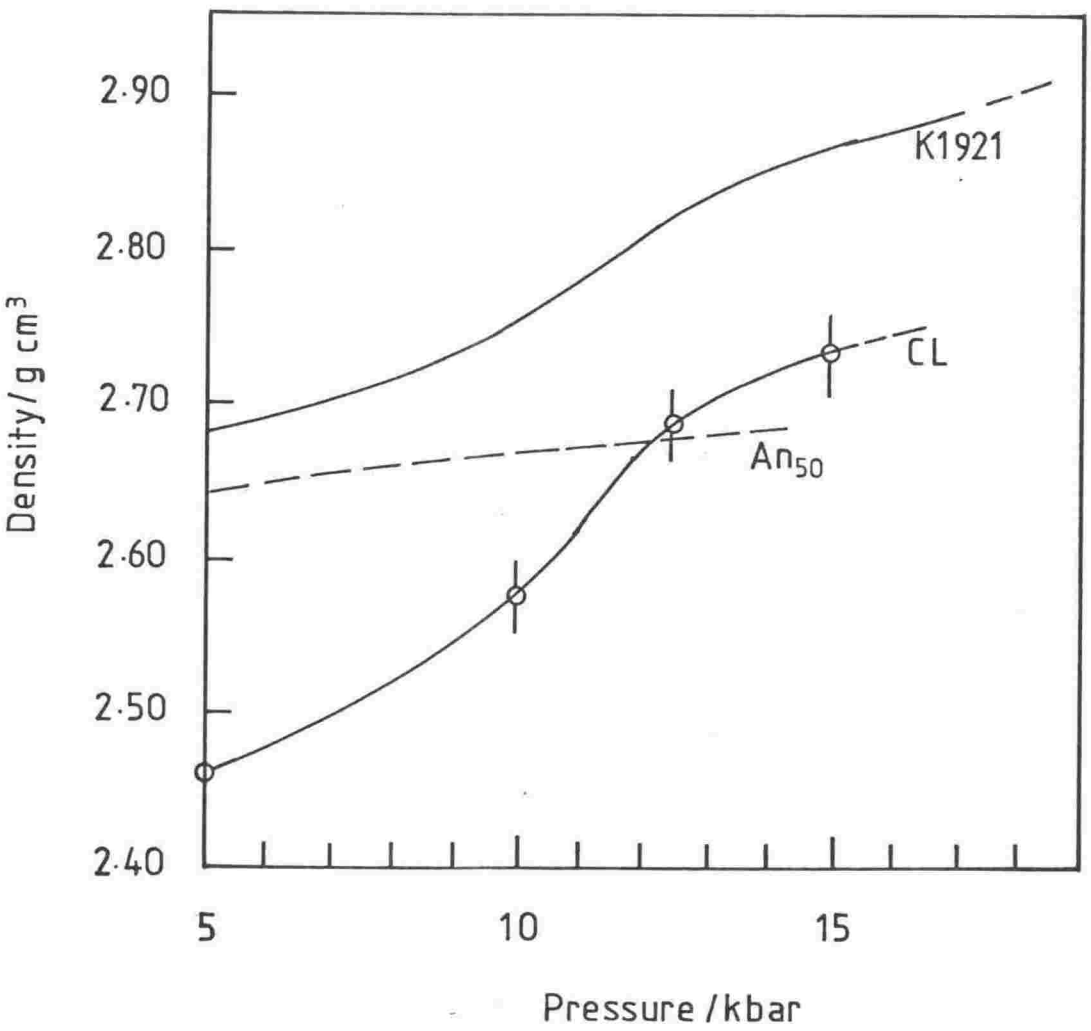

Figure 2.11—Density of a hydrous calc-alkalic andesite melt (CL) (2·86-2·98 wt%) at 10 kbar and 1175°C, 12·5 kbar and 1200°C and 15 kbar and 1200°C. The density at 5 kbar and 1175°C is for 2·63 wt% H_2O. The dashed line is for the density of plagioclase (An_{50}) and (K1921) is a Kilauea olivine tholeiite (80).

Kushiro (80) has measured the density of a hydrous calc-alkaline andesite (Figure 2.11). This Figure compares the density of the hydrous calc-alkaline andesite melt with molten tholeiite and plagioclase. The density is more pressure dependent for the hydrous andesite and the tholeiite than for the plagioclase. The more open structure of tholeiite and hydrous andesite is more compressible than the strong three-dimensionally bonded plagioclase.

Epel'baum et al. (46) have measured the surface tension of water bearing felsic magmatic melts. They found that the water bearing melt is 0.032-0.072 Nm^{-1} or approximately 5-10 times less than that for dry melts. Pressure was found to have little effect on the surface tension between 500 and 1000 atmospheres.

At present there is a debate in the literature regarding whether or not water dissolves in silicate melts exclusively by reacting with bridging oxygen atoms to form silanol groups or whether water dissolves as both molecular and hydroxyl groups. Evidence for the latter theory (81), (82) comes from infrared spectra on quenched glasses which show absorptions indicative of molecular water. The evidence for the former is extensive and is based on the measurement of a number of different physical properties: transport properties, Raman spectroscopic studies and solubilities. Raman spectroscopy has failed to detect vibrations of molecular water but have detected vibrations of hydroxyl bearing groups. The ultimate test of the alternatives is Raman and infrared studies in the molten state.

2.2 NON-EQUILIBRIUM PROPERTIES OF LIQUID SILICA AND SILICATES

This section examines the way in which metal oxides and water affect the transport properties of molten silica together with the pressure and temperature dependence of those properties. Transport properties describe the set of kinematic phenomena which arise in a liquid as a result of an applied force. The entities in the liquid experience this force as a consequence of some potential gradient existing across a volume of the liquid. Transport properties describe non-equilibrium processes and those processes are, consequently, irreversible. The transport processes discussed here cover: electrical conductivity, viscosity and diffusion. They are defined in section 2.2.1. This is followed by a brief review of the transport theories which have been applied to molten silicates. Sections 2.2.5 and 2.2.6 summarise the experimental transport data on molten silicates.

2.2.1 Definition of Transport Properties

2.2.1.1 Electrical Conductivity

When an electrical field, E, is impressed on a liquid an electric current is produced which arises from the movement of ions in the liquid. The electric current, I, is defined as the rate of flow of charge,

$$I = dq/dt \qquad (2.1)$$

where dq is the charge that passes through a cross-sectional area in a dt time interval. If the conductors cross-sectional area is A then the current density, J, the net flux of charge is given by

$$J = I/A \qquad (2.2)$$

and the conductivity, κ, is given by

$$\kappa = J/E \tag{2.3}$$

and,

$$\rho = 1/\kappa \tag{2.4}$$

where ρ is called the resistivity. The conductor obeys Ohm's law if κ is independent of E. Under such circumstances the resistance, R, a measurable quantity, is defined as

$$R = \Delta V/I \tag{2.5}$$

where ΔV is the electrical potential difference between the extremities of the conducting path of length l. The potential difference ΔV is related to the electric field by

$$\Delta V = \int_0^l E.dl = El \tag{2.6}$$

Therefore,

$$\Delta V = Il/\kappa A \tag{2.7}$$

and,

$$\rho = R(A/l) \tag{2.8}$$

and,

$$\kappa = G(l/A) \tag{2.9}$$

where $G = 1/R$ and is called the conductance. The ratio (l/A) in a conductance cell refers to the distance, l, which separates two electrodes divided by their cross-sectional area, A. This ratio is

called the cell constant since for constant temperature and pressure it remains invariant. It is generally determined by calibration with an electrolyte of known conductivity. The theory and techniques involved in the calibration of electrical conductivity cells have been discussed by a number of authors including: Janz and Tomkins (83), Barthel et al. (84), and Juhasz and Marsh (85). Experimentally κ is determined by the measurement of G or R of a liquid in a cell for which the cell constant is known.

Conductivity has the units Sm^{-1} where S is the siemen, the S.I. unit for the reciprocal ohm. Conductivity is often quoted in Scm^{-1}, because, till recently the cell constant was always expressed in terms of cm^{-1}. 1 Scm^{-1} = 100 Sm^{-1}.

If it is considered that conductance arises from the movement of ions in an electrolyte and that the total current is the sum of the currents carried by the individual ions then an expression can be derived for their mobilities and transport numbers. The former refers to the velocities of the ions and the latter to the proportion of the charge carried by each type of ion. If an ion i, has charge $z_i e$, then, under the influence of an electric field E, it will give rise to an electric current density J_i:

$$J_i = |z_i| \, ev_i N_i / Al \qquad (2.10)$$

where: v_i is the terminal velocity of ion i, N_i is the number of i ions in volume Al, e is the charge on a proton and z_i is the number charges/ion. If c_i is the concentration of i ions, and if all velocities are considered positive then:

$$J_i = |z_i| \, Fv_i c_i \qquad (2.11)$$

where: F is the Faraday and is equal to the product of e and Avogadro's number. Therefore the total current density due to all ions is:

$$J = \sum_i |z_i| F v_i c_i \qquad (2.12)$$

Since $J = \kappa E$ the conductivity of an electrolyte solution is given by:

$$\kappa = \sum_i |z_i| F c_i (v_i/E) \qquad (2.13)$$

At low field strengths κ is independent of E. This implies that for a fixed concentration of ion i, the ratio of (v_i/E) must be constant and characteristic of ion i. This ratio is called the electric mobility, u_i, of ion i:

$$u_i = v_i/E \qquad (2.14)$$

The terminal velocity, v, of an ion is, therefore proportional to the applied field, E, and the proportionality constant is the ions mobility. When mobilities of ions are included in the expression for κ, equation (2.13) becomes:

$$\kappa = \sum_i |z_i| F u_i c_i$$

The transport or transference number, t_i of ion i, is defined as the fraction of the total current carried by that ion.

$$t_i = J_i/J \qquad (2.16)$$

From equations (2.3), (2.8), (2.11), and (2.14) an expression can be derived which relates transport numbers to κ:

$$t_i = |z_i| F c_i u_i/\kappa \qquad (2.17)$$

Thus, the transport number of ion i, can be calculated from its mobility and the sum of transport numbers over all ionic species is unity:

$$\sum_i t_i = 1 \qquad (2.19)$$

Experimental observations (86) have shown that electrolytic conductance depends on many different variables including: the thermodynamic variables, concentration, temperature and pressure, the valence type of the electrolyte, the field strength and the frequency used in the measurement. Particular care must be taken when measuring conductance so that one measures the conductance of the sample alone and not some combination of the sample and the measuring technique. In particular, polarisation effects at the electrodes have to be minimised or excluded. This is usually achieved by using an AC voltage. However frequency dispersion arising from this method has to be examined. Robbins and Braunstein (87) have discussed this problem and how to compensate for it.

The molar conductivity of an electrolyte is defined as,

$$\Lambda = \kappa/c \qquad (2.19)$$

where c is the concentration of the electrolyte. If the units of κ are Sm^{-1} and the units of c are mol m^{-3} then Λ has units Sm^2mol^{-1}

2.2.1.2 Viscosity

The theory of viscosity is based on Newton's law of viscosity which states that: 'the shear stress, η_s, in liquids undergoing laminar flow is proportional to the local velocity gradient perpendicular to the

stress'. Figure 2.12 illustrates this law. Newton's law can be expressed:

$$f_{xy} = -\eta_s(dV_x/dy) \qquad (2.20)$$

where the proportionality constant, η_s, is known as the shear viscosity coefficient. The frictional resistance to flow (a force equal and opposite to f_{xy}) is directly proportional to the shear velocity. A liquid which obeys equation (2.20) is known as a Newtonian liquid. The S.I. unit of viscosity is the $kgm^{-1}s^{-1}$ or the pascal second, Pa s.

Most liquids discussed in this thesis obey the Newtonian equation. However, molten silicates containing bubbles and/or solid material are, in general, non-Newtonian.

2.2.1.3 Diffusion

When a gradient of chemical potential exists in a liquid a diffusive flow of component, i, arises , due to the virtual diffusive force it experiences. The effective force, F_i, exerted on a mole of i ions may be written as

$$F_i = -\text{grad } \mu_i \qquad (2.21)$$

where μ_i is the chemical potential of ion i. If it is assumed that the chemical potential gradient has only a component in the x direction then equation (2.21) may be written as:

$$F_{ix} = -\left|\text{grad } \mu_i\right| = -d\mu_i/dx \qquad (2.22)$$

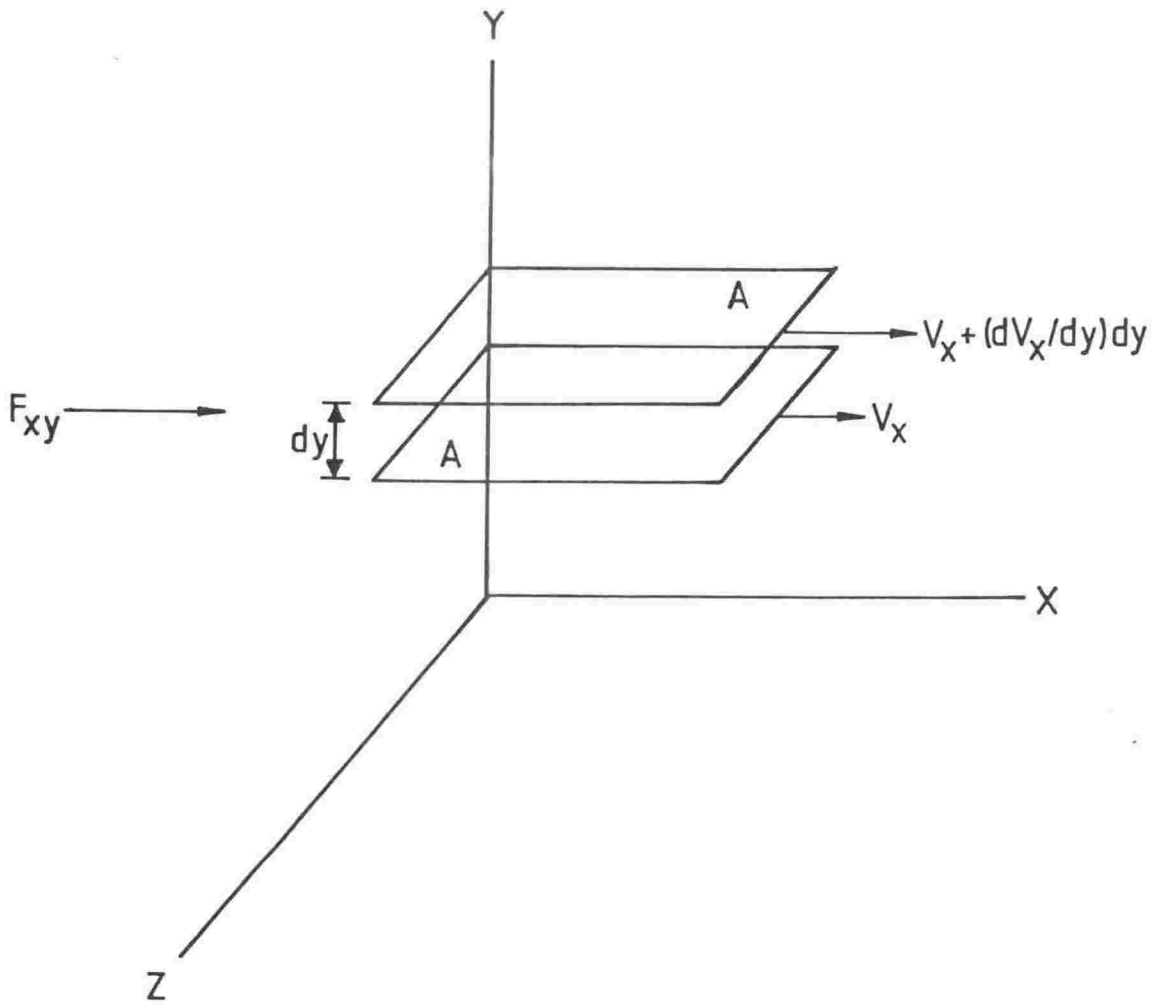

Figure 2.12—Laminar flow in the x-direction arising from shear force F_{xy} with velocity gradient in the y-direction.

If c_i, the concentration of component i, at every point is not too great then c_i is essentially the activity, a_i, of ion i and thus

$$\mu_i = \mu_i^o + RT\ln c_i \tag{2.23}$$

By differentiating with respect to x one obtains

$$(d\mu_i/dx) = (RT/c_i)(dc_i/dx) \tag{2.24}$$

which results in equation (2.22) becoming

$$F_{ix} = (RT/c_i)(dc_i/dx) \tag{2.25}$$

At any instant the application of F_{ix} results in a net, average flow velocity, v_{ix}, of one mole of i in the x direction, which is proportional to F_{ix}, i.e.

$$v_{ix} = KF_{ix} \tag{2.26}$$

K is a proportionality constant, dependent on the particular system in question. Equations (2.25) and (2.26) yield

$$v_{ix} = -K(RT/c_i)(dc_i/dx) \tag{2.27}$$

If A is the cross-sectional area, normal to the x direction of flow then the total number of moles of i flowing across A in unit time is Ac_iv_{ix}, which gives for the diffusive flux of i

$$J_{ix} = c_iv_{ix} \tag{2.28}$$

or,

$$J_{ix} = -k(RT/c_i)c_i(dc_i/dx) = -D_i(dc_i/dx) \tag{2.29}$$

where D_i is the diffusion coefficient of species i and is equal to KRT. Equation (2.29) is known as Fick's first law of diffusion. This law is valid for steady state conditions in which the concentration gradient of i is maintained constant by addition and removal of i from the extremities of the gradient. In this situation J_{ix} is independent of both x and time, t. In the case of a closed system, equation (2.29) is valid for particular instants of time. c_i and also J_{ix} will be functions not only of the x coordinate but also of time. This situation is described by Fick's second law of diffusion

$$(dc_i/dt) = D_i(dc_i^2/dx^2) \qquad (2.30)$$

The S.I. unit for the diffusion coefficient, D, is m^2s^{-1}, although it is frequently given in the literature as cm^2s^{-1}.

In the study of liquids the self-diffusion coefficient is frequently of interest to physical chemists. Unlike inter-diffusion as just described above, which results from a gradient of chemical potential, self-diffusion of a species arises from random motion caused by electrostatic interaction with neighbouring ions and molecules. It is usually measured by tracking the movement of isotopes of the diffusing species being examined. If m is the diffusing species being studied in a mixture of n components then the localised introduction of an amount of isotopically labelled m' into the system will result in a measurable diffusion of m' into the rest of the sample. Under such circumstances, if the system is otherwise homogeneous with respect to all other components, then

$$J_m + J_{m'} = 0, \text{ where } J_i = 0 \ (i = 1 \ldots n \neq m) \qquad (2.31)$$

and the diffusion coefficient of m' is the self-diffusion coefficient.

2.2.2 Relationships Between Transport Properties

There are several simple relationships between some of the transport properties which are valid for certain types of liquid. If the diffusive and conductive ionic mobilities are equated one obtains the Nernst-Einstein equation:

$$\Lambda = F^2(D_+ + D_-)/RT \tag{2.32}$$

This equation is formally valid for electrolytes of infinite dilution where there are no interactions between mobile species. For most ionic liquids the diffusive mobilities are greater than the conductive mobilities.

A simple hydrodynamic model for diffusion of a particle, i, consists of treating it as a sphere of radius r_i, moving with a velocity v_{ix} through a structureless medium of viscosity η. Under these conditions the drag force experienced by the particle i is given by Stokes's law:

$$F_{i,drag} = -6\pi\eta r_i v_{ix} \tag{2.33}$$

If it is assumed that the particle velocity, v_{ix}, is the same as the average diffusive velocity of ion, i, then the diffusive force per particle, F'_{ix}, is equation (2.22) divided by N_A, Avogadro's number:

$$F'_{ix} = (F_{ix}/N_A) = -(1/N_A)(d\mu_i/dx) \tag{2.34}$$

Therefore,

$$F'_{ix} = -(R/N_A)(1/c_i)(dc_i/dx) = (k/c_i)(dc_i/dx) \tag{2.35}$$

at steady state condition $F_{i,drag} = -F'_{ix}$ or

$$-6\pi\eta r_i v_{ix} = (k/c_i)(dc_i/dx) \qquad (2.36)$$

which yields

$$v_{ix} = -(kT/6\pi\eta r_i c_i)(dc_i/dx) \qquad (2.37)$$

By comparing equation (2.37) with equation (2.27) on obtains

$$K = 1/(6\pi\eta r_i N_A) \qquad (2.38)$$

and by substituting this expression for K into the expression for the diffusion coefficient $D_i = KRT$, yields

$$D_i = kT/(6\pi\eta r_i) \qquad (2.39)$$

which is the Stokes-Einstein equation. There is often remarkably good correlation between D_i and η for both molecular and ionic liquids although this is not the case for molten silicates.

2.2.3 Temperature and Pressure Dependence of Transport Properties

For ionic liquids well above T_g and over short ranges of temperature it is often found that the transport parameters: diffusion, D, fluidity, Φ $(=1/\eta_s)$ and electrical conductivity, κ, follow an Arrhenius temperature dependence, expressed as

$$D,\ \Phi,\ \kappa = D_o,\ \Phi_o,\ \kappa_o \exp(-E/RT) \qquad (2.40)$$

where: D_o, Φ_o, and κ_o are constants for their respective transport parameters and E is an activation energy which will depend on the transport parameter in question. R is the gas constant and T is absolute temperature. In the case of temperature intervals much closer to T_g an equation of the following form is often obeyed:

$$D,\ \Phi,\ \kappa = D_o,\ \Phi_o,\ \kappa_o \exp[-B/(T-T_o)] \qquad (2.41)$$

where T_o is a parameter that can be interpreted as the lower temperature limit of mobility of a transportable species. Similar equations with E and B replaced with PV^*, where P is the pressure and V^* an activation volume, express the pressure dependence of many liquids. Equations of this sort or with $(T-T_o)$ replaced with $(V-V_o)$ have given rise to various theories of transport processes in liquids and glasses. The Free Volume Theory (88) and the Configurational Entropy Theory (89) are notable examples.

2.2.4 Summary of Transport Theories Applied to Molten Silicates

There are three main transport theories which have been applied to molten silicates. These theories have been discussed and criticised extensively in the literature, consequently they will only be described here very briefly.

2.2.4.1 Transition State Theory

This theory was developed, under the name of absolute reaction rate theory, by Glasstone, Laidler and Eyring (90). Subsequently it was extended by Bockris et al. (91), (92) to apply to electrical conductivity and viscosity of molten silicates. An ion or atom, according to this theory will jump a distance, d, from one position to another in a quasilattice structure provided it acquires sufficient energy, ΔG^*, to surmount the energy barrier hindering the movement. The probability that an ion will receive this energy, (from the random thermal motion of the particles surrounding it) is proportional to

$\exp(-\Delta G^*/RT)$. Ions will move randomly in the absence of an applied field but will drift preferentially along a potential gradient in the presence of an applied field. Based on this molecular picture and together with the rate equation from the theory of absolute reaction rates, Bockris et al. (91) derived the following equation for conductivity in molten silicates:

$$\Lambda = (2/3)dFa(kT/h)\exp(-\Delta G^*/RT) \qquad (2.42)$$

where: d is the jump distance, F is the Faraday constant, k is Boltzman's constant, h is Planck's constant, R is the gas constant, T is absolute temperature and a is equal to XdzF/RT where X (Volt/cm) is the effective potential gradient acting on the ion. X is difficult to evaluate, but if it is written as $X = (\varepsilon + 2)/3$, where ε is the relative permittivity then

$$\Lambda = 3.62x10^{19}zd^2\exp(-\Delta G^*/RT) \qquad (2.43)$$

or,

$$\Lambda = 3.62x10^{19}zd^2\exp(-\Delta H^*/RT)\exp(\Delta S^*/R)$$

where $\Delta G^* = \Delta H^* - T\Delta S^*$ Thus a plot of log Λ against 1/T will have a slope of $-\Delta G^*$ with and intercept at $3.62x10^{19}zd^2$. ΔH^* and ΔS^* for the conduction process can then be evaluated.

2.2.4.2 Free Volume Theory

It has been found that an empirical equation, the Vogel-Tammann-Fulcher (VTF) equation:

$$W(T) = AT^{-1/2}\exp[-B/(T-T_o)] \qquad (2.44)$$

where $W(T) = \Lambda,\ D/T\ ,1/\eta$; A and B are constants for a particular transport function, describes the transport temperature dependence over a wide temperature range. Cohen and Turnbull (88) have proposed a model, called the Free Volume Model, to give a theoretical explanation for the applicability of the VTF equation.

In this model, originally designed to describe the diffusion process in a hard sphere fluid, mass transport occurs when, under the influence of an applied force, a molecule moves into a void of minimum volume V^* that is created by the redistribution of free volume. Free volume is defined as the volume of the liquid minus the close packed volume V_o. $V_f = V - V_o$. When free volume is defined in this way and if the redistribution of free volume is assumed to be without energy change then it is possible to evaluate the transition or jump probability, which is given by

$$P(V^*) = \exp(-\gamma V^*/V_f) \qquad (2.45)$$

where γ is a factor to allow for free volume overlap, $1/2 \leqslant \gamma \leqslant 1$. By making the additional assumption that the glass transition arises from the effective disappearance of free volume ($V_f \longrightarrow 0$, therefore $D \longrightarrow 0$ and $\eta \longrightarrow \infty$) which occurs at T_o, Cohen and Turnbull showed the diffusion coefficient is given by

$$D = g\ d\ v\ \exp(-\gamma V^*/V_f) \qquad (2.46)$$

where $g \doteqdot 1/6$, d is the distance through which the molecule moves in the jump and v is the velocity of the molecule. By substitution of D for Λ via the Nernst-Einstein equation the VTF equation can be obtained. By

plotting $\log \Lambda$ against $1/(T-T_o)$ the constants A and B can be evaluated and compared with the values calculated from the free volume equation.

2.2.4.3 Developments by Macedo and Litovitz

Macedo and Litovitz (93) assumed that two events must occur simultaneously before a molecule can undergo diffusion: (1) the molecule must attain sufficient energy to break away from its neighbours and (2) it must have an empty site large enough to jump into. Using the rate theory to calculate (1) and the FVT to calculate (2) a hybrid equation for the viscosity is obtained which contains both activation energy and free volume:

$$\eta = A_o \exp[(E_V^*/RT) + (\gamma V_o/V_f)] \qquad (2.47)$$

where E^*_V is the activation energy for viscous flow at constant volume, γV_o is the critical free volume, V_f is the free volume and A_o is a constant.

2.2.4.4 Application to Liquid Silicates

Bockris et al. (91), (92), have applied transition state theory to conduction and viscosity in molten silicates. Tickle (94) criticised this approach and explained his conductivity results in terms of the Free Volume Theory. In critique of the application of these theories to the conduction process in molten silicates, Smedley (95) concluded, "While neither the free volume theory nor the transition state theory can be regarded as providing an accurate description of electrical conductance in liquid silicates, the transition state formalism provides

a better correlation between the properties of the mobile cation (z_i, r_i) and the conductance of the melt". Moreover, the failure of the Nernst-Einstein equation for molten silicates (96), renders the Free Volume Theory for conduction inappropriate.

The interpretation of viscosity in molten silicates in terms of the FVT has been made by a number of workers including: Kumar (97), (98). Musikhin et al. (99), Sasek (100) and Cranmer and Uhlmann (101). The application of this theory to viscosity is more speculative (98) than conduction because the flow unit is not well defined.

Cohen and Grest (102) have extended the free volume model to describe the thermodynamic behaviour of dense liquids and glasses. They concluded that although the usual form of the FVT should describe the flow behaviour in the high temperature region ($\eta < 10^4$-10^5Pa s), a modified expression is required to describe viscosity over the full range of temperatures. Their modified expression is:

$$\log \eta = c + 2D/\{(T-T_o) + [(T-T_o)^2 + 4\zeta_o V_a T]^{1/2}\} \qquad (2.48)$$

where $D = 0.43 V_m \zeta_o$, V_m is the molecule volume, V_a is the hard core volume of the molecule and its vibrations at any temperature, ζ_o is a constant which reflects the interaction potential of the system and c is a constant. Cranmer and Uhlmann (101) have applied this version of the theory to the viscosity of molten mixtures of albite and anorthite ($CaAl_2Si_2O_8$) over a 800°C temperature range where the behaviour is non-Arrhenian. The modified equation gives a much better fit over this temperature interval compared to the usual equation which fits the data for only a 300°C interval at higher temperatures. They estimated the

radius of the flow unit to be 6Å which is larger by a factor of 1.3 than the radius of the formula unit estimated from density measurements. However due to approximations made in the calculations it was concluded that in liquid anorthite the flow unit is comparable in size to the formula unit. Although curve fitting is much better for the modified equation in these liquids it is not surprising with the addition of an extra adjustable parameter.

Macedo and Litovitz (93) have applied their hybrid equation to a number of liquids ranging from fused silica to liquid argon and including polyatomic van der Waals as well as hydrogen bonded liquids, with some success. In particular they applied it to liquid SiO_2, and GeO_2 and some silicate mixtures. Both SiO_2 and GeO_2 have Arrhenius temperature dependence for viscosity over a 1000°C temperature range; whereas the addition of alkali oxides to silica cause pronounced curvature over a similar temperature interval. Macedo and Litovitz (93) have given a explanation of this behaviour based on their hybrid equation. In the case of SiO_2 the density does not change much over this temperature interval (66), (103). This implies the free volume does not change since $\alpha_T \doteqdot 0$. Free volume thus effects only the magnitude of viscosity and not the temperature dependence. Thus $E_p^* = E_V^*$. A similar argument is believed to apply to germania.

The addition of alkali oxides does two things to molten silica: (1) it lowers the viscosity and (2) makes it non-Arrhenian. It has long been suggested that the alkalis act as network modifiers decreasing the extent of the network structure. This effect can be accounted for by E_V^*. In addition, another significant change occurs, that is, an increase in

thermal expansion. This increase in α is the cause of the non-Arrhenian behaviour. Further, the 'apparent' activation energy at low temperatures for 20 mol% Na_2O is close to that for fused silica. However, in this region α is no longer zero, E_V^* is possibly less than 42 kJ rather than the apparent 586 kJ comparable to pure silica.

The hybrid equation reduces to the commonly used equation under various conditions. The Arrhenius behaviour of liquids may occur if: (1) The liquid has a zero or very small expansivity coefficient in the temperature range being considered (i.e. V_f is independent of temperature) and (2) V_f is proportional to temperature. Condition (1) is exemplified by fused silica and germania. Condition (2) is typical of van der Waal and monatomic liquids.

Brummer (104), has criticised the Macedo-Litovitz model in spite of its apparent success, on the grounds that it ascribes all the volume dependence of the transport process to the p(V) term and that E_V is independent of density. The latter is contrary to experiment (105), (106), (107). Brummer correctly concluded that more detailed studies should be made not only as a function of temperature but also of density.

Goldstein (108), has observed that theories about transport processes, in general, are not well developed, even for solutions and simple low temperature molten salts for which there exists a large body of experimental data over wide temperature and pressure ranges. Consequently, it is not surprising that application of these theories to complex silicate liquids is not very successful. Moreover, at present data on silicate liquids at high temperatures and/or pressures have

relatively large errors and it is thus inappropriate to apply sophisticated transport theories. Until a much larger body of experimental data on liquid silicates exists, interpretation of transport properties can at best be only qualitative and will have to continue to rely on simple empirical relationships such as the Arrhenius law.

2.2.5 Transport Properties of Liquid Silica

Table 2.5 compares transport properties of liquid silica with the liquids: GeO_2, BeF_2, NaCl and H_2O. At the melting point of these liquids it is found that:

1. The conductivities of SiO_2, GeO_2, BeF_2 and H_2O are very low in contrast to the ionic liquid, NaCl.
2. SiO_2, GeO_2, and BeF_2 melt to form extremely viscous liquids; in contrast to NaCl and H_2O.
3. Self-diffusion of $^{22}Na^+$ in NaCl is a factor of 7 greater than self diffusion in H_2O. There are no reported measurements of self-diffusion in network liquids. However, it would be expected that self diffusion in network liquids would be much less than in NaCl due the strong covalent bonding in the former.

Bowen and Taylor (113) and Urbain et al. (114) have recently measured the viscosity of SiO_2 and Panish (115) has measured the electrical conductivity of silica from 1500 to 2600°C. The Arrhenius equation (equation 2.40) is obeyed over a wide temperature range for both of these transport properties and for viscosity it is obeyed to temperatures close to T_g. Figure 2.13 shows an Arrhenius plot for the viscosity of SiO_2, GeO_2, BeF_2.

TABLE 2.5

Non-equilibrium properties of liquids: SiO_2, GeO_2, BeF_2, NaCl and H_2O

	SiO_2	GeO_2	BeF_2	NaCl	H_2O
T_m /°C	1713	1115	552	801	0
T_b /°C	2230		1327	1465	100
At T_m					
κ /S cm^{-1}	7.7×10^{-4}[a]	$\sim10^{-3}$	1×10^{-6}	3.67	
E_κ /kJ mol^{-1}	70		>420		
η /Pa s	1.7×10^{7}	8.0×10^{5}	3.2×10^{5}	1.06×10^{-3}	1.7×10^{-3}
E_η /kJ mol^{-1}	515	293	240	21(?)	
D_s /$cm^2s^{-1}\times10^{-5}$				7.8(^{22}Na)	1.05
E_D /kJ mol^{-1}				29.8	
At $1.1T_m$					
T /°C	1911	1250	638	~900	
κ /S cm^{-1}		4.1×10^{-3}	3.9×10^{-5}	3.85	4×10^{-8}[b]
E_κ /kJ mol^{-1}		195	290		
η /Pa s	1.6×10^{6}	7.0×10^{4}	1.0×10^{4}	8.6×10^{-4}	8.5×10^{-4}[c]
E_η /kJ mol^{-1}	515	293	240	21	
D_s /$cm^2s^{-1}\times10^{-5}$					2.53[d]
At T_m + 200°C					
T /°C	2000	1315	755	1000	
κ /S cm^{-1}	$\sim10^{4}$[e]	1×10^{-2}	2.8×10^{-3}	4.03	
E_κ /kJ mol^{-1}		70		290	
η /Pa s	8.5×10^{5}	1.8×10^{4}	4.8×10^{2}	$7.3\times^{-4}$	2.8×10^{-4}[f]

[a]1800°C; [b]18°C; [c]27°C; [d]25°C; [e]2700°C; [f]100°C.

Data from references (109), (110), (111), and (112).

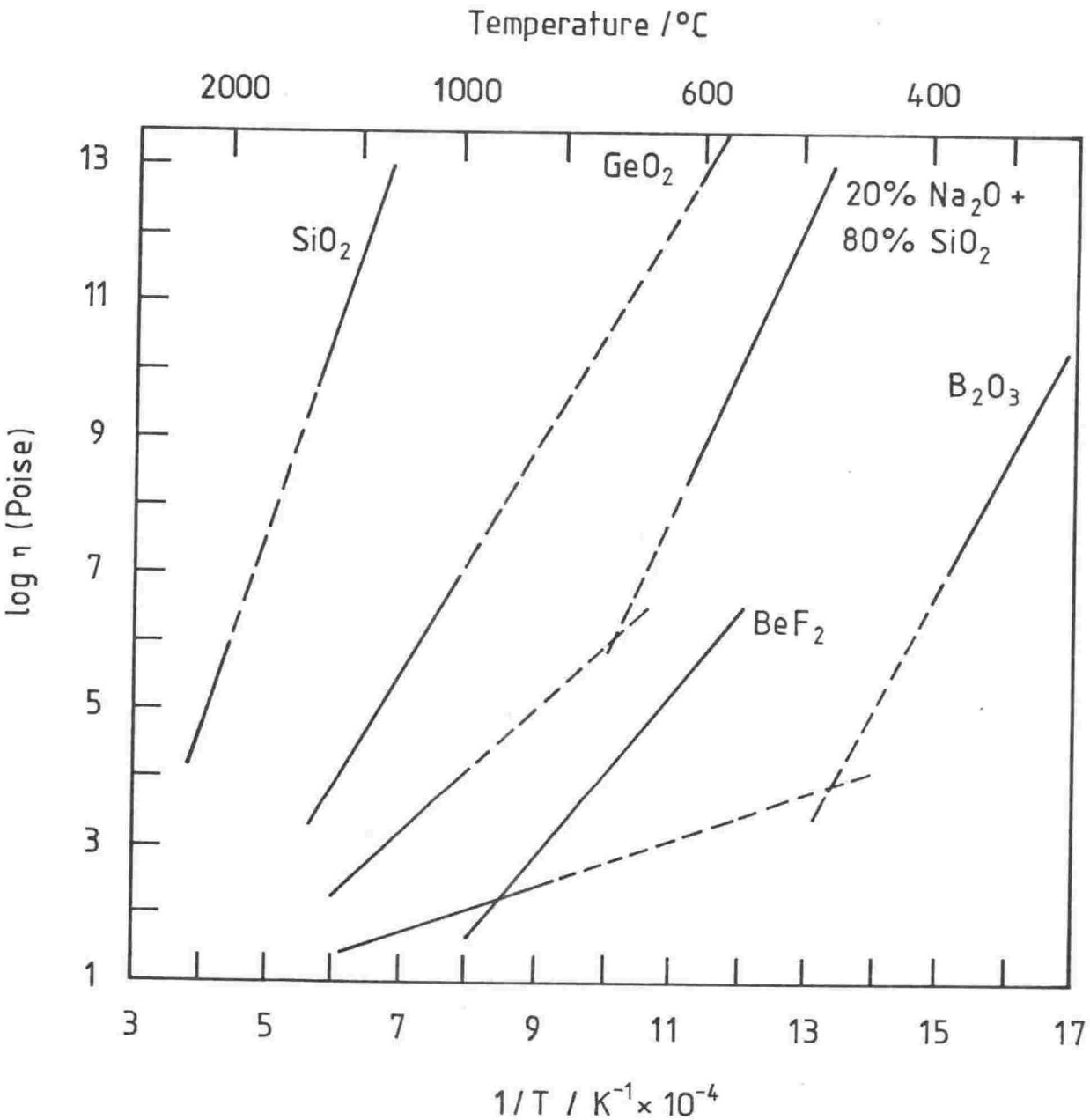

Figure 2.13—Log of viscosity versus reciprocal absolute temperature for several molten oxides and BeF_2. Solid lines are best fit to actual data and dashed lines are extrapolations (93).

There have only been a few studies reported in the literature on the effect of pressure on the transport properties of molten oxides. Sharma et al. (116) have measured the viscosity of GeO_2 as a function of pressure to 10 kbar. They found that viscosity decreases as a function of increasing pressure. This unusual phenomenon has been found in only a few liquids including water and some silicates. In water it has been attributed to hydrogen bonds being broken as pressure increases allowing some smaller entities to flow more readily. In silicates it was initially observed in alumino-silicates and was attributed to coordination changes of aluminium. However it has also been observed in silica rich silicates which do not contain aluminium. In their study on GeO_2, Sharma et al. (116), could find no evidence for coordination changes from Raman spectra of the quenched melt. They attributed the reduction in the viscosity to a weakening of the network structure due to decreases in the Ge-O-Ge and O-Ge-O bond angles with an accompanying increase in the bond length as pressure increases. These authors argued that because of the analogous crystal polymorph structures and transport properties of GeO_2 to SiO_2 the latter might be expected to undergo a similar viscosity decrease as pressure increases. Computer simulation experiments on SiO_2 have confirmed this expectation (15).

Sperry and Mackenzie (117) have measured the viscosity of B_2O_3 as a function of pressure to 300 bar. He observed a slight increase in the viscosity over this pressure range. This may be explained by the more open network structure of B_2O_3 compared to GeO_2. The density of GeO_2 is more than twice that of B_2O_3 at the same temperature. Thus the effect of pressure on B_2O_3 is not to break bonds but to force the entities in the liquid closer together hindering flow.

Mackenzie (118) has also argued that for highly associated liquids the difference between E_p and E_v is negligible. Therefore measurement of transport properties at constant volume are considered unnecessary.

2.2.6 Effect of Metal Oxides and Volatile Components on the Transport Properties of Liquid Silica

2.2.6.1 Binary and Ternary Silicates

Electrical Conductivity

Prior to the work by Bockris et al. (91), (119), (120), (122) in the late 1940's and early 1950's, the study of molten silicates was largely technological and ad hoc in character and consisted mainly of measurements of complex systems. It was generally thought that molten silicates and slags consisted of undissolved oxides (123) and silicate 'compounds' in solution. An exception to this view is found in a paper published in 1892 by Barus and Iddings (124). They concluded from a study on the conductivity of molten and partially molten rocks that molten magmas are largely dissociated into ions. However, the work of Bockris and co-workers on conductivity and electrochemical studies of simple binary silicate systems established the ionic nature of these liquids and that the small metal cations are the principal charge carriers. Subsequent to this work by Bockris and co-workers there has only been one other study, by Tickle (94), of a systematic nature on the conductivity of simple silicate liquids.

Bockris et al. (91), (119) measured the electrical conductance up to 1800°C covering the binary systems Li_2O-SiO_2 (33-57 mol% Li_2O), Na_2O-SiO_2 (20-34 mol% Na_2O), K_2O-SiO_2 (17-34 mol% K_2O), MgO-SiO_2 (39-55 mol% MgO), CaO-SiO_2 (27-60 mol% CaO), SrO-SiO_2 (24-58 mol% SrO), BaO-

SiO_2 (21-54 mol% BaO), MnO-SiO_2 (35-77 mol% MnO), Al_2O_3-SiO_2 (1-7 mol% Al_2O_3) and TiO_2-SiO_2 (8 mol% TiO_2). The composition limits were imposed by the volatility of the metal oxides, by their immiscibility, and by inadequate refractory materials at these high temperatures. All the conductivity results, over approximately a 500°C temperature range, were found to obey an Arrhenius equation. However, Tickle (94), who measured the resistivity of the binary alkali oxide silicates and some mixed alkali oxide silicates, from 400 to 1400°C, found that over this temperature interval an Arrhenius plot showed marked curvature (Figure 2.14). At the higher temperatures the line was approximately straight, as found by Bockris, but as T_g is approached there is substantial deviation from linearity.

Bockris et al. interpreted their data in terms of activation theory and a discrete ion model, discussed in sections 2.2.4.1 and 2.4.2.1 respectively. Metal cations are divided into three categories: (1) Network formers, (2) Network breakers and (3) Intermediate between (1) and (2). Cations with a high ion-oxygen attraction, for example: Si^{4+}, Al^{4+} and Ti^{4+}, will tend to bind strongly to oxygen atoms to form a three-dimensional network structure. Cations, such as the alkali cations, with a low ion-oxygen attraction do not build into the network but rather the reverse; breaking it into small ionic entities. These cations are regarded as network breaders. Intermediate cations, such as Fe^{2+} and Mg^{2+}, display a trend in their properties towards network forming as evidenced by relatively high ΔG^* and ΔH^* values compared with other divalent cations in spite of increasing the conductivity of silica.

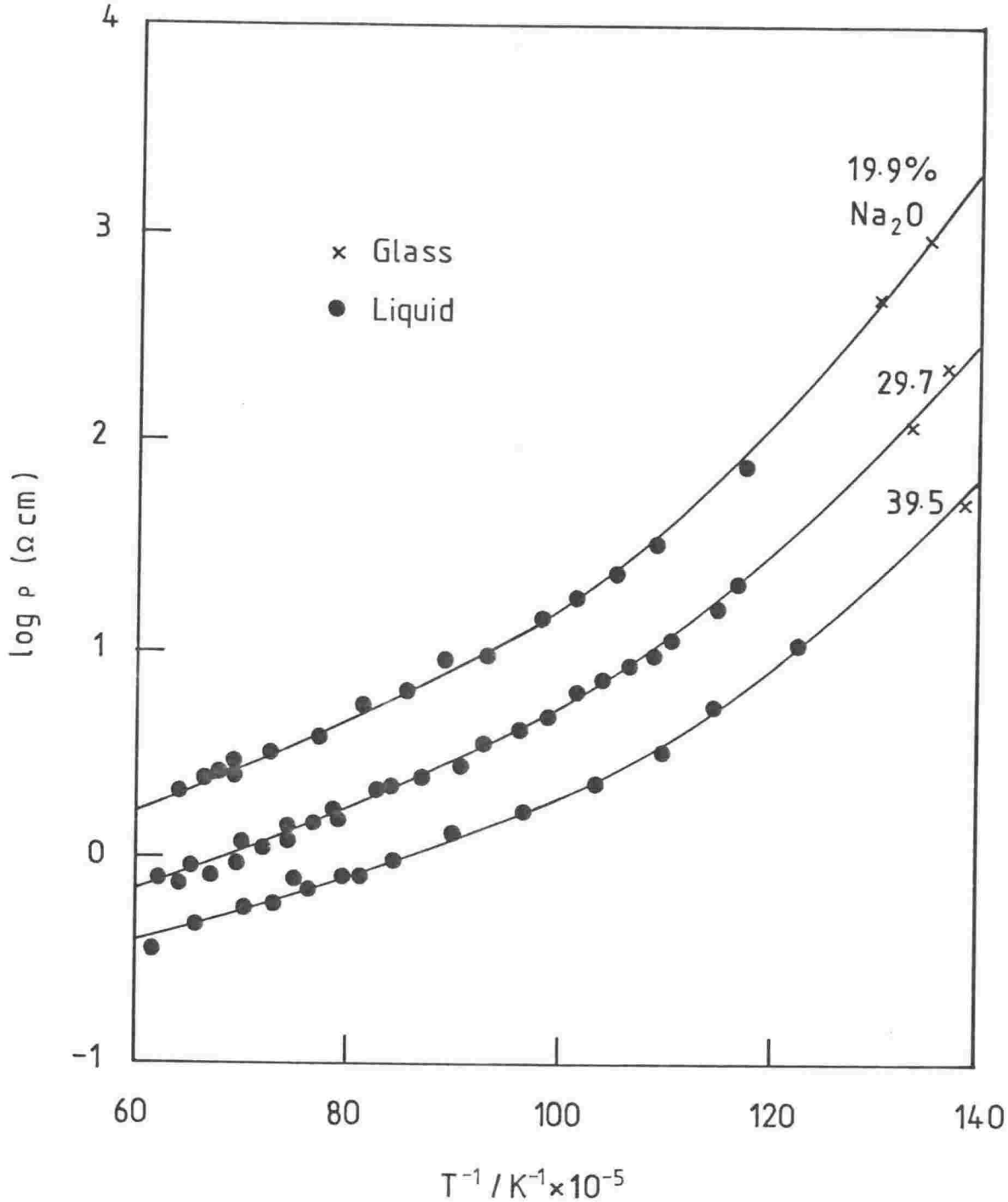

Figure 2.14—Log resistivity versus reciprocal absolute temperature for three compositions in the SiO_2 - Na_2O system over the temperature range 450-1400°C (94).

Activation energies are shown in Figure 2.15. A marked difference is observed between binary systems containing alkali oxides and alkaline earth oxides, although within each group activation energy is almost independent of cation species. $E_{a,\kappa}$'s for Group I oxide silicates are independent of composition whereas in Group II increasing concentration of metal oxide results in a rapid decrease in the activation energy. PbO falls close to the Group II line but TiO_2 and Al_2O_3 occupy quite different positions again. These observations suggest that cation charge plays an important part in the conduction mechanism. Bockris et al. (91), (119) attempted to give an explanation of this variation by assuming that the addition of a metal oxide to silica results in the breakdown of the 3-dimensional network to give different ions and then correlating the free energy of activation for conduction, ΔG^*, with a function of the electrical interaction in the melt, I, the ion-oxygen attraction. ΔG^* is dervied from applying absolute reaction rate theory to the conduction process and is given by equation (2.43). The relationship between ΔG^* and I is shown in Figure 2.16. For the ions of Group I ΔG^* decreases steadily as the ionic radius decreases. Thus it is probable that steric effects predominate. Group II oxides and other metals fall on a line with a minimum at I = ~0.9 for Fe^{2+}. Thereafter an anomalous increase in ΔG^* occurs, possibly indicating an increasing difficulty of cation movement. It is likely that this is due to the multivalent cations Al^{3+} and Ti^{4+} competing with Si^{4+} ions for oxygen in the lattice to form, for instance TiO_4^{4-} thus leaving fewer ions to carry the charge.

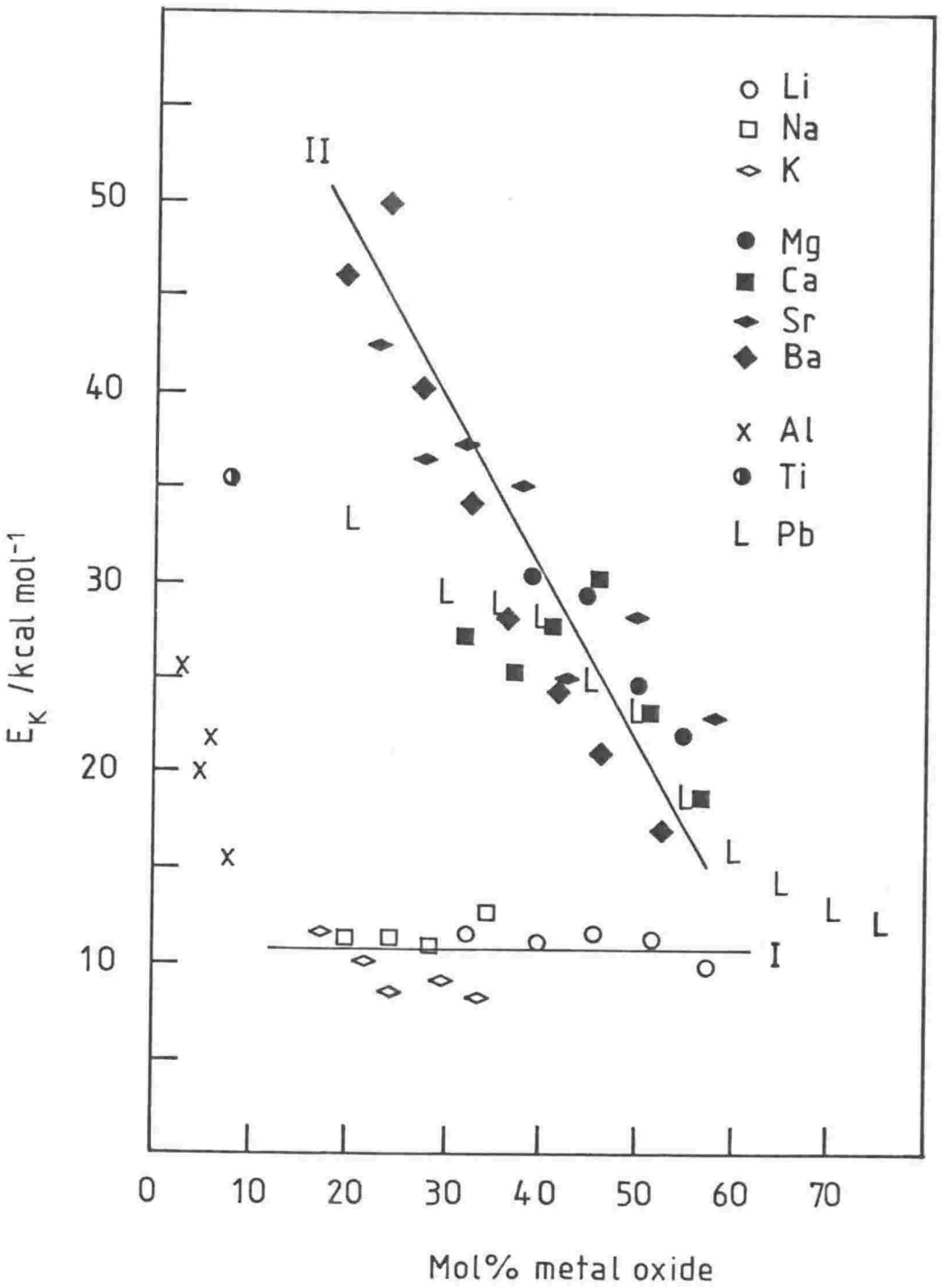

Figure 2.15— Activation energy for electrical conduction in molten binary silicates as a function of metal oxide composition (125).

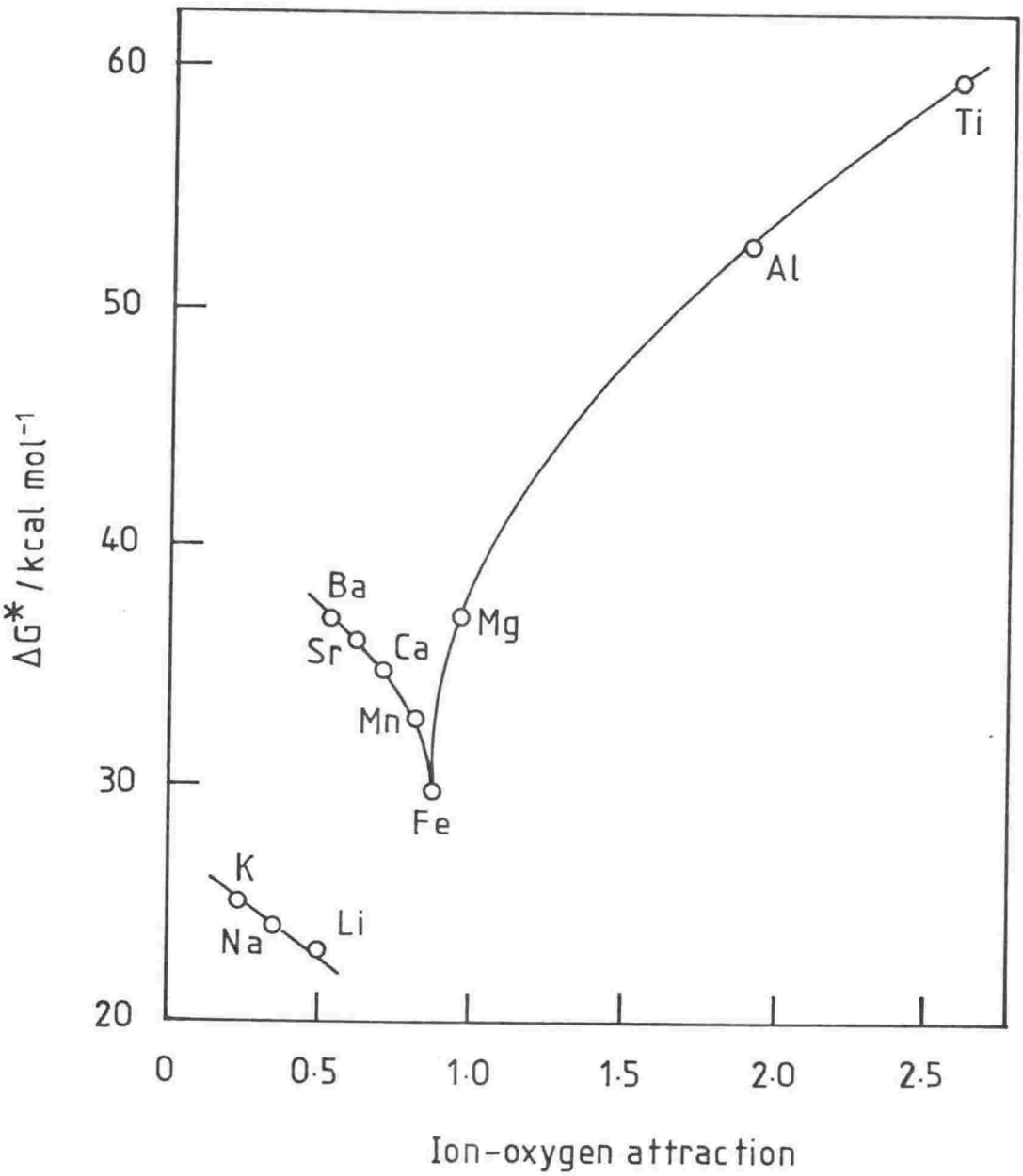

Figure 2.16—Free energy of activation versus ion-oxygen attraction (126).

Molar conductivity is found (91) to increase by ~5 orders of magnitude on the addition of small concentrations of alkali or alkaline earth metal oxides. Similar behaviour is observed for both MnO and PbO silicate systems. However, the conductivity isotherms of Al_2O_3-SiO_2 melts, in contrast to the above melts, undergo an initial increase in conductivity to about 5 mol% Al_2O_3 followed by a decrease and levelling off as further alumina is added.

In the binary alkali silicates it is found that the molar conductance decreases in the order $Li_2O > Na_2O > K_2O$ but below about 22 mol% M_2O the order of Li_2O and Na_2O is reversed. In the alkaline earth metal oxides the order is MgO > CaO > SrO > BaO. The conductivities of these systems fall into the following order: Group I > Group II, including MnO and FeO > Al_2O_3 and TiO_2

The addition of a second different alkali oxide to an existing binary oxide produces an interesting effect known as the mixed alkali effect (94) (Figure 2.17). While maintaining the mole fraction of SiO_2 constant and progressively replacing one alkali metal oxide with another the conductivity passes through a minimum. The minimum occurs for a $30(R'_2O + R''_2O).70SiO_2$ at about 15 mol% R'_2O (Figure 2.17). Doremus (127) has found an identical phenomenon for the same system in the vitreous state at 250°C. Bockris et al. (91) found, however, that for the system CaO-MnO-SiO_2 there was a smooth transition in κ, E_κ, ΔH^*, ΔG^* and ΔS^* on replacing Ca^{2+} progressively with Mn^{2+}.

An important study of the electrolysis of binary silicates has been carried out to determine the applicability of Faraday's laws (120), (121). The amounts of oxygen liberated at the anode or metal deposited

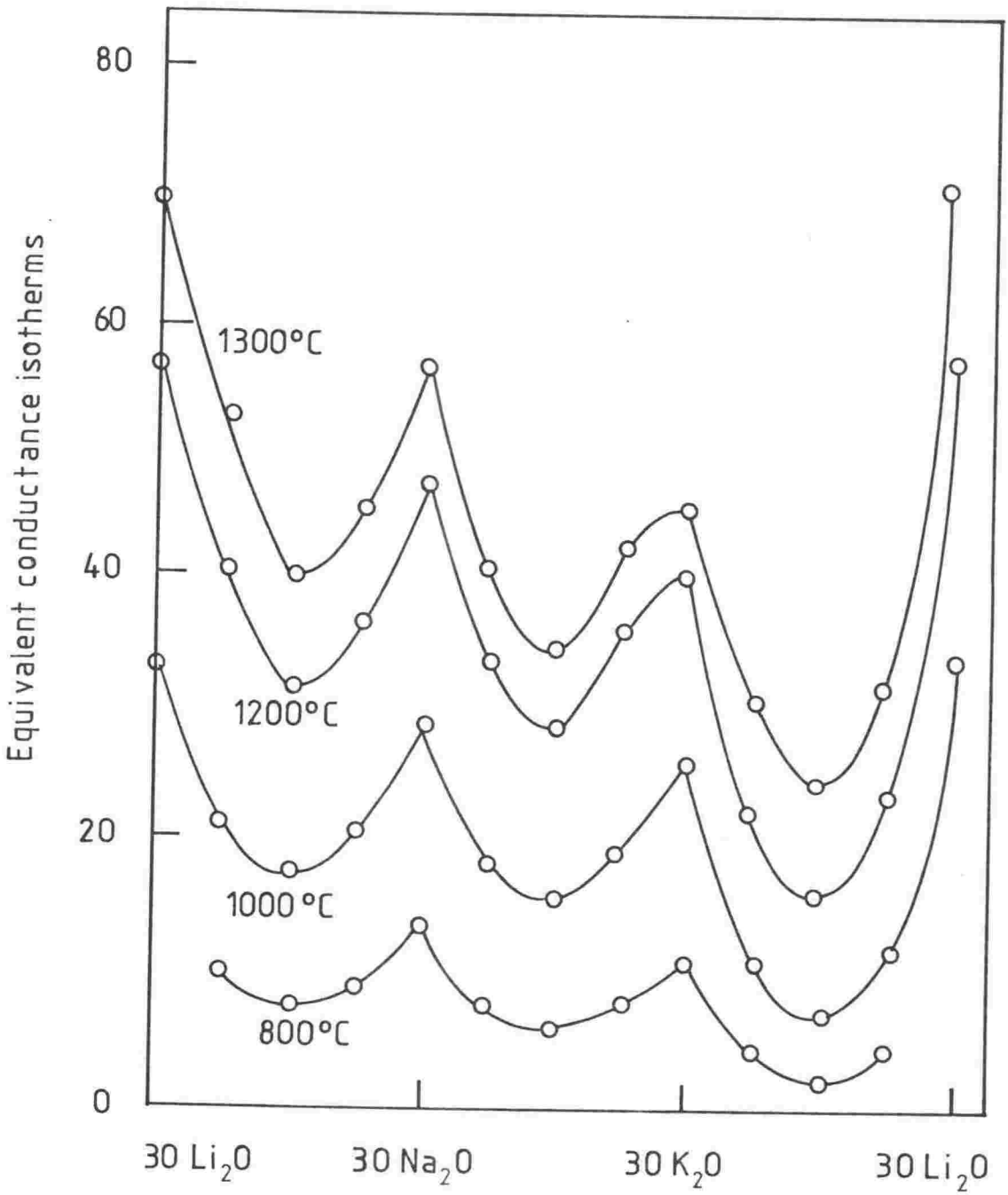

Figure 2.17—Equivalent conductance isotherms for the three mixed alkali oxide-silica systems (94).

at the cathode, have confirmed that for most binary silicates conduction is exclusively ionic. Further, studies of transport numbers (121) have shown that for K_2O-SiO_2 (22-34 mol% K_2O), Li_2O-SiO_2 (47 mol% Li_2O), and FeO-SiO_2 and CoO-SiO_2 containing 66 and 71.5 mol% metal oxide respectively, conductance is entirely cationic. Radiotracer determination by Esin and Kir'yanov (128) of the migration of Ca^{2+} in CaO-Al_2O_3-SiO_2 give transport numbers near unity. Simnad et al. (129) obtained unity for Fe^{2+} in 57 mol% FeO-SiO_2. This was confirmed by Baak (130) who used a moving boundary method.

Reliable studies on the quantitative effect of pressure in molten binary and ternary systems do not exist.

Viscosity

The addition of metal oxides to molten silica cause substantial reductions in viscosity (Figure 2.18). The first 20 mol% of metal oxide causes the largest reduction and further metal oxide produces relatively small reductions. The magnitude of the viscosity depends on the particular oxide. Bockris et al. (4), (92) found that at the same composition and temperature Li_2O reduces the viscosity more than Na_2O followed by K_2O. A similar trend, however, is not observed in the alkaline earth oxides when added to silica. They all lie very close together without any specific pattern, as Group II oxides are descended in the periodic table. Alumina behaves similarly to alkali oxides in reducing the viscosity of silica.

Bockris et al. (4) interpreted these results in terms of network formers and breakers and the transition state theory.

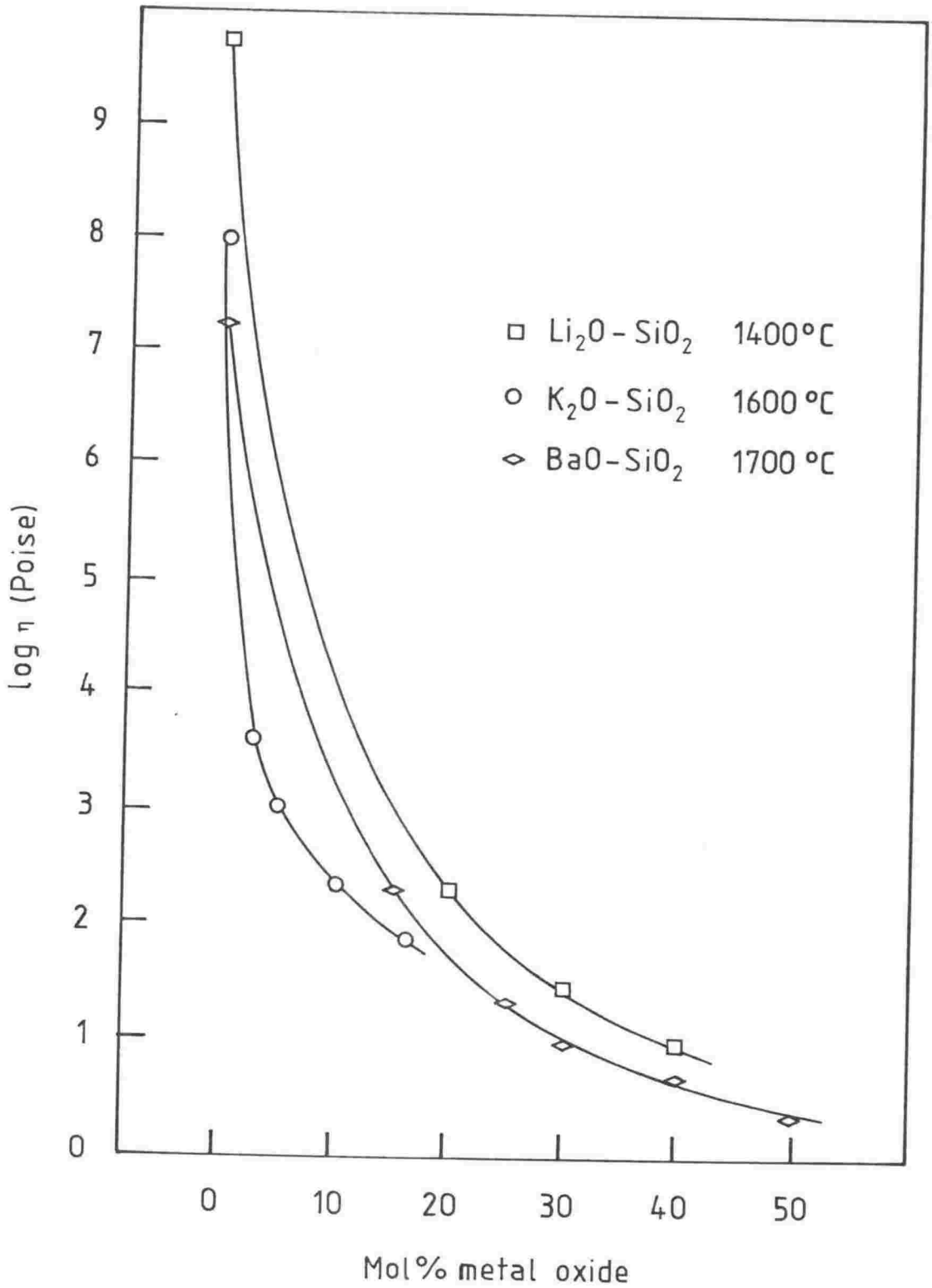

Figure 2.18—Effects of metal oxides on the viscosity of silica (24).

Activation energies of viscosity for the alkali and alkaline earth binary silicates have been found to fall on two different lines as a function of increasing mole fraction of metal oxide. $E_{a,\kappa}$(alkaline earth) > $E_{a,\kappa}$(alkali). Within each group activation energy is independent of the cations until relatively high mole fractions of metal oxide are reached. In Group II this holds till about 55 mol% MO; whereas for Group I, beyond ~40 mol% M_2O there is a sharp decrease in activation energy particularly for SiO_2/Na_2O melts (Figure 2.19). Since activation energies for Groups I and II fall on two distinct lines, led Mackenzie (131) to propose that the partial substitution of one alkali oxide for another would not effect the viscosity or activation energy greatly. The same observation would also be true for Group II silicates. He found (131) that the ternary systems still obeyed the Arrhenius law over the temperature range investigated (900 to 1400°C) and that the viscosities and activation energies did fall close to what he predicted. However, replacement in part of one alkali with another while maintaining constant SiO_2 reduces the viscosity slightly and replacement in part of one alkali oxide with an alkaline earth oxide, maintaining constant SiO_2, increases the viscosity. It appears then that the ternary systems containing combinations of alkali or alkaline earth metal oxides behave like the binary alkali or alkaline earth silicates, respectively.

Riebling (32) found that for a ternary soda-alumina-silica melt if the mole fraction of silica was held constant and soda was replaced by alumina, then the viscosity passes through a maximum. This maximum in viscosity is interpreted in terms of a dual role of aluminium in the silicate network. The addition of alumina to silica rapidly reduces the

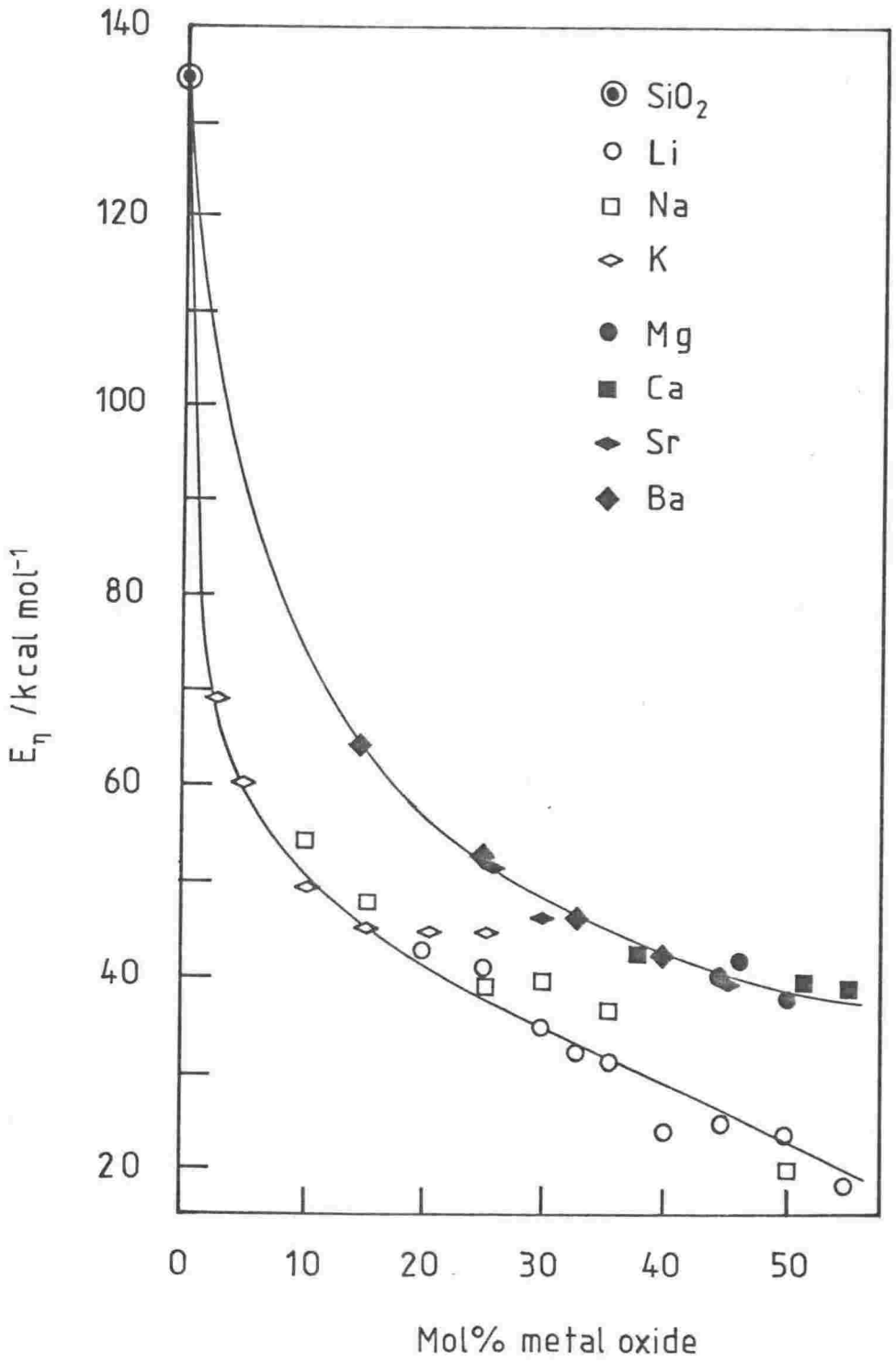

Figure 2.19—Energy of activation for viscous flow in binary liquid silicates (125).

viscosity (114). Al^{3+} apparently acts as a network modifier in this situation and is predominantly in six-fold coordination with oxygen. However, the addition of monovalent or divalent cations allows Al^{3+} to enter the tetrahedral sites while preserving charge balance:

$$-O-Si(-O-)(-O-)-Si-O- + MAlO_2 \longrightarrow -O-Si(-O-)(-O-)-Al(-O-)(-M^+)-O-Si-O-$$

In this situation aluminium acts as a network former, polymerising the melt and thus increasing the viscosity. Maxima in isotherms have been observed for melts containing Na_2O, CaO, MgO with Al_2O_3 (32), (132), (33).

It has been found that the effect of pressure on some silicates reduces the viscosity. This effect was first predicted by Waff (133) for alumino-silicates and subsequently observed for those silicates and for other silicates not containing aluminium (Figure 2.20). Silicates with a high concentration of SiO_2 tend to show a decrease in viscosity, although at a sufficiently high pressure it would be expected that viscosity would begin to increase monotonically with increasing pressure. For melts containing a high concentration of network modifiers the viscosity increases as pressure increases. It may also be expected that for a melt of intermediate composition viscosity may be independent of pressure at low pressures (Figure 2.20). This is discussed further in section 2.2.6.2.

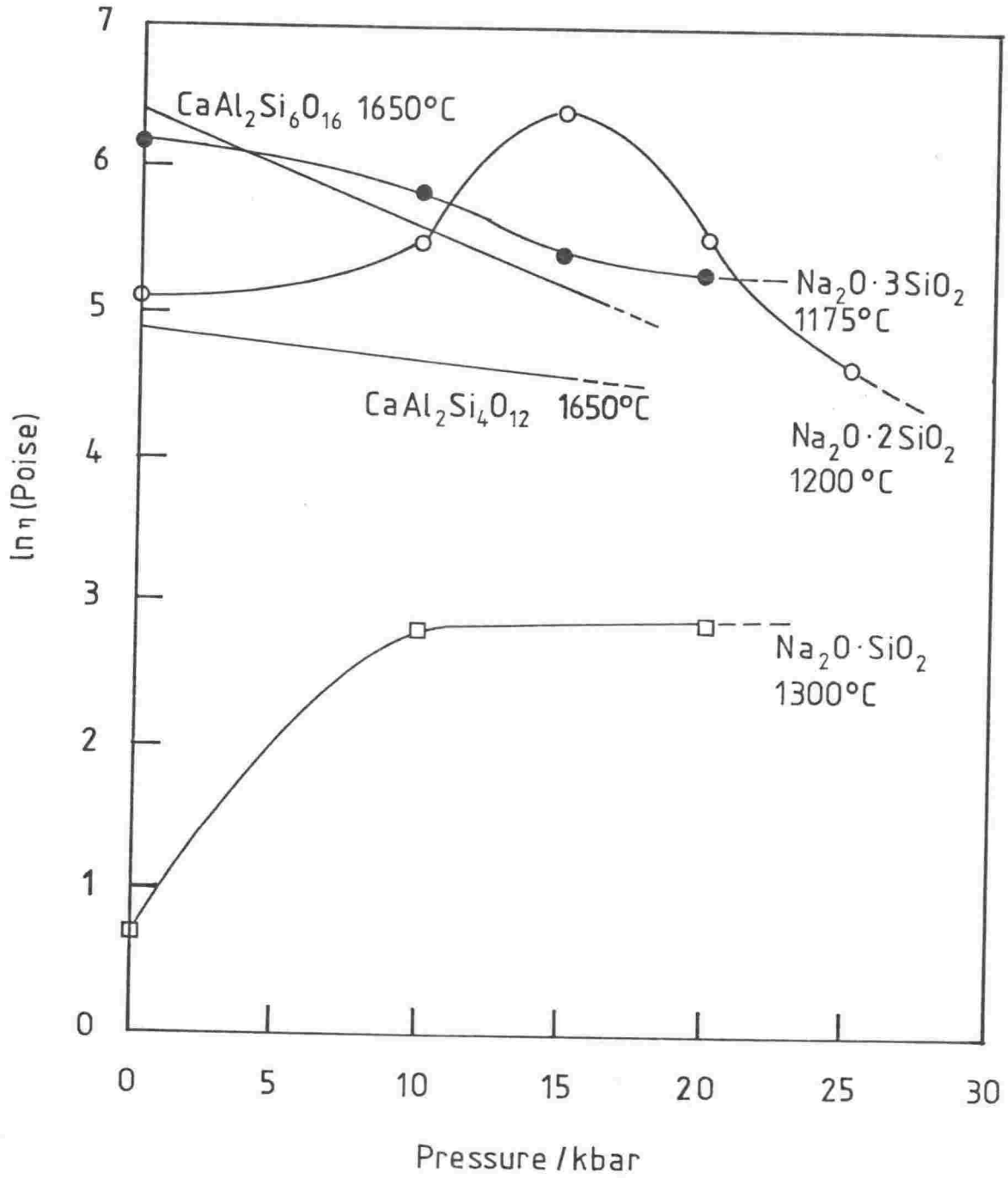

Figure 2.20—Pressure dependence of viscosity for several silicate melts (134).

Diffusion

There have been very few studies of diffusion in binary or ternary silicates. The ternary system $CaO-Al_2O_3-SiO_2$ appears to be the most widely studied (96). Figure 2.21 shows tracer diffusion in this melt for oxygen, calcium, aluminium and silicon species. All these species were found to obey an Arrhenius law with oxygen having the highest diffusion coefficient followed by Ca, Al and Si in that order. Henderson et al. (135) and Henderson (136) have given a qualitative explanation for the diffusion of Ca, Al and Si in terms of the dominant size of anionic complexes formed by these cations. However, they were unable to explain the high diffusivity of oxygen. The activation energy of diffusion for the above species fall in the range 290 +/- 80 $kcalmol^{-1}$, whereas the activation energy for conduction in this melt is only 125 +/- 40 $kcalmol^{-1}$ which seems to indicate a different process is involved in the transport of Ca in electrical conduction compared to diffusion.

Langanke and Schmalzried (137) have measured tracer diffusion in $PbO-SiO_2$ melts with $0.1 \leqslant X_{silica} \leqslant 0.6$. They developed theoretical relations using irreversible thermodynamics that relate tracer diffusion and interdiffusion for quasibinary silicate melts. Several diffusion experiments were performed on this melt at the metasilicate composition as a function of temperature between 850 and 1000°C. They found activation energy of diffusion to be 118 $kJmol^{-1}$, which in contradistinction to the above ternary melt just discussed, is very close to the activation energy for conduction.

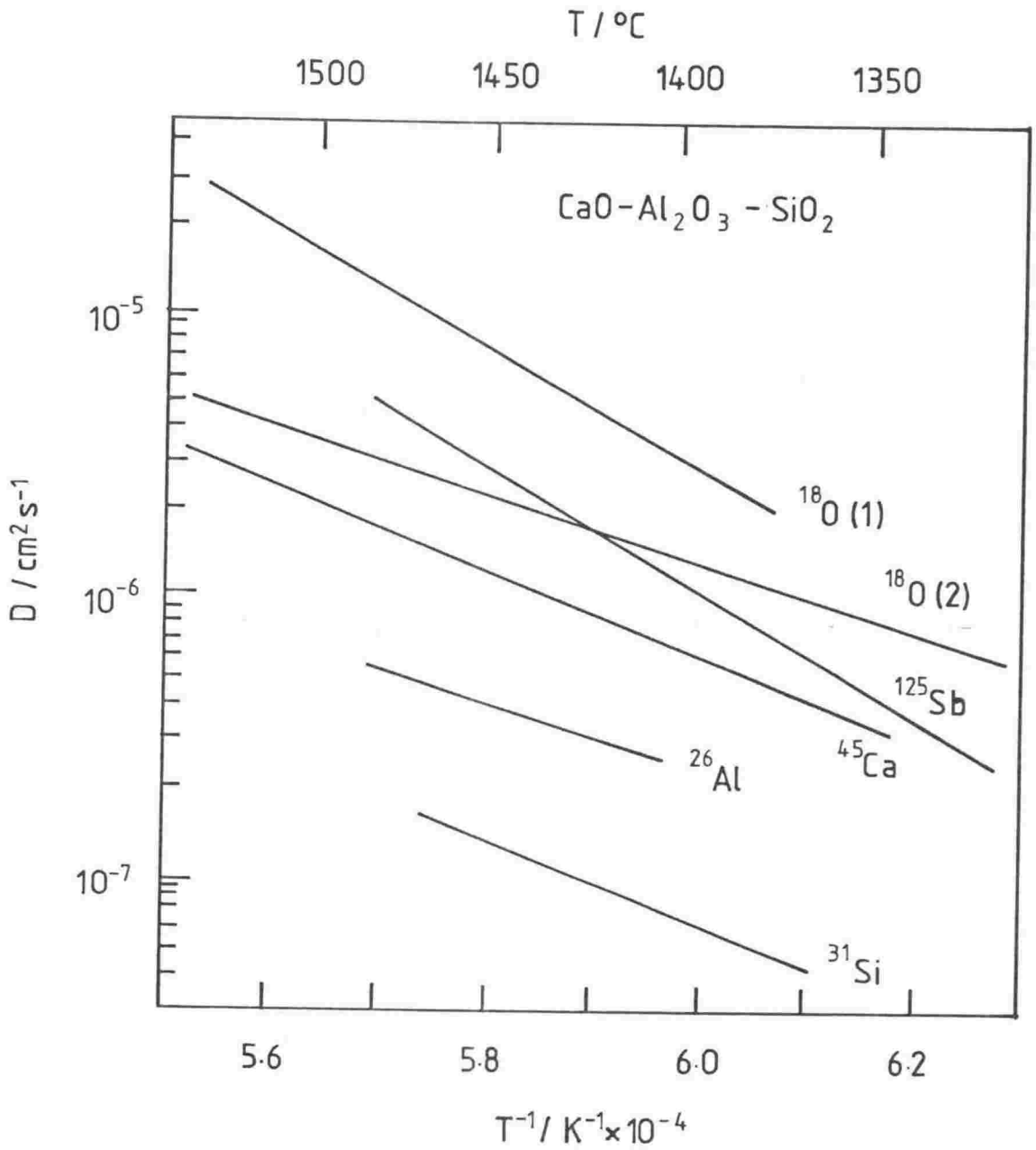

Figure 2.21 — Tracer diffusion of various species in the system $CaO - Al_2O_3 - SiO_2$ (96).

2.2.6.2 Multicomponent and Naturally Occurring Silicates

Electrical Conductivity

The conductivity of silicate minerals has been summarised by Waff (138), Smedley (95) and briefly by Shankland (139). Interest in the conductivity of molten silicate minerals has arisen because geomagnetic depth sounding experiments on the earth's crust and upper mantle have suggested that there is an anomalous region of high conductivity in the asthenosphere (140). There are three studies on these materials which examine the liquid state. The remaining studies carried out on silicate minerals examine conductivity changes during melting phenomena.

Waff and Weill (141), studied the effect of temperature, oxygen fugacity, and composition on the conductance of ten diverse silicate melts, see Table 2.6 for their compositions. They found that conductivity increased with increasing temperature for all silicates and that for HA, HA(2N) and HA(3N) compositions, log κ versus 1/T was linear, whereas the remaining compositions showed marked curvature. They found that for melts with a small $\Sigma M^{2+}/\Sigma M^{+}$ ratio Arrhenius temperature dependence was obeyed while for a relatively large $\Sigma M^{2+}/\Sigma M^{+}$ ratio Arrhenius behaviour was not followed. Activation energies decreased steadily as temperature increased. For those melts with a large $\Sigma M^{2+}/\Sigma M^{+}$ ratio they proposed that conduction is principally via movement of M^{2+} cations. Due to their high charge/radius ratio the divalent cations polarise the oxygens of the surrounding polymerised units to a greater degree than M^{+} cations. The mobility of M^{2+} cations surrounded by oxygen will be dependent on the degree of polymerisation in the melt which in turn is temperature dependent. Monovalent cations,

TABLE 2.6

Electron microprobe analyses (wt.%) of glasses studied by Waff and Weill

Oxide	70-15	PG16	BCR2	V-31	HA	HA(2N)	HA(3N)	HA(3F)	HA(6F)	HA(10F)
SiO_2	47.1	47.5	53.9	61.8	57.9	57.6	57.0	57.1	55.4	53.4
TiO_2	3.03	1.54	2.58	0.79	0.63	0.63	0.62	0.62	0.60	0.58
Al_2O_3	15.2	15.1	13.3	14.2	19.0	18.9	18.6	18.7	18.2	17.5
FeO	12.2	14.6	13.3	9.1	4.99	4.96	4.90	7.83	10.4	13.7
MnO	0.21	0.13	0.02	0.15	0.09	0.09	0.09	0.09	0.09	0.08
MgO	7.58	6.91	3.57	0.38	3.10	3.08	3.05	3.05	2.97	2.86
CaO	9.5	9.8	7.5	3.50	7.7	7.6	7.5	7.5	7.33	7.06
Na_2O	2.59	2.95	3.44	4.62	4.15	6.18	7.18	4.09	3.97	3.83
K_2O	0.74	0.60	1.74	4.46	1.06	1.05	1.04	1.04	1.01	0.98

70-15 and PG16 - Tholeiite basalt.

BCR2 - Alkali olivine basalt.

V-31 - Latite.

HA - Andesite.

Compositions HA(2N), HS(3N), HA(3F), HA(6F) and HA(10F) correspond to base composition HA with additions of 2.1% Na_2O, 3.2% Na_2O, 3.0% FeO and 10 % FeO respectively. Total Fe is arbitrarily given as FeO.

Table from reference (141).

however, polarise neighbouring oxygen ions to a lesser degree and are less dependent on the silicate anion structure and thus on temperature. A more general way to account (95) for the differences between Arrhenius and non-Arrhenius behaviour is by observing that melts rich in M^{2+} cations have higher T_g values than alkali rich melts. Non-Arrhenian behaviour is found for melts as they approach T_g and their temperature dependence is best explained in terms of a theory that is based on a cooperative mechanism such as the configurational entropy theory. The melts low in M^{2+} are probably well above T_g at the temperature at which this study was carried out and would be expected to show Arrhenian behaviour.

Waff and Weill found that electrical conductivity was essentially independent of oxygen fugacity and hence the ratio of Fe^{2+}/Fe^{3+}. The effect of compositional variations within the magmatic range account for much less than an order of magnitude variation in electrical conductivity at a fixed temperature. This contrasts with an increase of 2 orders of magnitude, for most magmas, on melting. Thus conductivity differences between liquids of magmatic compositional extremes will always be much less than those between solid and liquid. Under mantle conditions it is postulated that the bulk conductivity will arise predominantly from the liquid fraction in a partially molten magma.

Rai and Manghnani (142) measured the electrical conductivities of 6 ultramafic melts to 1820 K under known oxygen fugacity conditions. They found that above ~1350 K there are two regions of Arrhenius behaviour as a function of increasing temperature. The temperature at which the change in slope of log conductivity versus 1/T occurs, appears to depend

on composition and is possibly related to partial melting. They observed that the conductivity of basalts ($\sim 10^{-1}$ Scm^{-1}) is higher than ultramafic magmas ($\sim 10^{-3}$ Scm^{-1}) which in turn are higher than olivines ($\sim 10^{-4}$ Scm^{-1}). Although at temperatures greater than 1550 K the conductivities of basalts and ultramafic melts overlap.

Murase and McBirney (44) measured the electrical conductivity of 6 silicate systems covering the range 62 to 87 wt% total X, where $X = (SiO_2 + Al_2O_3 + TiO_2)$ wt% . At 1500°C the conductivity increases as X decreases. Activation energies were constant with temperature for only the systems with low X and showed most variation for the systems with high X. The latter silicates are much closer to T_g where it is normal for non-Arrhenius behaviour to be observed.

Measurements of the effect of pressure on conductivity of natural silicate melts are not consistent. The measurements made prior to 1980 have been summarised by Waff (138). Khitarov et al. (143), reported a limited amount of data on basaltic melts indicating that conductivity decreases by a factor of 2 between 2.4 and 27 kbar. Watanabe (144), however, found that the conductivity of an olivine basalt increases by a factor of 3 between 0 and 24 kbar. Waff (138), also found a drop in conductivity, of about 20%, in a basaltic liquid between pressures of 0 and 55 kbar. More recently, Tyburczy and Waff (145), measured the conductivity of basalt and andesite melts to 25 kbar and found that the conductivity decreases as pressure increases to about 10 kbar and thereafter it decreases at a slower rate to 25 kbar. The overall reduction in both melts is approximately 80% in this pressure range. Similar trends have been observed for molten $NaNO_3$ (146). No

explanation for the change in the pressure coefficient of conductivity in molten $NaNO_3$ has been given although Tyburczy and Waff (145) argued that in the case of the silicate melts they examined, structural alterations in the melt at 8-10 kbar are responsible for the abrupt change in pressure coefficient.

Viscosity

The extension from binary to ternary silicates has shown the dual role Al^{3+} may have as a network former or breaker depending on the presence or absence of alkali or alkaline earth metal oxides. In a study by Turkdogan and Bills (147), which draws on the work by Bockris et al. (119) on binary $CaO-SiO_2$, Kozakevitch (148), (149) on ternary $CaO-Al_2O_3-SiO_2$ and Machin (150), (151) on quaternary $CaO-MgO-Al_2O_3-SiO_2$ melts, they show the silica equivalence of alumina, at least for low Al_2O_3/CaO ratios, and that CaO and MgO are viscometrically equivalent in the quaternary melt. For a given temperature and viscosity, the silica equivalence of alumina (N_a) is given by the difference between the silica concentrations of the binary and ternary melts, i.e.:

$$N_a = N_{silica}(binary) - N_{silica}(ternary) \qquad (2.49)$$

It was found that, although the effects of alumina and silica on the viscosities of slags are similar, the total acid concentration cannot be represented by the sum of the molar concentrations of silica and alumina. N_a was found to vary with the Al_2O_3/CaO ratio and alumina concentration. CaO and MgO are found to have, on a molar basis, the same effect on the viscosity. Therefore for a given temperature, a viscosity-composition relationship can be shown by a curve for the quaternary

melts $CaO-MgO-Al_2O_3-SiO_2$ by plotting viscosity against $N_{silica} + N_a$. This simple relationship applies over a very wide composition range. In a further study, Bills (152) has shown that the simple empirical relationship between viscosity and the silica equivalence in the $CaO-MgO-Al_2O_3-SiO_2$ system no longer holds when these melts contain CaF_2. This is due to the decreased electrostatic bonding between the large silicate anions normally brought about by the presence of divalent calcium and magnesium ions. However, FeO and BaO, at least up to 10 wt% behave on a molar basis similarly to MgO. At larger concentrations of FeO the difference between Fe^{2+} and Mg^{2+} becomes apparent, the lower attraction of the ferrous ion for the silicate anions leads to lower viscosities than expected from a comparison with melts containing no ferrous oxide.

The study of the viscosity of naturally occuring lavas has shown (Shaw (153), (154), Murase (155)) that the melts are Newtonian above the liquidus temperature. Below the liquidus temperature a mixture of nonvesicular basalt liquid and up to 20% of crystals by volume is still found to behave as a Newtonian liquid, at least for low shear rates. However, with either vesiculation or with increased crystal content the viscosity of the mixture behaves like a Bingham plastic fluid (142).

The effect of pressure on melt viscosity has proved very interesting and has been particluarly important in modelling magma movement in the earth's crust and upper mantle. Considerable impetus has been given to the study of the pressure dependence of viscosity subsequent to the prediction by Waff (133) that Al^{3+} may undergo a coordination change from 4- to 6-fold thus changing from a network former to a network

breaker with a concomitant reduction in viscosity. In the cases of tholeiite and andesite melts, Waff predicted decreases in viscosity by factors of 14 and 47 respectively arising from the Al^{3+} coordination change. Later work (156), (157), (158) has shown that a decrease does take place, although it is not yet clear whether it is the result of coordination changes or not. Melts without aluminium have also been found to undergo viscosity decreases as pressure increases. Further, there does not appear to be any spectroscopic evidence supporting coordination changes in aluminium. Melts which are highly polymerised appear to exhibit viscosity reductions; whereas depolymerised melts show an initial reduction followed by an increase in viscosity with increasing pressure. Viscosity decreases with increasing pressure have been found in andesites, tholeiites, basalts and synthetic melts rich in silica. It has been proposed (116) that changes in bond angles and lengths take place under pressure and may be responsible for a rearrangement in the structure giving entities that flow more readily. The methods of determining viscosity under pressure are at present not very accurate nor reliable and thus there must be some caution in interpreting these results. However, recent computer simulation experiments on liquid silicates to high temperatures and pressures by Angell et al. (15), (159), (160) have confirmed the viscosity reductions as a function of increasing pressure.

Empirical equations have been derived to calculate the viscosity of a lava, based on the contribution of each component to the viscosity, see for example the work by Carron (161), Bottinga and Weill (162) and Shaw (163).

Diffusion

Diffusion is frequently the rate controlling process for many chemical and physical processes. In the case of igneous processes, for example, the growth of crystals is accomplished largely by the diffusion of material to crystalline nucleii (164) and it is important in trace element partitioning (165). Recent experimental work on diffusion has been critically reviewed by Hofman (96) and also briefly by Shankland (166), both of whom concluded that there is still much experimental work to be done to elucidate the diffusion mechanism and the relation of the diffusion mechanism to melt structure. The principal findings are that the Arrhenius law is almost universally obeyed over the temperature and pressure ranges which have been covered and there is a strong correlation betweeen D and ionic size and charge.

There are three papers that will be considered in this context, two (167), (168) subsequent to the above reviews and one just prior (169). Watson (169) investigated the diffusion of calcium, using tracer diffusion of ^{45}Ca, in an alumino-silicate melt ($Na_2O/CaO/Al_2O_3/SiO_2$ 29/5/10/56 mol%) at temperatures in the range 1100 to 1400°C and pressure to 30 kbar. Calcium diffusion was found to depend on both temperature and pressure. Arrhenius equations for temperature and pressure dependence of diffusion describe the behaviour for 1 and 10 kbar isobars but there is deviation for the isobar at 20 kbar. The temperature dependence is enhanced by increases in pressure. The pressure dependence is relatively minor at high temperatures but becomes more dependent at low temperatures.

In a later paper, Watson (167), measured the diffusion of Cs in the same alumino-silicate as above. The diffusivity of Cs is reduced by approximately an order of magnitude as pressure is increased from 1 to 30 kbar at constant temperature for three temperatures examined: 1100, 1200 and 1300°C.

Jambon (168) has measured tracer diffusion of Na, K, Rb, Cs, Sr, Ba, Ce and Eu in granitic melts to 1300°C and 1 bar together with the effect of pressure to 3 kbar on diffusion of Cs in granitic obsidian. Figure 2.22 is an Arrhenius plot for the diffusion of the alkalis in obsidian. The effect of pressure on diffusion up to 3 kbar is found to be minimal. Although there was a 84 kJ/mole difference in activation energy between 0 and 30 kbar the errors involved make this difference uncertain. It would seem from Watson's experiments (169) that pressures of the order of tens of kilobars are required to observe significant variation in the pressure coefficient of diffusion. For small cations such as Na^+ the effect of pressure may be even less significant.

Jambon showed that variations in diffusion coefficient are principally related to the diffusing species (charge, radius, coordination etc) rather than the composition and properties of the medium through which it is moving. This is illustrated in Figure 2.23 which shows Na and Cs diffusion in a number of different media. Although there are some differences in D for different silicate media, D for a particular species always falls within a narrow range in comparison to variations that are observed with increasing temperature or between different species.

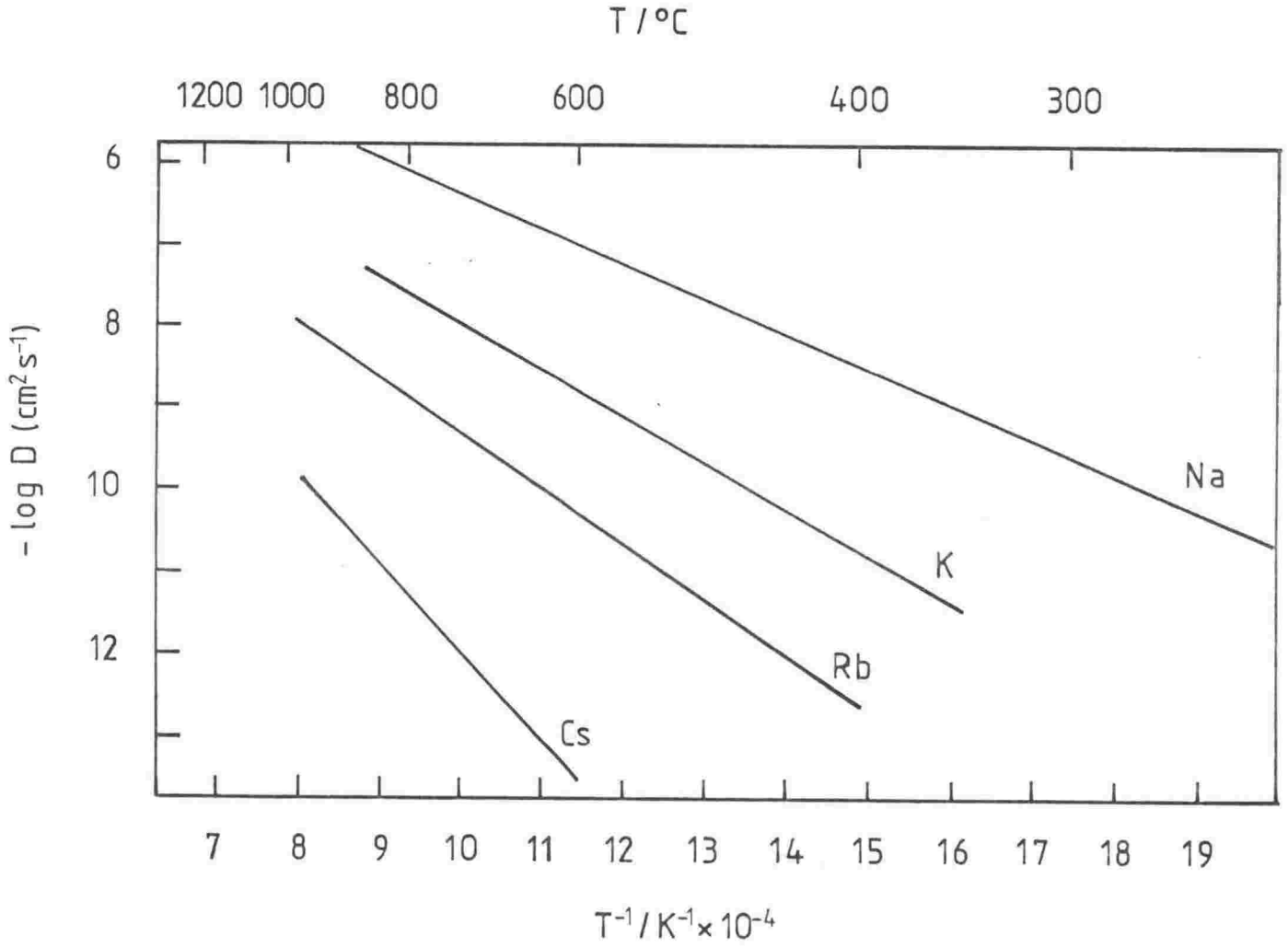

Figure 2.22— Arrhenius plot for the diffusion of the alkalis in obsidian (168).

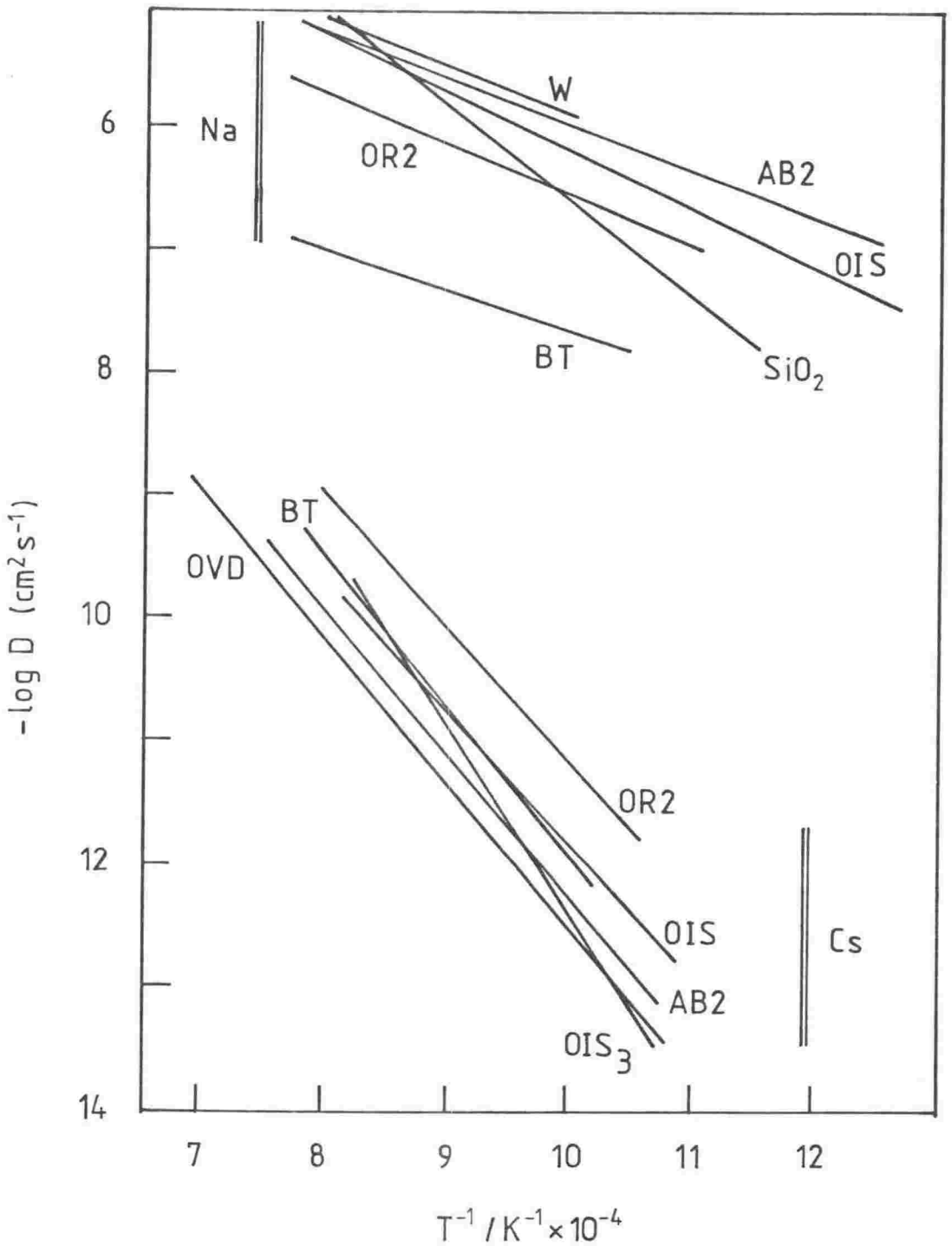

Figure 2.23—Diffusion of Na and Cs in several silicate systems. AB2-, OR2- albite and orthoclase glasses, BT-basaltic glass, W-CaO-Al_2O_3-SiO_2, OIS-granitic obsidian, OIS_3-granitic obsidian at 3kbar, OVD-dehydrated obsidian (168).

Jambon found a strong correlation between activation energy and ionic radius and also between activation energy and cationic charge.

The glass transition apparently does not effect the diffusivity of the species studied. Obsidian glasses behave as supercooled liquids and no distinction can be made between glassy and molten obsidian from diffusion measurements. Thus the diffusion mechanism must be identical for both glasses and melts since no discontinuity occurs at the T_g. Jambon showed that the Stokes-Einstein equation is invalid in these melts. The diffusivities determined in obsidians are far larger than predicted by the Stokes-Einstein equation.

Jambon proposed a model for diffusion in which diffusion arises by movement of a sphere in an elastic medium. This model permits a fair prediction of activation energy of diffusion as a function of cation radius and charge. He derived the following equation for activiation energy:

$$E = 8 + 128(r - 1.34)^2 + 33z^2/(r + 1.34)$$

where E is the activation energy, r is the cationic radius and z cation charge. The terms on the right hand side of the equation arose from making simplifying assumptions about the contributing energy terms to the activation energy:

$$E = E_s + E_c + E_r + E_p + E_v \qquad (2.50)$$

where E_s is the shear energy corresponding to the elastic repulsion of the neighbours upon jumping to the next stable position. E_c is the Coulombic energy, E_r, E_p, E_v are the repulsive, polarisation and van der

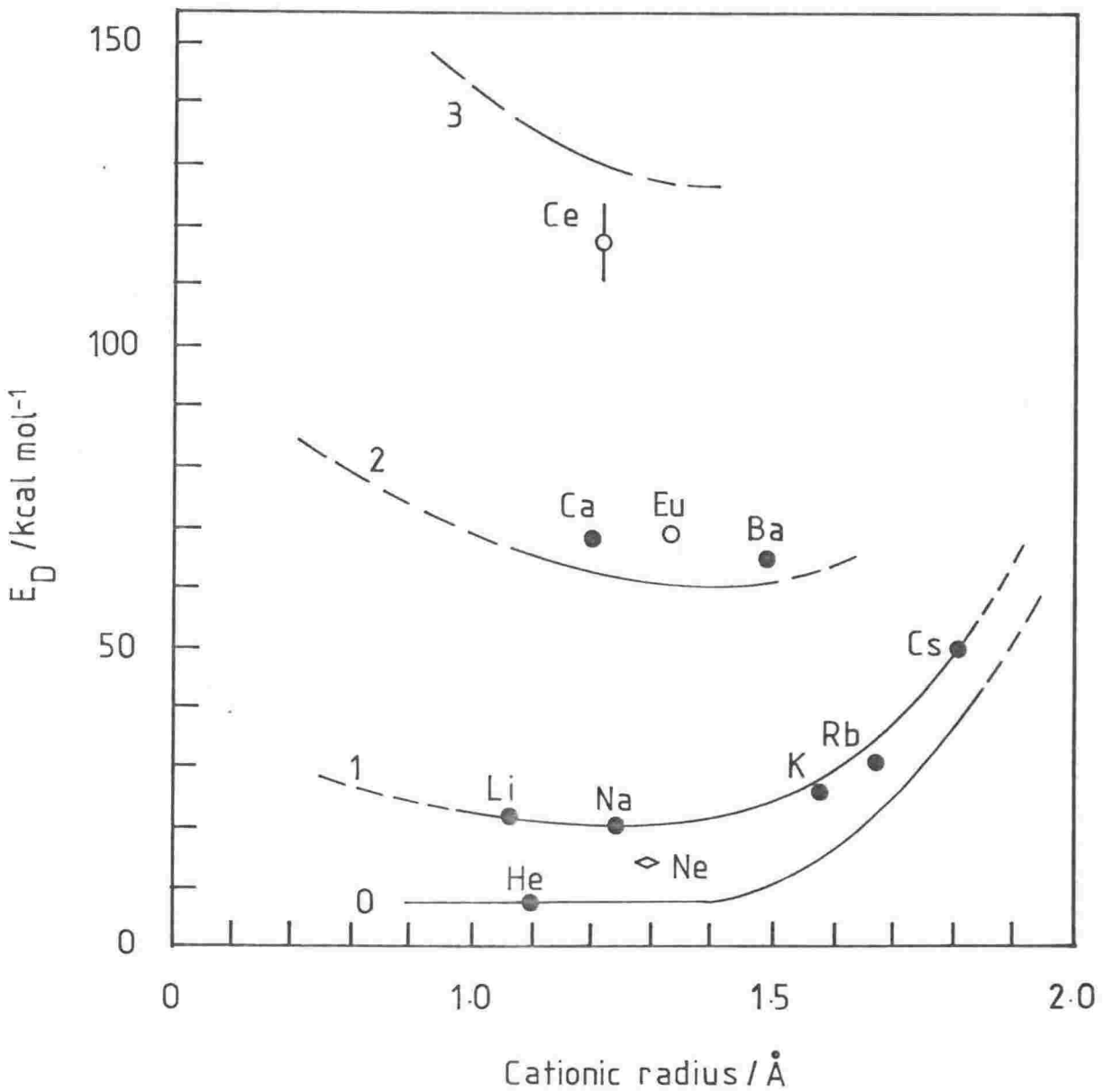

Figure 2.24—Comparison between measured activation energy of diffusion (OIS: solid circles; OVD: open circles) and predication according to equation (2.50) (168).

Waals energy, respectively. E_p and E_v are negligible. A plot of E against radius is shown is Figure 2.24. The lines represent species of constant charge. The fit is surprising considering the assumptions and simplifications made.

2.2.6.3 Hydrous Silicates

The majority of measurements reported on the transport properties of hydrous systems are on naturally occuring silicates.

SiO_2-H_2O

Electrical Conductivity

Figure 2.25 shows a plot of log κ versus mol% H_2O in a SiO_2-H_2O melt at 1200°C. The addition of 20 mol% H_2O causes an increase in conductivity of two orders of magnitude, whereas addition of a further 30 mol% H_2O results in only a small increase in conductivity. This appears to be the only work reported on this system.

Viscosity

Khitarov et al. (171) have measured the viscosity of SiO_2-H_2O as a function of temperature and pressure. Their results are shown in Figure 2.26 and compared with hydrous albite, granite and basalt silicates. The first 3 wt% H_2O at 1200°C reduces the viscosity by a factor of 10^7, in comparison with $10^{3.5}$ for granite and $10^{1.5}$ for basalt. Further water has only a small effect on viscosity. The order of the silicates in Figure 2.26 with decreasing viscosity is of decreasing mol% of silica in the melt. H_2O has the most effect on pure SiO_2 and highly polymerised melts such as albite but much less effect on melts containing less SiO_2 and higher concentrations of network

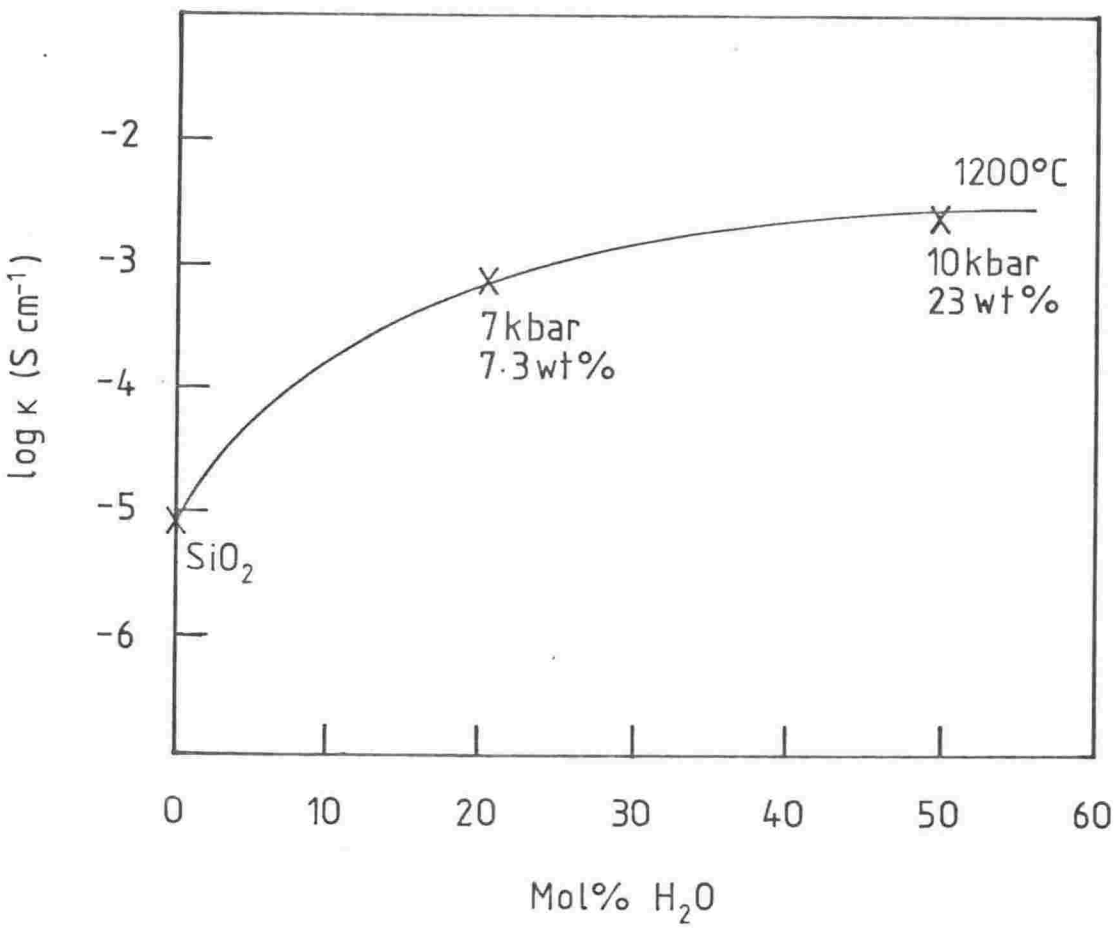

Figure 2.25—Log conductivity versus mol% H_2O for water saturated SiO_2 - H_2O melts at 1200°C (170).

breakers. Activation energies are plotted in Figure 2.27 and compared with binary alkali silicates. The trends for the hydrous silicate are identical with the metal oxide silicate.

The above results for conductivity and viscosity indicate that H_2O depolymerises SiO_2. However, there seems to be a limit to the degree of depolymerisation. Figures 2.25 and 2.26 show that depolymerisation does not reach the point where SiO_4^{4-} ions only are present, since the curves becomes independent of H_2O content long before the stoichiometrical ratio of 2 H_2O/1 SiO_2 is reached.

Diffusion

Khitarov et al. (171) have measured the diffusion of H_2O in molten silica. The value of D at a water pressure of 3000 atmosphere and at temperatures between 1100 and 1400°C is 0.58 - 1.21 x 10^{-5} cm^2s^{-1} and the value at 1200°C and between 3000 and 5000 atmosphere is 0.95 - 2.8.cm^2s^{-1}.

Binary and Ternary Silicates Containing Water

There do not appear to be any reports of any measurements on these systems.

Multicomponent and Naturally Occurring Silicates Containing Water

Electrical Conductivity

Lebedev and Khitarov (170) have summarised the literature on the effect of water on the conductivity of complex silicates. The addition of the first few wt% H_2O has the most dramatic effect in increasing the conductivity, further water has relatively little effect. Lebedev and Khitarov (172) found that the presence of water greatly reduced the temperature of the beginning of melting of granite with a concomitant

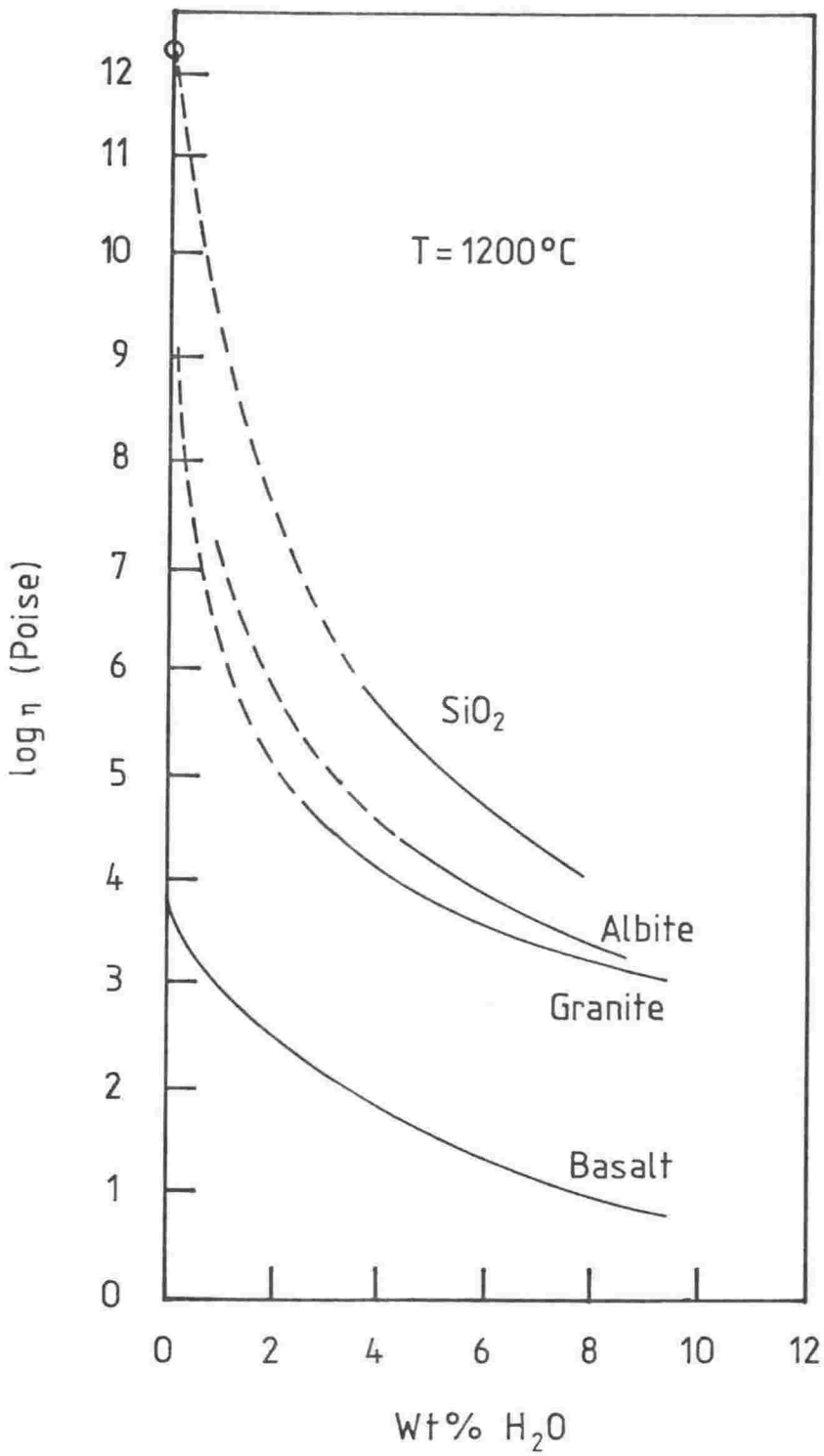

Figure 2.26—Effect of water content at 1200°C on the viscosities of molten silica, albite, granite and basalt (171).

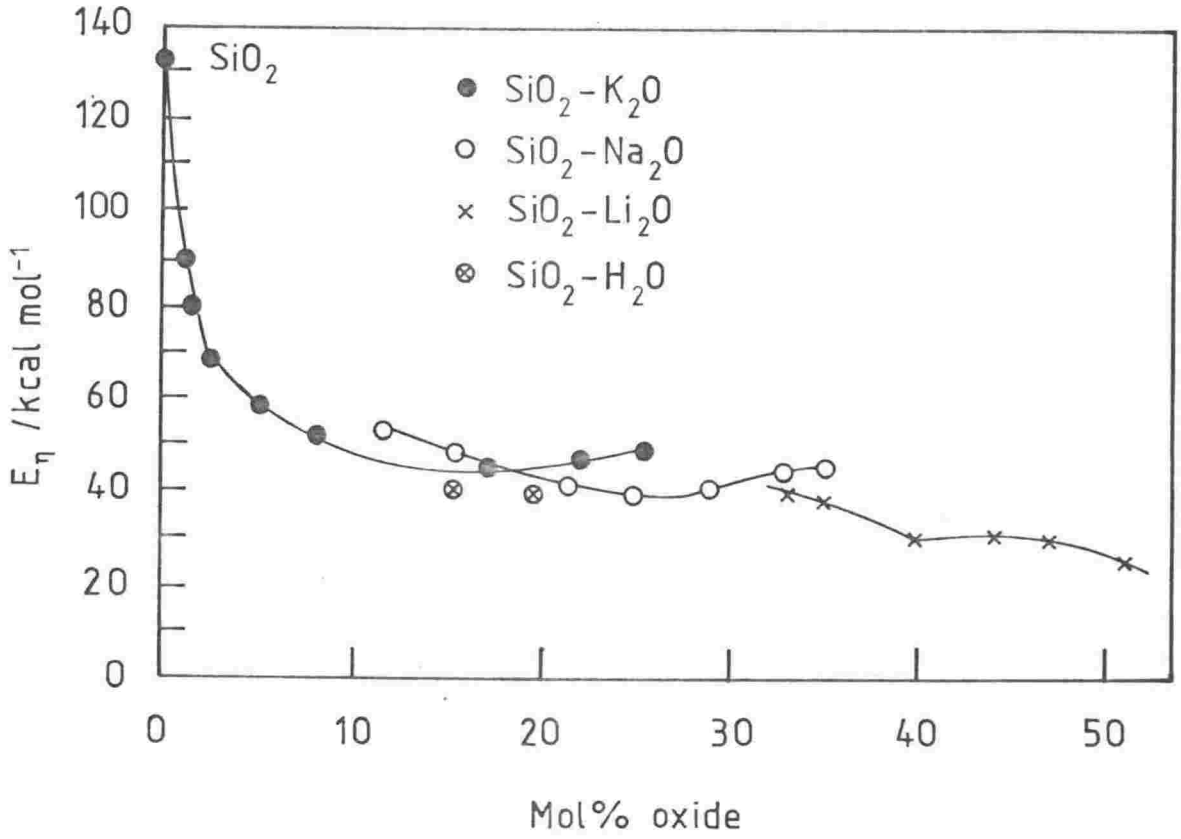

Figure 2.27—Comparison between activation energies for viscous flow in SiO_2-H_2O melts and binary alkali silicate melts (171).

increase in the conductivity. At 1200°C conductivity increaed as the water pressure increased from 1 bar to 8 kbar. Khitarov et al. (173) compared the effects of pressure for dry and water saturated melts on conductivity (Figure 2.28). For the basalt melt they examined conductivity shows very little dependence on pressure. However, the effect of water increases the conductivity over a 10 kbar range by ~one order of magnitude. This pressure dependence of conductivity for dry and water saturated melts parallels exactly the pressure dependence of viscosity (153).

Viscosity

The effect of volatile components on predicting and understanding magmatic and igneous processes has become very important subsequent to the discovery that water, for example, can decrease the viscosity of a magma by several orders of magnitude. Thus, a magma saturated with water will rise to the earth's surface much faster than a dry melt.

Shaw (174) measured the viscosity of hydrated obsidians and found that at 635°C 6 wt% H_2O caused a drop in viscosity of 7 orders of magnitude. The temperature dependence followed an Arrhenius law with activation energy following the same patterns as for binary alkali silicates when plotted against mol% H_2O. Friedman (175) observed similar reductions in viscosity for a hydrated rhyolitic glass. The addition of 0.6 wt% H_2O caused a 2.5 order of magnitude drop in viscosity.

Scarfe (176), found that although water caused a dramatic drop in viscosity its effect depended on the composition of the original silicate. The viscosity of a melt of basic andesite at 1150°C was lowered from 10^3 to 2.5×10^2 Pa s and a tholeiite melt was lowered from

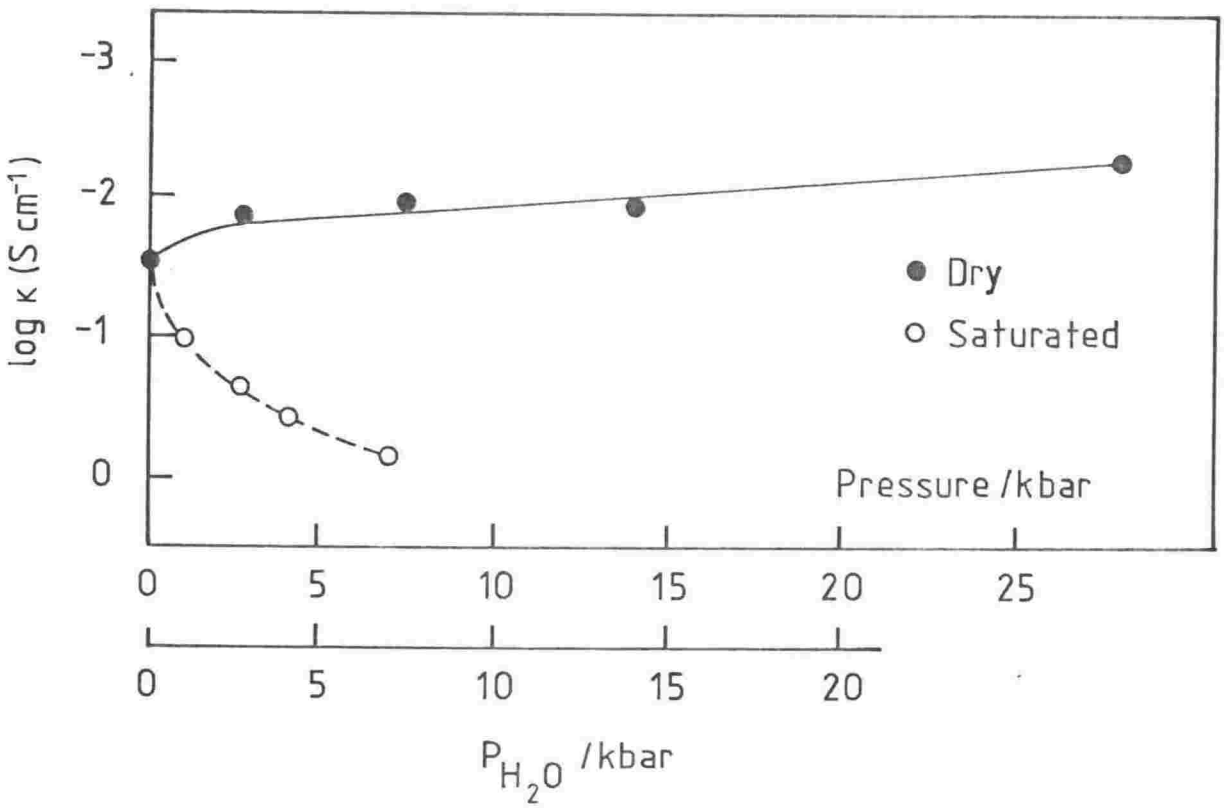

Figure 2.28—Comparison between electrical conductivity of dry and water-saturated basalt at 1400°C as a function of pressure (173).

$1.6x10^2$ to $6x10^1$ Pa s. However, an olivine basalt showed no measurable reduction in viscosity. Melts more basic than basalt appear to be depolymerised to the extent that water has no further network breaking action. Scarfe plotted log viscosity and activation energies against R, where R = O/(Si + Al + P) which indicates the ratio of the molecular percent of non-bridging oxygens to network forming cations. All of the different compositions fitted onto one curve. When R > ~2.6 then the melt is highly depolymerised and the viscosity is low and the activation energy is low as well. As R decreases there is a rapid increase in both viscosiy and activation energy.

Khitarov et al. (173) and (177) investigated the effect of pressure on viscosity. For molten basalt the viscosity increases by a factor of 100 as pressure is raised from 1 bar to 23 kbar at 1400°C. However, the addition of water to saturate the melt reduces the viscosity by 1.5 orders of magnitude from 1 bar to 5 kbar. In the case of tholeiitic melts the presence of H_2O to saturate the melt caused a decrease in viscosity by 1.5-2 orders of magnitude. The effect of pressure from 1 bar to 24 kbar was to increase the viscosity by a factor of 5 only. Undersaturated melts had reductions in viscosity intermediate between dry and saturated.

Viscosity reductions are greatest at lower temperatures for acid magmas and least for basic magmas.

Diffusion

Diffusion of various cationic species including H_2O in hydrous silicates has recently been investigated by some geophysicists. The principal finding is that diffusivity is enhanced by the presence of

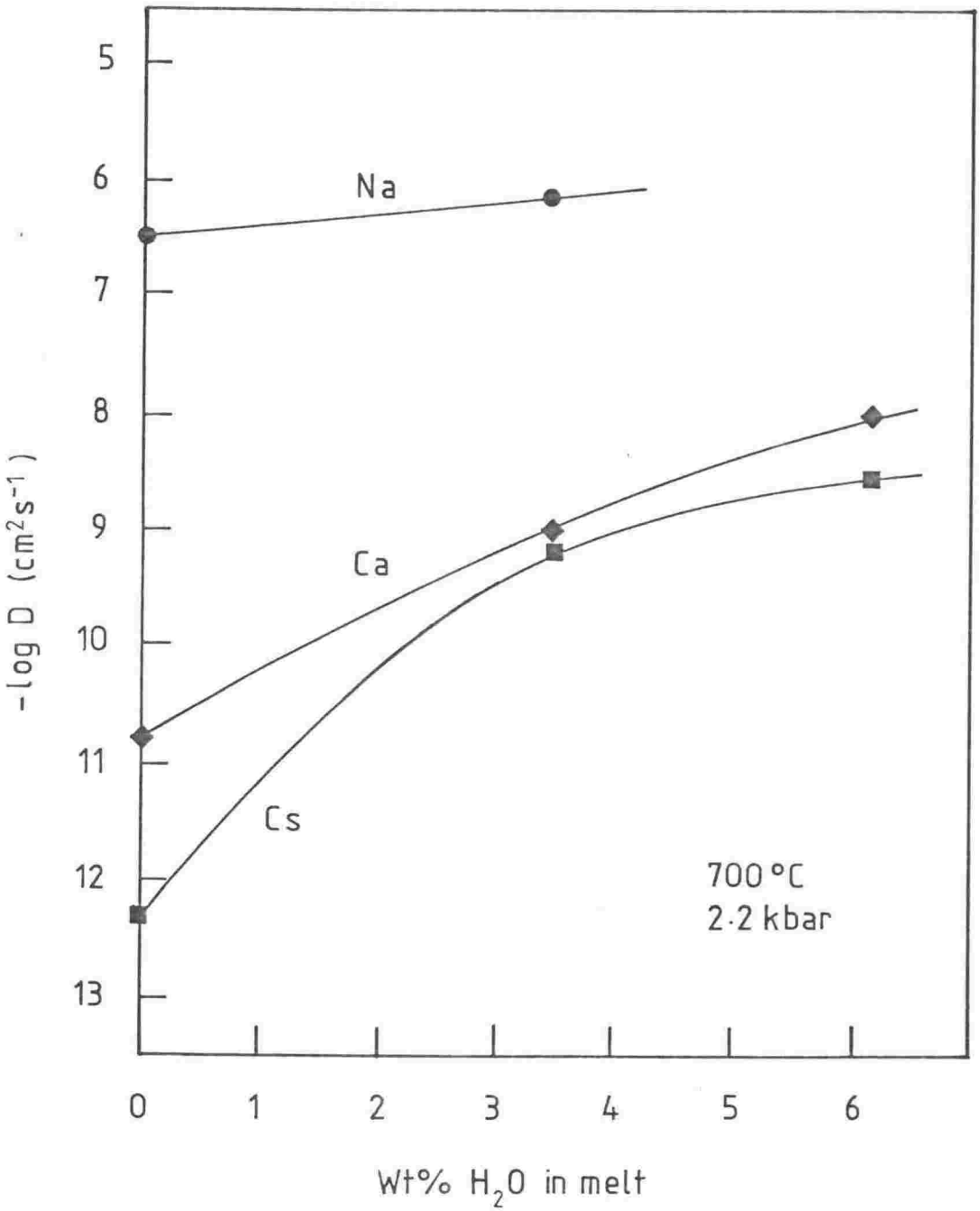

Figure 2.29—Dependence of log diffusivity on H_2O content for Na, Ca and Cs in a granitic melt (167).

water (178), (179), (167). Watson (167) examined the diffusion of Cs, Ca, and Na in granite melts and compared them with dry melts (Figure 2.29). The large cation Cs has an increased diffusivity of ~4 orders of magnitude with the addition of 6 wt% H_2O, whereas the singly charged and slightly smaller Na diffuses at a similar rate through either dry or hydrous granite melt.

Karsten et al. (180) and Shaw (181) have measured the diffusion of H_2O in rhyolite and granite melts respectively. Diffusivities of H_2O in rhyolite are exponentially dependent on concentration and vary from $\sim 10^{-8}$ cm^2s^{-1} at 650°C to $\sim 10^{-7}$ cm^2s^{-1} at 950°C with 2 wt% water. Thus H_2O diffuses faster than Cs but slower than Na. The activation energy for diffusion in both rhyolite and granite are very close, 80 and 63 $kJmol^{-1}$, respectively and is close to E_D for Na in granite. Diffusion of water is therefore relatively fast in comparison to many cations (168).

Watson (182) has measured diffusion of CO_2 in basalts and an aluminosilicate (SiO_2 60%, Na_2O 30%, Al_2O_3 10%). Diffusion has an Arrhenius dependence on temperature with an activation energy of ~192 $kJmol^{-1}$, more than double that for water. Diffusion of carbonate, the most likely diffusing species, is ~1-2 orders of magnitude slower than H_2O in granite melts but faster in basalts. Diffusion of CO_3^{2-} is almost independent of the concentration of CO_3^{2-} but more temperature dependent than H_2O.

2.3 SPECTROSCOPIC STUDIES OF MOLTEN SILICATES

Spectroscopic methods are powerful tools for elucidating the structure of matter, particularly the solid phase, but of recent times their application to liquids and glasses has become very important. They provide structural information, such as bond lengths and angles, which cannot be obtained from equilibrium and transport studies. Wong and Angell (183), in a recent book, have given an extensive review of the application of spectroscopic techniques to glassy material including silicate glasses. This book covers the entire electromagnetic spectrum from γ-ray spectroscopy (Mossbauer effect) to radio frequency spectroscopy (EPR and NMR). Included in the methods reviewed are the techniques of scattering X-rays, neutrons, and electrons. Although these diffraction methods are not strictly speaking a branch of spectroscopy, since they deal with elastic diffraction rather than emission or absorption of radiation, they are included because they are of great importance in structural studies of vitreous materials.

Spectroscopic studies of silicates have generally been carried out on glasses formed by quenching melts from high temperatures and/or pressures. Since the liquid state is often the state of interest in these studies, the question arises as to whether the structural features of a liquid are 'frozen-in' when the liquid cools to a glass. Some comparative studies on glasses and their melts show that the structures are similar although there is also evidence to the contrary. Infrared studies on melts and glasses in the soda-silica system (184) and Raman spectroscopic data on GeO_2 and melts and glasses in the system SiO_2-Al_2O_3-Na_2O (185) did not reveal structural differences between the

glass and its melt. Taylor et al. (186) reached a similar conclusion for glassy and molten albite. However, Nukui et al. (187) found structural differences between liquid and vitreous silica. In vitreous silica a closed structure exists in which the quartz-like arrangement predominates over the cristobalite-like structure; whereas the melt possesses an open structure with a large amount of cristobalite-like arrangement. Thus it is not certain to what extent structural features of a melt are 'frozen' into a glass particularly in view of the large volume decreases accompanying glass formation in some liquids such as alkali silicates.

Comparative spectroscopic studies of glass and liquids at high pressures and temperatures have not been conducted. These studies will be the ultimate test for structural similarities between a glass and its melt together with pressure and temperature dependence on structure.

Raman and infrared spectroscopy and X-ray diffraction have been utilised more extensively than other techniques on glassy and molten silicates. These spectroscopic methods have been applied to a wide range of silicates. The main structural information obtained is the number of bridging oxygens per silicon, coordination numbers and bond angles. Determining coordination numbers is very important in understanding the role of cations such as Al^{3+} and Ti^{4+}. For example, as already mentioned in section 2.2.6.2, it has been predicted that Al^{3+} changes coordination in silicate melts on application of sufficiently high pressures. X-ray diffraction has established that the SiO_4^{4-} tetrahedron is the basic structural unit in molten and vitreous silica and silicates. There has been some debate as to the bond angles of the tetrahedra and thus the

way they are joined together to make a three-dimensional network. This has been discussed by Richardson (10), Mackenzie (188) and Nukui et al.(187).

Dissolution of H_2O in silicate melts is of interest to petrologists for modelling the behaviour of hydrous magmas. Many researchers, from physical (section 2.1.2.3) and spectroscopic studies, have claimed that dissolution of water in silicate melts takes place by the formation, almost entirely, if not completely, of OH^- groups on silicate anions. Others workers, notably Stopler (81), (82), claim, contrary to the above, that water may be present in the molecular form as well as in OH^- groups. Evidence for molecular water, being present in silicate melts comes principally from NMR studies on silicate glasses (189), and infrared and near-infrared spectroscopic investigations on silicate glasses (190), (81). The systems examined in these studies are glasses quenched from high temperature and high pressure conditions where water was dissolved in the melt. Stopler (81), who argues the case for molecular water, concedes that the final proof of its existence in silicate melts rests on conducting spectroscopic experiments at high temperatures and pressures.

2.4 THEORIES AND MODELS OF THE STRUCTURE OF LIQUID SILICA AND SILICATE

The previous sections have summarised the principal experimental data on the properties of liquid silica and silicates, along with various empirical relations between some of the properties of these liquids, for example the relationship between activation energy and ion-oxygen attraction. The structure of molten silicates has recently been reviewed

by Mysen (134). In this section the structural models which have been proposed to account for the experimental observation are discussed. Attention is also drawn to analogous systems such as H_2O, GeO_2, BeF_2 etc. These liquids exhibit similar behaviour to silica and a comprehensive model of one must fit the others as well. Models of molten silica are discussed first since it is the parent material and on which models of silicates are based. This is followed by a discussion of the models of molten silicates. These are divided into two subgroups (i) Models based principally on kinetic experiments and (ii) Thermodynamic models. The latter group is divided into two categories: (a) Polymer models and (b) Mixing models. Polymer models are included here because the predictions of these models are activities of components in the melt. Finally parametric equations for calculating viscosity and density of liquid silicates are discussed briefly.

2.4.1 Models of Molten Silica

The random network theory is the most widely accepted model of vitreous and liquid silica. Proposed originally by Zachariasen in 1932 (191), (192), it has been extended more recently by Bell and Dean (193) and by Gaskell and Tarrant (194) among others. The present form of this theory states that vitreous silica consists of a three-dimensional random interlocked network of SiO_4^{4-} tetrahedra. The four oxygens of this molecular unit are tetrahedrally bound to a central silicon atom. Neighbouring tetrahedra are joined at the vertices by sharing bridging oxygen atoms. Although the SiO_4^{4-} entities are regarded as internally symmetrical, the orientation of adjacent units about a central unit is

variable, constrained by two factors: (1) the intermolecular Si-O-Si bond angle, θ, must lie between 120^{o} and 180^{o}, its mean value being approximately 150^{o}, and (2) each tetrahedral unit can lie in any position obtained by rotating the unit about the Si-O bond linking it with an adjacent tetrahedral unit. A further restriction placed on the tetrahedral units is that they must be continuously connected, thus forming a three-dimensional network structure.

According to this theory, in its original form (191), there is no short range order beyond the SiO_4^{4-} tetrahedra and thus no 'crystal-like' features. However, X-ray, Raman and neutron diffraction studies (195) indicate some short range structure beyond ~1.62 nm, the radius of the SiO_4^{4-} tetrahedra, although within the constraints of this theory it is possible to have the order extended beyond the basic unit. Testing the applicability of this theory has raised a number of problems, since mathematical or laboratory simulation of such an arrangement of silicon and oxygens atoms is extremely complicated (193) and as yet there is no direct proof of this model. The only way to test the theory is to construct a model of SiO_2 within the constraints of the theory and compare the predicted radial distribution function with that obtained from X-ray studies on silica glass. Bell and Dean (193) have pointed out, however, that to calculate the R.D.F the coordinates of the atoms are required and the theory does not predict individual atomic positions. Nevertheless, several workers (196),(197) have constructed geometrical models which could account for the observed X-ray and neutron R.D.F. out to ~4 nm. Bell and Dean (193) have improved on this and extended it to 8 nm. They have published the coordinates of a

geometrical model containing 614 atoms. Gaskell and Tarrant (194) have done further experiments and have confirmed the model of Bell and Dean.

Bottinga et al. (195) have summarised recent work on silica glass including Raman, X-ray and NMR studies which support the existence of tridymite-like regions of dimensions up to 20 Å, comprising several SiO_4^{4-} units. However, there is still insufficient evidence for microcrystalline regions indicative of the 'crystallite' model of Lebedev (198). According to this theory glasses and liquids are composed of small crystalline regions surrounded by completely disordered material.

Even though there are still problems with the randon network theory, particularly in explaining the amount of short-range order which is believed to be present in silica glass, it is still superior to alternative models which have been proposed. Further, the equilibrium and non-equilibrium experimental data cited earlier are consistent with the general picture of molten silica given by the random network model. The volume-temperature data indicates that vitreous and liquid silicates have a looser structure than any of the cystalline polymorphs. The viscosity, conductivity and diffusion data show that molten silica is an associated liquid and that the flow unit in the case of viscosity is the SiO_4^{4-} unit, since activation energy is constant over a wide temperature range.

Another line of approach to the structure of silica is via the silica/silicate analogues, particularly water. This has been discussed by Bockris and Reddy (12) who noted a number of similarities between water and silica. More recently Angell et al. (14), (15) via computer

simulations have extended the study of the properties of silica over very wide temperature ranges and have found remarkably similar properties: (1) a decrease in viscosity as a function of increasing pressure and (2) a density maxima.

2.4.2 Models of Molten Silicates

2.4.2.1 Ionic Models

The main models in this category include the network model, the discrete-ion model and the 'iceberg' model. These models are based on the electrical conductivity, viscosity and other experimental data cited in previous sections and attempt to account for the ionic character of molten silicates. They have been described in the following papers (199), (65), (92) (131), (29), (30) and have been reviewed by Mackenzie (24), (125), Bloom and Bockris (200) and Bockris and Reddy (12). These models will be described here very briefly.

(1) The network Model

This model applying to binary silicate liquids was proposed by Endell and Hellbrugge (199). It is essentially an extension of the random network theory postulating a progressive breakdown of the three

TABLE 2.7

The Network Theory of Liquid Silicate Structure

Range of composition mole % M_2O	Silicate entities present
0	Continuous three-dimensional (3-D) network of SiO_4 tetrahedra with small degree of thermal bond breaking
0-33	Essentially 3-D network of SiO_4 tetrahedra with number of broken bonds equal to number of added O atoms from M_2O; end of 3-D boundary at 33 %
33	"Infinite" 2-D sheets of SiO_4 tetrahedra; M^+ ions and O^{2-} ions between sheets
33-50	Region of sheets and some chains of tetrahedra
50	Chains of infinite length
50-60	Chains of decreasing length
66	SiO_4^{4-}

Data from (12).

At 33 mol% infinite two dimensional sheets are believed to exist. As further metal oxide is added these sheets collaspe into chains which in turn decrease in length till at ~66 mol% only SiO_4^{4-} anions exist. Beyond 66 mol% the entities present are not specified in this model. This model fails in at least two important ways: (1) It cannot account for the sharp changes which occur at ~12 mol% for both thermal expansivities and activation energy for viscous flow, and (2) In the composition range 33-66 mol% metal oxide this model would predict large changes in the activation energy of viscous flow since infinite sheets are broken down into single SiO_4^{4-} units and thus the flow unit would be expected to change dramatically. However, experimentally the activation energy is relatively constant in this region to about 50 mol% after which there is a sharp drop for soda-silica melts (Figure 2.19). Further there is an enormous change in activation energy on addition of the first 10 mol% metal oxide. This model predicts very little change in this region which is contrary to fact.

(2) The Discrete-Ion Model

Bockris and coworkers (4), (92) have proposed a model, which, although having features of the network model, can explain the experimental observation where the network model failed. It postulates the existence of discrete silicate anions: dimers, trimers, rings etc, instead of sheets and chains, in the composition range 10-66 mol% metal oxide. The anions present in each composition range are shown in Table 2.8. The following observations from experimental data are taken into account in this model. Since transport numbers show conduction to be cationic the anions must be considerably larger in size compared to

TABLE 2.8

The Discrete Polyanion Model of Liquid Silicates

Range of composition mol % M_2O	Silicate entities present
0	Continuous 3-dimensional networks of SiO_4 tetrahedra with some thermal bond breaking and a fraction of SiO_2 molecules
0-10	Essentially SiO_4 network with number of broken bonds approximately equal to number of added O atoms from M_2O, having fraction of SiO_2 molecules and radicals containing M^+
10-33	Discrete silicate polyanions based upon a six-membered ring ($Si_6O_{15}^{6-}$)
33-55	Mixture of discrete polyanions based on $Si_3O_9^{6-}$ and $Si_6O_{15}^{6-}$ or $Si_4O_{12}^{8-}$ and $Si_8O_{20}^{8-}$
~55-66	Chains of general form $Si_nO_{3n+1}^{(2n+1)-}$, e.g., $Si_2O_7^{6-}$
66-100	SiO_4^{4-} + O^{2-} ions

Data from (12).

the cations. The distinct changes in several properties which occur at ~12 mol% suggest that structural changes are taking place at this composition. Further, the sharp increases in transport properties and activation energies with decreasing amount (<10-20 mol%) of metal oxide indicates that polymerisation of silicate anions is occuring. However, between 10 and 66 mol% there is probably very little structural change since there is only a relatively small change in activation energy of viscosity. The flow unit in this region consequently must be of similar size throughout this region. These observations indicate that there are three distinct regions (i) 0-(10-20) mol%, (ii) (10-20)-66 mol% and (iii) 66-100 mol% metal oxide. It was argued that, as metal oxide is added to silica, in region (i), the network structure of silica becomes unstable with respect to discrete polyanions, and over a small composition range (0 - 10 mol%) the network depolymerises producing a liquid of low viscosity and high conductivity. On further addition of metal oxide rings and polyanions are broken down to give dimers and short chains. Throughout region (ii) the size of the postulated anions does not change greatly even though various anions are envisaged to exist at certain composition regimes. At 66 mol% metal oxide and in the rest of region (iii) only SiO_4^{4-} anions can exist and possibly some O^{2-} ions based on the quadrivalency of silicon and the requirements of stoichiometry.

(3) The 'Iceberg' Model

In spite of the improvements of the discrete-ion theory over the network model there are two properties of molten silicates which are difficult to explain in terms of the previous models: (1) The discrete-

ion model predicts an abrupt change in partial molar volume of SiO_2 at ~10 mol% metal oxide. However, the partial molar volume of SiO_2 changes negligibly in the range 0-33 mol% metal oxide and (2) The existence of a miscibility gap is not readily explicable in terms of the discrete-ion theory which predicts complete mixing at all compositions. This miscibility gap is most pronounced in the 12-33 mol% region of the alkaline earth binary silicate melts. A silica rich phase and a metal rich phase becomes apparent.

It has been proposed by Bockris et al. (29), (30) that two structures may be present in the region 12-33 mol% metal oxide, one similar to vitreous silica and the other similar to the anions which exist at 33 mol% in the discrete anion theory. The vitreous silica exists in the form of 'icebergs' surrounded by a 'sea' of anions. It has been suggested (12) that these 'icebergs' are similar to the clusters which are found in water, and, like the clusters in water, are probably continually breaking down and reforming. The existence of these postulated SiO_2 rich 'icebergs', would, at certain compositions, explain the phenomenon of two immiscible phases. This model for the 10-33 mol% M_2O region is consistent with the almost constant partial molar volume of SiO_2 observed for the composition range 0-33 mol% M_2O, because most of the SiO_2 is postulated to exist in the 'icebergs' which have the same -Si-O-Si- angle as that in vitreous silica. The sudden change in thermal expansion at 12 mol% is explained in terms of the 'icebergs' being separated from one another at ~12 mol% by ionic layers which have a greater expansivity coefficient than the 'icebergs'. The flow process in this model is somewhat different from the previous models since the

'icebergs' and the ionic film can slip past each other without the need for Si-O-Si bonds to be broken.

Both the discrete-ion and 'iceberg' models are speculative, since no direct evidence exists for the postulated anions or silica-rich 'icebergs'. Although, in neither model are the polyanions envisaged as the exclusive ones present but only the predominant ones. However there is some indirect evidence for silica 'icebergs' by analogy with $ZnCl_2$; there is a puzzling persistence of $ZnCl_2$ polymer bands in Raman spectra of $ZnCl_2$ + alkali chloride melts (201). Further indirect evidence comes from the wide range of anions which are known to exist in crystalline mineral silicates and from the potential variations in structure based on the crystalline structure of silica (202).

A point to be noted is that although molten silicates may be ionic liquids it doesn't mean that they are completely dissociated into the smallest possible ions. Thus they may be described as partially ionised liquids. The above theories attempt to account for this by postulating that for all compositions with less than 66 mol% metal oxide there exists a range of silicate anions containing undissociated silica.

2.4.2.2 Thermodynamic Models

Two types of model will be discussed under this heading: polymer theories and mixing models. An example from each will be discussed. These theories to a limited extent contribute to a structural understanding of silicate melts. Amongst other things they are special cases of the discrete-ion theory since they postulate the existence of a range of silicate polyanions. The theories are generally applicable only

to binary systems. An advantage of the mixing model discussed here is that it deals directly with pressure and the solubility of H_2O as an oxide component.

(1) Polymer Theories

In recent years the principles of organic polymer chemistry developed by Flory (203), have been applied to liquid silicates (204), (205), (206) since they can be regarded as inorganic polymers. For example the random network theory of silica explicitly contains the idea of a three-dimensional polymer. A number of polymer models have been proposed (207), (208), (209), (210). The simplest of these models is by Masson (207). In molten silicates, according to his model, it is assumed that the simplest and most abundant anionic species is the orthosilicate anion, SiO_4^{4-}, regarded as a monomer. Two of these monomers can undergo condensation to form a dimer, $Si_2O_7^{6-}$, with the elimination of O^{2-}. Three monomers or a dimer and a monomer can condense to form a trimer, $Si_3O_{10}^{8-}$, and so forth. At equilibrium an infinite number of these and other ions is considered to be present with a concomitant equilibrium constant for each polymerisation/depolymerisation equilibrium reaction. The aim of polymer theory is to calculate the activity of a component via the equilibrium reaction as a function of composition. Since the number of possible ion types is infinite, a number of simplifying assumptions have to be made and there are three such assumptions in Masson's theory:

1. The self-condensation of chains to give rings or network structures does not occur, i.e. only linear and branched chains are considered. Without this assumption intractable mathematical difficulties arise.

2. All functional groups of the same kind are chemically equivalent. For example the O^- groups are chemically equivalent regardless of the size of the polyanions to which they are attached. This is the principal of equal reactivity.
3. The activity of a component may be calculated from the product of the ion fractions of M^{2+} and O^{2-}:

$$a_{MO} = X_{M^{2+}} + X_{O^{2-}}$$

This is known as Temkin's law and for a binary system the ion fraction of the cation is unity.

By applying the above principles and assumptions theoretical activities can be calculated and compared with experiment. Comparison for binary melt up to 40 mol% silica are adequate.

The essential structural conclusions arising from the application of polymer theory to silicates are as follows:

1. The most abundant anionic silicate species is the SiO_4^{4-} monomer and is independent of mole fraction of silica.
2. The monomers exist in equilibrium with a range of other silicate anions including chains, branched chains, rings and networks. Although the theory can treat chains and branched chains explicitly it cannot satisfactorily treat rings and networks.
3. At a particular temperature the extent of polymerisation is defined by an equilibrium parameter k which determines the distribution of silicate anions for a given binary melt.

Although polymer theories describe the structure of silicate melts at least on a semi-quantative level, they have a number of serious limitations:

VICTORIA UNIVERSITY OF WELLINGTON

1. The condensation reaction producing O^{2-} is an essential feature of the theory. This ion, if present, will contribute significantly to the chemical and physical properties of the melt. Its effect on the melt structure is not taken into account in the theory. Further, there is no unequivocal evidence for its presence in silicate liquids with mole fraction of silica > 0.33.
2. Although postulating the existence of similar anions as the discrete-ion theory it also suffers in that there is little evidence for their existence. Direct evidence, supporting the existence of the silicate anions postulated in polymer theories, has come from trimethylsilylation studies by Lentz (211). However, this evidence has been disputed (195).
3. Treatment of cations is limited to Si^{4+}. Structure forming cations such as Al^{3+}, Ti^{4+} and Fe^{2+} are ignored as are also the structure breaking alkali and alkaline earth metal cations.
4. Most polymer theories rely on some form of Temkin hypothesis about ideal mixing of anions and cations in spite of enormous variations in size, field strength and preferred cation associations in the melt.
5. It is difficult to develop polymerisation models with mole fraction of SiO_2 > 0.5 because of the extensive network structure. Attempts have been made by Gaskell et al. (35), Baes (208) and Dron (210) to extend the application to silica-rich regions; however, comparisons with experimental results are poor.

(2) Mixing Models

A number of thermodynamic mixing models have been proposed to predict various thermodynamic parameters of mixing of metal oxides and silica, see for example Wasserburg (212), Shaw (75), Nichols (213), Bottinga and Richet (214) and Burnham (215). The model developed by Burnham (215) will be discussed here as an example of this approach to molten silicates because of its relevance to the present thesis since it treats the effect of pressure and dissolved water.

Burnham has proposed a model for the mixing of water in an albite melt which is based on the experimentally observed effects of water on the viscosity, volume relationships, electrical conductivity and thermodynamic properties of hydrous silicates. Associated silicates, such as albite, can be regarded as quasi-crystalline near the melting point. During melting long-range order is lost but short range order is maintained. This finding is supported by a low entropy of fusion (S_f(albite) = 3 $Jmol^{-1}K^{-1}$) (215) which is a measure of the change in the degree of atomic ordering upon melting. The structure of albite near its melting pont is thus assumed to be made up of four-membered units of $(AlSi)O_4$ tetrahedra, where each O^{2-} ion is shared either within the unit or between adjacent units. It is further assumed that H_2O, in order to dissolve, must react chemically with the albite melt. It is proposed that water enters the melt by reaction with bridging oxygens to produce $2OH^-$ ions, thereby breaking the bridge and lowering the degree of polymerisation. The addition of 1 mole of water per mole of albite is sufficient to break the three dimensional polymeric framework into sheets, about one four membered unit thick which are orientated perpendicular to the plane of projection and parallel to the Na^+

cations. The addition of a further mole of water per mole of albite is sufficient to break the sheets into chains.

Burnham adduced qualitative support for this model from viscosity, conductivity, ir spectra supporting existence of OH^- ions and partial molal volume data on hydrous albite melts. He found quantitative support for this model from calculated solubilities of water in albite compared to experimental observed solubilities. He also found support for this model from Henry's law constant, k, which is independent of melt composition within the range of applicability of the model since the activity of water has the same value at a given pressure, temperature and mole fraction of water for a range of alumino-silicates.

Although the model provides insight into the nature of the water-melt interaction, more precise data over a wider range of composition and conditions is required before it can be extended to provide a quantitative basis for an analysis of transport properties such as conductivity and viscosity.

2.4.2.3 Parametric Equations for Calculating Viscosity and Density of Liquid Silicates

Several attempts have been made to calculate the viscosity of multicomponent silicate systems, especially of geological interest, by empirical linear projection of experimental data of simple systems. Mackenzie (131) was the first to attempt this approach to estimate the viscosity of binary and ternary alkali and alkaline earth silicates. By using the viscosity data of synthetic silicate liquids Bottinga and Weill (162) and Shaw (163) have calculated the contribution, positive or negative, made by suitably chosen components. The viscosity of the liquids is then given by an equation:

$$\ln \eta = \sum_i X_i \ln \eta_i$$

where η is the viscosity of the mixture and η_i is the viscosity contribution from component i of mole fraction X_i An analogous approach has been applied by Bottinga et al. (37), (38) to partial molar volumes to calculate densities.

Although these empirical equations allow viscosity and density of multicomponent systens to be calculated they give no insight into the structure of silicate liquids.

Chapter III

EXPERIMENTAL

3.1 INTRODUCTION

This project was initiated to study transport (viscosity and electrical conductivity) and PVT properties of molten and water-rich silicates. In particular, the effects of pressure and water concentration on transport properties were of special interest, since these variables are important in magmatic processes. In order to carry out such a study, temperatures up to 1200°C and pressures up to 5 kbar are required. Further, due to the corrosive nature of molten silicates, special materials have to be used to contain these liquids while they are subjected to the above temperatures and pressures. This temperature and pressure regime requires the use of an internally heated pressure vessel (I.H.P.V.), the general features of which are described in section 3.2.1.1. These are large and complicated pieces of experimental apparatus requiring further ancillary equipment to operate them. Section 3.2 describes the commissioning of an I.H.P.V. facility.

Initial studies using the I.H.P.V. have been on the electrical conductance of both hydrous and anhydrous silicates over a range of composition. A simple conductance cell was made from platinum and alumina. This cell was designed to be capable of being used under pressure, without bursting or altering the cell constant, by hermetically sealing a collapsible platinum bag to the cell. In this way

there was a zero pressure gradient across the wall of the cell. The experimental equipment and techniques used for the electrical conductance study are described in section 3.3.

The measurement of viscosity as a function of pressure is very difficult. A method has been developed which utilizes the piezoelectric properties of quartz crystals. This quartz crystal viscometer, although not yet sufficiently refined to be used at high temperatures and pressures, has been extensively tested at room temperature with satisfactory results. Section 3.4 summarises these previous developments and describes further improvements, as part of this thesis, to extend the range of operation of the viscometer to higher tempertures.

3.2 INTERNALLY HEATED PRESSURE VESSEL

Figure 3.1 is a schematic diagram of the internally heated pressure vessel facility that has been constructed as part of this project and described in this section. The pressure vessel and its ancillary components are described first, followed by the pressure generation system. Finally, the furnace and the electrical equipment to operate it are described.

3.2.1 Pressure Vessel

3.2.1.1 General Description of I.H.P.V.'S

An internally heated pressure vessel, as the name implies, has a furnace inside the pressurised vessel. The walls are water cooled to maintain the strength of the metal. Such vessels can be used at higher temperatures and pressures than externally heated vessels since they do

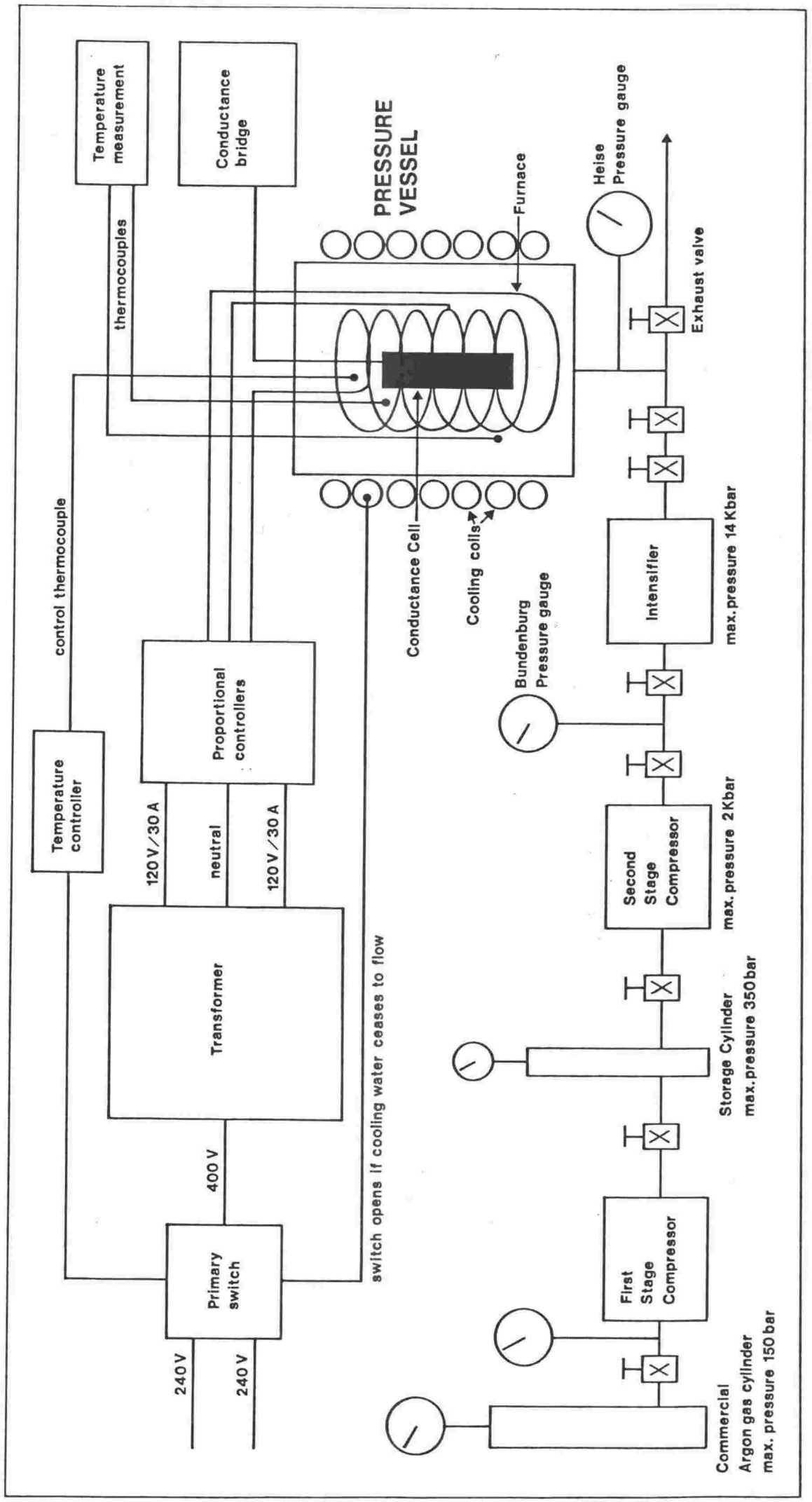

Figure 3·1 — Schematic Diagram of INTERNALLY HEATED PRESSURE VESSEL Facility

not depend on the hot-rupture strength of the metal used in their construction but are limited only by the furnace windings, the insulation and wall thickness. Generally, argon or nitrogen gas is used as the pressurising medium because it transmits a uniform hydrostatic pressure to the sample and does not react with materials exposed to it. Internally heated vessels are much larger, both in overall dimensions and pressurised volumes than externally heated ones because of the necessity to incorporate a furnace. The large internal volume also makes it possible to incorporate complex and delicate equipment inside the vessel, giving this equipment considerable experimental flexibility. Internally heated vessels are required for experiments in the 1-10 bar pressure range if the operating temperature is to exceed ~900°C.

Due to their larger gas volumes and the necessity of taking several electrical and other leads through the mushroom heads of internally heated vessels, they are more complicated, dangerous and expensive to operate than externally heated vessels. Holloway (216) and Edgar (217) discuss the necessary safety precautions. However, in spite of the advantages of these vessels there are at least three problems common to all I.H.P.V.'s:

1. There is only a limited number of leads which can be sealed into the mushroom heads. This constrains the type of apparatus to be operated inside the vessel.
2. Temperature control is difficult and requires at least two independent elements to enable control of temperature gradients.
3. All dead space must be filled with a suitable non-porous, inert material to minimize both convection currents and the volume of high pressure gas.

3.2.1.2 Design and Description of Pressure Vessel

Plate 3.1 shows the large pressure vessel used in this project and Figures 3.2 to 3.6 show the design drawings giving the dimensions of the different parts of the vessel. The overall length of the vessel is 1170 mm, it is 200 mm in diameter and has a 50 mm bore through it. The complete vessel weighs ~400 kg.

The pressure vessel was designed by Torrie, Smedley and Bird and the design calculations are given in the appendix of Torrie's thesis (2). It was calculated (2) that an internal volume of 50 mm diameter and at least 700 mm long was required for the measuring equipment. This length was necessary because of the dimensions of the quartz crystal viscometer and the need to keep the crystals in the cool zone below the furnace.

The design was based on Burnham's I.H.P.V. which is discussed in detail by Holloway (216). However, rather than using a Bridgman unsupported-area seal (218), as in Burnham's vessel, which can occupy up to half the internal volume, a simpler modified mushroom head with 'O' ring seals was adopted. This method has the added advantages that more leads can be sealed into the mushroom heads and the internal volume is greatly increased. For a pressure vessel giving the required internal volume and rated to 5 kbar, Bohler US Ultra 1 ESR ISODISC steel was used which has a yield strength of 13.1 kbar.

Bohler Steels Pty Ltd[1], were contracted to machine and heat treat to the specified hardness, the vessel and its components as in Figures 3.2 to 3.6. However, mushroom heads A and B were machined at the Victoria University of Wellington Workshops. Following heat treatment, the

[1] Bohler Steels Pty Ltd, 146 Botany Street, Waterloo, N.S.W. 2017, Australia.

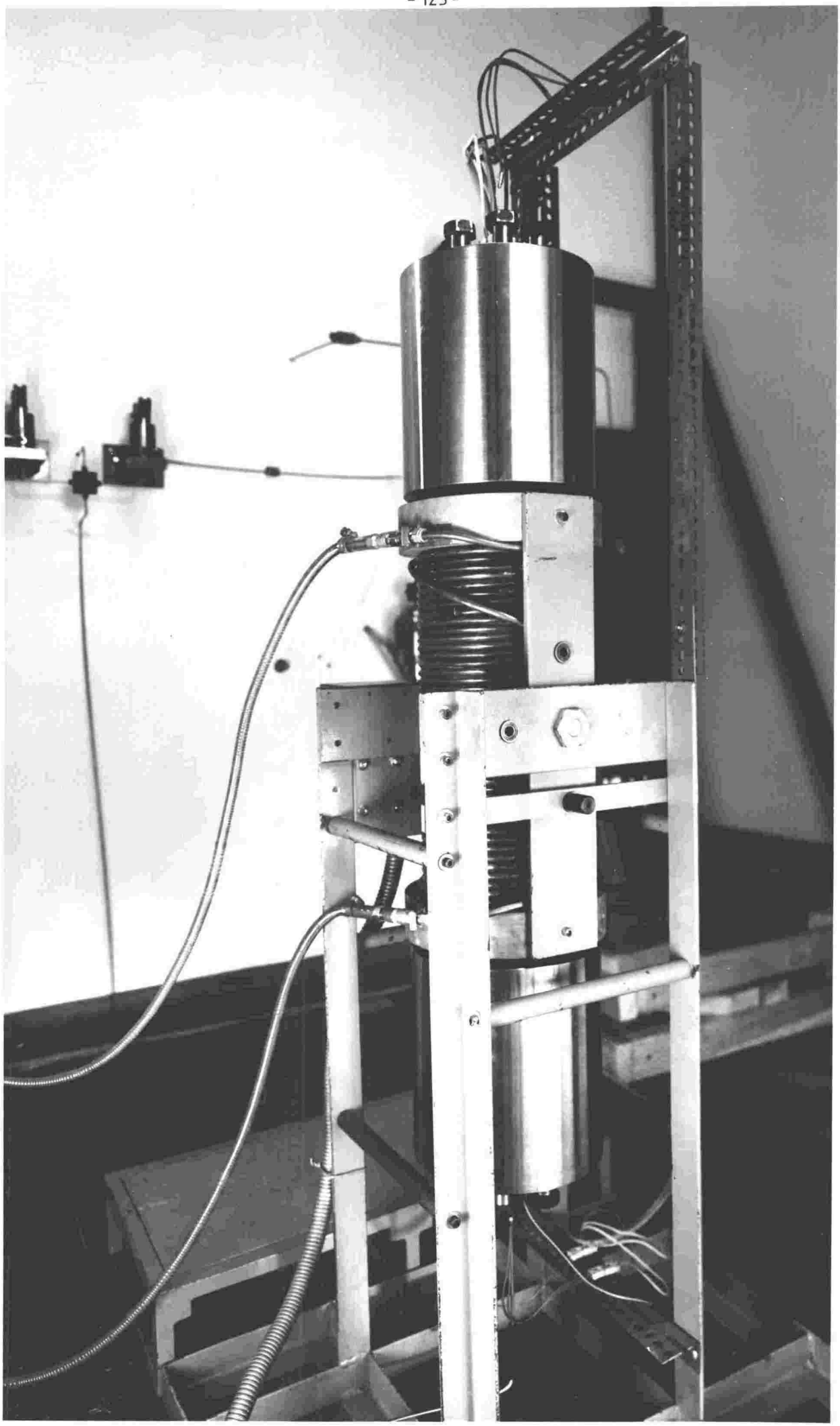

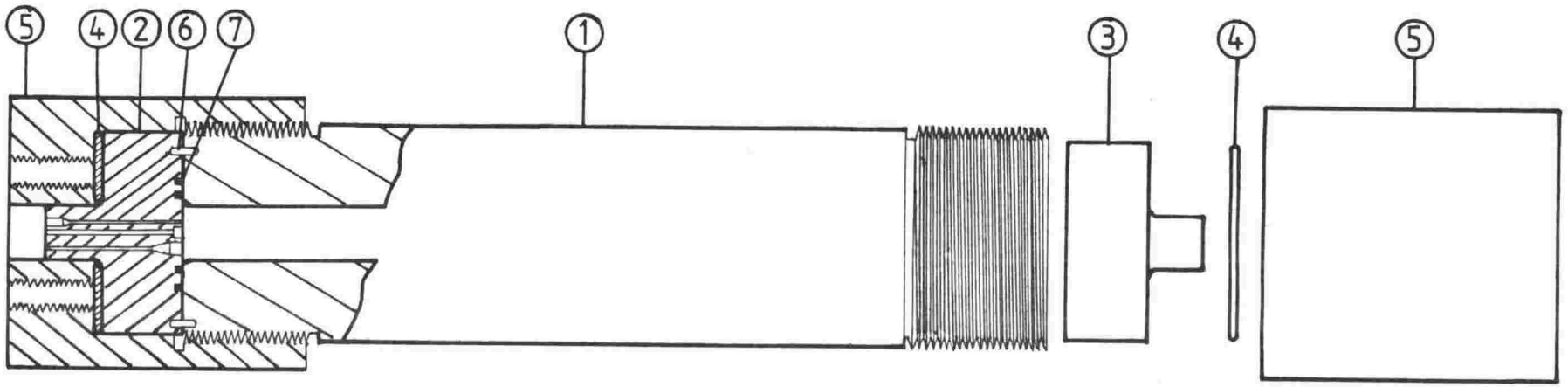

Item no.	Description
1	Pressure vessel body
2	Mushroom head A
3	Mushroom head B
4	Compression ring
5	Closure head
6	Dowel pin
7	"O" ring

Figure 3.2—5 kbar Internally Heated Pressure Vessel

General Assembly

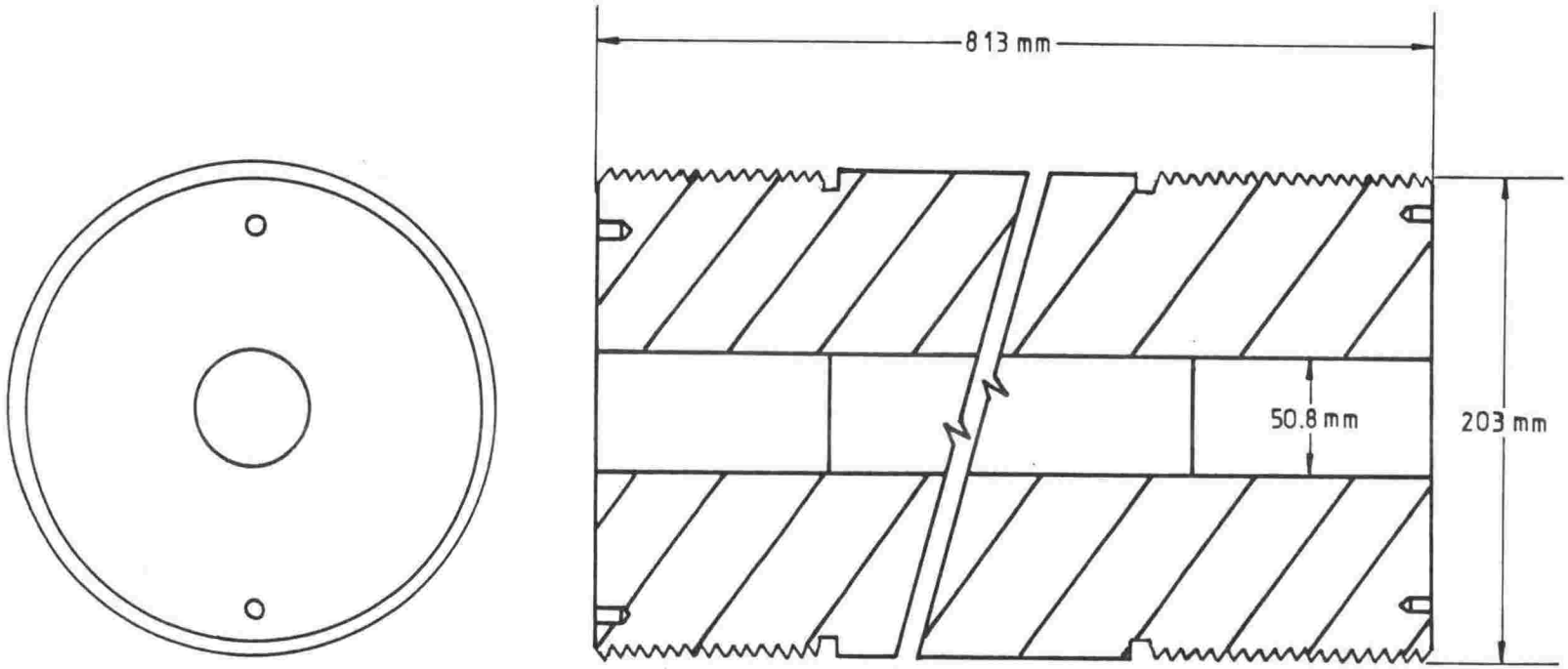

Figure 3.3—5kbar Internally Heated Pressure Vessel
Pressure Vessel Body

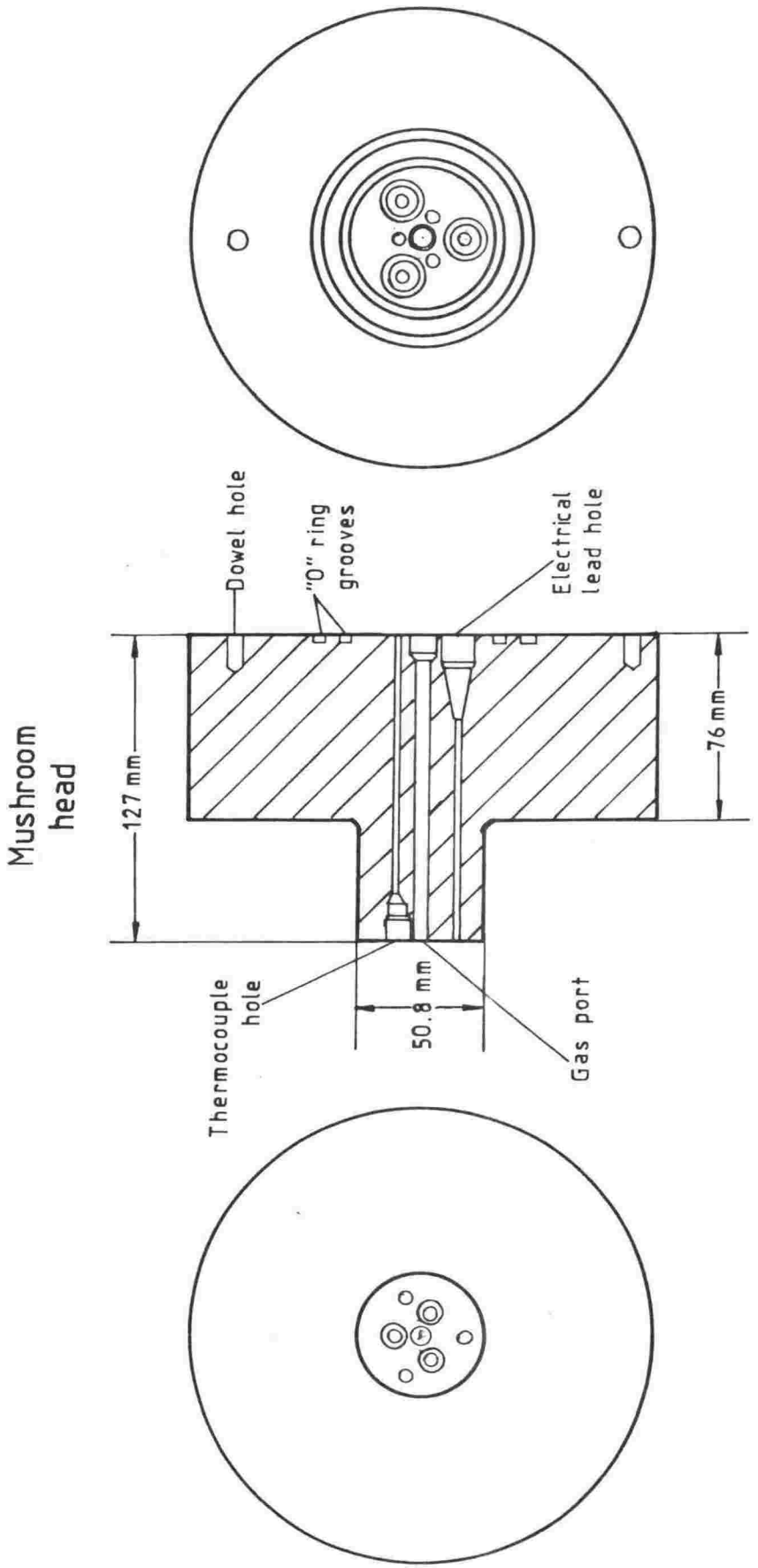

Figure 3.4 – 5kbar Internally Heated Pressure Vessel
Mushroom Head A

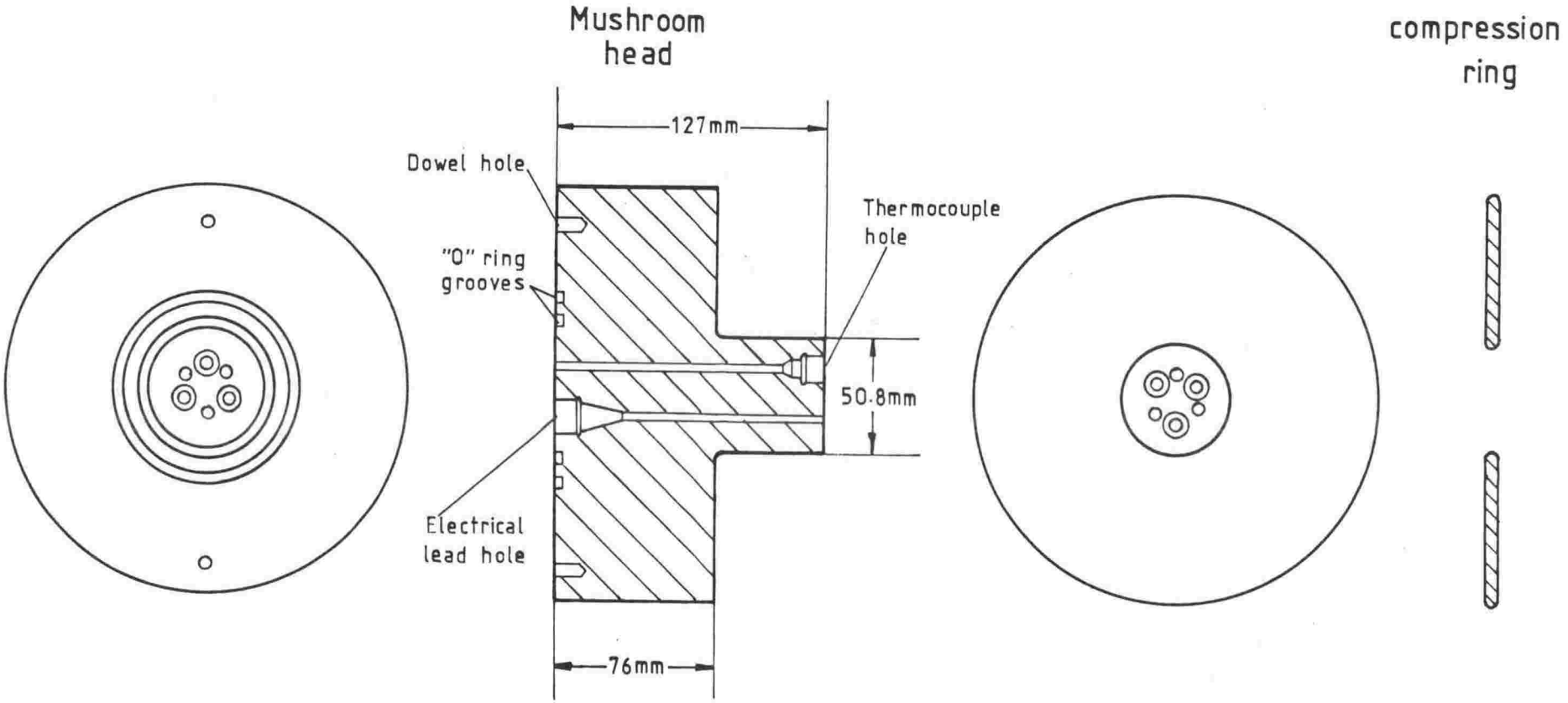

Figure 3.5—5 kbar Internally Heated Pressure Vessel
Mushroom Head B and Compression Ring

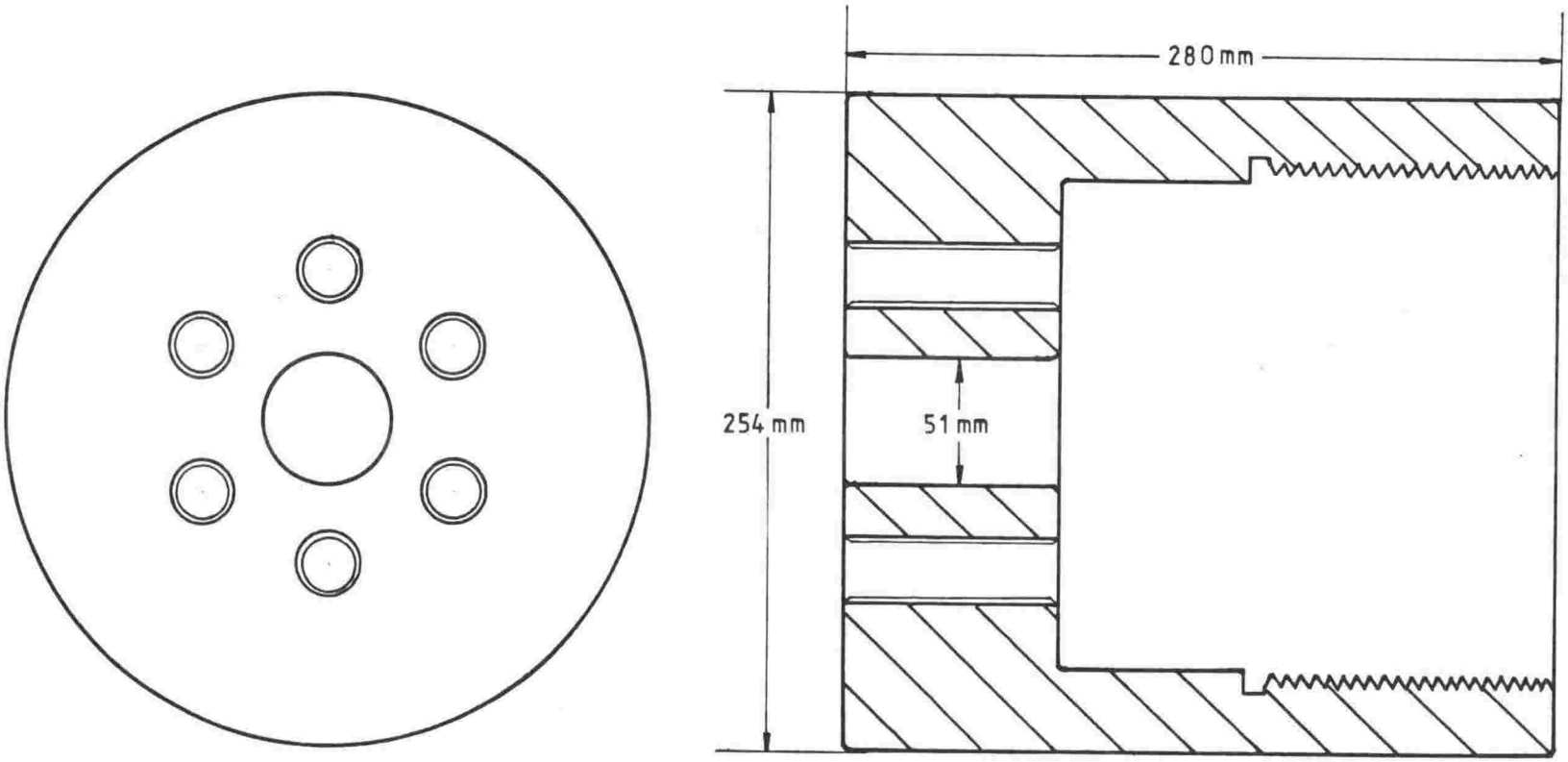

Figure 3.6—5kbar Internally Heated Pressure Vessel
Closure Head

compression rings and mushroom heads were ground by Bohler Steels as part of the contract. Further grinding and lapping of the faces of the pressure vessel body and mushroom heads was necessary to ensure that adjoining faces mated sufficiently well for the '0' ring sealing method to work. This was accomplished by grinding each of the faces with silicon carbide grit of varying size down to 600 mesh, followed by lapping together the two mating faces using 600 mesh grit and brasso. Suitable sealing faces were obtained when, on blueing one surface and torquing the bolts in the closure head to 80 ft lb, the dye uniformly and continuously covered the adjoining face.

An important requirement for I.H.P.V.'s is, that the temperature of the wall in the bore of the pressure vessel does not exceed 300^{o}C. Copper cooling coils were fitted by Victoria University of Wellington Workshops to the pressure vessel body and the top closure head (Plate 3.2).

As already noted, gas pressurised internally heated vessels are potentially dangerous. For safety reasons the pressure vessel was housed in a specially designed room in the Joint Mineral Sciences Research Laboratory, Cotton Building, Victoria University of Wellington. The safety features of this room include the following:

1. Sufficient volume in the room (3.2 x 3.0 x 3.6)m to contain a gas explosion.
2. Wall cladding that would absorb energy from a gas explosion and also dissipate the energy of projectiles rather than reflecting them.

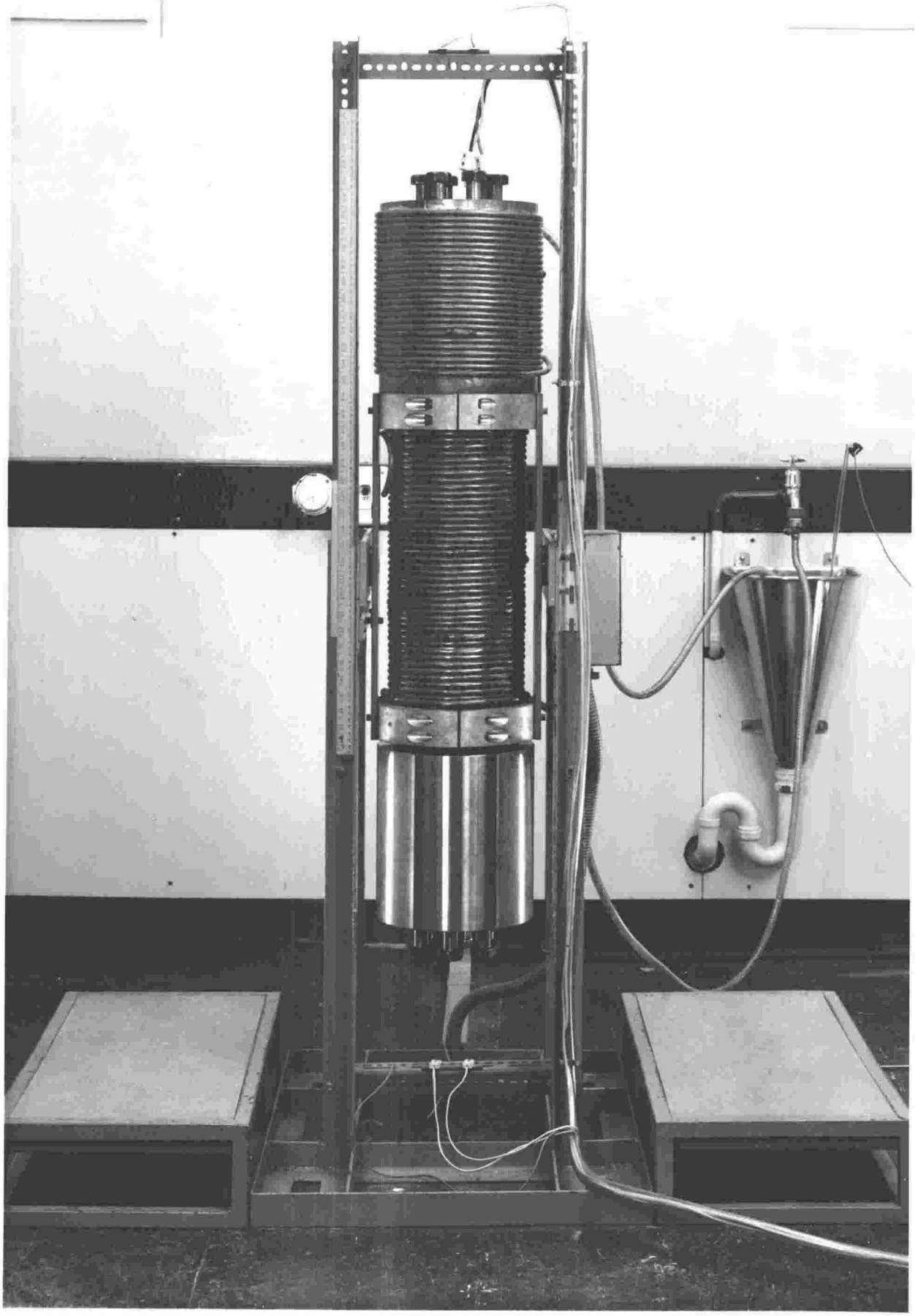

3. Four large swinging doors, each (0.8 x 3.6)m, make up one wall. These heavy doors are designed to absorb energy from a shock wave resulting from a gas explosion.

This room was also equipped with a 1 ton chain and block which hangs from a carriage running on a R.S.J. beam. This crane is used for moving the pressure vessel (~400 kg), for lowering the mushroom head assemblies (~20 kg) and the closure heads (~40 kg) into position. Experiments in the vessel were monitored from outside the safety room.

At each end of the pressure vessel there are six bolts which have to be tightened down to seal the mushroom head 'O' rings against the pressure vessel face. It was found that these bolts required torquing to 180 ft lb to achieve a seal up to the experimental pressures reached.

3.2.2 High Pressure Seals

3.2.2.1 Introduction

Internally heated pressure vessels, in general, require four types of high pressure seal:

1. Seals between the pressure vessel body and the mushroom heads to seal the pressure vessel components together.
2. Seals made on the inside of the mushroom heads to seal in, for example, power leads, instrument leads, or thermocouples.
3. Seals made on the outside of the mushroom heads; usually to seal in metal sheathed thermocouples.
4. Pressure port seals. In most I.H.P.V. systems there is only one pressure port. It allows the gas pressurising medium to enter or leave the vessel

The principles of high pressure sealing are discussed by Holloway (216) and Edgar and Platt (219) and have been followed here. However, although these principles are straightforward, it was found that substantial trial and error was involved to overcome specific problems associated with some of the seals. Even though the pressure vessel body and components were designed to withstand 5 kbar, the maximum experimental pressure is limited to the pressure that the poorest seal will hold and may be much less than 5 kbar. This section describes the progress towards, and the final way in which each type of sealing was achieved.

3.2.2.2 Mushroom Head "O" Ring Seals

Although the fully supported 'O' ring method of sealing (Figures 3.4 and 3.5) was designed to withstand 5 kbar it was found that viton 'O' rings extruded from their housing and eventually burst, inspite of torquing the closure head bolts to 180 ft lb. The rate of this extrusion was also found to increase when the pressure in the vessel was increased beyond 2 kbar - the normal maximum operating pressure of this type of 'O' ring. It was initially thought that the cause of the collapse of these viton 'O' rings by extrusion might be that they shear too easily. They were replaced by a set of copper 'O' rings, machined in the laboratory. These copper 'O' rings, however, failed at 700 bar. Copper, although requiring a much greater force to shear it than does viton lacks the resilence of viton. It appeared from these attempts to seal the vessel that the mushroom heads were flexing under pressure. This means a small gap was appearing on the outer edge of the 'O' ring housing, sufficient to allow viton or other resilient type 'O' rings to

extrude and keep extruding till the '0' ring burst. Also, in the case of copper '0' rings under the same conditions, since they lack resilience, gas would escape when the mushroom head flexed under pressure. To overcome this flexing problem it was necessary to have a resilient '0' ring, so as to take up the gap when the mushroom head flexed and a way of stopping the '0' ring extruding. The latter was achieved by machining anti-extrusion rings (Figure 3.7). They were fitted into the grooves in the mushroom heads. When the closure head bolts were torqued down these rings were clamped against the surface of the pressure vessel face. These anti-extrusion rings plus neoprene or viton '0' rings proved satisfactory, with very little extrusion, to 2 kbar. Other seals in the pressure vessel caused problems and so these anti-extrusion rings were not tested above 2 kbar.

3.2.2.3 Pressure Port Seal

Mushroom head A (Figure 3.4) was machined to allow 1/4 inch diameter pressure tubing to be used for the pressure port. However, this size tube did not allow sufficient room to rotate the hexagonal heads of the three thermocouple gland nuts without them being reduced in size. This in turn increased the difficulty of tightening these gland nuts and consequently their respective seals. A 3/16 inch diameter tube, however, left adequate space to rotate the three gland nuts without the need to mill the hexagonal heads down. This size tube was threaded at one end, fitted with a sleeve to take up the difference in diameter, and silver-soldered in place. A cone with 59° included angle was machined on the inside end of this sleeve. The cone and tube was then coated with

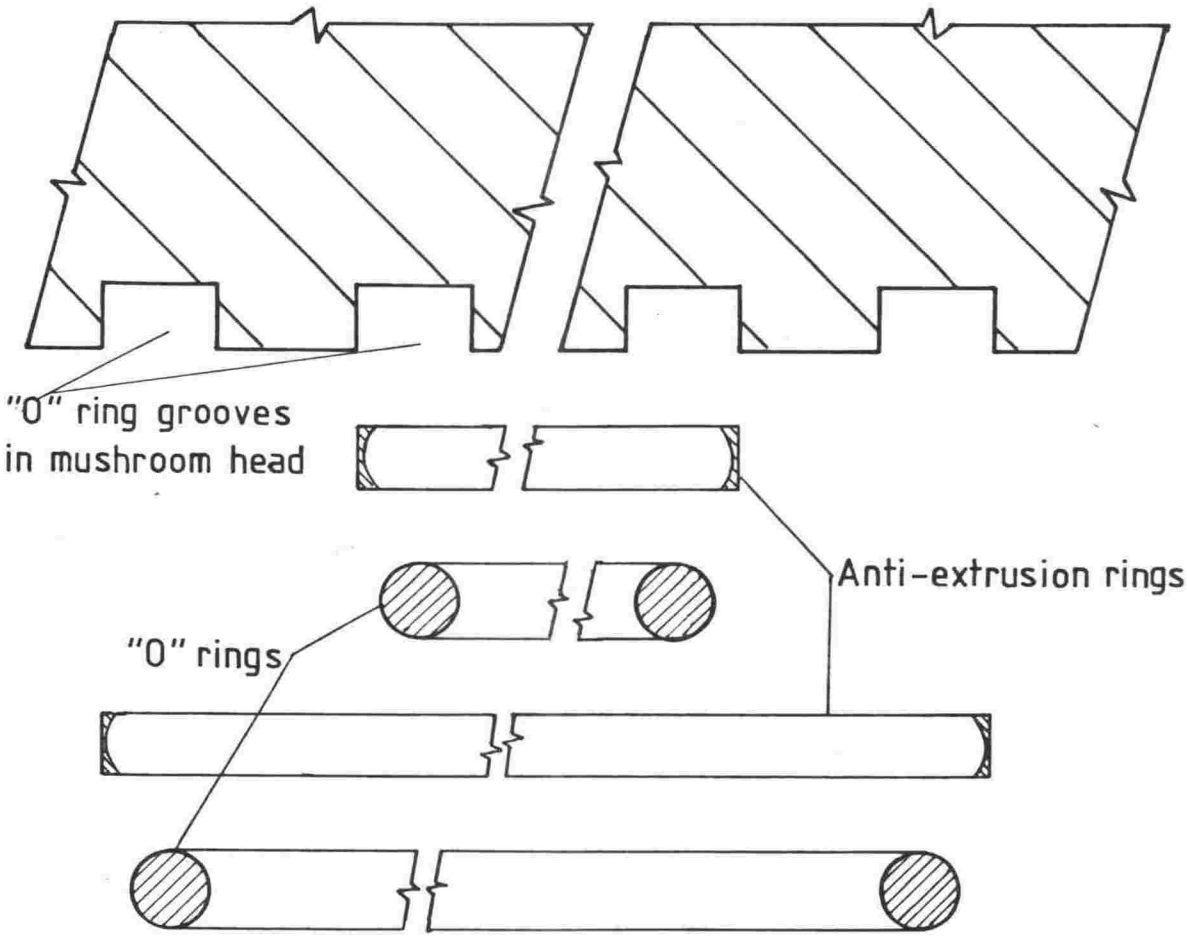

Figure 3.7— Anti-extrusion rings.

plumbers' solder as was also the inside of the counter-bored hole in the mushroom head. Finally, the tube was pressed, using a hydraulic press, into the mushroom head causing the cold solder to flow and thus cause a seal. The free end of this short piece of high pressure pressure tubing was connected onto the high pressure gas line.

3.2.2.4 Power and Conductance Lead Seals

These were made in the 18^{o} included angle counter bored cones on the inside of the mushroom heads (Figure 3.4). The power leads had to be insulated to carry 120 volts at 30 amperes. The principle involved in this type of seal is as follows: a gland nut forces a conical plug into a cone in the mushroom head to create an initial seal; the pressure in the vessel aids the seal by pushing the plug further into its cone. Beryllium-copper conical plugs were machined and 2.34 mm diameter brass rods were silver-soldered into the nose and tail of the cone. A hollow pyrophyllite (non-heat treated) cone, coated with teflon spray, was used to insulate the beryllium-copper plug from the mushroom head. To insulate the tail of the beryllium-copper cone from the gland nut and to insulate the brass rod passing through the centre of the gland nut appropriately shaped pieces of pyrophyllite were machined and heat treated. However, this pyrophyllite proved too fragile and was replaced with a teflon plug which was machined to fit over the brass rod and act as a washer between the end of the gland nut and the tail of the beryllium-copper cone (Figure 3.8). The only drawback with teflon was that it flowed under pressure and the gland nuts consequently required torquing down several times to 50 ft lb before an initial seal was

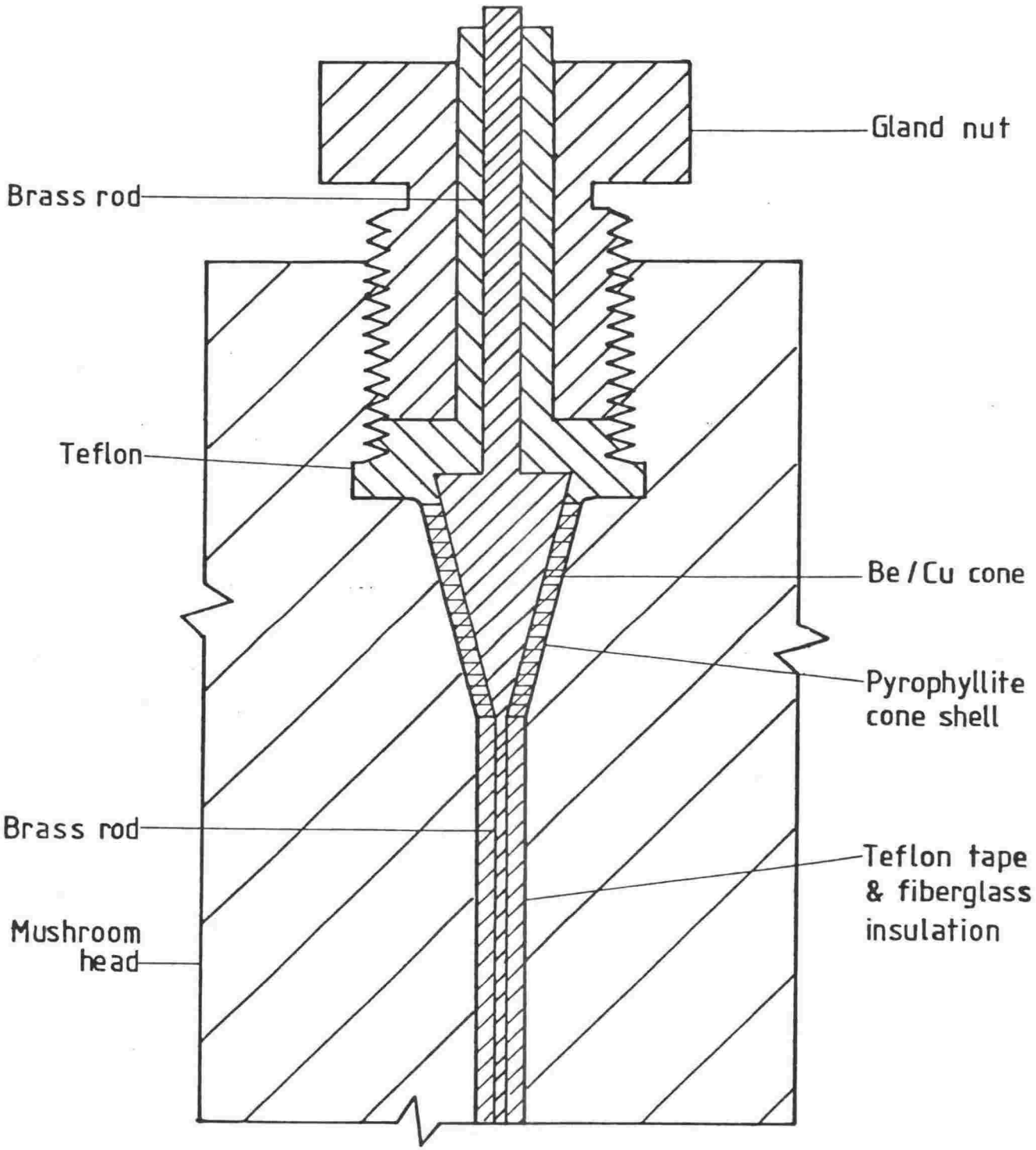

Figure 3.8—Power lead seal.

achieved. The brass rods passing through the mushroom head were insulated with teflon tape and fibre glass sleeves. A megger was used to check that the leads were electrically insulated from the mushroom head.

The conductance leads were sealed in an identical way to the power leads except that less insulation was required since the voltage of the conductance leads was very small compared to the power leads. One of the type 'C' holes in mushroom head A was not required for a conductance lead and was sealed with a dead plug.

3.2.2.5 Thermocouple Seals

These seals were made on the outside of the mushroom heads in a 60^{o} included angle cone for: (1) ease of replacement and (2) because of insufficient room on the inside of the mushroom head. This type of seal is made by deforming a soft stainless steel conical plug in a counterbored cone in the mushroom head. A stainless steel cone and tail was silver-soldered onto a 1 mm diameter inconel sheathed thermocouple (Figure 3.9). To take up the discontinuities in the counterbored cone in the mushroom head an annealed silver cone shell was fitted before the conical plug on the thermocouple was tightened down with a gland nut.

These seals, compared to the other three types, were found to leak first and thus they set the maximum sustainable experimental pressure - ~1400 bar. The experimental pressure, although much less than 5 kbar - the maximum design pressure, was not, however, a design fault but rather the result of poor machining. Further steel has been obtained to re-machine the mushroom heads and thus rectify this problem.

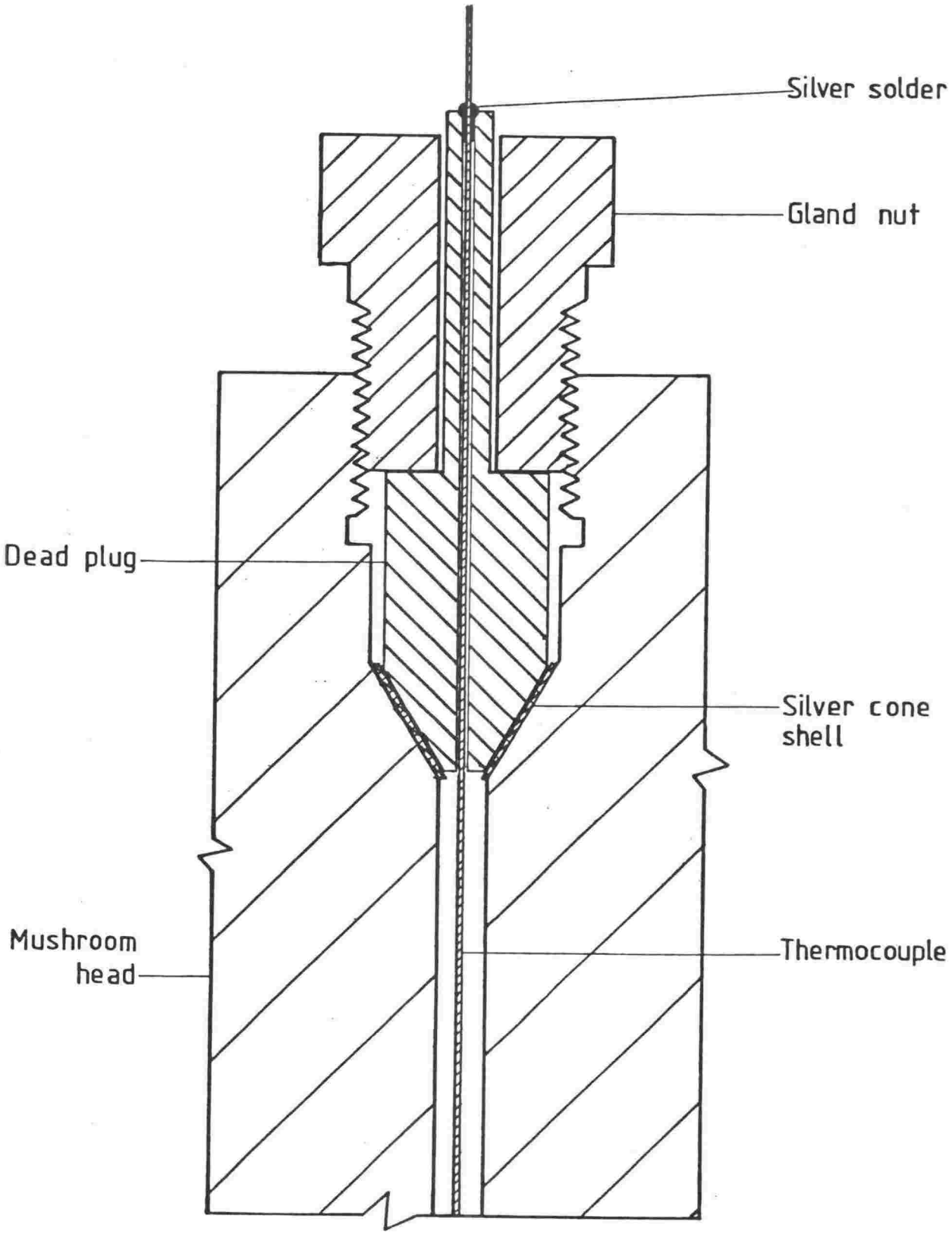

Figure 3.9— Thermocouple seal.

3.2.3 Pressure Generation and Measurement

Pressure is generated by a two stage compressor system (Plate 3.3) plus an intensifier (Plate 3.4) and is capable of producing up to 14 kbar gas pressure. The first compressor (Hochdruck[1], diaphragm transfer compressor) receives gas from a commercial argon cylinder (18-150 bar) and pressurises it to 350 bar in a storage cylinder. The second stage compressor (Hochdruck[1], diaphragm transfer compressor) increases the pressure to 2 kbar and passes it to the intensifier (Harwood[2]) which can generate gas pressures up to 14 kbar as required. Since the experimental pressure in this study did not exceed 2 kbar, the intensifier was not used.

Argon gas pressure from the second compressor was measured by a 250 mm diameter Budenberg gauge, capable of measuring pressures up to 3.5 kbar. A Heise gauge of 450 mm diameter with 10 bar divisions up to 7 kbar was used to measure the pressure in the pressure vessel. All high pressure tubing and fittings used, linking compressors, gauges and the pressure vessel, were made by Aminco[3]. However, the two high pressure needle valves (Plate 3.4) for isolating the pressure vessel were made by Victoria University of Wellington Workshops. These valves were based on a design by Stanford University Earth Sciences Laboratory.

---

[1] Andreas Hofer, Hochdruck-Apparatebau GmbH, 433 Mulheim, Friedrich-Freye-Straße 59-61, West Germany.

[2] Harwood Engineering Company, Inc., South Street, Walpole, Mass., U.S.A.

[3] American Instrument Company, now known as: Superpressure Inc., 8030 Georgia Avenue, Silver Spring, Maryland 20910, U.S.A.

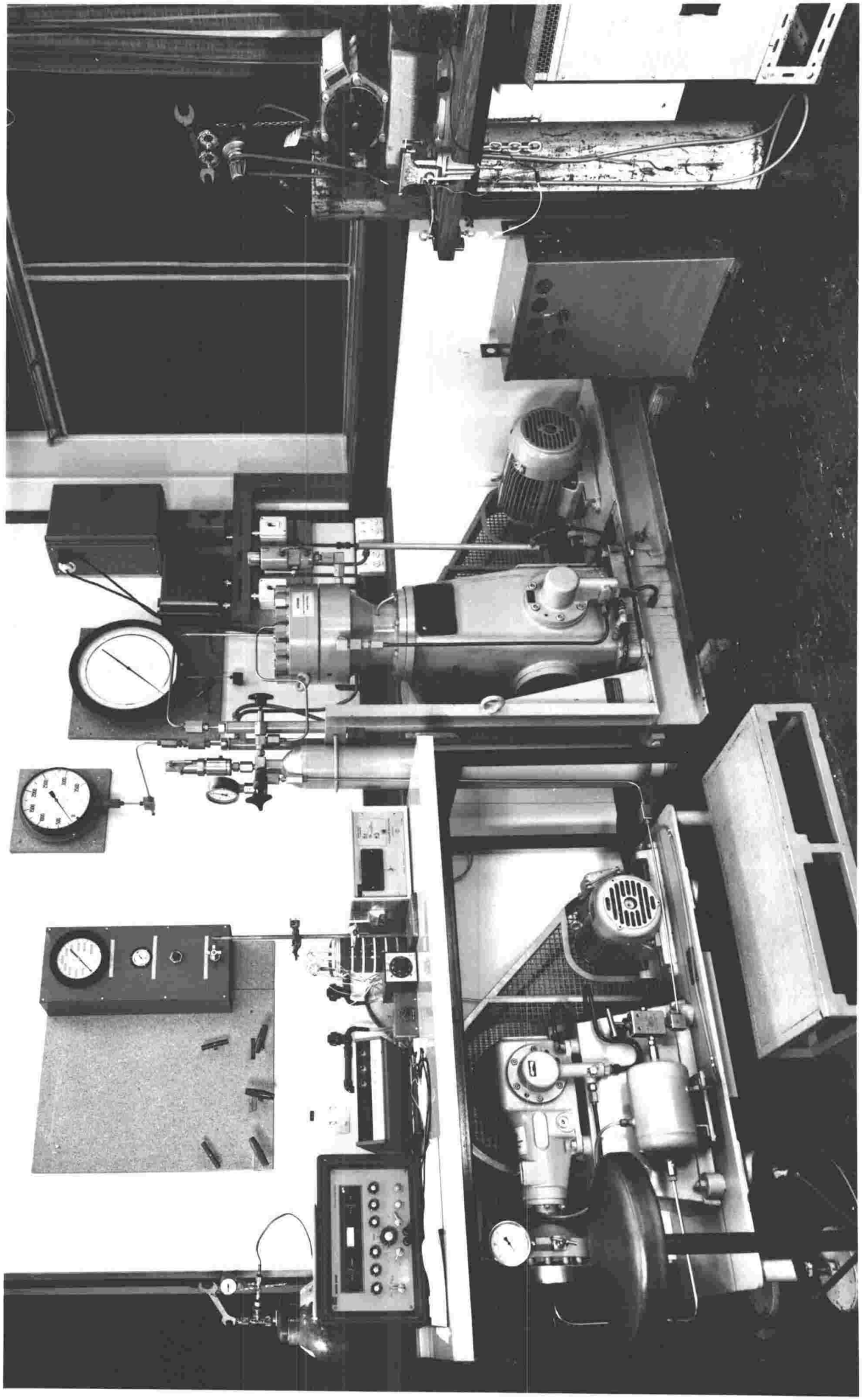

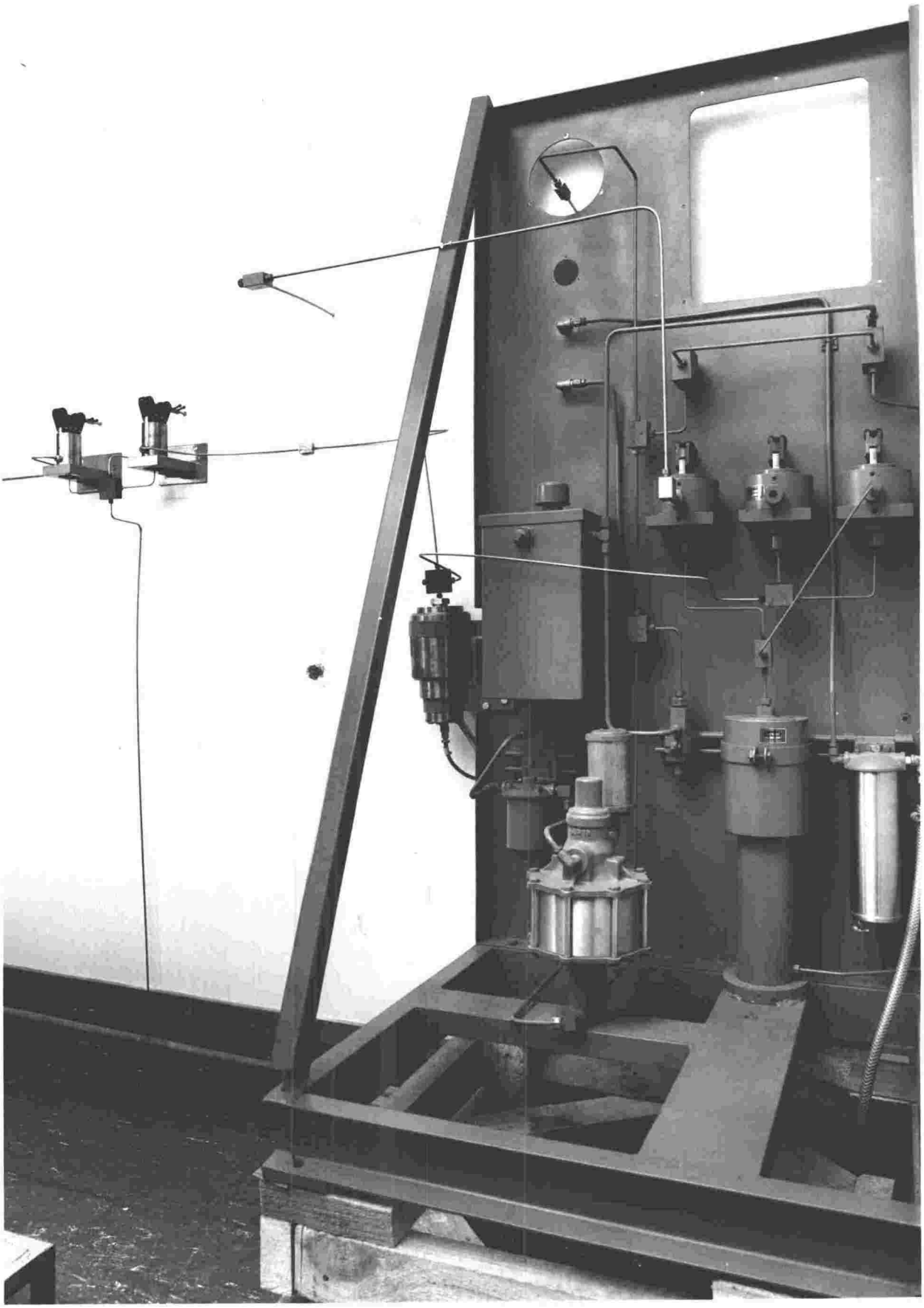

3.2.4 Furnace and Furnace Mounting

Generally a furnace for an internally heated pressure vessel is of the helically-wound resistance element type (216). Since the temperature distribution, which is established by gas convection, must be controlled over the largest possible region of zero-temperature-gradient, the furnace is normally operated with its long axis vertical. The flow of convecting gas can be minimised by filling all open space with pyrophyllite. Changes in temperature and pressure alter the density of the gas medium and this causes the position of the zero-temperature-gradient region to shift. In order to control the length and position of this region it is necessary to have at least two separately powered resistance elements. The power requirements of the furnace and thus its length, diameter of resistance wire, and the number of turns/inch are determined by the length of the region of zero-temperature-gradient, maximum temperature and pressure required. The above considerations imply that the furnace has to be designed first, and then the electrical equipment to operate such a furnace.

The furnace for the present I.H.P.V. was required to reach and maintain a constant temperature of 1200°C over an adjustable length of ~60 mm. The design of the furnace was constrained by the bore (50 mm) of the pressure vessel (restricting the interior diameter of the furnace and space for insulation) and by the fact that there can only be a maximum of three power leads to the furnace (limiting the number of independent elements to two). Based on the above requirements and constraints, and following the guidelines given by Holloway (216) a furnace was designed and is described in the following paragraph.

The furnace is of the helical element type with a centre tap. The internal diameter of the furnace is 23 mm and it is ~250 mm long. 16 gauge Kanthal A1 resistance wire (rated to 1300°C) is used to form a helically wound element with 10 turns/inch. Each 125 mm of winding contains ~3600 mm of resistance wire which has a resistance of ~4 ohm. At a maximum of 120 volt each winding produces ~3.6 kwatt which is more than sufficient to maintain the desired conditions.

A furnace was fabricated by positioning a helically wound element onto a wooden former and coating it with an alumina cement. When the cement was dry, the wooden former was slowly burnt out leaving the element encased in cement. Plate 3.5 shows a furnace after this process along with a furnace sleeve. The furnace sleeve was designed to fit between the cell and the furnace wall so that if the cell ruptured the furnace would not be contaminated.

The whole furnace assembly is shown in Plate 3.6. The furnace was positioned to be in the centre of the pressure vessel along its longitudinal axis. A pyrophyllite column was made to fill the space between the top of the furnace and the face of mushroom head B. This column consists of pyrophyllite disks cemented together with sauereisen cement along with a 30 mm length of pyrophyllite plugging the top of the furnace. Further sauereisen was used to seal the pyrophyllite column to the furnace. Three holes near the edge of the column allow the power leads to be threaded through with minimal clearance. Two smaller holes near the centre of the column permit the thermocouples to be inserted into the furnace from the exterior of the mushroom head. The three power leads emerging from the column were silver-soldered to the brass rod

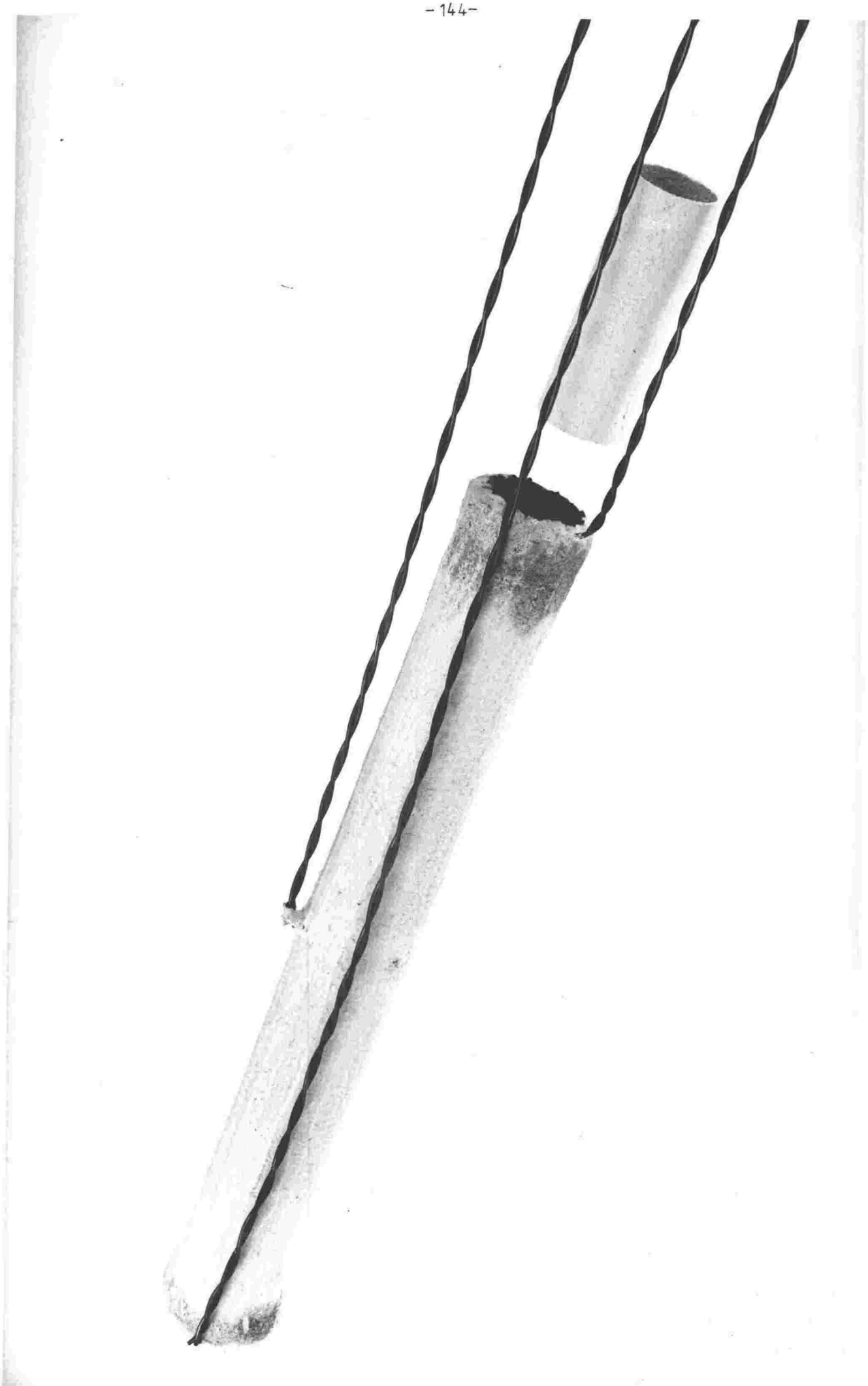

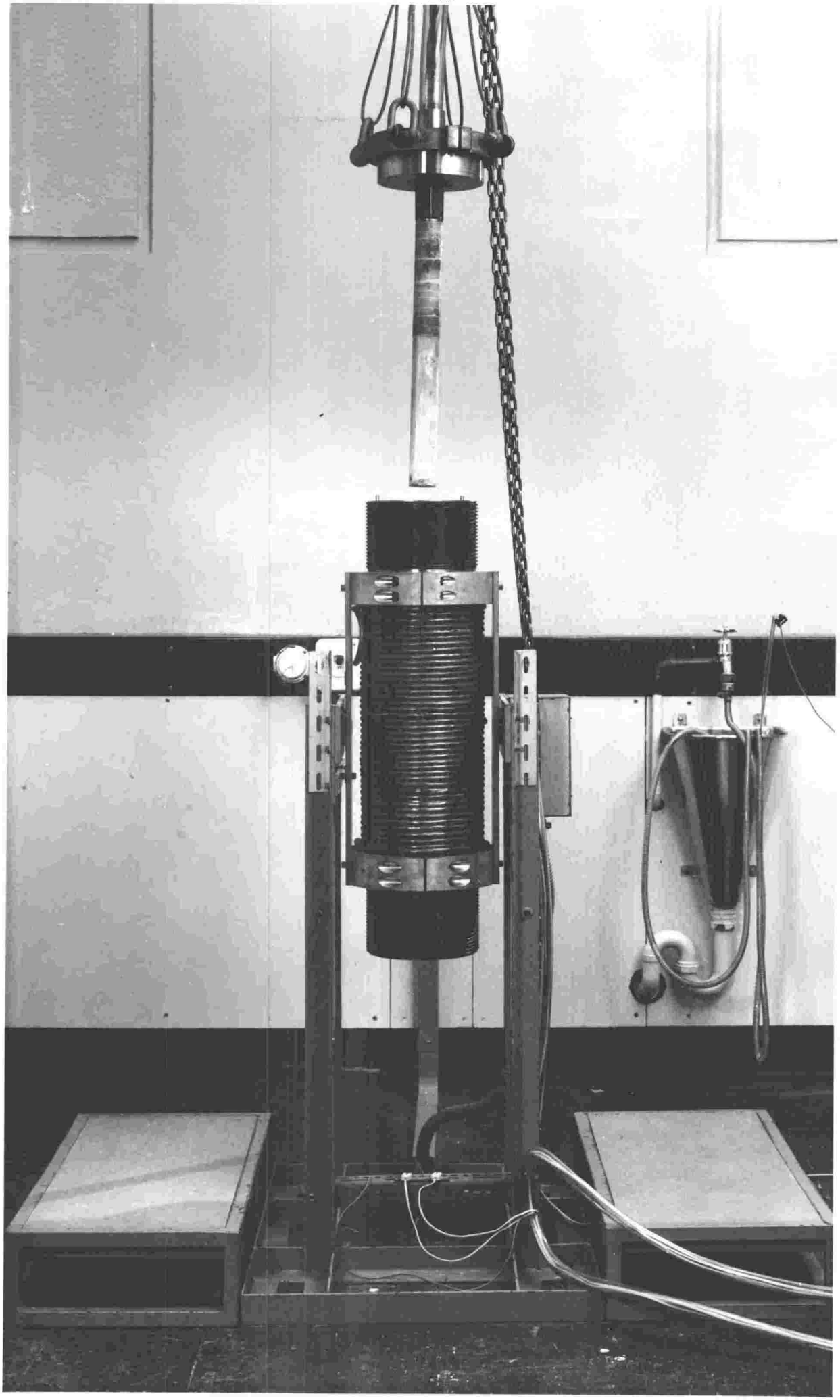

tails of the beryllium-copper cones sealed into the mushroom head. To support the furnace assembly beneath the mushroom head a metal plate was attached to the top of the column with three screws; from this plate a rod screwed directly into the mushroom head and was held firm with locking nuts. Once attached in this manner further pyrophyllite pieces were fitted around the power lead gland nuts to fill the remaining space.

3.2.5 Furnace Insulation and Minimizing Convection Currents

To achieve the desired temperature distribution inside the furnace of an I.H.P.V., careful attention must be paid to the furnace insulation. Not only is this insulation to minimize gas convection, a major problem in this type of high pressure work, and to retain the heat in the furnace, but also to keep the temperature of the pressure vessel wall below 300°C (216). The latter requirement is important because the rupture pressure of the vessel is greatly reduced as the temperature of the metal increases.

Holloway (216) describes two types of furnace, one of which is insulated with a high temperature fibre or cloth and the other with a similar insulation material but soaked in a slurry of alumina cement before being wrapped around the furnace. The first type was operated up to 900°C although no indication of temperature gradients in the furnace was given. The second type, as described by Holloway, could be operated at 950-1000°C with a 75 mm long region of zero-temperature-gradient. A high temperature silicate fibre insulation, fibrafax, similar to what Holloway describes, was tried in the present work. It was found to work

well at one atmosphere with the temperature of the pressure vessel wall not exceeding 150°C when the temperature in the furnace was 1000°C. However, when the vessel was pressurised to ~500 bar a ~200°C temperature gradient was produced over the length of the cell. This gradient increased as pressure was increased. Fibre insulation under these circumstances is unsuitable because it is too porous and thus allows convection of the gas pressurising medium.

Fibrafax insulation was replaced with a non-porous alumina cement. The furnace (Plate 3.5) was attached to the pyrophyllite column by threading the power leads through it. Sauereisen cement was used to cement the furnace to the pyrophyllite column and block up all gaps. This minimized the path for diffusing gas from the top of the furnace. The column and furnace unit was then placed in a wooden mould with an internal diameter just less than the bore of the pressure vessel. Alumina cement was poured around the furnace till the mould was full. It was left to dry and then fired to remove all water.

After positioning this furnace assembly in the pressure vessel (Plate 3.6) the clearance gap was packed with alumina powder. A fibrafax gasket, fitted over the end of the furnace, kept the powder in place when the pressure vessel was inverted. The distance between the end of the furnace and the open end of the pressure vessel was measured and the length of the conductance cell assembly (section 3.3.2) was adjusted so that, when it was lowered into position, the larger diameter part of the pyrophyllite column pushed firmly against the fibrafax gasket. In this way the interior of the furnace was partially sealed from the rest of the pressure vessel interior. The path for convecting gas on the outside

of the furnace was minimized by the non-porous cement. It was found, over the temperature and pressure ranges of this study, that the temperature gradient between the ends of the cell could be reduced to +/-5°C. Also, it was found that the power requirements, using the non-porous insulation, were greatly reduced compared to the porous insulation.

3.2.6 Electrical Equipment and Power Supply for the Furnace

The design of the electrical system for the I.H.P.V. depended in the first instance on the type of furnace that would reach and maintain the desired temperatures. The furnace designed, described in section 3.2.4, operates at 120 volt. The reason for operating at 120 volt is to allow the optimum resistance wire diameter to be used. Since mains voltage is 240 volt a transformer was necessary. A 9 KVA single phase transformer with dual primary (230 and 400 volt) and with a centre-tapped secondary delivering 120 volt either side of centre with taps at 40 volt intervals all rated at 35 ampere was constructed by N.Z. Transformers Ltd[1]. The dual primary, extra taps and surplus power to the present requirements were included to give the system increased flexibiltiy in case of alternative furnace designs. It was found that once adequate insulation around the furnace was achieved the design requirement of 7.2 kWatt was much more then was necessary.

The 400 volt primary of the transformer was supplied by connecting across two phases through a control box (Plate 3.3) containing two three-phase power relays and two specially made 5 ohm resistors. These

---

[1] N.Z. Transformers Ltd., 5-17 Gregory Street, Naenae, Wellington, New Zealand.

form a two-stage start, to limit the peak current should the transformer core saturate momentarily during the first few cycles at switch-on. This control box also contains facilities to switch the electrical system off should the cooling water supply fail.

An electric cable, in conduit, was taken from the secondary side of the transformer to a box bolted onto the pressure vessel frame. From this box three heavy-duty flexible leads emerge with ceramic connectors on their free ends for attaching to the power leads in mushroom head B.

3.2.7 Temperature Control and Measurement

The overall temperature of the furnace was controlled using a potentiostatic thermostat controller (Ether mini, series 17-90 B). This controller activated, via an electronic system the two three-phase relays on the primary side of the transformer. A chromel/alumel thermocouple, positioned about 35 mm below the top of the furnace, was used as the temperature sensor for the controller.

To adjust the temperature gradient in the furnace, two proportional power controllers, mounted in the transformer, were fitted to each phase on the secondary side of the transformer. These controllers allowed the power supply to each half of the furnace to be independently varied from zero to full power.

Plate 3.7 shows the temperature monitoring equipment and the furnace controller. Chromel/alumel thermocouples, 1 mm in diameter, inconel sheathed and earthed were used to measure the temperature. They were initially calibrated against the melting points of ice ($0^{\circ}C$), zinc ($419^{\circ}C$) and sodium chloride ($800.4^{\circ}C$). The thermocouples were

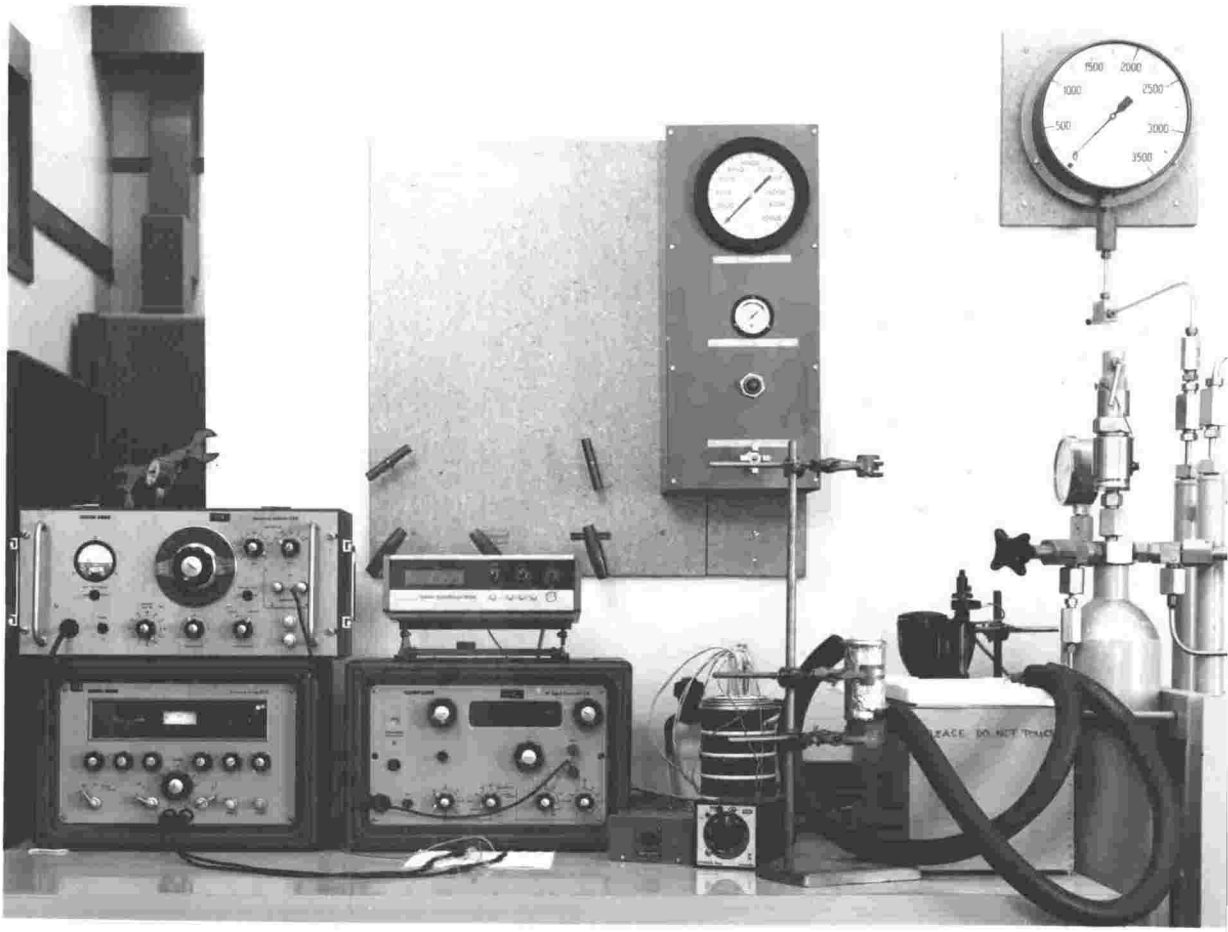
1500
2000
1000
2500
500
3000
0
3500

connected, using compensating cable, through an ice/water junction, via a switching box, to a digital voltmeter with a +/-0.1 mV accuracy. Four thermocouples were used to measure the temperature at various positions in the furnace. Two were part of the furnace assembly, of these, one was used as the control thermocouple and also to measure the temperature at the top of the furnace and the other one measured the temperature at the top of the cell. The two remaining thermocouples were positioned in the furnace as part of the conductance cell assemblage, one to measure the temperature at the base of the cell and the other to monitor the temperature of the lower element.

It was initially calculated that the region of zero-temperature-gradient would occur approximately in the middle of the upper element. The conductance and furnace mountings were thus constructed so that the cell would be in that position. With the extensive power adjustment available with the two proportional controllers it was found that the cell in this position could be kept in a region of almost zero-temperature-gradient.

3.3 EXPERIMENTAL EQUIPMENT AND TECHNIQUES USED FOR THE ELECTRICAL CONDUCTANCE STUDY

Although electrical conductance is one of the easiest transport properties to measure, under the conditions of very high temperature and pressure the experimental difficulties increase enormously compared to laboratory bench conditions. This section describes the experimental techniques relating to the electrical conductance part of this project. In particular, it discusses the design requirements of the cell, problems in obtaining parts and fabrication difficulties. The experimental run procedure is also described.

3.3.1 Electrical Conductance Cell

3.3.1.1 Introduction

The electrical conductance cell for this study on molten silicates had to meet the following conditions:

1. That it remained hermetically sealed during both temperature and pressure variations to allow variable concentrations of water from dry to saturated silicates and to exclude argon gas, the pressurising medium.
2. That the pressure in the pressure vessel was transmitted to the sample via a volume change in the container resulting in a zero pressure gradient across the wall of the cell.
3. That during the volume change mentioned in (2) the cell constant remained invariant.

Design problems were further complicated by the fact that molten silicates and particularly molten hydrous silicates are extremely corrosive liquids. The only materials, from which to construct the cell, that are inert with respect to these liquids are noble metal and high purity oxides. Even in the case of the oxides they are slowly attacked. Platinum, gold and alumina were the most readily available and suitable materials from which to construct the cell.

3.3.1.2 Description of Cell

The conductance cell designed to meet the above constraints is illustrated in Figure 3.10 and Plates 3.8 and 3.9. Initially, it was thought that a platinum bellows would be the best means of satisfying requirement (2). A bellows would also have the added advantage of

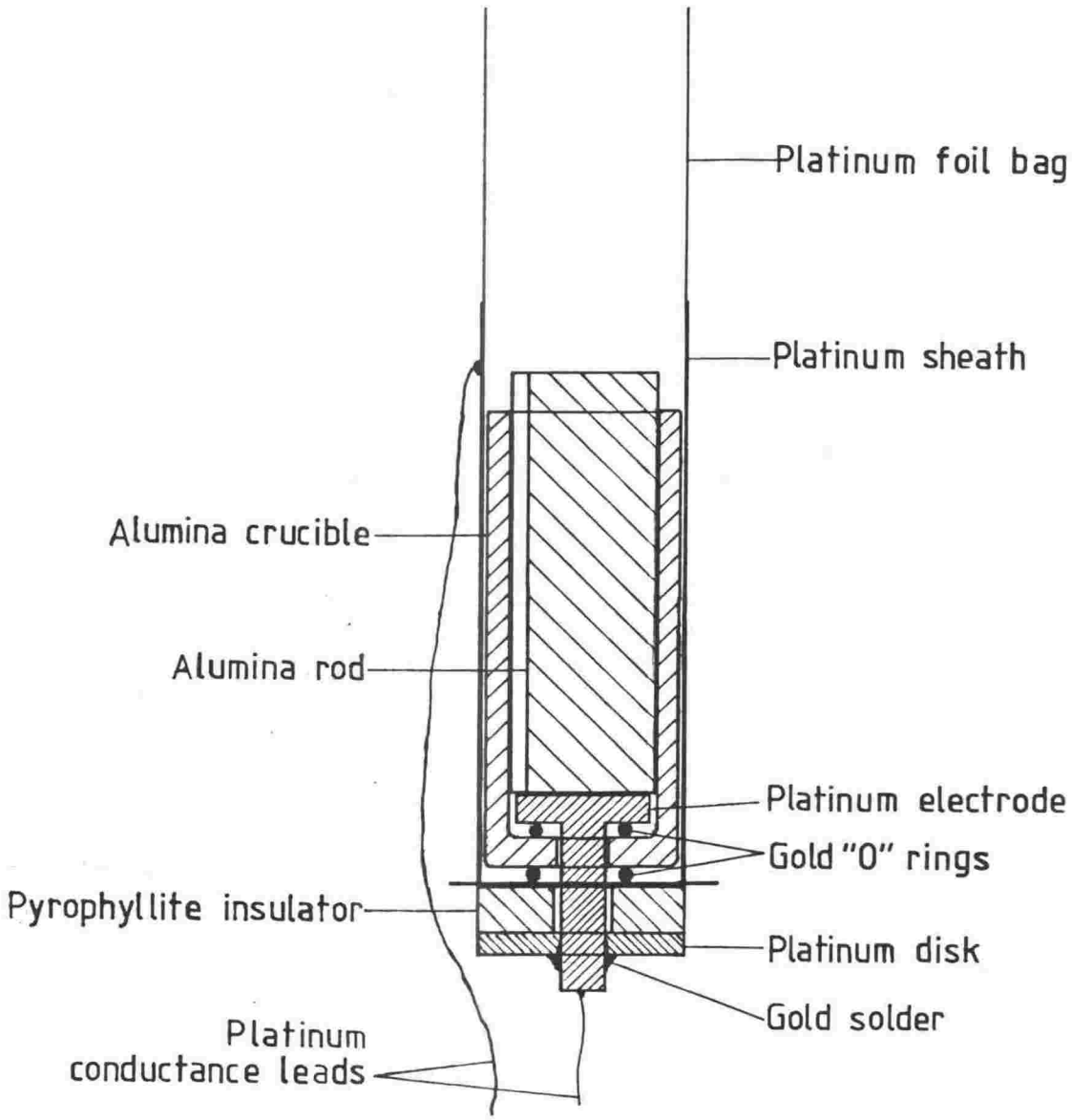

Figure 3.10— Electrical conductance cell.
(Length- 65 mm, diameter- 14 mm.)

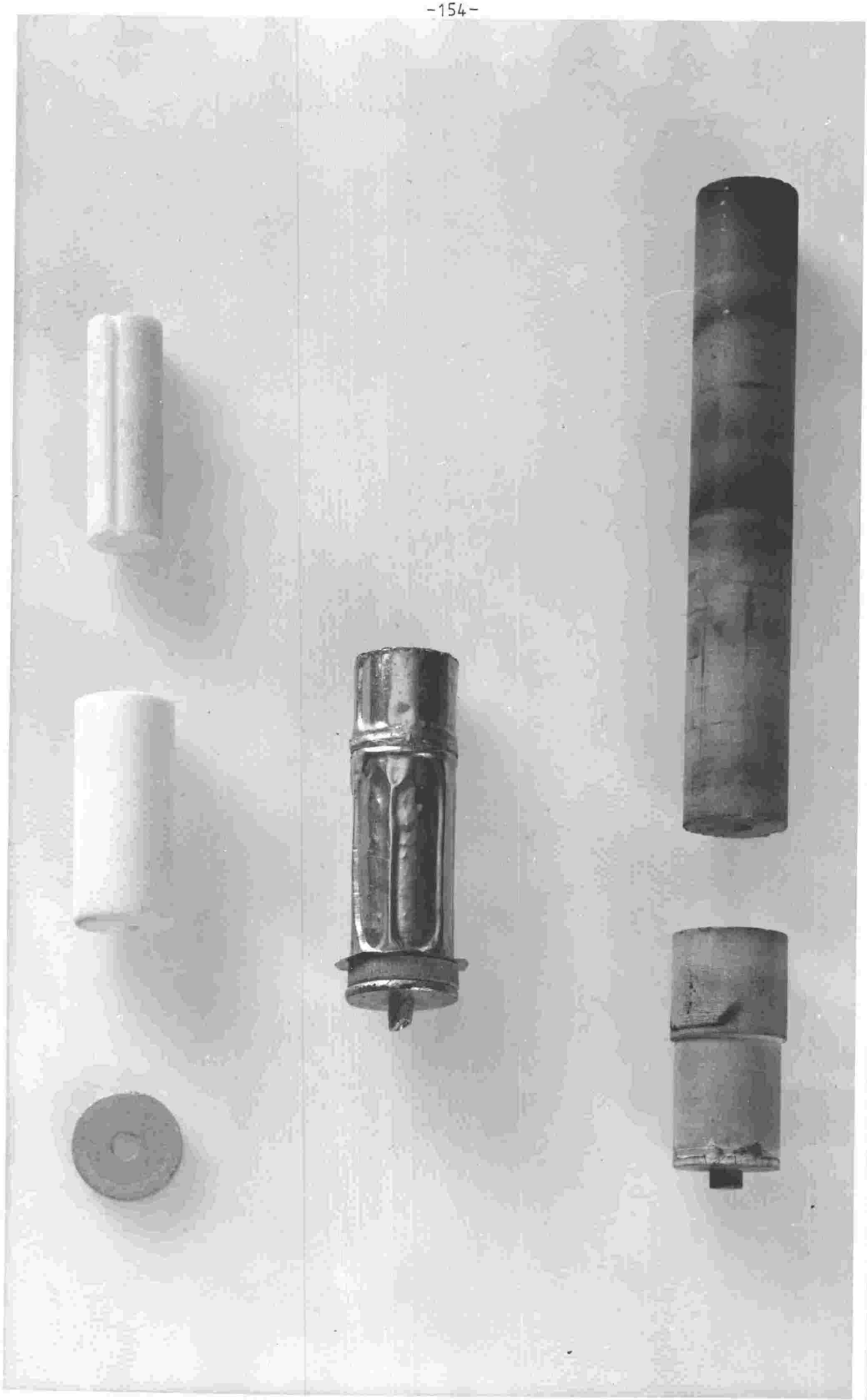

allowing PVT properties of water rich silicates to be measured. However, after a long and unsuccessful search for a manufacturer of such an item, the idea of using a platinum bellows was discarded. Instead, a thin platinum foil bag was used. This foil bag began as a cylindrical tube sealed with gold solder to the platinum sheath around the alumina crucible. After the sample had been loaded into the cell the open end of the bag was crimped in a three-fold manner and sealed with gold solder. This method worked remarkably well. Plate 3.9 shows the cell following an experimental run. At 1000°C the metal was continuously annealed, therefore the process of expanding and contracting due to pressure changes did not cause work hardening of the metal. If the metal had work hardened, fractures along creases in the platinum bag would have been expected. Nevertheless, it was found that the platinum bag had to be replaced after each run due to cleaning problems (section 3.3.1.5). This work with the platinum foil bag showed that a bellows would be difficult to clean and thus impractical.

The alumina crucible and rods were made by Thermal Syndicate[1] and the platinum and gold parts (Figure 3.10) were fabricated in the laboratory. A special jig (Figure 3.11) was used to seal the electrode and crucible into the base of the platinum sheath by clamping together the base parts of the cell and distorting two soft annealed gold '0' rings. While the cell was held in this position gold was melted around the electrode stem and platinum disk to hold the electrode in place. While the cell was still in the jig and hot from the gold soldering operation a platinum wire lead was gold soldered to the protruding stem of the platinum

---

[1] Thermal Syndicate Ltd., P.O Box 6, Neptune Road, Wallsend, Tyne and Wear NE28 6DG, ENGLAND.

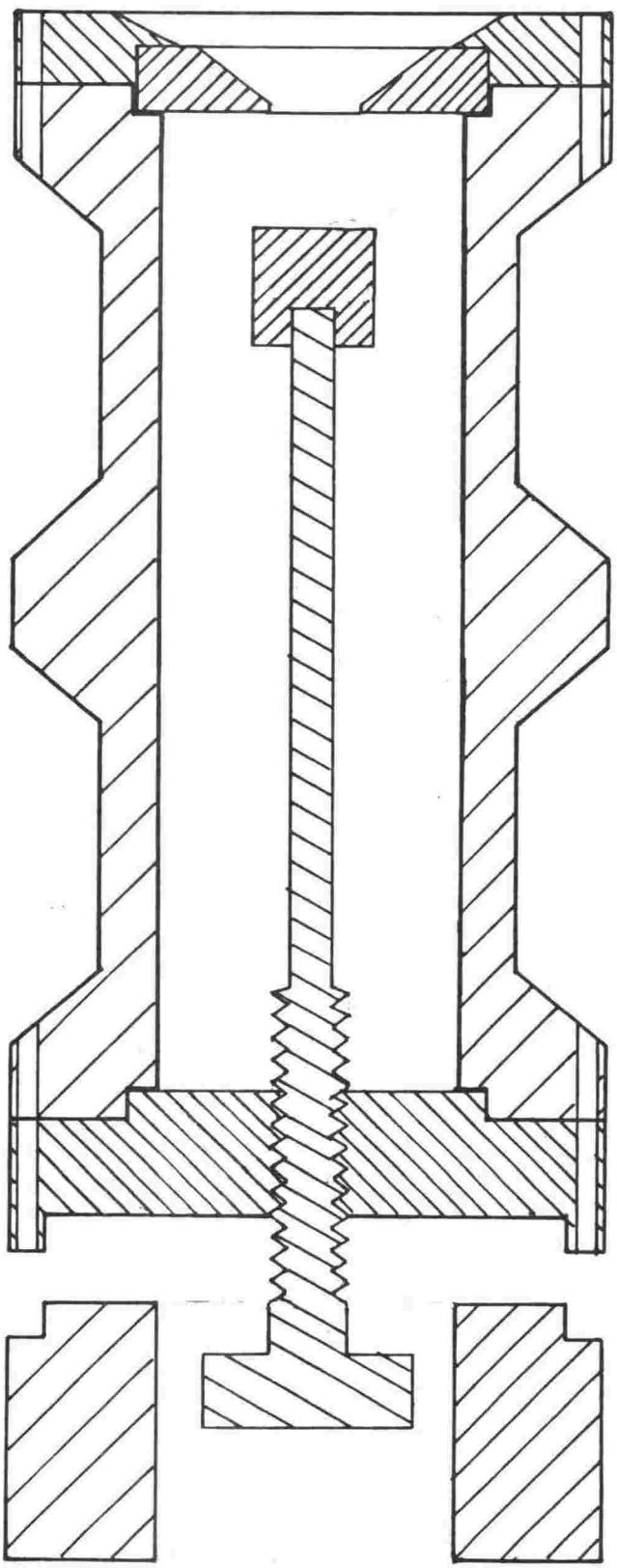

Figure 3.11—Jig for sealing central platinum electrode and alumina crucible into the base of the electrical conductance cell.

electrode. When the cell was removed from the jig a second platinum wire was gold soldered to the platinum sheath, the second electrode. A calculation of the expansivities of the metals, alumina and pyrophyllite showed, that the seal did not open up when the cell was heated to 1000°C, in fact the 'O' rings were distorted still further.

Gold was used in the cell construction because (1) suitable 'O' rings could be made from it, and (2) it was easier to use as a solder for joining the platinum parts together than gold/platinum solders. The use of gold set the maximum experimental temperature to 1000°C

3.3.1.3 Cell Calibration

The cell constant was calibrated using either 0.01M KCl at 25°C in a waterjacket (Plate 3.7) or using literature data of the conductivity of identical silicate compositions to the experimental ones. Conductivity of 0.01M KCl solution at 298.15 K is found by using the Chui-Fuoss equation (85) which holds for concentrations between 0.01 and 0.10 mol dm^{-3}.

$$\Lambda = 14.988 - 9.485c^{1/2} + 2.547c\ln c + 22.0c - 22.9c^{3/2}$$

where Λ, the molar conductivity, has units mSm^2mol^{-1} and c is concentration with units of $moldm^{-3}$. Thus for a 0.01M KCl solution Λ = 14.12 mSm^2mol^{-1} which is equivalent to 0.001412 Scm^{-1} at 25°C. In the present case it was not always possible to achieve a satisfactory calibration due to minuscule leaking of the fluid. However, leaking would not occur with silicate liquids which are ~3 orders of magnitude more viscous than water. In such cases the cell was calibrated against

the literature conductivities of identical silicate compositions as the experimental ones.

It was found that during calibration the conductance varied by 3-4% over a frequency range of 1-20 khz. Consequently, no special procedures were used to determine the cell constant by extrapolation. The value of the conductance used for calibration was measured at 1592 hz.

3.3.1.4 Loading and Sealing the Cell

With the central rod in position (Figure 3.10), included to increase the resistance path between the electrodes, dried silicate powder was carefully placed in the cell with a micro spatula with constant tapping of the cell to ensure maximum packing. When the cell was about three quarters full the top of the bag was shaped to make its rim join along three folds radiating symmetrically from the centre (Plate 3.9). The top was opened slightly and the remaining space in the cell was filled with powder. Gold foil was used to solder together the folds in the top of the platinum bag. In the cases where water was included in the sample, water was weighed into the cell first followed by weighing in the powder. The cell was then placed in an acetone/ice solution to keep the water in the base of the cell frozen while the top of the cell was sealed in the same manner as described above. Following drying, the cell was reweighed to check if there was a weight loss during sealing. After sealing, the cell was cemented with sauereisen to the top of the pyrophyllite column

3.3.1.5 Cleaning the Cell Following an Experimental Run

At the completion of an experimental run the cell assembly was withdrawn from the pressure vessel. After the cell was removed from the top of the pyrophyllite mounting, it was weighed and then opened at the top of the platinum foil bag. A sample of the glass was kept for analysis. The cell was then inverted and slowly lowered into a furnace at 1000°C so that the glass at the end of the cell would melt first to allow room for the expansion of the glass, on fusion, at the closed end of the cell. There is a large volume change on fusion of silicate glasses. However, frequently, but especially after the cell had been frozen under pressure, for example when water was present, this melting process resulted in the platinum sheath rupturing and the alumina crucible cracking. After several runs it became clear that a new cell would be required for each run. The maximum number of cell parts were retrieved by melting out the glass and removing the remaining glass or very viscous glass melts using sodium carbonate at ~850°C as a flux. Carbonate was then easily removed by boiling in concentrated hydrochloric acid.

3.3.2 Conductance Cell Mounting

The conductance cell was mounted on the end of a pyrophyllite column (Figure 3.12). This column positioned the cell in the middle of the top half of the furnace. It also filled the space below the cell in the furnace and from the end of the furnace to the lower mushroom head. Four, 1.5 mm diameter holes, drilled longitudinally through this column, allowed the two platinum wire conductance leads to pass through it and

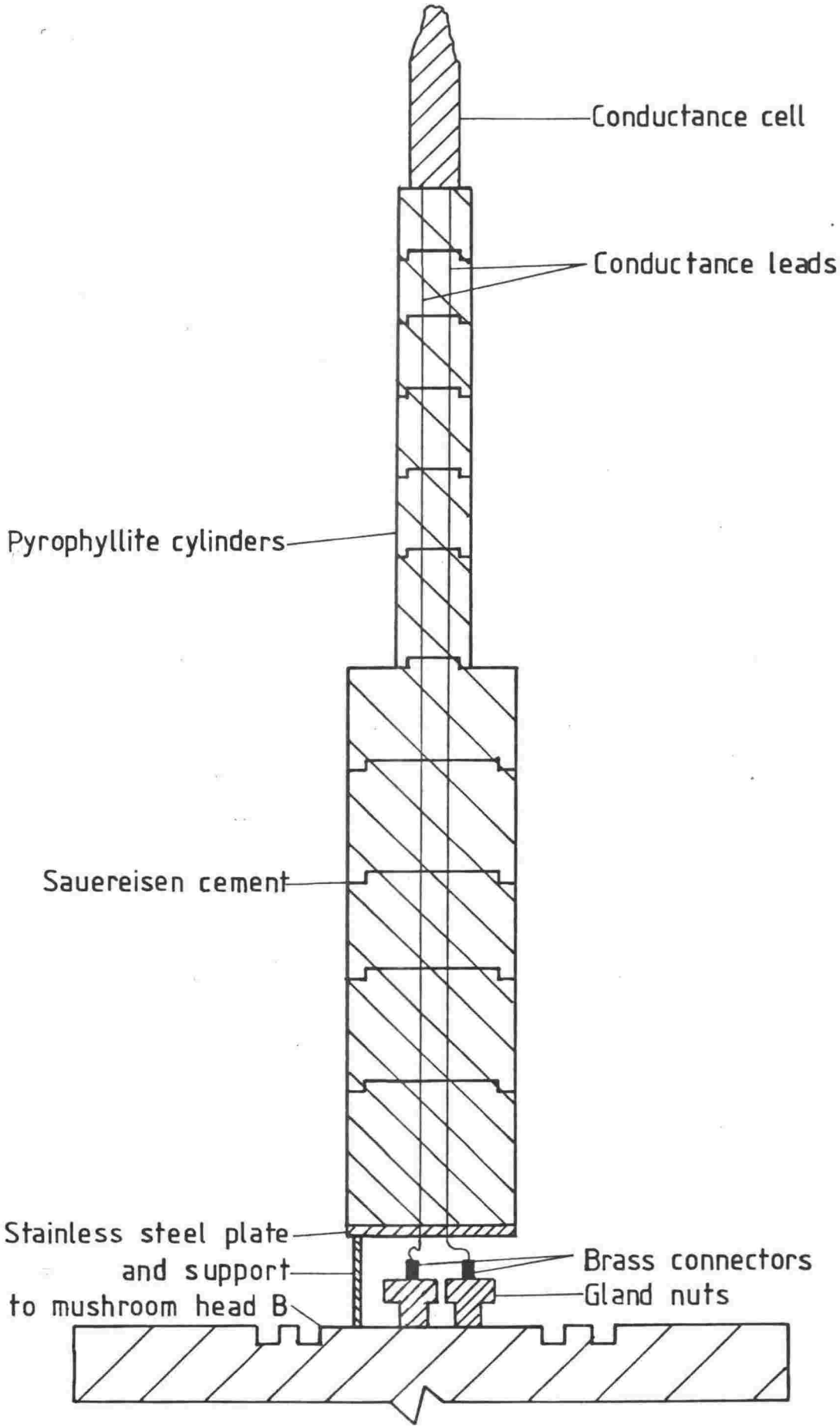

Figure 3.12— Electrical conductance cell assembly.

two thermocouples to be positioned in appropriate places. The pyrophyllite assemblage was attached to the mushroom head in a similar manner to the furnace mounting. Brass connectors were used to join the platinum wire leads to the brass rods emerging from the seals in the mushroom head. Remaining space around the connectors and thermocouples was filled with pieces of pyrophyllite.

3.3.3 Equipment Used to Measure Electrical Conductance

Electrical conductance was measured using a Wayne-Kerr B221 manual conductance/capacitance bridge which operates at 1592 hz. To monitor the effect of frequency on conductance a Wayne-Kerr Waveform A F Signal Generator S121 and a Wayne-Kerr Waveform Analyser A321 (5-20 khz range) were used in conjunction with the Wayne-Kerr B221 bridge. Plate 3.7 shows the equipment in position.

3.3.4 Sample Materials

All synthetic samples were prepared from analytical reagent grade chemicals. Precipitated SiO_2 and the appropriate quantities of metal carbonates (CO_2 is lost on fusion) were mixed and vibrated together for 15 minutes to homogenize the powders. The samples were then stepwise fused in a platinum crucible. The stepwise fusion was necessary because of the large volume decrease on fusion of the powder. When all the powder was melted into the crucible the melt was heated to 1350°C for 12-14 hours to ensure complete homogenization of the components and to remove evolved CO_2. The sample was then poured onto an aluminium plate and the resulting glass ground to a fine powder in a Tema mill. A

comparison of the composition determined by a microprobe analysis of the glass following an experimental run with the composition calculated from the mass of the initial components (Table 3.1) shows close agreement. This implies that there was very little volatilisation of Na_2O during the preparation of the sample.

The raw sample of Mount Erebus lava[1] contained crystals, probably of orthoclase. However, these crystals did not dissolve when a sample of the lava was heated to 1000°C. Since homogeneous melt is required for electrical conductivity work, these crystals were removed. An X-ray diffraction pattern of the remaining sample after removing the crystals showed it to be amorphous. Table 3.2 compares the composition of the glass in the raw sample with the composition after an experimental run, determined by microprobe analysis. This analysis shows the compositions to be very similar. Following removal of the crystals the glass was ground to a fine powder in a Tema mill.

A sample was dried in an oven at 150°C for at least 24 hours before being loaded into the conductance cell.

3.3.5 Experimental Run Procedure

1. The furnace assemblage, attached to the mushroom head, was lowered into position, the closure head screwed on and the bolts torqued to 180 ft lb. The pressure vessel was then inverted. Alumina powder was packed around the furnace and a fibrafax gasket placed over the end of the furnace. This end of the pressure vessel was only removed to replace neoprene 'O' rings or

---

[1] Kindly supplied by Dr Ray Dibble, Geology Department, Victoria University of Wellington.

TABLE 3.1

Electron microprobe analysis of sample No. 7 subsequent to an experimental run

Oxide	Wt %	Mol %[1]
SiO_2	71.671	71.83
Al_2O_3	0.415	0.25
MgO	0.042	0.06
Na_2O	23.837	23.16
CaO	4.303	4.62
K_2O	0.041	0.03
TiO_2	0.071	0.05
	100.308	100.00

[1] Initial composition from mass of oxides: 72/24/4 mol% $SiO_2/Na_2O/CaO$.

TABLE 3.2

Electron microprobe analyses of original Mount Erebus lava and subsequent to an experimental run

Oxide	Wt %[1]	Mol %[1]	Wt %[2]	Mol %[2]
SiO_2	56.198	62.69	65.968	63.68
Al_2O_3	19.234	12.73	29.548	12.87
TiO_2	1.089	0.91	1.008	0.85
FeO	4.763	4.44	4.416	4.13
MnO	0.47	0.23	0.35	0.33
MgO	0.951	1.58	0.881	1.47
CaO	2.368	2.83	1.913	2.29
Na_2O	9.480	10.25	9.222	9.99
K_2O	5.515	3.93	5.516	3.94
Cl	0.190	0.59	0.235	0.45
	100.035	100.00	100.158	100.00

[1]Original lava.

[2]Subsequent to experimental run.

the furnace, and not after every experiment.

2. After sealing the cell it was fitted to the pyrophyllite column with the platinum wire leads threaded through the column. Sauereisen cement was used to hold the cell in position so it would not hang by the platinum wires while the conductance cell assemblage was being lowered into the pressure vessel.
3. This pyrophyllite column and cell unit were then attached to the mushroom head B positioning thermocouples at the same time. The platinum wires were connected to conductance lead seals in mushroom head B. All holes in the pyrophyllite column where wires or thermocouples emerged were filled with sauereisen cement to help minimize gas flow.
4. Mushroom head B, in a special clamp, with the conductance assemblage suspended below it, was carefully lowered into the pressure vessel, the closure head screwed on and the six bolts torqued to 180 ft lb.
5. The pressure vessel was rotated 180° to the operating position and all external connections made. The safety doors were closed.
6. Before switching the furnace on the pressure vessel was flushed with argon gas to remove oxygen gas. When working with anhydrous samples a small pressure of argon was admitted, approximately 20 bar, before the furnace was switched on. The sample was heated, over a period of approximately 1 hour, to the maximum operating temperature of $1000^{\circ}C$ before the vessel was pressurised. When working with hydrous samples pressure and temperature were increased together.

7. When the system reached experimental run conditions, the temperature controls on the transformer were adjusted until the temperature gradient over the length of the cell was at a minimum. Then the conductance was monitored till it reached a stable value. It usually took approximately 30 minutes for equilibrium to be reached. Pressure was changed at constant temperature, then the temperature was reduced and the pressure range traversed again. It took up to 18 hours to measure the conductance of a sample over the ranges of temperature and pressure available.
8. At the completion of a run the pressure was reduced till it was ~20 bar then the furnace was switched off. In the case of hydrous samples, temperature and pressure were reduced together in a stepwise manner so that the pressure was always greater than the water vapour pressure in the cell to avoid bursting it.

3.4 QUARTZ CRYSTAL VISCOMETER

3.4.1 Introduction

The accurate measurement of the viscosity of a liquid while it is subjected to high pressures and temperatures presents an enormous challenge. The conventional methods of measuring viscosity: timing flow in a capillary tube or measuring changes in the torque of a rotating cup, for example, are inappropriate at high pressures not least because of the impracticality of sealing them into a pressure vessel. Part of this overall project to measure transport properties and density as a function of temperature and pressure, and PVT relations of molten and

water-rich silicates, is the measurement of viscosity as a function of pressure. This raised the problem as to how viscosity was to be measured. An important part of this project, then, has been to find and develop a viscometer to make these measurements. Robinson and Smedley (1) found that a recent and accurate method for measuring viscosity using an oscillating quartz crystal, first described by Mason (220), was ideally suited, on further refinement, for operation inside a pressure vessel. Not only would it be possible to operate it easily under pressure, since it requires only two electrical wires to be sealed into a pressure vessel, but also the sample liquid could be sealed in a closed container which was, incidentally, also essential for the work on molten silicates. Moreover, this device allows for the possibility of studying shear-rate dependent liquids and is also able to give a continuous and quantitative measurement of viscosity even if the viscosity is changing due, for example, to a chemical reaction. Consequently, since this instrument offered the possibility of measuring viscosity as a function of pressure, and further, because of its potential versatility, it was decided to develop it for high pressure and temperature operation. A part of this thesis has been spent on the development of this viscometer, particularly in extending its use to temperatures well above room temperature.

Section 3.4.2 describes the mode of operation of the viscometer along with important equations used for calculating viscosity. A detailed derivation of these equations from first principles can be found in Torrie's thesis (2) and Robinson and Smedley (1). Section 3.4.2 describes only the principles by which the viscometer operates and not

technical matters relating to its assemblage. The electronic instruments necessary to operate the the viscometer are described in section 3.4.3; while section 3.4.4 discusses the technical problems associated with assembling the viscometer and operating it above room temperature. Overcoming these problems is now the only obstacle before it can be used in the internally heated pressure vessel. Further, section 3.4.4, summarises the results and problems encountered in the initial developments at room temperature and in attempting to extend its use above room temperature. The final section, 3.4.5, describes the contribution to the development made as part of this thesis. This development proved arduous and time consuming. However, it was found that by mounting the quartz crystals on flexible springs the effect of thermal expansion, found to be a major problem at high temperatures, could be minimised and viscosities as a function of temperature were obtained. Unfortunately, these results were limited since commissioning of the internally heated pressure vessel and measurement of the electrical conductance of molten silicates took precedence and were the principal part of this thesis.

3.4.2 Description and Theory of Viscometer

The instrument being developed for operation in an I.H.P.V. consists of two α-quartz piezoelectric crystals butted together. On one end of this assemblage is cemented a glass or metal rod. Figure 3.13 illustrates these dynamic components of the viscometer. Each piezoelectric crystal has four electrodes plated longitudinally with opposite pairs connected electrically as illustrated in Figure 3.13. A

crystal driver applies an AC voltage, V_d, to one pair of electrodes on the drive crystal, which forces it into the torsional mode of oscillation. The other crystal, the gauge crystal, because it is mechanically fixed to the drive crystal, must oscillate in the torsional mode as well. The voltage, V_g, induced by the oscillation of the gauge crystal is fed back into the crystal driver making the whole device a closed loop crystal oscillator.

At conditions of minimum drive voltage the frequency of oscillation will be the fundamental frequency of the crystals, in this instance 40 khz. The rod butted to the quartz assemblage is tuned by grinding the ends with carborundum paper to a resonant length, that is, an integral number of half-wavelengths, $n\lambda/2$. It is this rod that is used as a probe; it is immersed in a liquid to a depth of $\lambda/4$ from the free end or an integral number of quarter wavelengths, $n\lambda/4$, where $n=1, 3, 5, \ldots$. These distances from the free end of the rod correspond to nodal points. It is, therefore, possible to touch the rod at these points, with, for example, '0' ring seals, without significantly perturbing the resonant response of the system. By moving an '0' ring along the rod the nodal positions can be located. A cup can then be attached around the probe with a seal made at a node. If the top of the cup is also sealed then it is possible to determine the viscosity of a liquid in a closed container. With the viscometer in the configuration of Figure 3.13 and with a cup attached, it becomes possible to measure the viscosity of hot, corrosive or electrically conducting fluids.

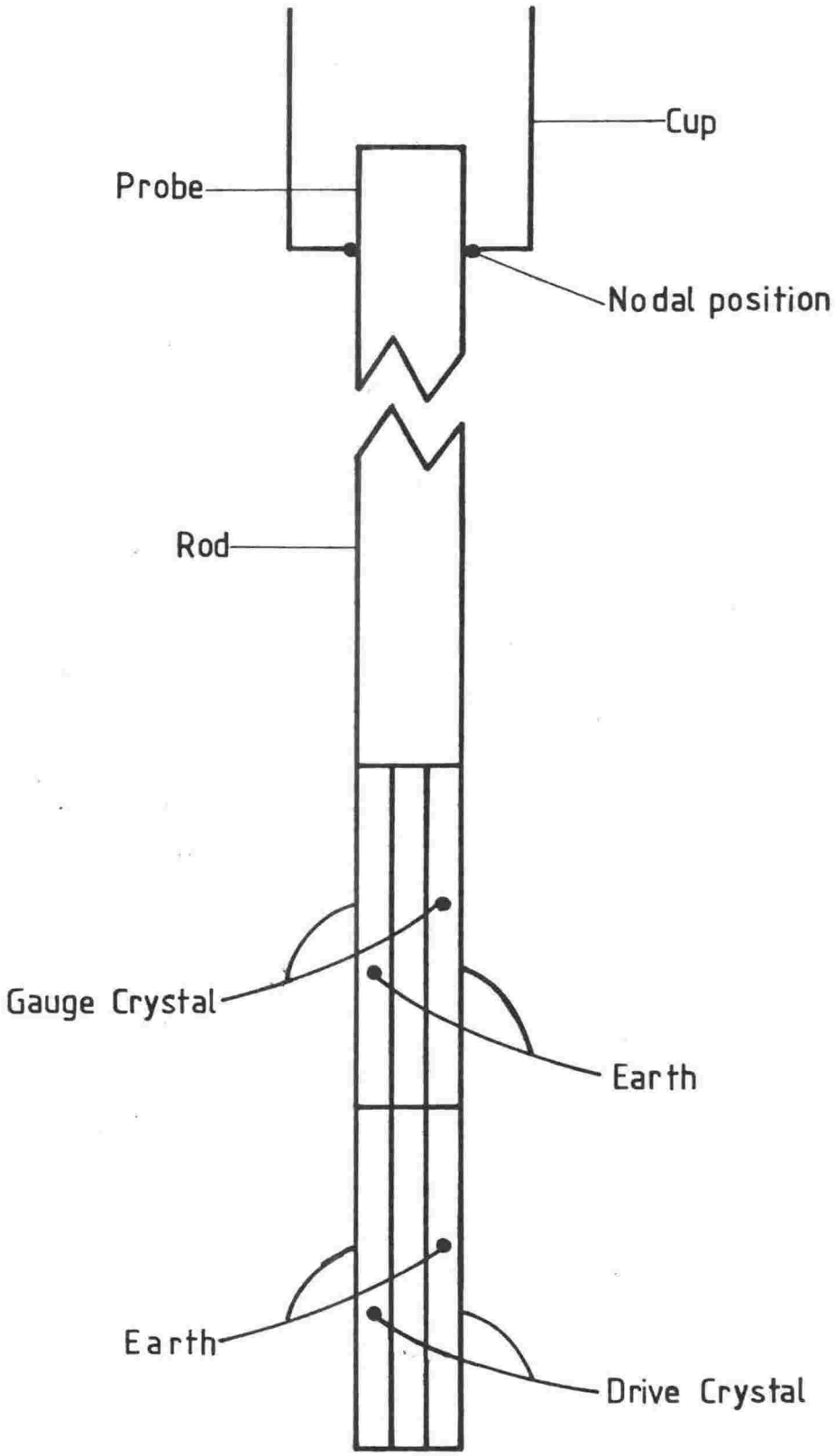

Figure 3.13—Quartz crystals and rod assemblage. (The electrode positions are distorted on the diagram for clarity of illustration.)

When the probe is immersed $\lambda/4$ into a fluid the liquid dampens the vibration and thus increases the resonant period, τ, of the oscillating assemblage. The crystal driver is designed to maintain V_g at a preset value and to increase V_d in response to the mechanical damping. To determine the viscosity of a liquid, V_d, V_g and τ are measured without the liquid present and then remeasured with the liquid present. Both measurements being made under identical temperature and pressure conditions and also with the phase angle between V_d and V_g adjusted to 90^o. Under the latter condition V_d is a minimum. Viscosity can be calculated from either of two equations. One equation relates viscosity to the change in drive voltage and the other to the change in resonant period. For some liquids viscosity is given by an appropriate combination of $\Delta(V_d/V_g)$ and $\Delta\tau$. For non-elasticoviscous fluids the viscosity is given by:

$$\rho\eta = C[Q^{-1}(\eta)]^2 \tag{3.1}$$

or,

$$\rho\eta = 4C\,[(\tau_{fluid} - \tau_{background})/\tau]^2 \tag{3.2}$$

where: ρ - density, η - viscosity, $Q^{-1}(\eta)$ - mechanical damping, τ- resonant period and C is a constant dependent on the physical properties of the crystal assemblage.

$$C = \pi/4\tau\,[\textstyle\sum_i m_i a_i^2/a^3(2n\lambda + 1/2h\pi a)]^2 \tag{3.3}$$

where: m - mass of crystals and rod, a - radius of crystals and rod, λ - wavelength of oscillation, h - number of flat surfaces immersed in the liquid and n = 1, 2, 3, ... $Q^{-1}(\eta)$, the mechanical damping due to the fluid can be calculated from:

$$Q^{-1}(\eta) = K\,[(V_{d,fluid} - V_{d,background})/V_g] \tag{3.4}$$

where K is a constant that can be calculated from the electromechanical properties of the system and is given by:

$$K = 16N^2/\omega C_m \sum_i m_i a_i^2 \tag{3.5}$$

where N - transformer ratio, ω - radial frequency and C_m - capacitance load on the gauge crystal. K can be determined by substituting into equation (3.4) or by measuring, if it is symmetrical, the half-width resonance response and (V_d/V_g) and then substituting into:

$$Q^{-1}(\eta) = [(n^2 - 1)^{-1/2}(\tau_2 - \tau_1)/\tau_r] \tag{3.6}$$

where $n = V_{d,1}/V_{d,r} = V_{d,2}/V_{d,r}$, τ_1 and τ_2 are the periods when $V_d = V_{d,1} = V_{d,2}$ and $V_{d,r}$ and τ_r are the values of V_d and τ at resonance, respectively. The constants C and K can also be determined by calibrating the instrument using liquids of known viscosity.

For elasticoviscous fluids, that is, fluids which exhibit elastic properties, the complex viscosity is written as:

$$\eta^* = \eta_1 - i\eta_2 \tag{3.7}$$

where,

$$\rho\eta_1 = 2C\,[(\Delta\tau/\tau)Q^{-1}(\eta)] \tag{3.8}$$

and,

$$\rho\eta_2 = C/2\,\{[Q^{-1}(\eta)]^2 - 4[\Delta\tau/\tau]^2\} \tag{3.9}$$

the symbols are defined as before.

A significant advantage of this system above other viscometers is that it enables one to vary the shear rate by increasing the amplitude

of vibration, that is increasing V_g, and therefore to study shear rate dependent fluids. For non-shear rate dependent fluids the ratio V_d/V_g will be constant with varying shear rate, for shear thickening fluids it will decrease with increasing shear rate and conversely for shear-thickening fluids. Since the device is continually oscillating at its resonant frequency it provides a constant readout of viscosity and can therefore be used to study fluids with rapidly changing viscosities such as polymerisation reactions or drying films.

For high temperature and pressure operation the probe must be sealed into a closed container, both to exclude pressurising gas from the sample and also to contain dissolved volatiles in the sample from dry to saturated. This can be achieved by sealing the probe into the container at a node $\lambda/4$ from the free end. When used at high temperatures the piezoelectric crystals must be separated from the hot zone since α-quartz crystals undergo a phase change to non-piezoelectric β-quartz at 573°C. This can be achieved by having a sufficiently long rod attached to the quartz crystals so they can be outside a furnace. The effect of pressure on the piezoelectric properties of the quartz crystals can be allowed for since the background measurement is made under the same conditions as the test fluid. Throughout the development work on the viscometer it has been scaled to fit inside the 50 mm diameter bore of the internally heated pressure vessel that has already been discussed.

3.4.3 Electronic Equipment

A schematic diagram, Figure 3.14, illustrates the dynamic and the electronic equipment. The crystal driver was supplied by Solid State Electronics Ltd., Lower Hutt, New Zealand and is capable of operating from 0.1-1000 drive voltage, 0.001-10 gauge voltage and between 20-200 khz. It also has a built in phase shifter and filter. A Hewlett Packard multimeter 3465A coupled to the driver and via a switch box was used to measure the drive and gauge voltages. This gave an ultimate precision in voltage measurement of of +/-0.1%. A Hewlett Packard frequency counter, model 5245L, was used to measure frequency or period. In the period mode 1 part in 10^8 could be determined. An oscilloscope was used to monitor the drive and gauge voltages set by the phase shifter on the crystal driver to be 90^o out of phase.

The piezoelectric crystals were obtained from Valpey Corporation, Hopkinton, Mass., U.S.A. They were cut from natural quartz to operate in the torsional mode at 40 khz. Each crystal was 47 mm long and 5 mm in diameter with the longitudinal axis of the cylinder being the x-axis.

3.4.4 Summary of Previous Development

The preceding section described briefly: (1) the theory of an oscillating quartz crystal viscometer and (2) how in principle the dynamic components are used to determine the viscosity of a fluid. Technical problems such as: assembling the dynamic components, developing a suitable holder for the crystal, rod and cup, attaching a cup to a rod at a node and wires to the plated quartz crystal electrodes to make the viscometer operate correctly over a temperature range of

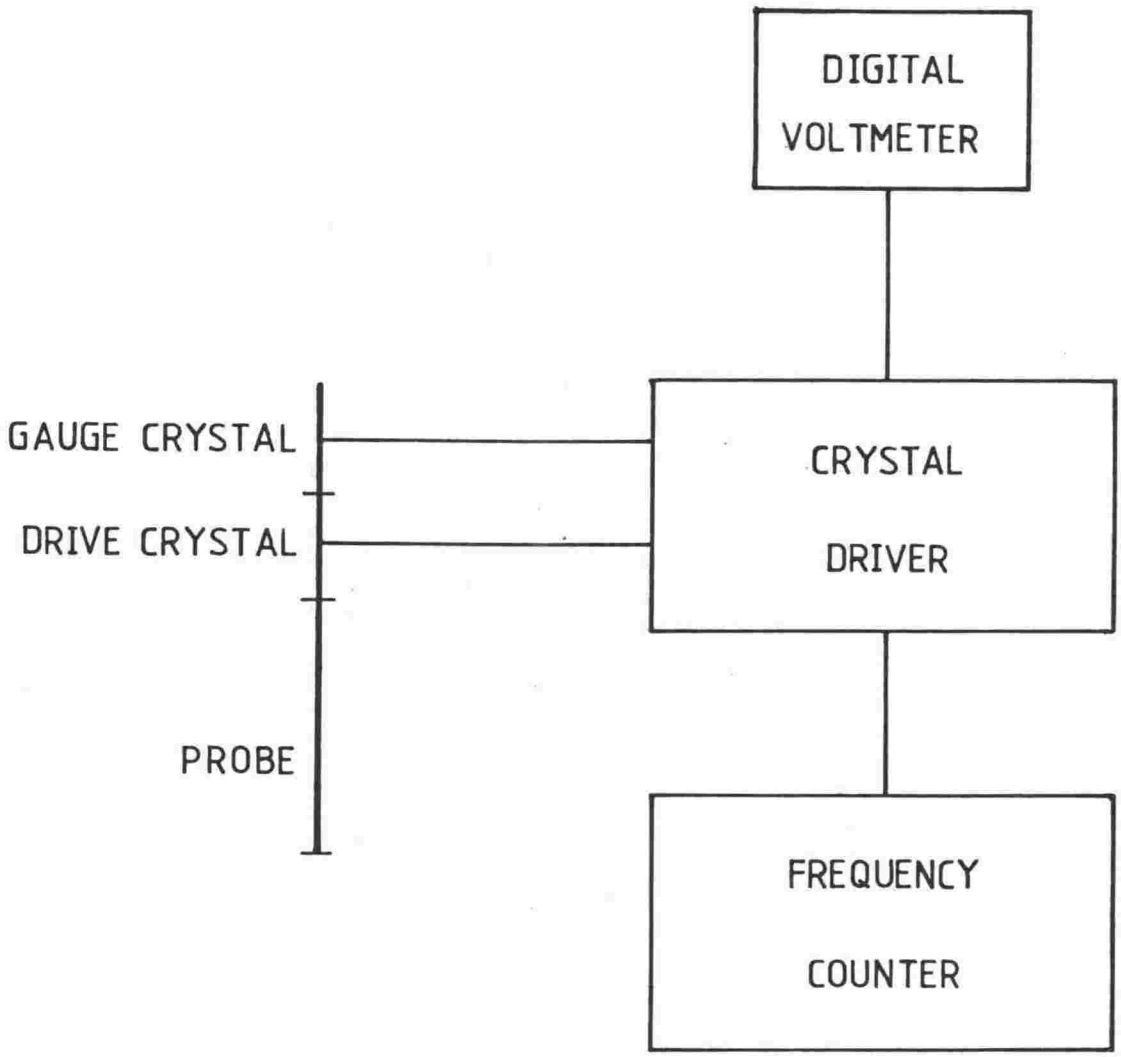

Figure 3.14— Schematic diagram of electronic apparatus and dynamic components of the quartz crystal viscometer.

1000°C and a pressure range of 5 kbar, were not dealt with. These problems present a substantial challenge. This section and the next describes the development of the viscometer up to the present. Preliminary testing of the viscometer at room temperature has been reported by Robinson and Smedley (1). A detailed description of the initial extensions to higher temperatures is found in Torrie's thesis (2).

The preliminary work (1) included a configuration of the crystal assemblage in which the viscometer was completely immersed in ethyl alcohol contained in a thermostated (25 +/- 0.05°C) jacket and evacuated to (10^{-3}mm Hg). Results from this configuration were never closer than 10% of the literature value and sometimes 30% too high. These discrepancies were explained in terms of the surface roughness of the crystal; a rough crystal surface adding an extra unknown inertial term. This was overcome by using a glass probe with a cup sealed, using a quickfit screw thread joint, onto a rubber 'O' ring positioned at a node $\lambda/4$ from the free end. Using this configuration and similarly thermostated and evacuated as previously the viscosities of H_2O, CCl_4 and three oils were measured. These liquids gave a range of viscosity from 0.00089 to 2.044 Pa s. Over this viscosity range the results agreed to within 1/2% of the literature values. Although these results showed that the viscometer gave reliable results over four orders of magnitude in viscosity, the materials used to construct the viscometer did not allow extension to temperatures much above room temperature. Further, Torrie (2) noted the following problems:

1. The positioning and seating of the rubber 'O' ring, and hence the background readings, could not be reliably reproduced.
2. The width and nature of the 'O' ring was such that the precise measurement of the length of the rod immersed in the fluid could not be obtained.
3. Any accidental bumping tended to alter the background reading slightly and hence invalidate any results.
4. The sample chamber had to be filled by gravity feed as the 'O' ring did not support a good vacuum. Hence the fluid touched the Quickfit screw thread as well as the rod, slightly increasing the background readings.

To overcome these problems Torrie fused a glass 'O' ring to the rod at the node and then fused a cup to this ring. He found that this virtually eliminated problems (1), (2) and (4) but tended to accentuate the effect of (3), as the seal, being at a node of maximum stress was less cushioned from the effects of any bumps or stress such as produced when applying or releasing a vacuum in the chamber. However, since this type of seal was more suitable for extension to higher temperatures it was persevered with.

A glass rod ~230 mm long was required so that the quartz crystals would be outside a furnace. With this length of rod and with a cup sealed to the rod at the free end it was necessary to find a way of supporting the system since the top heavy rod and cup was held only by a butted glue joint. This was achieved by using a pyrophyllite cylinder, with a bore sufficient to pass the rod through, firmly attached to the crystal holder and just long enough for the cup to be cemented onto the

top of the pyrophyllite. Several versions of this configuration were constructed, the most significant improvements were developments in the crystal holder and the method of attaching the electrode wires to the crystal surfaces.

Torrie found that this new arrangement proved to be extremely stable in air over a range of temperature. Preliminary data obtained on a 60/40 mol% melt of $Ca(NO_3)_2 - KNO_3$, the density and viscoelastic properties of which are well known, was self-consistent with the theory. Unfortunately, only isolated data were recorded, as every time the supercooled melt crystallised the resulting strain snapped the probe of at the node. However, the single measurement recorded in Torrie's thesis for this melt at 200.2°C compares favourably with the literature value:

$$(\rho\eta)_{freq} = 4C(\Delta\tau/\tau)^2 = 233.5$$

and,

$$(\rho\eta)_{Q^{-1}} = CK^2(V_d/V_g)^2 = 250.2$$

and the literature value of $(\rho\eta) = 238.6$.

To overcome the fragility of the glass rod it was decided to replace it with a stainless steel rod with a stainless steel cup silver-soldered at a node. Allowance had to be made for expansion when tuning the rod since the coefficient of thermal expansion for stainless steel, equal to $16\times10^{-6}/°C$ is 32 times greater than glass. However, as well as the expansion altering the resonant response of the system it also put strain on the electrode connections, since, at this stage of development the electrode wires not only made contact with the electrode plates on the crystal, but also held them in a rigid position. Torrie recorded no

measurements with the viscometer containing a stainless steel rod and cup. Figure 3.15 shows the viscometer at this stage of development.

This initial development of the viscometer showed that a wide range of viscosity can be measured and that it is capable of measuring viscosity as a function of temperature. However, there are still technical problems to be overcome to operate the apparatus continuously and reliably as a function of temperature.

The principal problems to be overcome at this stage were:

1. Relieving the effects of thermal stress on the system.
2. Harnessing fully the sensitivity of the piezoelectric quartz crystals.
3. Making positive contact between the plated electrodes on the crystals and the wire leads.

3.4.5 Further Development Above Room Temperature

It was decided, following the time consuming familiarisation of the theory and operation of the viscometer, to attempt to measure the viscosity of the molten oxide, B_2O_3. This oxide, for which the viscosity, density, and viscoelastic properties are well characterised (2), has over the same temperature range as molten silicates a similar range of viscosity. Consequently, it was regarded as an ideal liquid with which to test the capabilities of the viscometer. In order to conduct this experiment a silica-glass probe assemblage was persisted with, in spite of the problems encountered by Torrie, since silica has the most suitable properties of all the materials examined thus far for extending to the temperatures required to make these measurements. In

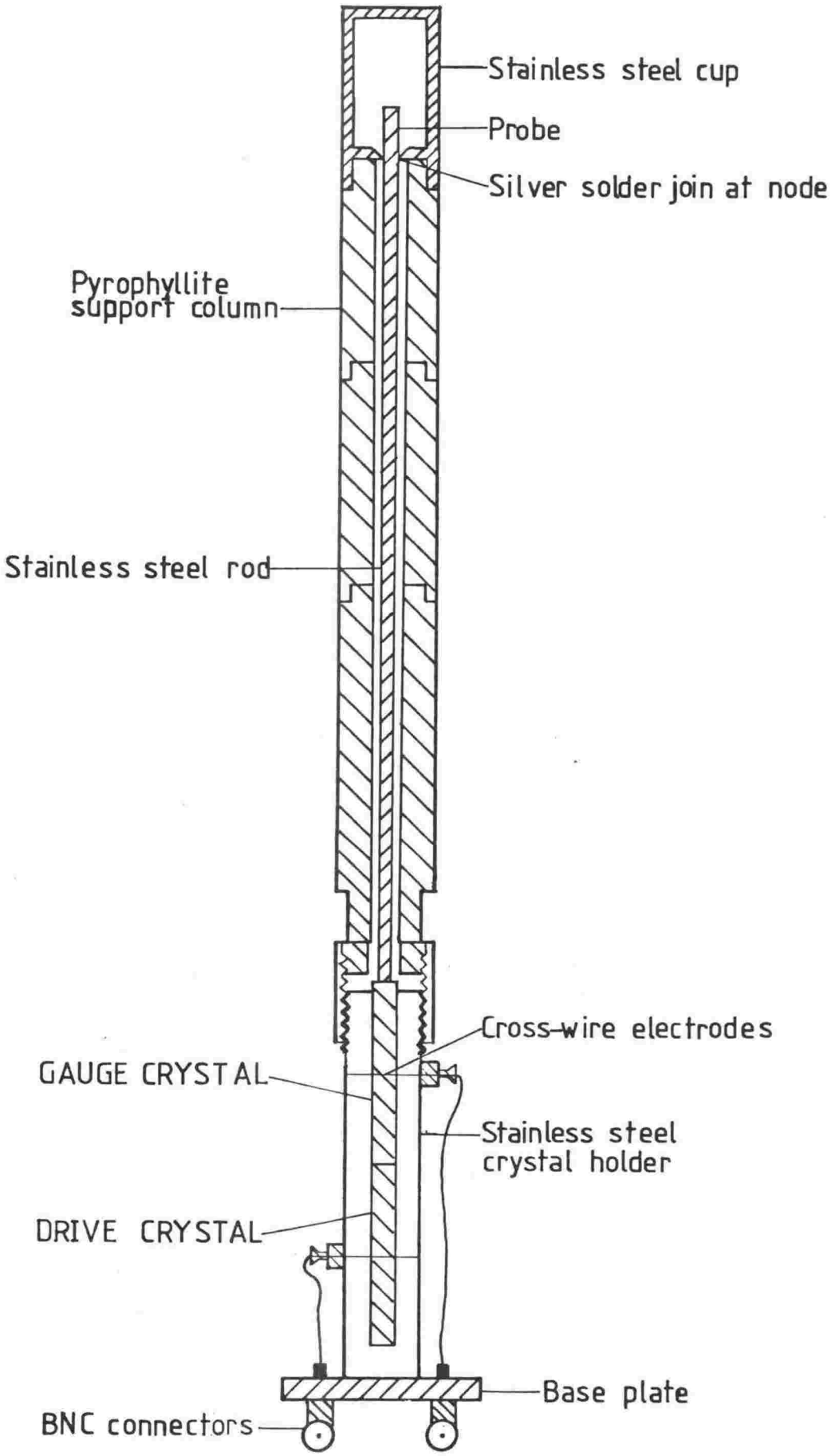

Figure 3.15—High temperature viscometer with stainless steel rod and cup and with cross-wire electrode connections.

particular, it has a low coefficient of thermal expansion ($5.4 \times 10^{-7}/^{\circ}C$); it can be heated to $1200^{\circ}C$ and it was found to have a stable resonant response as a function of temperature. Torrie's criticism that glass probes snapped whenever a melt cooled to a glass can be overcome by doing a background run first, followed by a run with the liquid present but ensuring that the melt does not overcool till the run is complete. At the completion of such a run the destruction of the silica probe and cup is probably inevitable. However, this experiment would provide a stringent test on the viscometer over the range of viscosities and temperatures that would be encountered when measuring the viscosity of molten silicates, thus showing its suitability for this project.

Although the background measurements were found to be stable, various problems hindered progress with this configuration. On several occasions the glue joint between the silica rod and crystals broke. This was caused by a combination of stress on the joint from expansion of the components, and the joint not being sufficiently baffled against the heat from the furnace. Cyanoacrylate adhesive was an excellent glue for room temperature work but it breaks above $100^{\circ}C$. A satisfactory alternative adhesive for higher temperatures could not be found: waterglass, araldite and sauereisen were tried and found to be unsuitable. The whole system proved extremely fragile, not only because the probe snapped when the melt undercooled, but also just in handling the components while assembling it. During heating it appeared that the electrode connections were being subjected to some stress as a consequence of thermal expansion. This problem was principally caused by the wires to the electrodes on the crystals not only making contact but

holding the crystal in a rigid position. Thus any pressure on the crystal due to thermal expansion effected the connections to the electrodes and, in turn, the resonant stability. Because of these problems it was concluded that the attempt to measure the viscosity of B_2O_3 was premature and that these problems ought to be solved first at lower temperatures.

It was decided to measure the viscosity, using the silica assemblage, of suitable liquids at much lower temperatures than required for B_2O_3. The viscosity of molten $Ca(NO_3)_2$ - KNO_3 60/40 mol% up to ~150°C was attempted. However, at low temperatures viscosity was 3 to 4 orders of magnitude to low. The glue joint, thermal expansion and fragility of the silica still continued to be problems. The complete silica rod and cup system was discarded. In its place a composite silica and stainless steel resonant assembly was developed. A half-wavelength of stainless steel was used with a stainless steel cup sealed on midway along the rod in conjunction with a tuned $n\lambda/2$ length of silica rod between the quartz crystals and the stainless steel rod. This combined the mechanical strength of stainless steel with the low thermal expansivity of silica. It showed signs of promise, but a satisfactory high temperature bond between the stainless steel and silica rods was not available, even for these lower temperatures. Also, an extra cement joint made the system even more fragile for handling than the previous one.

The only alternative was to use a complete rod and cup made from stainless steel and to seek the answer to the thermal expansion in an alternative manner. The answer was found by replacing the electrode connections, which held the crystals in a rigid position, with permanent

connections to the crystal, but with flexible leads from the connection to the crystal holder. It was achieved by cementing the end of a flexible copper wire spring onto the appropriate position on the electrode surface with a small drop of araldite and coating the connection with silver paint. Expansion of the metal rod now no longer strained the electrode connections. The remaining parts of the viscometer were the same as in Figure 3.15. By using this method of holding the crystals, the viscosity of a sample of Canadian Athabasca bitumen as a function of temperature was measured. This material was used because it has a wide viscosity range at relatively low temperatures.

While this thesis was being written, the temperature and viscosity range of the viscometer was extended still further. The viscosity of $Ca(NO_3)_2$ - KNO_3 60/40 mol% was measured as a function of temperature from 160°C to 200°C. This gave a viscosity range of 10^3 Pa s and the results agreed well with literature data. The viscosity of B_2O_3 up to 700°C and 10^3 Pa s was also measured[1].

---

[1] These viscosity measurements were made by Mrs Sandra Thang.

Chapter IV

EXPERIMENTAL RESULTS

This chapter presents the results from the electrical conductance measurements and the results obtained from the quartz crystal viscometer. The conductivity results are presented; first, as a function of pressure at constant temperature for each category of silicate examined; second, for the hydrous silicates, as a function of temperature; and third as a function of composition. Activation energies of conduction are calculated and displayed in tables and graphs. This is followed by a discussion of the experimental errors associated with the conductance measurements together with a discussion of the reliability and internal consistency of the results. The viscosity results obtained from the quartz crystal viscometer on Canadian Athabasca bitumen are presented as a function of temperature.

4.1 ELECTRICAL CONDUCTIVITY OF MOLTEN SILICATES

4.1.1 Introduction

Measurement of conductance was carried out above the liquidus temperature for all the silicates studied. There were, however, two constraints placed on the experimental temperature range, limiting it to only ~150°C. The upper temperature limit was 1000°C (section 3.3.1.2). Although the lower temperature limits were in fact set by the liquidus temperatures, the lowest experimental temperatures were considerably

greater since cooling to a glass had to be avoided. Increases in pressure were accompanied by temporary decreases in temperature caused by cold pressurising gas entering the pressure vessel. In such circumstances, if the temperature was sufficiently close to the liquidus temperature then vitrification was inevitable. It was found that if the melt vitrified, then on re-fusion the accompanying change in volume ruptured the cell. Thus, to avoid this occurrence, the lower temperature limit was kept well above the liquidus temperature.

In the case of hydrous silicates the amount of water present determines the temperature and pressure limits for which a homogeneous liquid exists - the region to be studied. At any given temperature of a molten hydrous silicate, the applied pressure must always be greater than the partial vapour pressure of water at the temperature in question. If the applied pressure was less than the partial pressure of water, then not only would bubbles form in the melt, but if the applied pressure was too low the cell would burst. Consequently, measurements were made on hydrous systems with the pressure not less than 300 bar. In the instance of bubbles being present in the melt it would be expected that the conductance measurements would vary erratically. This was not observed, nor did inspection of the glasses following an experimental run indicate that bubbles were present except in the case of hydrous Mount Erebus lava. On several occasions it was found that the cell was ruptured when the pressure vessel was dismantled. Subsequent inspection of the cell showed that the extruded melt had not flowed very far before vitrifying. Since these melts have a high fluidity it was concluded that the cell had ruptured during the close-

down procedure, when the pressure was released and not during the run. The results from these runs, therefore, were not discarded.

All experiments were carried out under the conditions of both stepwise increasing followed by stepwise decreasing pressure. No differences were observed between these two conditions, nor was any hysteresis observed in the measurements after altering the pressure. There was usually a delay of approximately 30 minutes before the cell returned to thermal equilibrium subsequent to a re-set temperature.

The experimental data are given in the Appendix. They were recorded under conditions of varying pressure at constant temperature. It was found that over a 20 khz frequency range the conductance varied by only ~3% and no further analysis of frequency effects were examined. Most of the experimental data were recorded at 1592 hz. Plots of log conductivity versus pressure give straight lines indicating the Arrhenius equation is obeyed.

4.1.2 Binary Silicates

The electrical conductivity results for the binary soda-silicates studied are presented in Figure 4.1, which amongst other things shows the effect of varying the concentration of Na_2O in silica. Conductivity has a much greater dependence on temperature and composition than on pressure. In fact, within experimental error electrical conductivity is independent of pressure.

For the binary systems with the following compositions: 60/40, 65/35, 75/25, mol% SiO_2/Na_2O the temperature gradients between the top and bottom of the cell were well above 10°C (Appendix), for

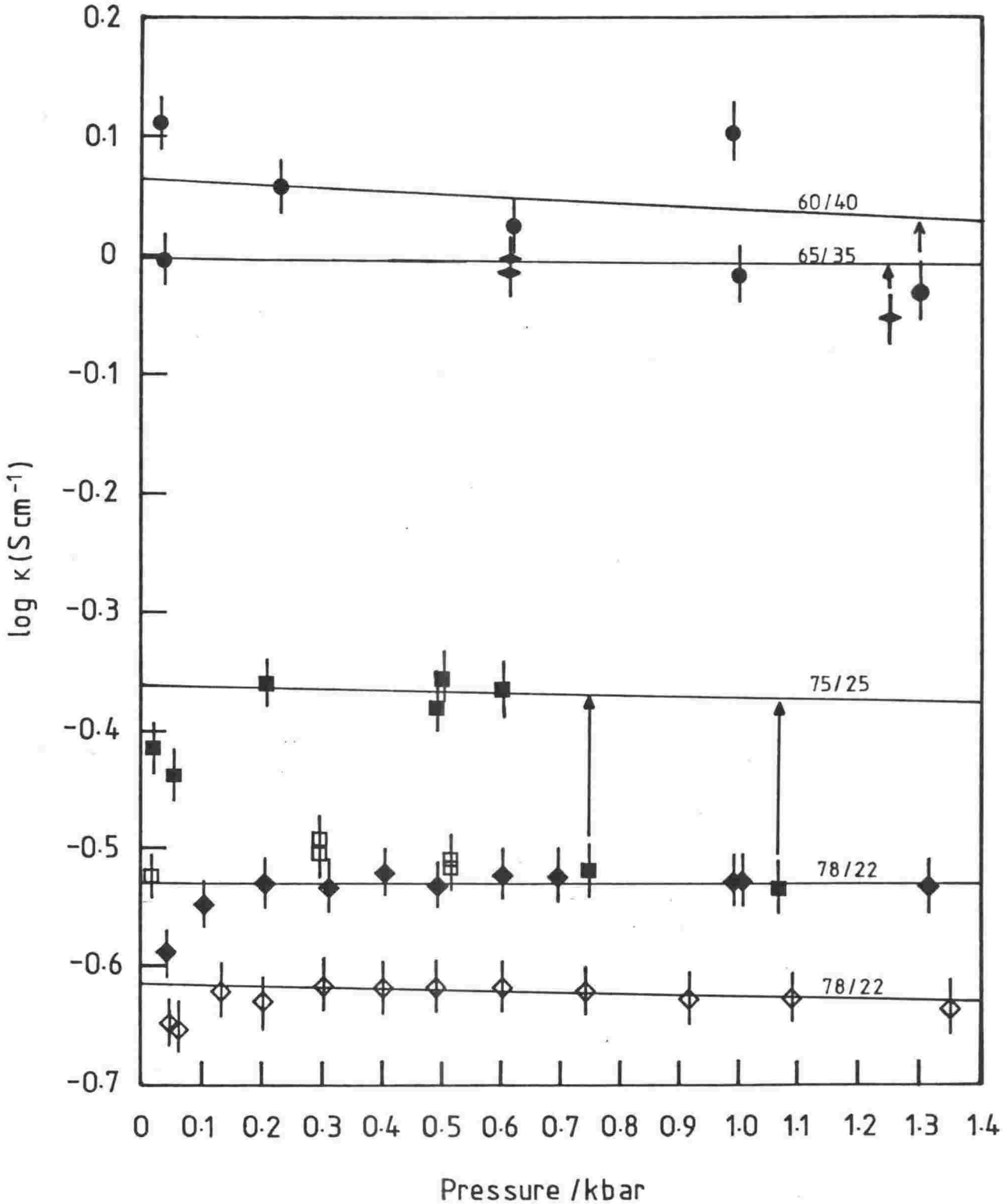

Figure 4.1— Log conductivity versus pressure at constant temperature for binary SiO_2/Na_2O melts. (●-60/40 mol% at 925°C; ◆-65/35 mol% at 1000°C; ■ and □-75/25 mol% at 1000 and 900°C, respectively; ◆ and ◇-78/22 mol% at 1000 and 943°C, respectively; the shift of some of the points, indicated by arrows, is explained in the text.)

pressures greater than ~500 bar, because of inadequate insulation around the furnace. These were the first silicate melts investigated and convection currents were still a problem. As soon as the temperature gradients were minimised by using suitable non-porous insulation around the furnace it was found that log conductivity was independent of pressure, see, for example, the system SiO_2/Na_2O in Figure 4.1. Based on the behaviour observed in the later experiments where temperature gradients were less than 10°C, isotherms have been drawn for these initial binary silicates studied, which reflect a similar pressure independence.

The cell constant was determined by extrapolating the conductance data to 1 bar at 1000°C and using the electrical conductivity value from Tickle's data under identical conditions. This value of the cell constant was used to calculate conductivities at pressures greater than 1 bar.

In the case of the 65/35 and 75/25 mol% SiO_2/Na_2O silicates two separate runs were carried out for each system. Similar behaviour was observed for the repeated experiment.

4.1.3 A Ternary Silicate: Silica/Soda/Lime, 72/24/4 mol%

The purpose of studying this silicate was to examine the effect of a doubly charged cation on the electrical conductivity. However, the binary alkaline earth metal oxide silicates all have liquidus temperatures greater than 1000°C making their study impossible in the present experimental equipment. But, by adding an alkaline earth metal oxide to a binary alkali silicate, the conductivity behaviour of which

is already known, the effect of the doubly charged ion can be examined. In this experiment a melt was prepared in which the ratio of SiO_2 to Na_2O was the same as in the binary 75/25 mol% melt but with the addition of 4 mol% CaO. Figure 4.2 shows the electrical conductivity results as a function of pressure for this ternary silicate. The cell constant was determined in the manner described in section 4.1.2 but using the data of Kroeger and Heckmann (221). The composition of the present melt was not, however, identical with the composition of any of their melts and two extrapolations were required to obtain an estimate of the conductivity of the present ternary silicate. Their results were extrapolated to 1000°C and then plotted, along with Tickle's data, as a function of soda content on a graph of log conductivity versus mol% Na_2O. Above 14 mol% Na_2O the two sets of data were approximately on the same curve. The conductivity of a melt containing 24 mol% Na_2O, extrapolated from Kroeger and Heckmann's data, was obtained from this plot. The addition of this small amount of CaO caused a small decrease in the electrical conductivity compared to the 75/25 mol% silica - soda melt. For this experiment the temperature gradient was less than 5°C except in two instances (Table A.8) and the isotherms are parallel to the pressure axis.

4.1.4 A Multicomponent Silicate: Mount Erebus Lava

An important feature of this lava is the unusually high content, 10 mol%, of Na_2O. A consequence of this is the relatively low melting point and high fluidity. The low liquidus temperatures made it possible to study this multicomponent silicate using the present experimental

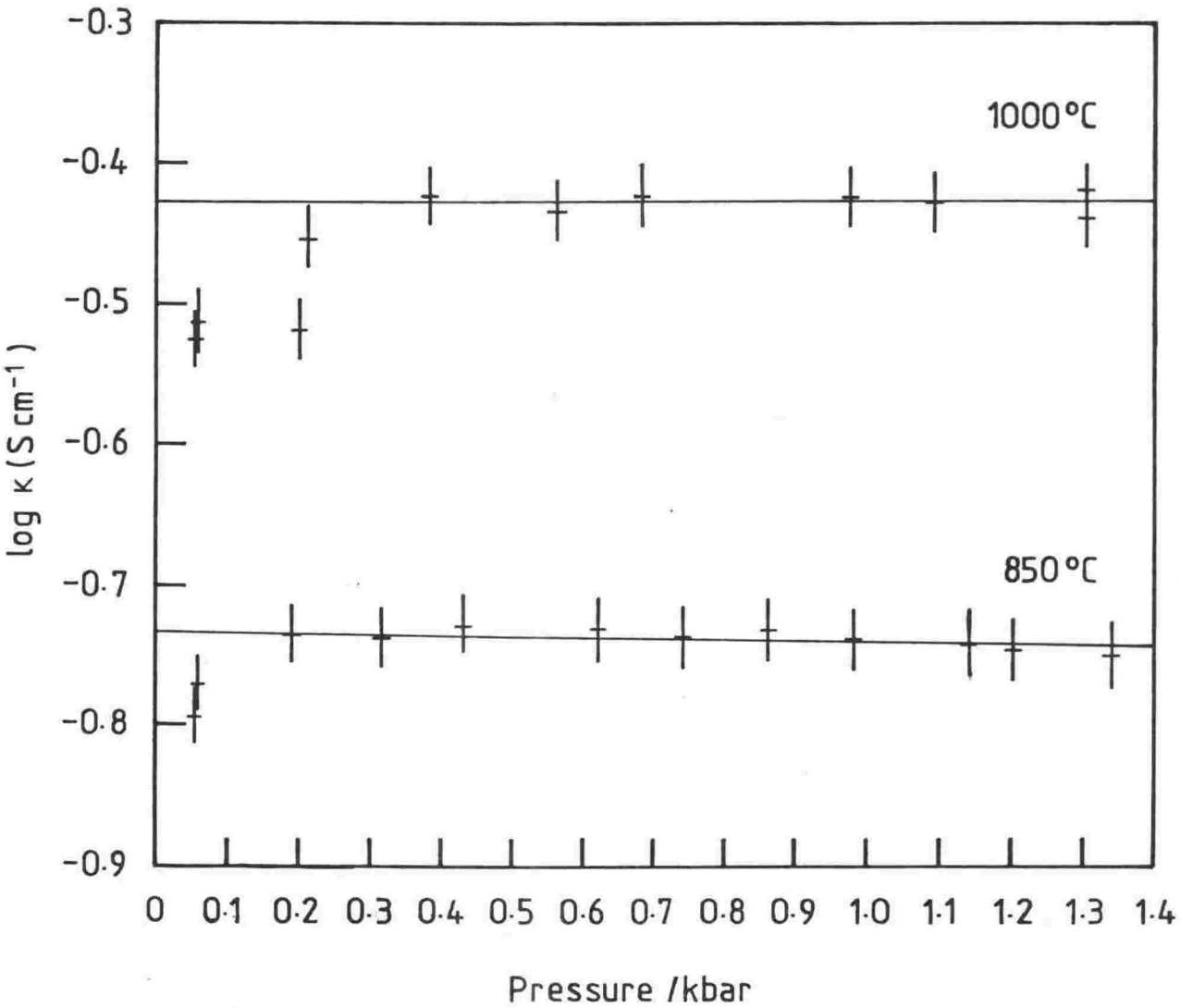

Figure 4.2— Log conductivity versus pressure at constant temperature for a ternary $SiO_2/Na_2O/CaO$ 72/24/4 mol% melt.

equipment. The results are presented in Figure 4.3. Calibration of the cell constant was made using 0.01M KCl. It was found that the electrical conductivity of this silicate was significantly less, by a factor of ~20, than the binary and ternary silicates. The 900°C isotherm shows slight negative pressure dependence.

4.1.5 Hydrous Silicates

4.1.5.1 The Binary Silicate: Silica/Soda, 78/22 mol% + ~5 wt% Water

The electrical conductivity results for this hydrous silicate, ~60/19/15 mol% when converted to mole% ratios, are presented in Figures 4.4 and 4.5. It was found that the electrical conductivity of this hydrous system was actually less than the parent anhydrous silicate (cf. Figures 4.1 with 4.4). There was a slight positive pressure dependence for the 1000°C isotherm but this dependence had disappeared in the 850°C isotherm. From a plot of log conductivity versus temperature at constant pressure it is possible that the isobars may pass through a maximum as in some liquids such as molecular and partial ionised liquids (95). This pattern becomes clearer from the results on hydrous Erebus lava.

4.1.5.2 Mount Erebus Lava + ~4 wt% Water

Figure 4.6 presents the results of log conductivity versus pressure plots at constant temperature. From the graph it can be seen that there is a positive pressure dependence on conductivity which becomes more positive as temperature is increased. It was found that the 1000°C isotherm intersects both the 900°C and 950°C isotherms and that it is not till a pressure of 1100 bar is reached that the 1000°C isotherm

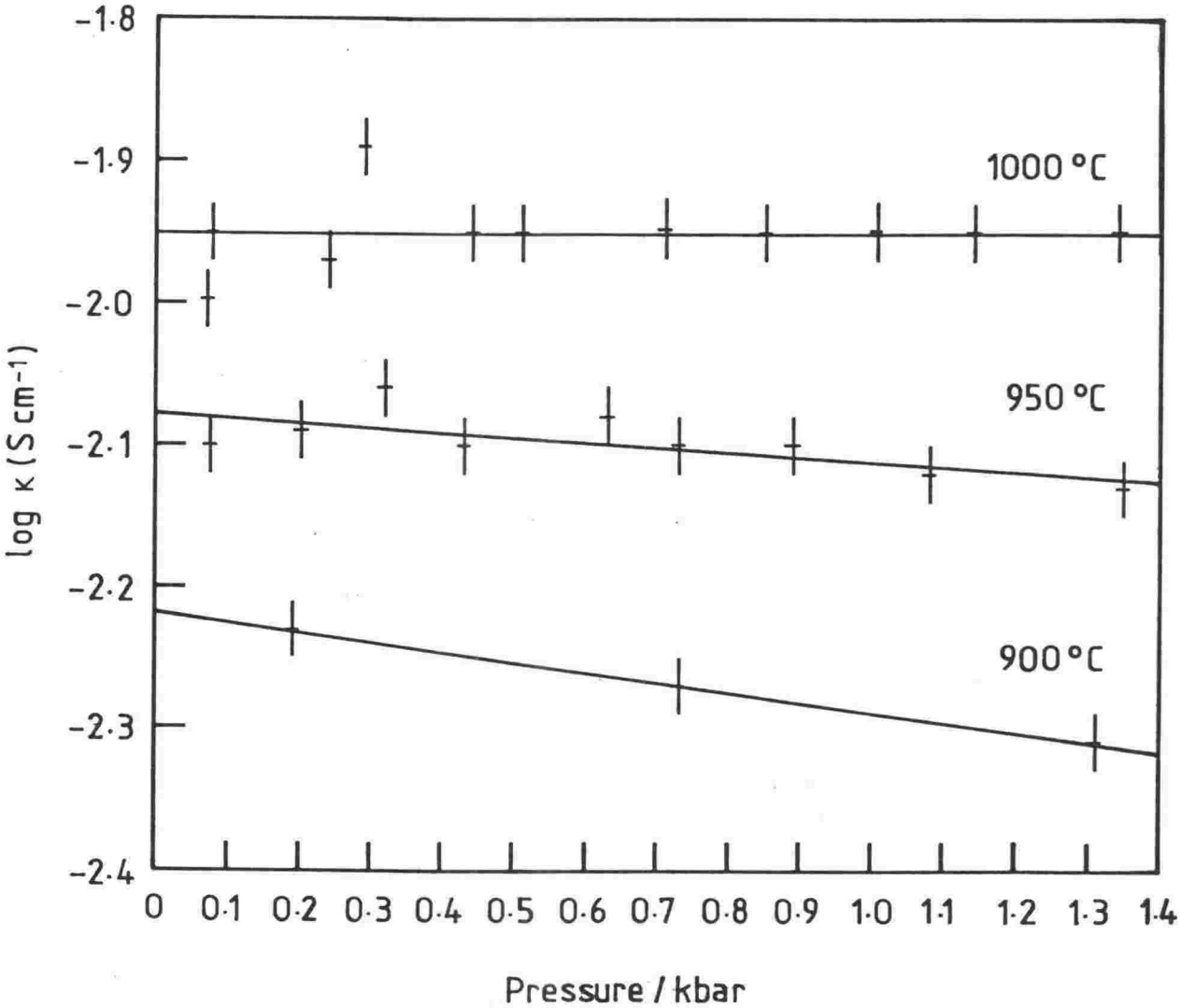

Figure 4.3—Log conductivity versus pressure at constant temperature for molten Mount Erebus lava.

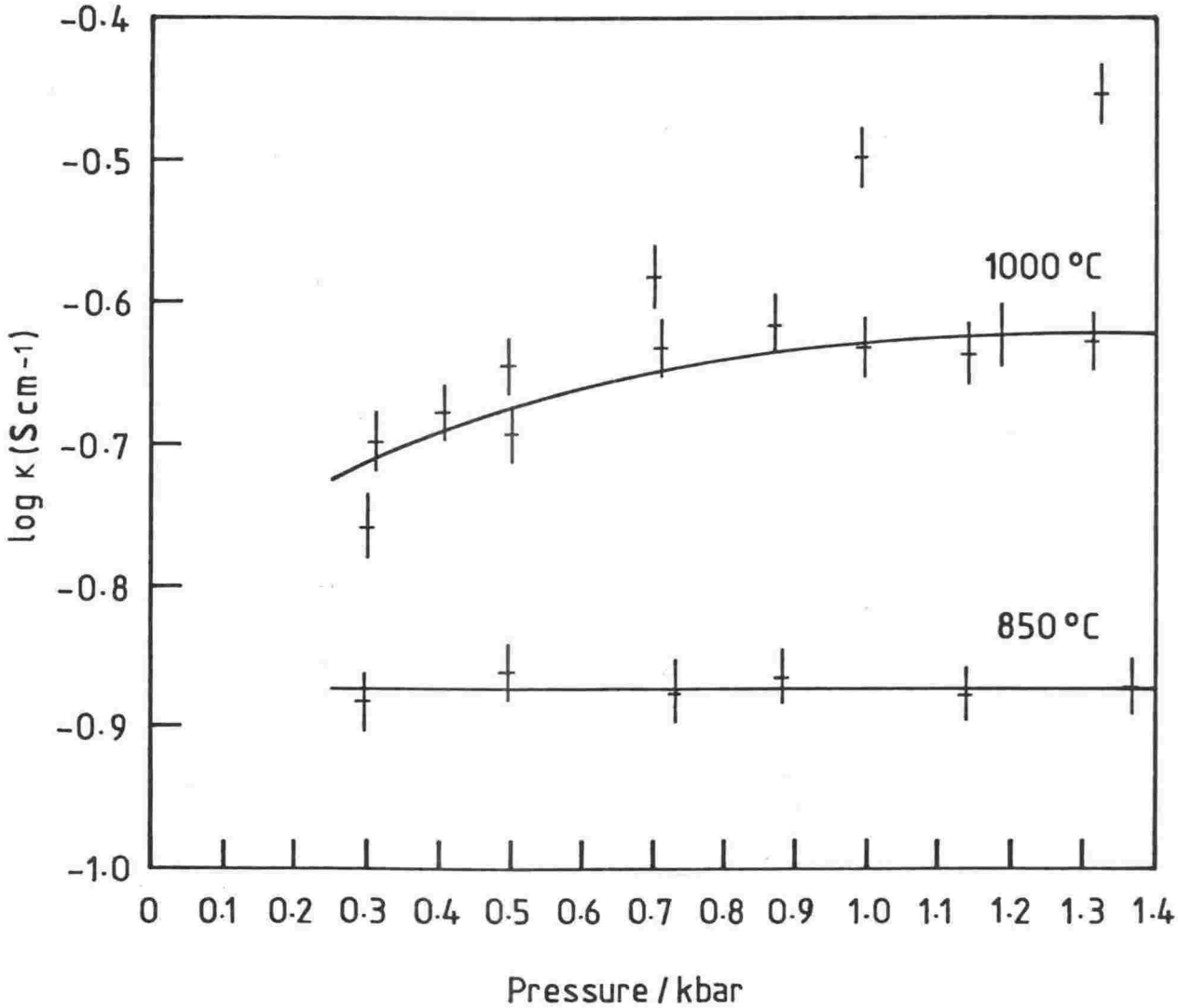

Figure 4.4 — Log conductivity versus pressure at constant temperature for a SiO_2 / Na_2O 78/22 mol% melt containing ~5 wt% H_2O.

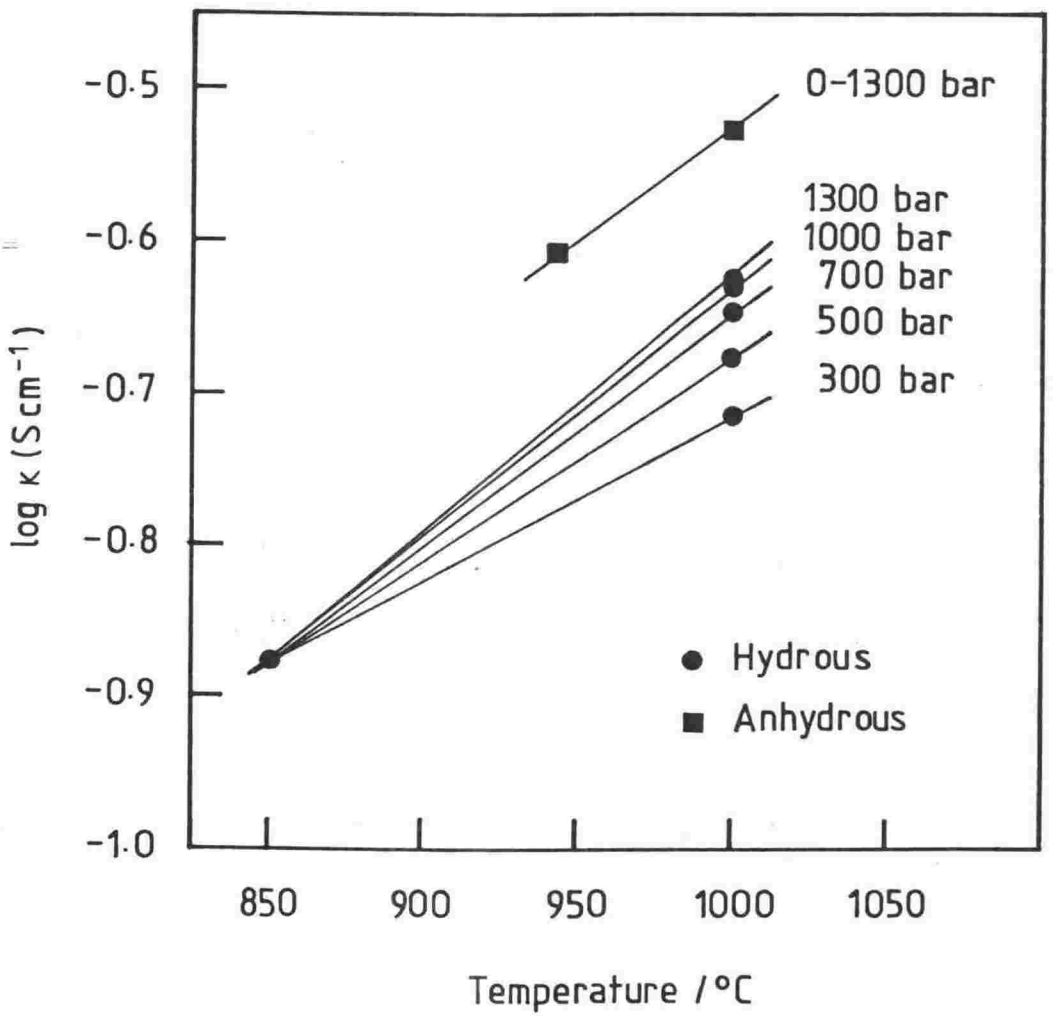

Figure 4.5 — Log conductivity versus temperature at constant pressure for hydrous and anhydrous SiO_2/Na_2O 78/22 mol% melts.

exceeds the 950°C one. When this data is plotted as log conductivity versus temperature (Figure 4.7) it is found that conductivity passes through a maximum with increasing temperature. The maximum shifts to higher temperatures as pressure is increased. The cell constant was determined by calibration with 0.01M KCl.

Table 4.1 shows one of several electron microprobe analyses performed on the hydrous lava subsequent of the experimental run. These analyses showed that there was, on average, a 3 wt% shortfall in the wt% total. This loss was assumed to be composed of the most volatile components in the glass, which, in this case, is water. The mol% ratios in the table have been calculated assuming the 3 wt% was water lost from the glass during analysis. This quantity of water present in the experimental glass compares favourably with the 4 wt%, which was the proportion of water added when preparing the sample.

4.1.6 Composition Dependence of Electrical Conductivity

The composition dependence of electrical conductivity for all silicates investigated is presented in Figure 4.8 by plotting log conductivity versus mol% Na_2O. Since the effect of pressure was minimal, the values have been plotted for the 1000°C and 1 bar conditions only and compared with Tickle's data under similar conditions. The four binary systems fall on the literature line since it was this data from which the cell constant was calculated. However, it was found that the ternary, multicomponent and hydrous silicates, independent of Tickle's data, still lie very close to the binary soda - silica curve. The conductivity is thus a strong function of the

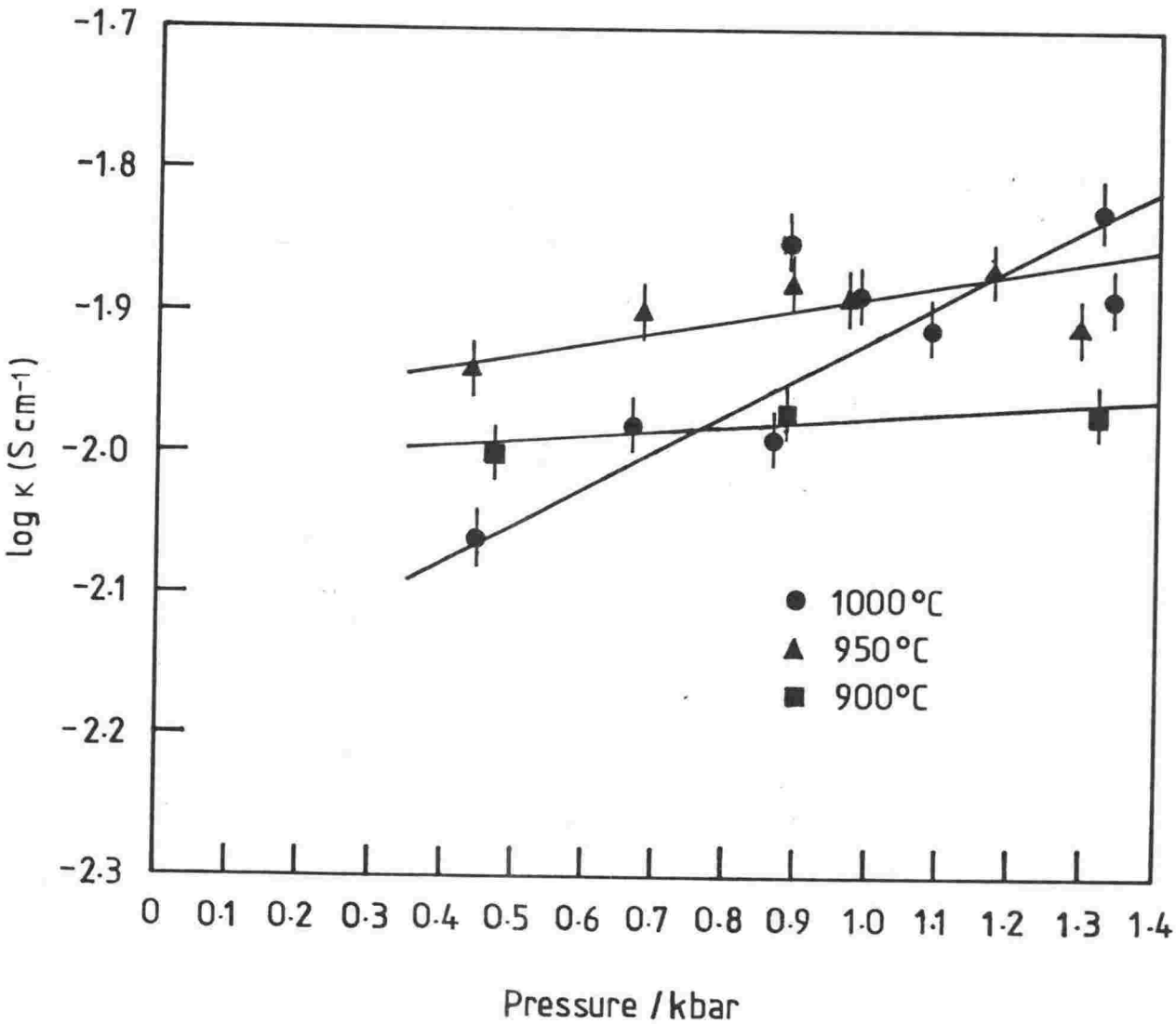

Figure 4.6—Log conductivity versus pressure at constant temperature for molten Mount Erebus lava containing ~4 wt% H_2O.

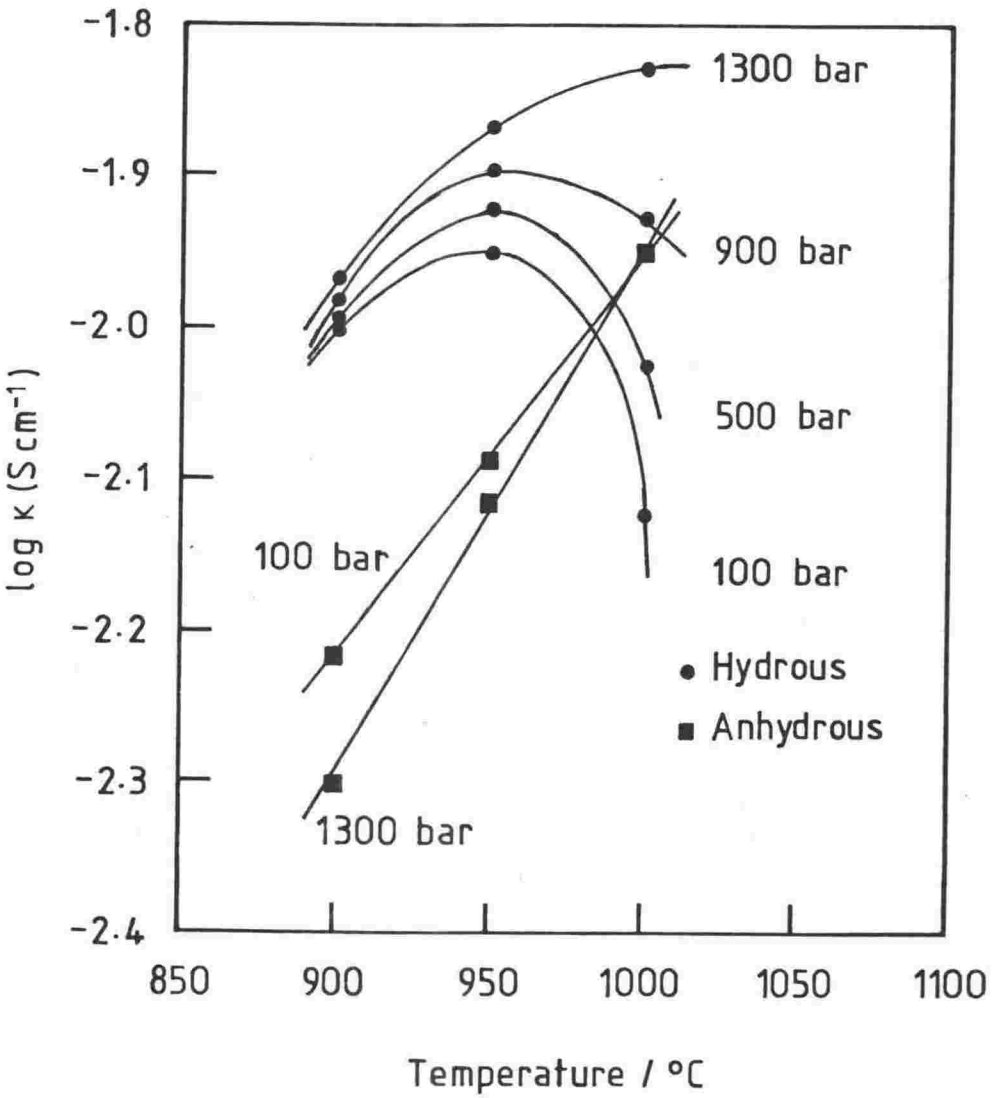

Figure 4.7—Log conductivity versus temperature at constant pressure for hydrous and anhydrous molten Mt. Erebus lava.

TABLE 4.1

Composition of Hydrous Erebus Glass Following Experimental Run

Oxide	Wt %[1]	Mol %[2]
SiO_2	55.677	57.33
Al_2O_3	18.822	11.42
TiO_2	0.915	0.71
FeO	4.200	3.62
MnO	0.305	0.27
MgO	1.022	1.57
CaO	2.154	2.38
Na_2O	9.054	9.04
K_2O	4.687	3.08
Cl	0.169	0.29
H_2O	[3.000]	10.30
	100.005	100.01

[1] Analysis by Electron Microprobe.

[2] Calculated assuming 3 wt% H_2O present.

concentration of Na_2O. For example, at 1000°C an increase by 20 mol% Na_2O to a melt already containing 20 mol% Na_2O causes an eightfold increase in the conductivity.

4.1.7 Activation Energies of Conduction

Where possible, activation energies were calculated. Unfortunately the activation energies could only be determined over a small, ~150°C, temperature range. Since generally there were only two points on a log conductivity versus 1/T plot, it had to be assumed that the isotherms were a linear function of log conductivity. However, for the anhydrous Mount Erebus lava, where there were three isotherms, log conductivity versus 1/T did produce a straight line. Nevertheless, although there are substantial errors (section 4.1.8) involved in the calculation of activation energy from log conductivity versus pressure plots, limiting the usefulness of this parameter, it was found that where experimental and literature data overlapped, there was good agreement (Figure 4.10). Table 4.2 lists the activation energies of conduction for the various silicates and compares the values at different pressures. On the same Table are the activation energies calculated from Tickle's data at 1 bar and for three temperatures. Figure 4.9 is a plot of the data in Table 4.2 as a function of pressure. Activation energies as a function of mol% Na_2O are plotted in Figure 4.10 and compared with literature data.

In Figure 4.9, where activation energy of conduction is plotted as a function of pressure, all silicates show an increase in activation energy with pressure. The large pressure dependence in the case of hydrous Erebus lava is a consequence of the conductivity isobars passing

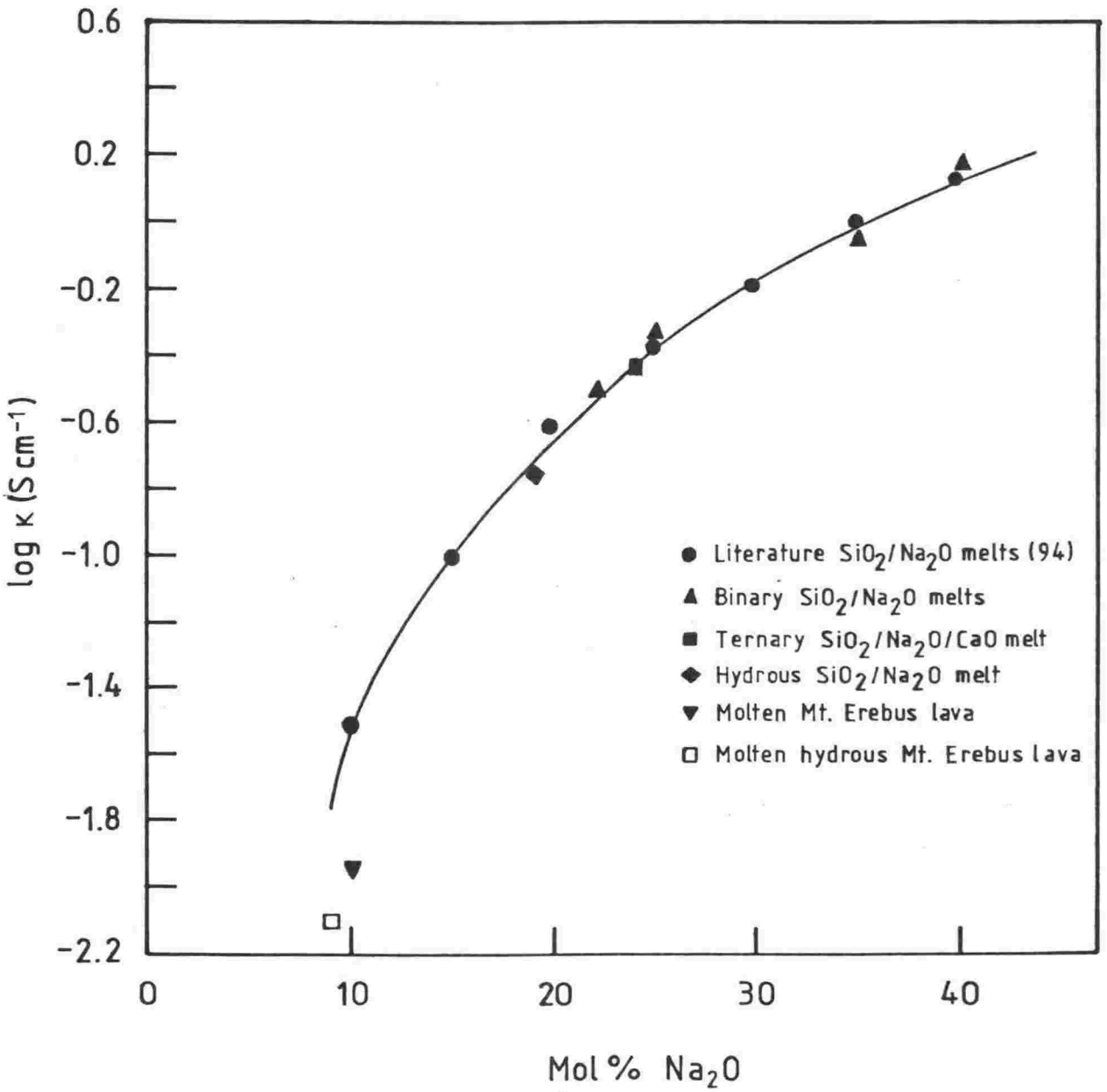

Figure 4.8—Log conductivity versus mol% Na_2O at 1000°C and 1 bar for the molten silicates of the present study and binary SiO_2/Na_2O melts from literature data.

TABLE 4.2

Activation Energies of Conduction

Mol% Na_2O	E_K /Jmolx10^4 1 bar	300 bar	600 bar	1000 bar	1300 bar
1. Anhydrous Silicates (900-1000)°C					
22	4.4			5.2	
25	3.9			4.7	
24 [+4% CaO]	5.4			5.7	
40	4.4			5.7	
10 [Erebus]	7.6			9.6	
2. Hydrous Silicates (900-1000)°C					
19 [+ ~15% H_2O]		2.9			4.6
9 [+ ~10% H_2O, Erebus]					
900°C	4.0	4.8	5.7	7.5	7.7
1000°C	-14.0	-12.0	-7.5	-1.9	-1.8

3. Literature data for SiO_2/Na_2O melts at 1 bar[1]

	800°C	900-1000°C	1100°C
15	6.8	5.2	4.3
20	5.4	4.5	3.7
25	4.9	4.0	3.5
30	4.5	3.8	3.4
35	4.2	3.6	3.5
40	4.1	3.5	3.4
45	4.1	3.8	

[1]Activation energies calculated from data in reference (94).

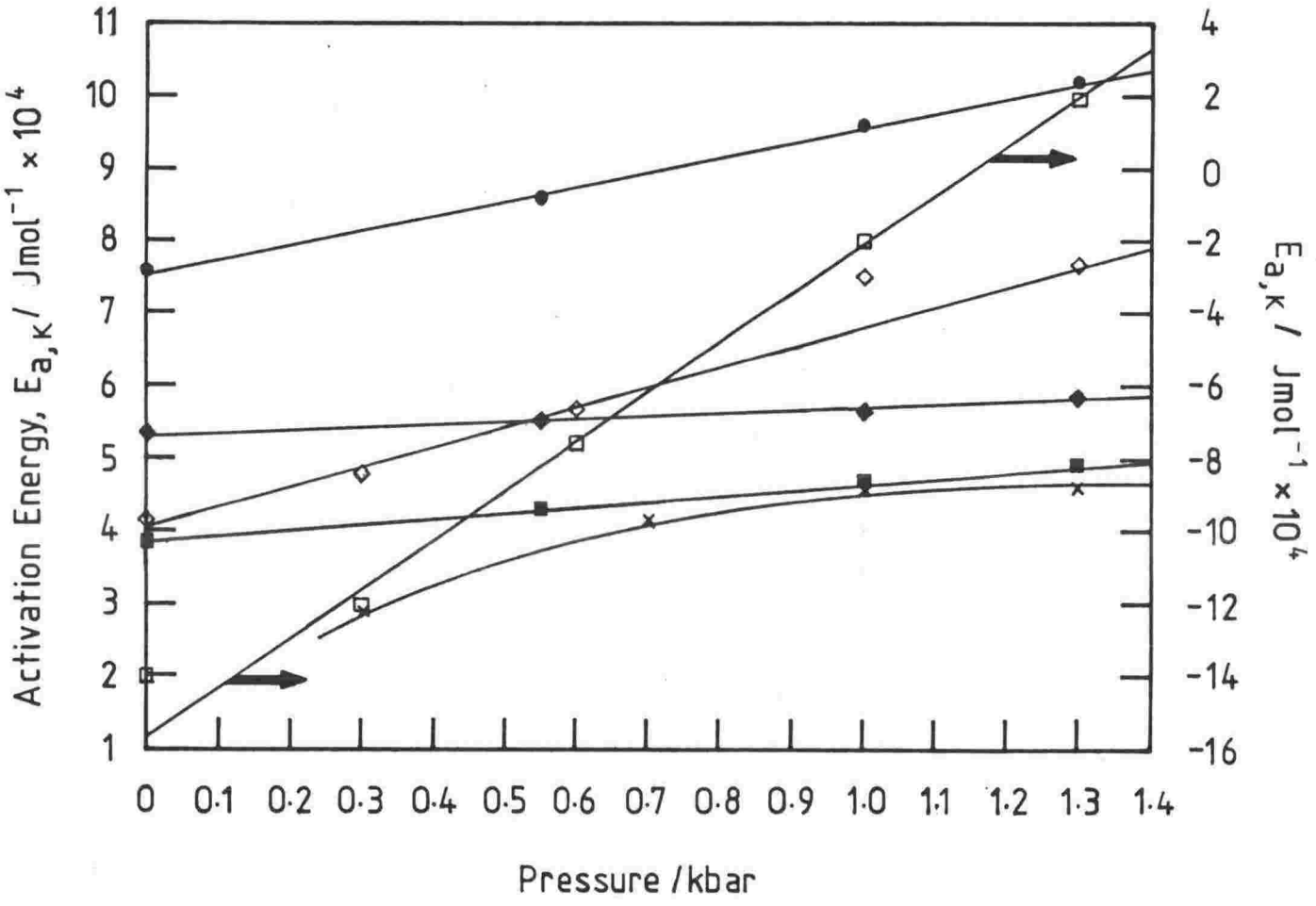

Figure 4.9— Activation energy of conduction versus pressure for some silicate melts selected from the present study. (●-Molten Mt. Erebus lava; □-Hydrous Mt. Erebus lava at 1000°C; ◇-Hydrous Mt. Erebus lava at 900°C; ◆-Ternary $SiO_2/Na_2O/CaO$ melt; ■-Binary SiO_2/Na_2O 75/25 mol% melt; X-Hydrous SiO_2/Na_2O 78/22 mol% melt.)

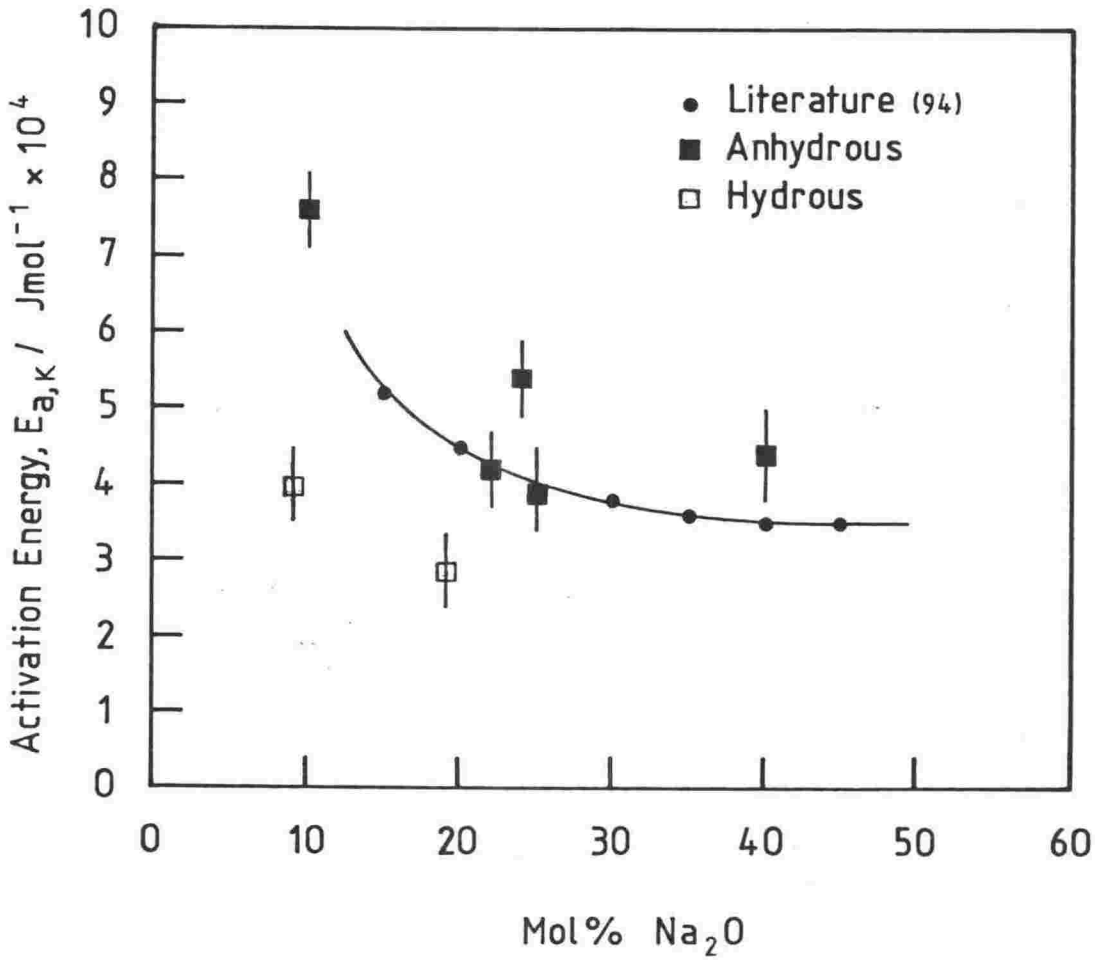

Figure 4.10— Activation energy of conduction versus mol% Na_2O at 1000 °C and 1 bar for the hydrous and anhydrous silicates studied and activation energies calculated from literature data.

through a maximum and the slope of the line changing sign (Figure 4.7). Activation energy according to Figure 4.10 is approximately a function of Na_2O composition. Increasing the amount of Na_2O in those melts examined here, decreases the activation energy of conduction irrespective of composition.

4.1.8 Discussion of Errors and Reliabilty of Results

Table 4.3 summarises the errors associated with each of the experimentally measured quantities and the derived parameters. The error in pressure is half the smallest division (5 bar) of the Heise gauge. In the case of the error associated with temperature, the value in Table 4.3 is the error of the individual thermocouple measurements converted from voltage to degrees centigrade. This is not to be confused with the temperature gradient over the length of the cell, which was determined by two independent thermocouples. The 6% error in the cell constant value was the result of either errors involved in the extrapolation process to determine the value from Tickle's data or errors arising from temperature variations during the calibration process. Also, during calibration with KCl, small leaks, which passed the gold "O" rings, in the base of the cell made it impossible to increase the precision of this measurement using the present cell design. Electrical conductance depends on both temperature and pressure. Since there is an uncertainty in measuring both of these parameters, the errors associated with each contributes to the overall error in conductance. There is also a contribution from the instrument error. The error arising from the effect of pressure is very small

TABLE 4.3

Summary of Experimental Errors

Pressure	+/-5bar	
Temperature	+/-3oC	
Cell constant	+/-6%	
Conductance	+/-4%	{0.25% instrument error {0.03% pressure error {3.57% temperature error
Conductivity	+/-10%	
log Conductivity	+/-0.04	
Silicate Composition	+/-3%	
Activation Energy	+/-25%	

(+/-0.03%), since conductance is almost independent of pressure, compared to the error from temperature uncertainty (+/-3.57%) and instrument error (+/-0.25%). These errors are consequently reflected in the error for conductivity (+/-10%) together with the cell constant. Silicate compositions have an error of +/-3% due to either the initial preparation of samples, particularly the hydrous ones, or the microprobe analysis. Electron microprobe analysis of synthetic glasses containing high concentrations of Na_2O, even with a defocussed beam, underestimates the quantity of Na_2O present due to its high volatility. The large percentage error in activation energy was caused by the relatively large error in conductivity coupled with the small differences in Δlog conductivities.

At this point it is appropriate to make some comments about the reliability and internal consistency of the experimental results. First, there are three important features of the results which should be borne in mind:

1. The results show little or no hysteresis during either increasing or decreasing pressure.
2. Frequency effects were very small, indicating a reliable cell design.
3. The effect of pressure on conductance is almost independent of pressure for the anhydrous silicates.

Second, although the electrical conductivity results for the binary silicates of necessity fall on the literature data (Figure 4.8), the activation energy of conduction which is independent of the cell constant falls, within experimental error, on the literature data.

Further, where the cell constant was determined by both calibration with KCl and the appropriate silicate there was good agreement. Also, the values of conductivity of all the silicates plotted against mol% Na_2O (Figure 4.8) form a consistent set of data with respect to increasing concentration of soda. (This will be discussed further in the following chapter). Third, the plots, Figures 4.9 and 4.10, of activation energy as a function of pressure and mol% Na_2O show an increase in activation energy with an increase in pressure and a decrease in activation energy with an increase in mol% Na_2O, respectively. Both of these results are to be expected and the latter results agree well with the literature data.

The foregoing shows there is a high degree of internal consistency within the experimental results and that there are excellent comparisons with literature data (section 5.1).

4.1.9 Summary of Electrical Conductivity Results

1. Electrical conductivity is independent of pressure, at least up to 1300 bar, for the anhydrous silicates studied. However, as T_g is approached pressure dependence becomes negative. There is a small positive pressure dependence for the hydrous systems. This dependence increases with temperature.
2. The electrical conductivity of molten silicates is a strong function of both temperature and Na_2O composition.
3. The addition of water to molten silicates, already containing 10 mol% or more Na_2O, gives rise to a reduction in the electrical conductivity.

4. Activation energy of conduction decreases with the addition of soda. In all cases activation energy has a positive pressure dependence.

4.2 VISCOSITY OF ATHABASCA BITUMEN

Table 4.4 presents the viscosity results on Canadian Athabasca bitumen using the quartz crystal viscometer[1]. Viscosity was calculated using the damping formula (equation 3.1). These results are shown graphically in Figure 4.11. To calculate viscosity via the damping formula a background run to determine $V_{d(background)}$ as a function of temperature was required. A plot of $V_{d(background)}$ versus temperature is found in Figure 4.12. The viscometer was calibrated to determine CK^2, in the damping formula, by using two different oils with viscosities of 2.044 and 0.965 Pa s, respectively, and liquid glucose at 100°C where its viscosity is 25 Pa s. CK^2 for calculation in the damping formula was taken as the average value of CK^2 determined for each of these three liquids and was equal to 0.82 $kg^2m^{-4}s^{-2}$.

The results in Figure 4.11 generally follow the characteristic viscosity behaviour of liquids, however, there is some unusual behaviour at both ends of the temperature range covered. Although there is no data with which to makes comparisons there are observational and experimental reasons to explain this behaviour. The increase in viscosity above 200°C can be explained in terms of either the formation of bubbles in the melt nucleated on the metal surface of the cup or rod, or decomposition and loss of volatile components. In the former

---

[1] These viscosity measurements were made by Mrs Karen Hamer.

TABLE 4.4

Viscosity of Canadian Athabasca #2 Bitumen

T /°C	V_d(liq)/ Volt	V_d(bkgd)/ Volt	Freq/khz	η/Pa s[1]	log η
118	3.12	0.0275	39.168	70	1.85
123	3.16	0.28	39.159	72	1.86
127.5	3.289	0.28	39.146	78	1.89
130	3.352	0.28	39.140	81	1.91
132	3.380	0.28	39.138	83	1.92
135	3.35	0.28	39.122	81	1.91
134	3.21	0.28	39.166	74	1.87
142	2.51	0.28	39.096	43	1.63
147	2.22	0.28	39.083	32	1.51
152	2.446	0.28	39.064	40	1.60
157	1.722	0.28	39.357	18	1.26
162	1.634	0.28	39.341	16	1.20
167	1.360	0.28	39.235	10	1.00
170	1.174	0.285	39.215	8.3	0.92
172	1.077	0.285	39.203	5.4	0.73
177	1.025	0.285	39.174	4.7	0.67
182	1.072	0.285	39.156	5.3	0.73
185	0.863	0.285	39.144	2.9	0.46
187	0.772	0.285	39.137	2.0	0.31
192	0.674	0.285	39.116	1.3	0.12
197	0.628	0.285	39.101	1.0	0.0067
202	0.675	0.285	39.085	1.3	0.12
209	1.086	0.285	39.054	5.5	0.74
224	1.96	0.29	39.040	24	1.4
225	1.99	0.29	39.004	25	1.4
227	1.9	0.29	39.997	22	1.3

[1]Calculated using the damping formula, equation (3.1), where $CK^2 = 0.82 kg^2 m^{-4} s^{-2}$ an average value determined by calibration using 2.044 and 0.965 Pa s oils at 25°C and glucose at 100°C.

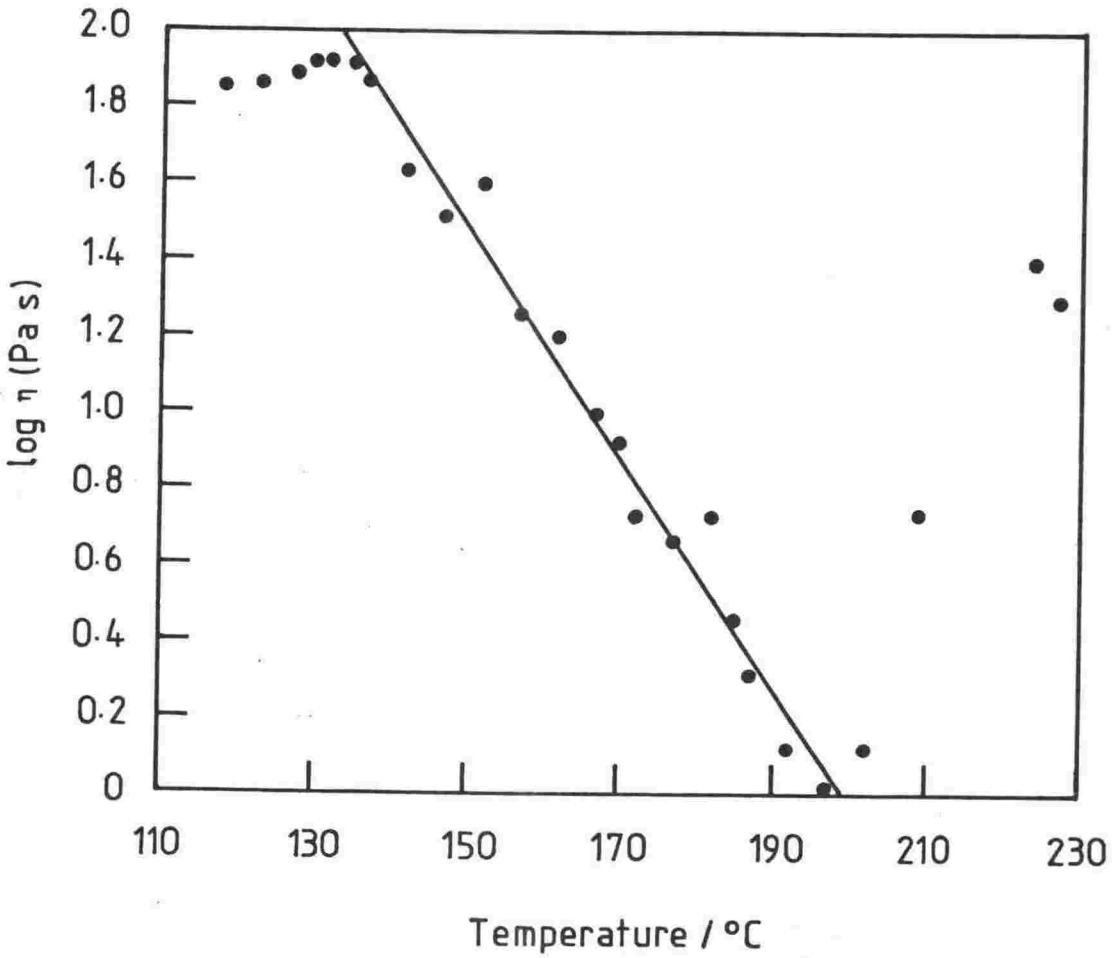

Figure 4.11—Log viscosity, η, versus temperature for Canadian Athabasca #2 bitumen.

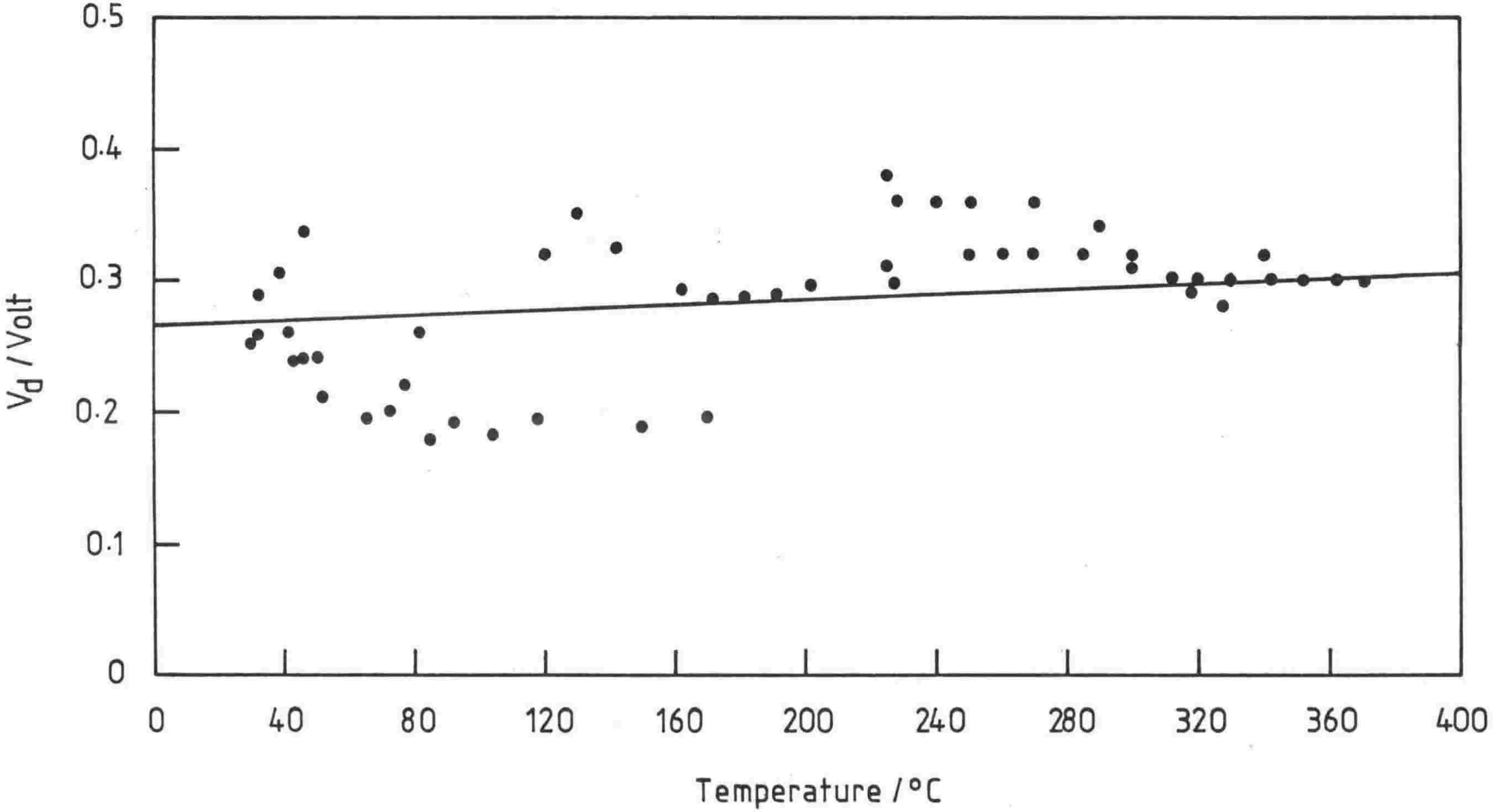

Figure 4.12—Drive voltage, V_d, versus temperature for quartz crystal viscometer background run.

situation it is well known that the formation of bubbles or froth in a liquid increase viscosity. In the latter case, with a reduction in the lighter solvent fractions in the bitumen, one would expect an increase in the viscosity. In the process of assembling the viscometer the quartz crystals were broken. A new set of crystals were substituted. However, the rod, already sealed in the cup, was not re-tuned to the resonant period of the new crystals. The resulting damping caused by the cup not being sealed onto the rod at a node would reduce the resonant response of the viscometer, particularly at high viscosities. There were no precautions taken to thermostat the quartz crystals.

Chapter V

DISCUSSION

In this chapter the results presented in chapter four are discussed. An attempt is given to interpret the conductivity results in terms of previous work on molten silicates, as described in chapter II, and the properties of other high temperature liquids, notably, partially ionised molten salts.

The chapter begins with a comparison of the conductivity results with previous studies. Composition dependence, temperature dependence and pressure dependence of conductivity are discussed in the next three sections respectively. The final section discusses the piezoelectric quartz crystal viscometer and viscosity measurements made above room temperature.

5.1 COMPARISON WITH PREVIOUS RESULTS

5.1.1 Anhydrous Melts

The only conductance measurements on binary soda-silica melts at one atmosphere which have been made in the temperature range of this study are by Tickle (94). These results were used to calibrate the conductance cell and consequently the conductivities of the two sets of results are not independent. However, the activation energies compare favourably with those calculated from Tickle's data (Figure 4.10). Tickle's results cover a wider range of temperature and composition than previous workers

and for temperatures greater than 1200°C his results compare well with those of Bockris et al. (91) and Urnes (222). Thus the present conductivity results for binary soda-silica melts are consistent with an extensive body of experimental data.

There are no previous conductivity studies on $SiO_2/Na_2O/CaO$ liquids in the temperature and composition range examined here.

The conductivity of Mt Erebus lava at 1000°C and 1 bar is within an order of magnitude of the conductivity of the complex silicates studied by Murase and McBirney (44) and Waff and Weill (141). These complex silicates have similar but not identical compositions to the Erebus lava. The amount of Na_2O present in melt NRO of reference (44) and melt HA(3N) of reference (141) is ~5 and ~7 mol%, respectively, in comparison with ~10 mol% for the Erebus lava. Figure 4.8 shows that conductivity is very dependent on Na_2O content. Thus the order of magnitude discrepancy in conductivity is the result of compositional differences in Na_2O. This will be discussed later.

No measurements on the pressure dependence of conductance for binary or ternary silicate melts have been reported in the literature. Previous work on the effect of pressure on conductance for complex silicates is described in section 2.2.6.2 (1).

The present results of zero pressure dependence on conductivity for binary and ternary systems and small negative pressure dependence at low temperatures for the Erebus lava are qualitatively in agreement with the results of Khitarov et al. (143), Waff (138) and Tyburczy and Waff (145). All of these groups of workers found that in the pressure range 0 to 25 kbar the conductivity decreases by ~80% or less. Therefore on

application of only ~1.3 kbar, the maximum pressure of the present study, even smaller decreases in conductivity would be observed. In the case of the Erebus lava, the pressure dependence became more pronounced as the temperature was reduced. An identical trend was found by Tyburczy and Waff (145) for both andesite and tholeiite melts.

Silicate liquids can be regarded as partially ionised liquids. This is explicit in both the 'iceberg' model and polymer theories of molten silicates, discussed in chapter two, where equilibria are postulated to exist between a range of silicate anions. For example, in the 'iceberg' model vitreous like SiO_2 islets exist in equilibrium with polyanions such as, $Si_3O_9^{6-}$ and $Si_6O_{15}^{6-}$. In a study of the pressure dependence of electrical conductivity for fused, partially ionised, mercuric halides, Cleaver and Smedley et al. (223) made a quantitative estimate of the activation volumes of conduction ΔV_κ. In molten salt systems where the cation radius (r_+) is very much less than the anion radius (r_-) and where the smaller ion is the most mobile, for example the lithium halides and nitrates, ΔV_κ approaches zero and thus the mobility of the cation is almost independent of pressure. Thus by assuming that ionic mobilities are independent of pressure and that conductance is proportional only to the concentration of the charge carrying ions they derived the following equation for ΔV_κ:

$$\Delta V_\kappa \doteq -N_A \beta_T \sum_i e_i^2 / 12 r_i$$

where: N_A - Avogadro's number, e - charge on a proton and r_i - radius of the charge carrying ion. This equation predicts that for a melt in which the size of the conducting species is not a function of pressure,

ΔV_K is proportional to β_T. Thus for a partially ionised melt of low compressibility, ΔV_K will be small and hence β_T will not be a strong function of pressure. The above equation has been tested satisfactorily for the mercuric halides as well as AlI_3, GaI_3 and I_2 (224). Since in molten alkali silicates $r_+ << $ radius of the silicate anions the mobility of the alkali cations is not expected to be pressure dependent. Further, alkali silicates have very low compressibilities, see section 2.1.2.1. Therefore, applying the above discussion on partially ionised melts to alkali silicate melts, it is predicted that these silicate melts will have small pressure coefficients of conductivity. The present experimental results confirm this prediction.

5.1.2 Hydrous Melts

Previous work on the effect of dissolved water on the conductivity of silicate melts has been restricted to water saturated systems with low mole fractions of alkali cations. Under these conditions the mole fraction of H_2O increases with increasing pressure and the conductivity is augmented by several orders of magnitude on addition of the first few wt% of H_2O. Beyond this initial amount of H_2O, addition of further water causes relatively minor concomitant increases in the conductivity. In contrast, the hydrous systems of this work: (1) contain a relatively high mole fraction of alkali cations; and, (2) the mole fraction of H_2O in the melt remains constant with increasing pressure. Under these conditions electrical conductivity was found to decrease, by ~40%, on addition of ~4 wt% water to a dry melt.

5.2 COMPOSITION DEPENDENCE OF CONDUCTIVITY AT 1 BAR

5.2.1 Anhydrous Melts

Figure 4.8, a plot of log conductivity versus mol% Na_2O, shows that conductivity is a strong function of soda content. This graph includes Tickle's data for binary soda-silica melts at 1000°C and 1 bar along with the results for the present binary and ternary melts, the Erebus lava and the hydrous melts. The important feature of this graph is that all the systems studied lie close to, or actually on the binary soda-silica line, implying that Na^+ is the principal conducting species even though some of the melts contain a variety of cations. Since conductivity is expected to be a function of the total alkali content, literature data and the results of this work were plotted versus mol% total alkali. This is shown in Figure 5.1 along with the the data for the binary Na_2O-SiO_2 and K_2O-SiO_2 systems. In spite of widely varying mole fractions of SiO_2, Al_2O_3, and alkaline earth metal oxides (MgO and CaO) the conductivity is predominantly a function of mol% (total alkali) and for the naturally occurring systems in Figure 5.1 Na_2O is the major alkali cation.

Figure 5.1 does, however, show some displacement from the binary soda-silica line particularly above 10 mol% total alkali where the points are all below the binary soda-silica line. There are three factors contributing to this displacement:

1. Compositional variations. In the complex silicates the contribution of non-alkali cations to the conductivity, although small, may be sufficient to account for some of the deviation from the binary line at least below 10 mol% total alkali.

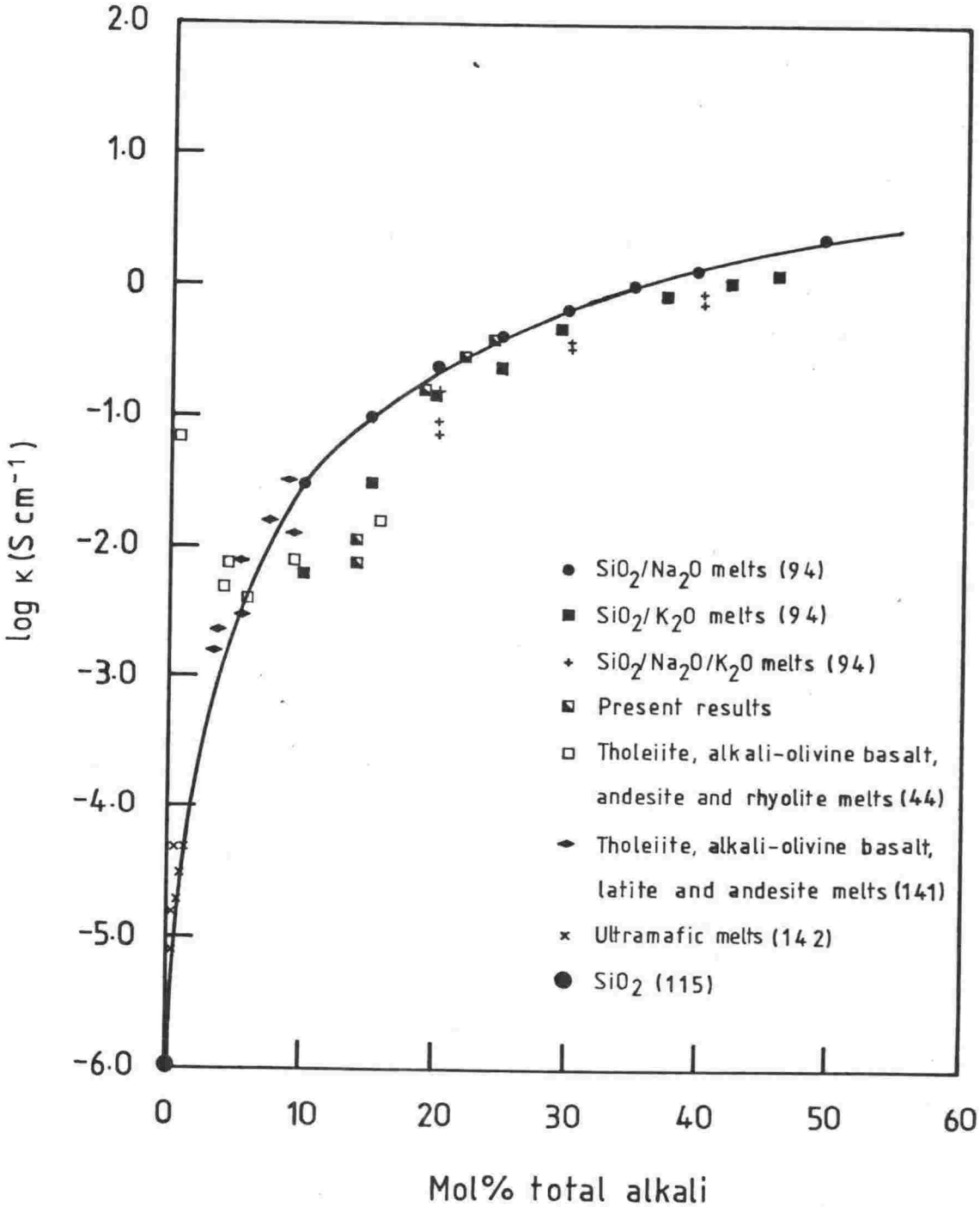

Figure 5.1—Log conductivity versus mol% total alkali at 1000 °C for a wide range of molten silicates.

2. Density variations. Conductivities of melts of different compositions should be compared via molar conductivities. This requires data on the density of the melts, which for the present melts and the lavas used in Figure 5.1 is not known. Bottinga et al. (37), (38), however, have developed an equation to calculate density of multicomponent silicates based on the fact that the partial molar volumes of most components of magmatic liquids are constant. The density, calculated from the Bottinga equation, of anhydrous melts at constant mol% ($Na_2O + K_2O$) varies by ~3-4% as the mole fraction of other oxides is altered. Density variations and hence changes in the concentration of mobile species, at least for anhydrous melts, will cause only relatively minor variations in the conductivity at a given mol% ($Na_2O + K_2O$).
3. Mixed alkali effect. This effect refers to deviations from additivity in isotherms of various physical properties as a function of composition as one alkali cation is progressively replaced by another. Both glasses and melts exhibit this phenomenon (225), (94). It is most pronounced and with negative deviations for conductivity isotherms, but almost nonexistent in the case of equilibrium thermodynamic properties such as molar volumes and heat capacities (226). This effect according to Isard (227) is observed only for systems containing approximately 10 mol% or more total alkali. In the absence of lithium cations the binary soda-silica line will be the upper limit of conductivity where the mixed alkali effect is operative, since the conductivity of K_2O-SiO_2 is less than Na_2O-SiO_2 and the

conductivity passes through a minimum as Na_2O is replaced by K_2O (94). This effect is observed for the ternary alkali silicates studied by Tickle shown in Figure 5.1 and may be responsible for the low conductivity values where there is a high total alkali mole fraction. Most naturally occurring silicates contain insignificant amounts of lithium and the mol% ($Na_2O + K_2O$) is generally less than 10%. Therefore a mixed alkali effect is unlikely to be observed for these melts.

Figure 4.8 shows that the addition of 4 mol% CaO to a soda-silica melt reduces the conductivity. This finding can be accounted for in the following way. Comparison of the conductivities of $CaO-SiO_2$ and Na_2O-SiO_2 binary melts (119), (221) shows that soda melts are significantly more conducting than calcium melts. The calcium ion has an ionic radius similar to that of sodium but with a higher charge, thus is more tightly bound to oxygen and consequently there is a low concentration of free Ca^{2+} ions. The conductivity of the $Na_2O-CaO-SiO_2$ ternary melt studied in the present work is identical to a binary Na_2O-SiO_2 melt containing the same mole fraction of Na_2O as the ternary melt. Since CaO is not participating in the conduction process it is, in effect, acting only as a diluent, reducing the concentration of Na^+ ions and hence the conductivity. In ternary melts at a high mole fraction of CaO in comparison to Na_2O, it appears, from the data of Kroeger and Heckmann (221), that CaO may cause a significant decrease in the conductivity. However, at present, there is insufficient data on ternary melts to confirm this.

The conclusion that Na^+ cations are the main conducting species in silicate melts except in the presence of significant quantities of other alkali ions has implications for estimating the conductivity of molten lavas. To a first approximation the conductivity of a molten lava of known composition can be obtained from a log conductivity versus mol% ($Na_2O + K_2O$) graph at the appropriate temperature.

5.2.2 Hydrous Melts

There are three ways in which H_2O may be envisaged to give rise to conductivity changes in molten silicates. These ways will be described briefly, followed by a discussion of how they, either individually or in combination, account for the present experimental results on hydrous silicates.

Changes in conductivity, on addition of H_2O to a molten silicate, can arise from:

1. Molar volumes changes. Burnham and Davis (65) have shown that the molar volume of albite increases considerably as H_2O is added, in contrast, to the addition of further Na_2O to an albite melt. The increased molar volume gives rise to a reduction in concentration of mobile species and hence the conductivity, provided the added water does not liberate extra ions.
2. Polymerisation of the melt. The addition of H_2O to highly polymerised melts, i.e. melts rich in SiO_2 and poor in metal oxides, results in a rapid decrease in viscosity (171) and an increase in conductivity (170). These observations have been explained in terms of water acting as a depolymerising agent,

i.e. a network breaker, in a similar way to metal oxides, rupturing the three dimensional silicate network structure. Smaller silicate anions are produced which offer less resistance to viscous flow and allow increased mobility of charge carrying cations. However, the large changes in transport properties are observed for only the first few wt% of water added. Addition of further water results in only small changes in the transport properties. Thus once a melt has reached a certain degree of depolymerisation addition of further depolymerising agents have little effect on the transport properties. A similar argument has been advanced by Shelby and McVay (228) to explain the effect of water on the viscosity of soda rich silica glasses. It might, therefore, be expected that melts rich in alkali oxides, as for the present melts, may undergo relatively minor changes in conductivity because they are already extensively depolymerised.

3. The mixed alkali effect. Several workers (190), (229) have observed decreases in the conductivity of glasses as a function of increasing water composition and have attributed the reduction in conductivity to the mixed alkali effect. If water participates in a melt in a similar way to an alkali oxide then it is possible that the conductivity isotherms may pass through a minima as water progressively replaces an alkali oxide in an analogous way to one alkali oxide replacing another. Thus a reduction in conductivity in the presence of H_2O, under some circumstances, may be explicable in terms of the mixed alkali effect.

The study by Burnham and Davis (65) has shown that, under similar conditions to the present study, ~4 wt% H_2O would cause a 10-14% increase in the molar volume of an albite melt. Assuming a similar molar volume change for the present melts a concomitant reduction in the conductivity by 10-14% would also be expected as a result of the decreased concentration of Na^+ cations, assuming further ions are not added by the water. Although this effect may be contributing to the reduction in the conductivity, it is insufficient to explain the ~40% decrease shown in Figures 4.5 and 4.7, at the highest temperatures, for the SiO_2/Na_2O 78/22 mol% and Mount Erebus lava silicate systems.

The depolymersing role of H_2O, as indicated in (2) above, may account for relatively small increases in conductivity for the composition range of the present silicates but it cannot account for the observed decrease in conductivity.

The mixed alkali effect is a possible means of accounting for the observed reduction in electrical conductivity. Takata et al. (190) found that the conductivity of $Na_2O.3SiO_2$ glass passed through a minimum as wt% H_2O increased. The minimum occurred at ~4 wt% H_2O. These authors summarised other experimental observations which were consistent with their conductivity results. Ass and Stevels (230), concluded from a study of internal friction and dielectric loss in glasses that deuterium behaves similarly to alkali ions; this interpretation has been questioned (231). Nevertheless, there is a substantial body of evidence in favour of decreases in both conductivity and mobility of species such as Na^+ when appropriate amounts of H_2O are added to glasses.

Since a mixed alkali effect is observed in both anhydrous and hydrous silicate glasses (225), (190) as well as molten ternary silicates (94), it is probable that this effect will occur in molten hydrous silicates. Even though the conduction mechanisms in glassy as compared to molten silicates are probably different, reflected in activation energies which are much lower in glasses (232) than in liquid silicates, the mixed alkali effect is still observed in glass and liquid. The difference in activation energy arises because the contribution to the activation energy caused by the motion of silicate anions falls to zero below the glass transition temperature, T_g, where the anions become stationary.

As already noted the composition range of the present study: total alkali > 10 mol%, falls into the region where the mixed alkali effect is likely to be observed (227). Moreover, the mole fractions of H_2O and Na_2O present in the melt are similar and the composition of the ternary melt is almost analogous to the hydrous glasses studied by Takata et al. (190) where a mixed alkali effect was observed.

The mixed alkali effect has been discussed by a number of authors including Isard (227) and Moynihan (226), (233), (234). Various theories have been proposed to explain this effect, the earliest ones are reviewed by Isard (227), but to date no comprehensive theory has been proposed. Moynihan (233) has summarised the data of a variety of binary mixtures to produce two important generalisations about monovalent cation internal mobilities in mixtures containing a common anion:

1. An increase in mole fraction of the salt with the larger cation will result in a decrease in both cationic mobilities.

2. The rate at which the mobility decreases with the addition of the larger cation will be greatest for the smaller cation.

More recently Ingram et al. (225) and Moynihan and Lesikar (234) have developed a weak electrolyte model to account for the phenomena in a quantitative way. This model supercedes previous ones that can be divided into two categories: (1) cationic interactions and (2) structural/mechanistic models (226). Two important features of the weak electrolyte model are that (i) alkali transport in single-alkali glasses is due to small concentrations of mobile species and (ii) adding a small amount of foreign alkali suppresses, by mass action, the mobile-species concentration.

In hydrous glass systems where the 'mixed alkali effect' has been invoked, the species arising from water and playing the part of the second alkali is disputed. For example: Day and Stevels (235) argued that cooperative movement of sodium ions and protons, in water containing $NaPO_3$ glasses, was responsible for a second peak in the internal friction as a function of temperature. In a study of the effect of water content on the electrical conductivity of sodium trisilicate glasses, Takata et al. (190), suggested that OH^- is the species taking the part of the second alkali. Shelby and McVay (228) were less specific, tentatively concluding, from measurements of viscosity and thermal expansion on sodium trisilicate glasses, that H_2O behaves similarly to an alkali oxide.

There is an increasing amount of attention being placed on the possibility that protons or H_3O^+ (236), (237), (238) are the species responsible for the 'mixed alkali effect' in hydrous glasses and that

partial ionisation of Si-OH(OH_2) groups play an important part in this process for silicate glasses. Doremus (238) concluded, from a study of the interdiffusion of alkali and hydronium ions in silicate glass surfaces, that SiO^- $^+H(OH_2)$ groups are totally ionised. Smit (239), however, has disputed this conclusion claiming that the experimental work of Grigorovich et al. (240), Bauche (241) and Scholze et al. (242) support the hypothesis of partial ionisation of silanol (SiOH) groups. Moreover, Smit (239) noted that Bauche (241), (243) and Scholze et al. (242) conclude from their experimental results that protons and not hydronium ions migrate under the influence of an electric field. Smit then elaborates on how he envisages protons to move through a glass, "...the so called "free" H^+ ions move through the lattice using free electron pairs on oxygen atoms in siloxane bridges, in silanol groups or in water molecules, if present, as points of stabilisation. This binding is much less tight than that of H^+ in silanol groups and also less tight than the binding with non-bridging oxygens with an alkaline earth ion in their vicinity" (239). It is likely that the extent of the ionisation of silanol groups is composition dependent and that H^+ ions or protons are the species playing the part of the second alkali. A similar explanation in favour of H^+ being present in molten hydrous silicates is likely since there is no spectroscopic evidence in favour of either molecular H_2O or H_3O^+ ions. This partial ionisation process is also consistent with the weak electrolyte theory of the mixed alkali effect (234).

The mixed alkali effect thus accounts qualitatively, although possibly in conjuction with molar volume increases, for the observed reduction in conductivity on addition of water.

5.3 TEMPERATURE DEPENDENCE OF CONDUCTIVITY AT CONSTANT PRESSURE

The temperature dependence of conductivity at constant pressure as shown in Figure 4.7 for hydrous Mount Erebus lava is similar to that exhibited by a large number of liquids (95). As temperature increases at constant pressure, conductivity initially increases to a maximum value and then decreases. The temperature at which the conductivity maximum occurs, T_{max}, shifts to higher temperatures with increasing pressure. This phenomenon has been discussed by a number of authors including Smedley (95) and Hensel (244). Both of these authors argue that if any molten salt or molecular liquid is heated to high enough temperatures at low pressures the conductance will pass through a maximum. The maximum is the result of two competing effects: the increase in ionic mobility and the decrease in ion concentration due to association at low densities at the higher temperatures. The former explains the increase which is eventually offset by the latter causing a decrease in the conductivity. Equilibria between ion-pairs and ionic species is shifted in the direction of ionic species as pressure is increased and thus T_{max} is shifted to higher temperatures.

Some aqueous salt systems have also been found to exhibit conductivity maxima as a function of temperature at constant pressure. In aqueous solutions of LiCl, KCl, and $CaCl_2$, conductivity, at high temperatures, passes through a maximum at constant pressure (245), (246). T_{max}, however, passes through a minimum as a function of increasing mole fraction of salt. The concentration of the salt at the minimum in T_{max} is ~1 mol kg^{-1}. A similar trend has been observed in KOH solutions (247). It has been argued (95) that in the dilute region

(< ~1 mol kg^{-1}) of these aqueous salts, T_{max} is the result of two competing effects: (1) increased ionic mobilities with temperature and (2) an increase in ion association as the relative permittivity of water decreases at higher temperatures. Hence any effect which would increase the degree of association, such as increased concentration, would affect the conductance at lower temperatures and cause a decrease in T_{max}.

Above concentrations of ~1 mol kg^{-1} T_{max} increases with increasing salt content, and is also believed to be the result of the two competing effects of increased mobility and ion association. However, at these concentrations ion association is not controlled by the relative permittivity of the solvent, rather, ion association arises at low-densities by the formation of gaslike ion pairs at high temperatures (248). This effect shifts to higher temperatures as the mole fraction of salt increases.

It is proposed that the above explanation is applicable to hydrous and anhydrous silicate liquids since they can be regarded as partially ionised molten salts. The conductivity data for the hydrous silicate melt in Figure 4.7 clearly exhibit maxima, that shift to higher temperatures with increasing pressure. The anhydrous systems do not show maxima in the temperature range that has been covered. However, the isobars for these systems are close together in this temperature range which is analogous to molten $BiCl_3$ at low temperatures in the pressure range 50 - 4000 bar (249). At higher temperatures the isobars for $BiCl_3$ become more widely spaced and pass through a maximum. Therefore it is expected that the anhydrous silicates will also pass through a maximum at temperatures much greater than 1000°C. Silicate liquids, thus,

exhibit the same qualitative features of the aqueous chloride solutions discussed above where T_{max} is lowered by increasing the water content.

Figure 5.2 illustrates the conductivity trends as a function of temperature at constant pressure for the hydrous and anhydrous silicates studied in the present work together with conjectured trends based on the explanation given above.

5.4 PRESSURE DEPENDENCE OF CONDUCTIVITY AT CONSTANT TEMPERATURE

In light of the discussion in the previous section it is not difficult to account for the pressure dependence at constant temperature in the compostion range of the present measurements. The anhydrous binary and ternary silicates of the present study lie in a temperature region which is well below T_{max}, between points T_1 and T_2 on Figure 5.2. In this region conductivity is governed principally by the ionic mobility of the charge carrying Na^+ cations. The mobility of these small cations is not expected to be significantly affected by the size of the silicate anions nor the effect of pressure. Hence the isobars are close together reflecting a zero or a small positive pressure coefficient of conductivity. However, as T_g is approached, for example the anhydrous Erebus lava, the pressure coefficient of conductivity changes sign, shown on Figure 5.2 at T_3 where the isobars cross over. The pressure coefficient of conductivity becomes more negative with decreasing temperature. Identical trends are observed in many liquids, including $Ca(NO_3)_2/H_2O$ mixtures and $MgCl_2.6H_2O$ solutions and these trends arise because the mobility of the charge carrying ions become more pressure dependent at temperatures close to T_g. These trends have been accounted

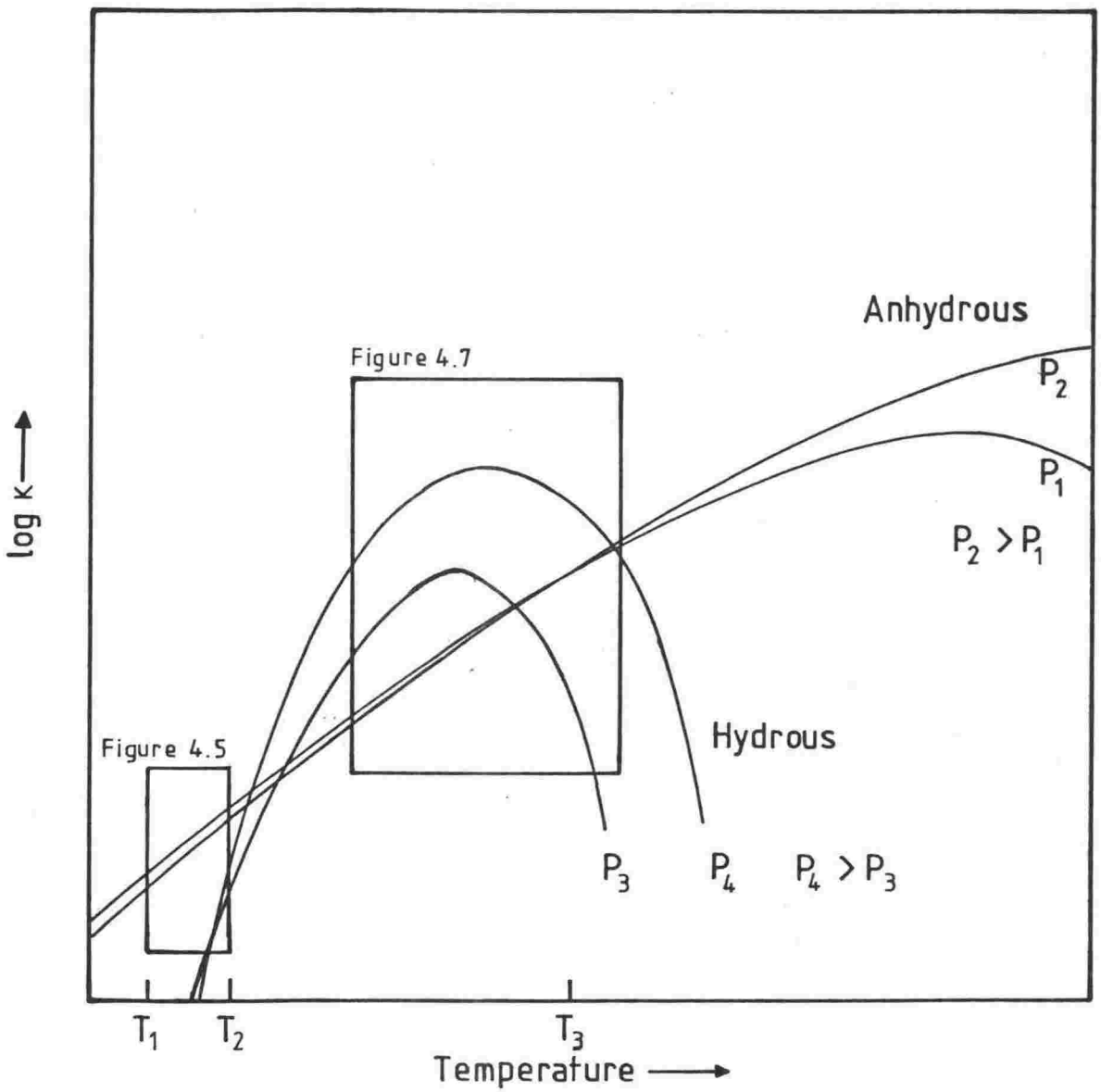

Figure 5.2—Schematic diagram of log conductivity versus temperature at constant pressure. Experimental results on molten hydrous and anhydrous silicates are shown in the two boxes. The extrapolated isobars are conjectured trends based on the discussion in section 5.3.

for in terms of the configurational entropy theory (250), (251). For the hydrous silicates studied the pressure dependence of conductivity becomes greater at higher temperatures. At temperatures greater than T_{max} small increases in pressure significantly increase the conductivity. This arises, because the effect of pressure shifts the equilibrium between species in the melt in the direction of small ionic entities. Ion-pair formation has a greater effect on conductivity at low pressures.

5.5 VISCOMETER

The purpose of developing a quartz crystal viscometer is to be able to measure viscosity as a function of pressure. In particular, it is intended to be used to study the temperature and pressure dependence of viscosity in molten hydrous and anhydrous silicates. As mentioned in section 3.4.1 it is virtually impossible to measure viscosity of a liquid inside a pressure vessel using conventional viscometers. A quartz crystal viscometer makes this possible since only electrical leads are required to pass between the inside and outside of a pressure vessel. Although it has been found to operate successfully at room temperature (1) it has proved difficult to extend its use to higher temperatures and ultimately to 1200°C. Part of this project has been spent on extending its use to temperatures above room temperature. The main problems were:

1. Maintaining good electrode connections between the holder and the crystals.
2. Expansion of the probe as a function of increasing temperature giving rise to strain on the electrode connections.

3. Lack of suitable high temperature cements.

4. Extreme sensitivity of the instrument.

The main achievement of the present development was to mount the crystals on flexible springs. This minimised the effect of (2) since expansion of the probe did not interfere with the electrode connections which had previously been rigid. A completely satisfactory high temperature cement was not found, although a high temperature araldite proved successful in some circumstances. This problem will not be as significant when the viscometer is operating in the internally heated pressure vessel since the temperature at the bottom of the furnace will be close to room temperature due to large temperature gradients (section 3.2.5). A serious drawback with this instrument is its extreme sensitivity: it is subject to ambient temperature variations and mechanical vibrations. This still presents a serious problem in its application.

Athabasca bitumen was used as a test fluid because it has relatively high viscosities at temperatures up to ~200°C. The results indicate the viscometer is behaving correctly over most of the temperature range covered. Abnormalities in the viscosity behaviour, at both ends of the temperature range, were discussed in section 4.2. Later work, mentioned in section 3.4.5, has extended the temperature and viscosity range considerably. As a consequence of this later work the viscometer can now be tested as a function of both temperature and pressure using a molten salt such as $Ca(NO_3)_2$ - KNO_3 60/40 mol% as a test liquid.

Extending the viscometer to study the temperature and pressure dependence of viscosity in molten silicates will require materials: (a)

which can be used to 1200°C and (b) which will withstand corrosive silicate liquids. The only materials which meet these criterion are noble metals. The probe, made from a platinum/iridium alloy, must be a single rod from the crystals to the liquid to avoid any high temperature bonds. Iridium, a very hard noble metal, is necessary to increase the resonant response of the probe. A platinum foil cup can be sealed to the probe at a node and the top of the cup sealed in a similar way to the conductance cell. One of the most important features when assembling the viscometer is that the whole system must be rigidly connected together apart from the electrode connections. Although this instrument lends itself to high pressure viscometric applications, it is an extremely sensitive and delicate instrument.

Chapter VI

CONCLUSIONS AND FURTHER WORK

6.1 CONCLUSIONS

This thesis describes the commissioning of an I.H.P.V. facility which enabled initial electrical conductivity studies to be carried out on some molten silicates over ranges of temperature and pressure. Although the number of results is limited, there are five significant conclusions arising out of the discussion of these results which contribute to the understanding of molten silicates:

1. Electrical conductivity is not a function of pressure for anhydrous and soda-rich melts except at temperatures close to T_g. However, electrical conductivity has a small positive pressure dependence for hydrous melts.
2. Electrical conductivity as a function of increasing temperature was found to pass through a maximum for hydrous melts.
3. In molten silicates containing ~10 mol% or more Na_2O the addition of H_2O results in a reduction of the electrical conductivity. This phenomenon can be accounted for in terms of the mixed alkali effect.
4. Both the temperature and pressure dependencies on conductivity and the effect of water on T_{max} are analogous to the behaviour, previously observed, for partially ionised liquids. This supports the theories of the ionic nature of molten silicates.

5. On the basis of previous data and the present work it was concluded that Na^+ is the principal charge carrier in multicomponent silicate melts.

The developments described in this thesis on the piezoelectric quartz crystal viscometer show that it is capable of measuring viscosity as a function of temperature. Viscosities up to $\sim 10^3$ Pa s have been measured over the temperature range 450-700°C using B_2O_3 as a test fluid. The viscometer is now at the stage where it can be tested, inside the I.H.P.V., as a function of both temperature and pressure. This work has shown that this method of measuring viscosity is ideally suited for measuring the viscosity of molten silicates provided that problems associated with high temperature and pressure applications can be overcome.

6.2 FURTHER WORK

There are a number of technical improvements to the experimental equipment which are necessary to extend the present work. The temperature and pressure ranges should be extended to their design maxima. The maximum design temperature of the furnace, 1200°C, can be utilised if all gold used in the cell construction is replaced with a suitable higher melting temperature noble metal. A gold/platinum solder could replace gold foil for sealing-up the cell. However, in conjunction with these changes, the conductance cell ought to be redesigned to: (i) overcome leaking problems associated with the gold 'O' rings and (ii) facilitate ease of cleaning subsequent to a run, thus allowing repeated use of the cell. To reach the maximum design pressure

of 5 kbar two new mushroom heads are required. This will enable satisfactory power, conductance and thermocouple lead seals to be made in the mushroom heads allowing 5 kbar to be reached and maintained. With these improvements it will be possible to increase the rate at which experimental runs can be performed and also to observe, with greater clarity, the trends in the pressure dependence of conductivity.

There are five avenues of research on molten silicates which arise out of the present work which ought to be pursued:

1. Examination in more detail the conductivity of $SiO_2/Na_2O/CaO$ melts over extended ranges of composition. This will enable the effect on conductivity to be observed as Na_2O is progressively replaced by CaO while maintaining constant mole fraction of SiO_2. It will be of interest to determine if a mixed alkali type effect is observed and the way Na^+ and Ca^{2+} interact in a melt. This work should be repeated with the trivalent cation Al^{3+} in place of Ca^{2+}. If Al^{3+} acts as a network former in the presence of alkali cations then the progressive replacement of Na^+ with Al^{3+} should result in the conductivity passing through a maximum.
2. Investigation of the effect of H_2O on conductivity over greater ranges of alkali mole fractions than the present work to examine in detail the effect of H_2O on conductivity.
3. With the extended pressure range to 5 kbar available, it will be of great interest to measure the conductivity of low melting temperature anhydrous silicates at constant pressure as a function of increasing temperature to determine if conductivity passes through a maximum as predicted in the above discussion.

4. With the viscometer operating as a function of both temperature and pressure it will be possible to measure accurately the viscosity of molten silicates as a function of pressure. This will allow interesting comparisons with the conductivity work.
5. Measurement of the conductivity of multicomponent silicates containing varying mole fractions of alkali cations from zero through to high mole fractions. From this data a parametric equation for estimating the conductivity of naturally occurring silicates based on compositional variations can be developed.

Appendix

TABLES OF EXPERIMENTAL RESULTS

TABLE A.1

Sample No. 3: SiO_2/Na_2O 65/35 mol%

P /bar	T /°C Top of cell	T /°C Bottom of cell	ΔT /°C	C /μF	G /mS	G_c /mS[a]	log G_c	log κ (Scm^{-1})[b]
10	994	1004	10	0.085	16.38	17.42	-1.759	-0.215
12	994	999	5	0.081	15.64	16.60	-1.780	-0.780
525	1002	1002	0	0.034	25.80	28.51	-1.545	-0.00094
500	996	996	0	0.0030	24.80	27.29	-1.564	-0.0199
1000	999	965	34	0.036	24.25	26.67	-1.574	-0.0299
1300	971	933	38	0.048	24.46	26.92	-1.570	-0.0259
1300	996	948	48	0.040	22.98	25.12	-1.600	-0.0559
Switched furnace off and reheated the following day. Subsequent results are not consistent with the initial ones.								
9	996	999	3	0.400	25.05	27.61	-1.559	-0.0149
60	996	999	3	0.648	43.97	52.48	-1.280	0.264
60	996	999	3	0.749	44.85	53.70	-1.270	0.274
60	993	999	2	2.498	61.65	79.80	-1.098	0.446
570	986	945	41	2.690	71.68	97.55	-1.011	0.533

[a] Conductance corrected for leads resistance (3.7 Ω).

[b] Cell constant ~35 cm^{-1} determined from literature data (94) at 1000°C and 1 bar.

(Unless otherwise stated all conductance values in these Appendix tables were measured at 1592 Hz)

TABLE A.2

Sample No. 3: SiO_2/Na_2O 65/35 mol%

P /bar	T /°C Top of cell	T /°C Bottom of cell	ΔT /°C	C /μF	G /mS	G_c /mS[a]	log G_c	log κ (Scm^{-1})[b]
10	993	993	0	0.022	4.14	4.21	-2.376	-0.427
10	999	993	6	0.021	4.16	4.23	-2.374	-0.425
45	996	999	3	0.022	8.46	8.73	-2.059	-0.110
45	996	999	3	0.023	7.83	8.07	-2.093	-0.144
45	993	1001	8	0.022	7.69	7.91	-2.102	-0.153
620	996	993	3	0.0032	10.69	11.12	-1.954	-0.00461
615	999	993	6	0.029	10.48	10.91	-1.962	-0.0126
1250	999	963	31	0.020	9.59	9.94	-2.002	-0.0526

[a] Conductance corrected for leads resistance (3.7 Ω).

[b] Cell constant ~89 cm^{-1} determined from literature data (94) at 1000°C and 1 bar.

TABLE A.3

Sample No. 1: SiO_2/Na_2O 75/25 mol%

P /bar	T /°C Top of cell	T /°C Bottom of cell	ΔT /°C	C /μF	G /mS	G_c /mS[a]	log G_c	log κ (Scm^{-1})[b]
10	986	991	5	0.108	48.47	59.06	-1.229	-0.627
10	986	996	10	0.205	71.79	97.72	-1.010	-0.408
52	973	973	0	0.210	68.45	91.62	-1.038	-0.436
490	999	999	0	0.072	75.26	104.23	-0.982	-0.380
1068	988	910	78	0.073	57.74	73.45	-1.134	-0.523
1454	852	772	80	0.056	35.26	40.55	-1.392	-0.790
746	897	887	10	0.086	59.19	75.86	-1.120	-0.518
500	999	1004	5	0.082	78.70	110.92	-0.955	-0.352
500	1001	993	8	0.078	77.24	108.14	-0.966	-0.367
250	999	1001	2	0.106	77.92	109.40	-0.961	-0.359
205	1001	1001	0	0.110	77.68	108.89	-0.963	-0.360
600	999	996	3	0.087	77.54	108.64	-0.964	-0.362
15	973	1001	38	0.200	70.91	96.16	-1.017	-0.415
12	899	897	2	0.261	58.56	74.82	-1.126	-0.524
220	899	897	2	0.208	61.85	80.17	-1.096	-0.494
220	897	897	0	0.207	60.50	77.98	-1.108	-0.506
470	899	899	0	0.186	59.30	76.03	-1.119	-0.517
470	899	899	0	0.169	59.68	76.56	-1.116	-0.514

[a] Conductance corrected for leads resistance (3.7Ω).

[b] Cell constant ~4 cm^{-1} determined from literature data (94) at 1000°C and 1 bar.

TABLE A.4

Sample No. 1: SiO_2/Na_2O 75/25 mol%

P /bar	T /°C Top of cell	T /°C Bottom of cell	ΔT /°C	C /μF	G /mS	G_c /mS[a]	log G_c	log κ (Scm^{-1})[b]
18	965	965	0	0.165	45.90	55.34	-1.257	-0.585
350	963	968	5	0.250	61.72	79.98	-1.097	-0.425
755	965	855	110	0.250	54.26	67.92	-1.168	-0.496
500	968	870	98	0.270	56.50	71.45	-1.146	-0.474
210	965	965	0	0.284	63.20	82.41	-1.084	-0.412
60	968	968	0	0.254	58.81	75.16	-1.124	-0.452
60	897	897	0	0.255	50.18	61.66	-1.210	-0.538
535	899	818	81	0.228	48.80	59.57	-1.225	-0.553
735	897	796	101	0.209	44.26	52.97	-1.276	-0.604
300	902	899	3	0.250	53.98	67.45	-1.171	-0.499
60	897	897	0	0.255	50.14	61.52	-1.211	-1.211
56	820	825	5	0.190	39.89	46.77	-1.330	-0.658
320	813	818	5	0.208	43.84	52.36	-1.281	-0.609
700	828	707	121	0.115	26.74	29.65	-1.528	-0.856
500	823	779	54	0.178	38.52	44.88	-1.348	-0.676
55	821	823	2	0.202	40.15	47.21	-1.326	-0.654
5	998	998	0	0.358	56.25	70.96	-1.149	-0.477
12	973	970	3	0.330	56.40	71.29	-1.147	-0.475
320	957	973	16	0.294	64.23	84.33	-1.074	-0.402
748	927	816	111	0.260	48.16	58.61	-1.232	-0.560
210	965	965	0	0.314	64.25	84.33	-1.074	-0.402

[a] Conductance corrected for leads resistance (3.7 Ω).

[b] Cell constant ~4.7 cm^{-1} determined from literature data (94) at 965°C and 1 bar.

TABLE A.5

Sample No. 5: SiO_2/Na_2O 60/40 mol%

P /bar	T /°C Top of cell	T /°C Bottom of cell	ΔT /°C	C /nF	G /mS	G_c /mS[a]	log G_c	log κ (Scm^{-1})[b]
10	947	980	33		9.329	426.6	-0.370	0.0102
210	996	970	26	4.0	9.322	413.1	-0.384	-0.00373
500	988	985	3	2.9	9.341	453.9	-0.343	0.0372
1300	983	962	21	2.9	9.316	400.9	-0.397	-0.0168
1048	985	980	0	2.7	9.322	412.7	-0.384	-0.00415
790	985	987	2	3.0	9.326	420.7	-0.376	0.00418
390	988	988	0	3.4	9.325	418.8	-0.378	0.00222
58	988	990	2	5.0	9.328	424.6	-0.372	0.00819
32	924	927	3	6.9	9.321	411.2	-0.386	-0.00574
30	929	924	5	7.9	9.372	540.8	-0.267	0.113
230	922	919	3	8.5	9.350	475.3	-0.323	0.0572
620	918	922	4	8.0	9.336	441.6	-0.355	0.0252
1000	924	919	5	8.0	9.318	404.6	-0.393	-0.0128
1300	927	902	25	8.0	9.307	385.5	-0.414	-0.0388
890	924	932	8	8.2	9.369	530.9	-0.275	0.105
160	932	924	8	8.2	9.352	480.8	-0.318	0.0622
152	855	850	5	13.6	9.206	264.9	-0.577	-0.197
155	852	855	3	13.6	9.202	261.8	-0.582	-0.202
660	855	857	3	14.0	9.248	304.8	-0.516	-0.138
1020	852	845	7	14.2	9.216	273.5	-0.563	-0.183
1310	847	825	22	15.1	9.188	250.6	-0.601	-0.221
875	857	852	3	13.1	9.245	301.3	-0.521	-0.141
60	855	859	4	15.4	9.198	258.2	-0.588	-0.208
60	983	993	10	6.6	9.382	575.4	-0.240	0.140

[a] Conductance corrected for leads resistance (104.85 Ω).

[b] Cell constant ~2.4 cm^{-1} determined from literature data (94) at 988°C and 1 bar.

TABLE A.6

Sample No. 4: SiO_2/Na_2O 78/22 mol%

P /bar	T /°C Top of cell	T /°C Bottom of cell	ΔT /°C	C /μF	G /mS	G_c /mS[a]	log G_c	log κ (Scm^{-1})[b]
40	1001	1001	0	0.282	52.04	64.42	-1.191	-0.589
203	998	998	0	0.260	57.92	73.79	-1.132	-0.530
403	1001	1003	2	0.211	58.90	75.34	-1.123	-0.521
602	1001	1001	0	0.208	58.70	74.99	-1.125	-0.523
1005	1003	1001	2	0.197	58.14	74.13	-1.130	-0.528
1312	1001	1001	0	0.184	57.56	73.11	-1.136	-0.534
990	1001	1001	0	0.197	57.93	73.79	-1.132	-0.530
695	1003	1001	2	0.214	58.44	74.65	-1.127	-0.525
495	1001	1001	0	0.221	57.86	73.62	-1.133	-0.531
310	1006	1003	3	0.231	57.55	73.11	-1.136	-0.534
105	1001	998	3	0.308	55.85	70.47	-1.152	-0.550
60	940	940	0	0.258	46.15	55.59	-1.255	-0.653
200	940	942	2	0.256	48.26	58.75	-1.231	-0.629
400	940	942	2	0.235	49.17	60.12	-1.221	-0.619
603	940	947	7	0.231	49.24	60.26	-1.220	-0.618
915	937	940	3	0.215	48.28	58.78	-1.231	-0.629
1350	937	947	10	0.190	47.66	57.81	-1.238	-0.636
1090	940	942	2	0.196	48.31	58.88	-1.230	-0.628
740	940	947	7	0.207	49.01	59.84	-1.223	-0.621
495	942	942	0	0.218	49.40	60.40	-1.219	-0.617
300	942	940	2	0.228	49.30	60.26	-1.220	-0.618
130	945	942	3	0.249	48.88	59.70	-1.224	-0.622
45	945	942	3	0.270	46.66	56.36	-1.249	-0.647

[a]Conductance corrected for leads resistance (3.7Ω).

[b]Cell constant ~4 cm^{-1} determined from literature data (94) at 1000°C and 1 bar.

TABLE A.7

Sample No. 4: SiO_2/Na_2O 78/22 mol% + ~5 wt.% H_2O

P /bar	T /°C Top of cell	T /°C Bottom of cell	ΔT /°C	C /nF	G /mS	G_c /mS[a]	log G_c	log κ (Scm^{-1})[b]
1325	1001	996	5	0.01	66.28	87.82	-1.056	-0.454
990	1001	998	3	0.082	61.32	79.32	-1.101	-0.499
700	1001	1003	2	0.069	52.76	65.56	-1.183	-0.581
500	998	1003	5	0.064	42.63	50.61	-1.296	-0.694
304	1001	993	8	0.066	37.58	43.65	-1.360	-0.758
408	998	1003	5	0.066	44.13	52.74	-1.278	-0.676
870	998	998	0	0.072	49.46	60.54	-1.218	-0.616
1185	996	998	2	0.074	48.78	59.52	-1.225	-0.623
1312	996	1001	5	0.074	48.29	58.80	-1.231	-0.629
995	996	1003	7	0.078	48.00	58.80	-1.234	-0.632
495	993	998	5	0.087	46.80	56.60	-1.247	-0.645
312	1003	1003	0	0.086	42.22	50.04	-1.301	-0.699
710	998	996	2	0.072	47.93	58.26	-1.235	-0.633
1140	998	1003	5	0.070	47.62	57.81	-1.238	-0.636
1365	850	854	4	0.048	29.80	33.49	-1.475	-0.873
882	850	850	0	0.053	30.30	34.13	-1.467	-0.865
494	850	852	2	0.054	30.51	34.39	-1.464	-0.862
296	852	852	0	0.050	29.12	32.64	-1.486	-0.884
730	847	845	2	0.047	29.60	33.24	-1.478	-0.876
1135	847	854	7	0.049	29.49	33.10	-1.480	-0.878

[a]Conductance corrected for leads resistance (3.7Ω).

[b]Cell constant ~4 cm^{-1}

TABLE A.8

Sample No. 7: $SiO_2/Na_2O/CaO$ 72/24/4 mol%

P /bar	T /°C Top of cell	T /°C Bottom of cell	ΔT /°C	C /nF	G /mS	G_c /mS[a]	log G_c	log κ (Scm^{-1})[b]
200	963	988	25	2.0[c]	3.894	3.951	-2.403	-0.528
200	986	1001	15	8.6	3.900	3.957	-2.403	-0.528
560	996	996	0	9.0	4.822	4.910	-2.309	-0.434
975	996	996	0	7.6	4.943	5.035	-2.298	-0.423
1305	998	1001	3	7.0	4.876	4.966	-2.304	-0.429
1305	1001	1001	0	7.0	4.800	4.887	-2.311	-0.436
1090	998	1001	3	7.6	4.909	5.000	-2.301	-0.426
680	996	1001	5	8.5	4.959	5.052	-2.297	-0.422
382	1001	996	5	9.0	4.942	5.034	-2.298	-0.423
210	1001	996	5	8.8	4.605	4.685	-2.329	-0.454
54	1001	996	5	8.5[d]	3.924	3.982	-2.400	-0.525
54	1001	996	5	2.0[d]	4.017	4.078	-2.390	0.515
54	1001	996	5	8.5	3.924	3.982	-2.400	-0.525
52	847	845	2	4.8	2.127	2.144	-2.669	-0.794
315	850	845	5	4.2	2.424	2.446	-2.612	-0.737
620	850	845	5	4.0	2.460	2.483	-2.605	-0.730
860	850	845	5	4.0	2.455	2.478	-2.606	-0.731
1140	850	845	5	4.0	2.394	2.415	-2.617	-0.742
1340	847	847	0	4.0	2.395	2.371	-2.625	-0.750
1340	847	847	0	1.8[e]	2.366	2.387	-2.622	-0.747
1200	847	850	3	3.9	2.363	2.384	-2.623	-0.748
980	852	850	2	4.0	2.411	2.433	-2.614	-0.739
740	845	850	5	3.9	2.425	2.447	-2.611	-0.736
430	847	850	3	3.8	2.464	2.487	-2.604	-0.729
195	847	850	3	3.8	2.430	2.452	-2.610	-0.735
55	845	850	5	4.0	2.259	2.278	-2.642	-0.767

[a] Conductance corrected for leads resistance (3.7 Ω).

[b] Cell constant ~75 cm^{-1} determined from literature data (221) at 1000°C and 1 bar and calibration with KCl.

[c] 10 kHz.

[d] 20 kHz.

[e] 10 kHz.

TABLE A.9

Sample No. 10: Mount Erebus Lava

P /bar	T /°C Top of cell	T /°C Bottom of cell	ΔT /°C	C /nF	G /μS	G_c /μS[a]	log G_c	log κ (Scm^{-1})[b]
410	998	1003	5	3.1	505.3	506.2	-3.296	-2.30
580	996	998	2	3.18	567.6	568.8	-3.245	-2.25
800	1001	998	3	3.28	608.4	609.8	-3.215	-2.22
1000	998	996	2	3.3	622.0	623.4	-3.205	-2.21
1210	1001	998	3	3.47	676.4	678.1	-3.169	-2.17
1390	998	996	2	3.48	687.5	689.3	-3.162	-2.16
980	1001	998	3	3.90	800.0	802.4	-3.096	-2.10
980	998	993	5	3.94	820.0	822.5	-3.085	-2.09
700	996	998	2	4.21	895.3	898.3	-3.047	-2.05
490	996	1001	5	4.46	952.6	956.0	-3.020	-2.02
290	996	998	2	4.64	996.5	1000.0	-3.000	-2.00
290	998	998	0	4.64	1060.0	1064.0	-2.973	-1.97
Furnace left switched on overnight.								
290	1001	1001	0	5.4	1331.0	1338.0	-2.874	-1.88
290	998	1001	3	5.5	1334.0	1341.0	-2.873	-1.87
Due to a technical fault the furnace was switched off. After reheating the run was continued. There did not appear to be any discontinuities in the results arising from remelting the glass.								
290	998	1006	8	4.9	1302.0	1308.0	-2.883	-1.89
290	993	1001	8	4.9	1290.0	1296.2	-2.887	-1.89
75	988	1008	20	4.9	1122.0	1126.7	-2.948	-1.95
440	998	998	0	4.0	1133.0	1137.8	-2.944	-1.95
710	998	996	2	4.0	1144.0	1148.9	-2.940	-1.94
1003	998	996	2	4.0	1120.0	1124.7	-2.949	-1.95
1340	996	1001	5	4.0	1116.0	1120.6	-2.951	-1.95
1140	998	993	5	4.2	1125.0	1129.7	-2.947	-1.95
850	996	1001	5	4.2	1158.0	1163.0	-2.934	-1.95
510	998	998	0	4.6	1124.0	1128.7	-2.947	-1.95
240	1001	994	7	5.0	1080.0	1084.3	-2.965	-1.97
70	994	1001	7	5.0	1034.0	1038.0	-2.984	-1.99

Continued.

TABLE A.9

Sample No. 10: Mount Erebus Lava - Continued

P /bar	T /°C Top of cell	T /°C Bottom of cell	ΔT /°C	C /nF	G /μS	G_c /μS[a]	log G_c	log κ (Scm^{-1})[b]
75	945	955	10	4.0	798.0	800.4	-3.097	-2.10
320	950	955	5	3.38	864.0	866.8	-3.062	-2.06
630	952	947	5	3.29	825.2	827.7	-3.082	-2.08
890	950	945	5	3.29	798.6	801.0	-3.096	-2.10
1350	947	945	2	3.23	739.8	741.8	-3.130	-2.13
1080	947	947	0	3.25	764.0	766.2	-3.116	-2.12
730	950	947	3	3.44	797.1	799.5	-3.097	-2.10
430	952	945	7	3.54	803.0	805.4	-3.094	-2.10
200	947	947	0	3.78	818.8	821.3	-3.085	-2.09
190	899	894	5	3.22	592.1	593.4	-3.227	-2.23
730	897	902	5	3.00	541.6	542.7	-3.265	-2.26
1310	897	902	5	3.00	495.0	495.9	-3.305	-2.31

[a]Conductance corrected for leads resistance (3.7Ω).

[b]Cell constant ~10 cm^{-1} determined by calibration using KCl.

TABLE A.10

Sample No. 10: Mount Erebus Lava + ~4 wt.% H_2O

P /bar	T /°C Top of cell	T /°C Bottom of cell	ΔT /°C	C /nF	G /mS	G_c /mS[a]	log G_c	log κ (Scm^{-1})[b]
865	1001	998	3	4.0	1.690	1.701	-2.769	-1.99
1090	998	996	2	4.9	2.070	2.086	-2.681	-1.91
1340	993	998	5	5.1	2.165	2.183	-2.661	-1.89
985	996	996	0	5.4	2.208	2.226	-2.652	-1.88
670	1001	1001	0	5.0	1.762	1.774	-2.751	-1.98
450	1001	996	5	5.0	1.452	1.460	-2.836	-2.06
885	1001	998	3	6.0	2.352	2.373	-2.625	-1.85
1325	996	1001	5	6.6	2.490	2.513	-2.600	-1.83
1295	950	952	2	6.2	2.064	2.080	-2.682	-1.91
975	950	950	0	6.6	2.130	2.147	-2.668	-1.89
680	952	950	2	6.6	2.084	2.100	-2.678	-1.90
440	950	947	3	6.6	1.928	1.942	-2.712	-1.94
890	950	947	3	7.0	2.200	2.218	-2.654	-1.88
1175	947	950	3	7.5	2.230	2.249	-2.648	1.87
1320	899	899	0	6.6	1.800	1.812	-2.742	-1.97
880	897	902	5	6.6	1.788	1.800	-2.745	-1.97
470	899	899	0	6.2	1.664	1.674	-2.776	-2.00

[a] Conductance corrected for leads resistance (3.7Ω).

[b] Cell constant ~6 cm^{-1} determined by calibration using KCl.

REFERENCES

1. Robinson, W.H. and Smedley, S.I., Piezoelectric method of determining viscosity at 40 kHz., J. Appl. Phys. 49, 1070-1076, (1978).

2. Torrie, I., A viscometer for use at high temperature and pressures, M.Sc. Thesis, Victoria University of Wellington, Wellington, New Zealand (1979).

3. Rochow, E.G., Silicon, in: Comprehensive Inorganic Chemistry, (Trotman-Dickenson, A.F. ed.), Pergamom Press, New York (1973), vol. 1, pp. 1323-1467.

4. Bockris, J.O'M., Mackenzie, J.D. and Kitchener, J.A., Viscous flow in silica and binary liquid silicates, Trans. Faraday Soc. 51, 1734-1748, (1955).

5. Bacon, J.F., Hasapis, A.A. and Wholley, J.M., Viscosity and density of molten silica and high silica content glasses, Physics Chem. Glasses 1, 90-98, (1960).

6. Riebling, E.F., Structure of molten oxides. II. A density study of binary germanates containing Li_2O, Na_2O, K_2O and Rb_2O, J. Chem. Phys. 39, 3022-3030, (1963).

7. Cantor, S., Ward, W.T. and Moynihan, C.T., Viscosity and density in molten beryllium fluoride-lithium fluoride, J. Chem. Phys. 50, 2874-2879, (1969).

8. Bockris, J.O'M. and Richards, S.R., The compressibilities, free volumes and equation of state for molten electrolytes: some alkali halides and nitrates, Proc. R. Soc. A241, 44-66, (1957).

9. Kingery, W.D., Surface tension of some liquid oxides and their temperature coefficients, J. Am. Ceram. Soc. 42, 6-10, (1959).

10. Richardson, F.D., Physical Chemistry of Melts in Metallurgy, Academic Press, London (1974).

11. Weast, R.C. (ed.), Handbook of Chemistry and Physics, C.R.C. Press, Cleveland, Ohio (1976-1977), 57th Edition.

12. Bockris, J.O'M. and Reddy, A.K.N., Modern Electrochemistry, Plenum Press, New York (1970), Vol. 1, pp. 594-618.

13. Kanno, H. and Angell, C.A., Volumetric and derived thermal characteristics of liquid D_2O at low temperatures and high pressures, J. Chem. Phys. 73, 1940-1947, (1980).

14. Angell, C.A. and Kanno, H., Density maxima in high pressure supercooled water and silicon dioxide, Science 193, 1121-1122, (1976).

15. Angell, C.A., Cheeseman, P.A. and Tammadon, S., Water-like transport property anomalies in liquid silicates investigated at high temperature and pressure by computer simulation techniques, Bull. Mineral. 106, 87-97, (1983).

16. Richet, P., Bottinga, Y., Denielou, L., Petitet, J.R. and Tequi, I., Thermodynamic properties of quartz, cristobalite and amorphous SiO_2: drop calorimetry measurements between 1000 and 1800K and a review from 0 to 2000K, Geochim. Cosmochim. Acta 46, 909-919, (1982).

17. Riebling, E.F., Structural similarities between a glass and its melt, J. Am. Ceram. Soc. 51, 143-149, (1968).

18. Bockris, J.O'M. and Kojonen, F., The compressibilities of certain molten alkali silicates and borates, J. Am. Chem. Soc. 82, 4493-4497, (1960).

19. Bloom, H. and Bockris, J.O'M., The compressibility of silicates: the Li_2O-SiO_2 system, J. Phys. Chem. 61, 515-518, (1957).

20. Baidov, V.V. and Kunin, L.L., Speed of ultrasound and compressibility of molten silica, Soviet Phys. Dokl. 13, 64-65, (1968).

21. Bucaro, J.A. and Dardy, H.D., Equilibrium compressibility of glassy SiO_2 between the transformation and melting temperature, J. Non-Cryst. Solids 20, 149-151, (1976).

22. Laberge, N.L., Yasilescu, V.V., Montrose, C.J. and Macedo, P.B., Equilibrium compressibilities and density fluctuation in K_2O-SiO_2 glasses, J. Am. Ceram. Soc. 56, 506-509. (1973).

23. Fray, D.J., The structure of alkali silicate melts, Physics Chem. Glasses 11, 219-222, (1970).

24. Mackenzie, J.D., Structure of some inorganic glasses from high temperature studies, in: Modern Aspects of the Vitreous State (Mackenzie, J. D., ed.), Butterworths, Washington (1960), pp. 188-218.

25. Levin, E.M., Robbins, C.R. and McMurdie, H.F., Phase Diagrams for Ceramists, American Ceramic Society, Columbus, Ohio (1964).

26. Kracek, F.C., The cristobalite liquidus in the alkali oxide-silica systems and the heat of fusion of silica, J. Am. Chem. Soc. 52, 1436-1442, (1930).

27. Boettcher, A.L., Burnham, C.W., Windom, K.E. and Bohlen, S.R., Liquids, glasses and the melting of silicates to high pressures, J. Geol. 90, 127-138, (1982).

28. Shartsis, L., Spinner, S. and Capps, W., Density, expansivity and viscosity of molten alkali silicates, J. Am. Ceram. Soc. 35, 155-160, (1952).

29. Bockris, J.O'M., Tomlinson, J.W. and White, J.L., The structure of liquid silicates: partial molar volumes and expansivities, Trans. Faraday Soc. 52, 299-310, (1956).

30. Tomlinson, J.W., Heines, M.S.R. and Bockris, J.O'M., The structure of liquid silicates: Part 2- Molar volumes and expansivities, Trans. Faraday Soc. 54, 1822-1833, (1958).

31. Barrett, L.R. amd Thomas, A.G., Surface tension and density measurements on molten glass in the $CaO-Al_2O_3-SiO_2$ system, J. Soc. Glass Technol. 43, 179-190, (1959).

32. Riebling, E.F., Structure of sodium aluminosilicate melts containing at least 50 mol% SiO_2 at 1500°C, J. Chem. Phys. 44, 2857-2865, (1966).

33. Riebling, E.F., Structure of magnesium aluminosilicate liquids at 1700°C, Can. J. Chem. 42, 2811-2821, (1964).

34. Segers. L., Fontana, A. and Winand, R., Specific density and molar volumes of mixtures of calcium oxide, silicon dioxide and manganese oxide, Electrochim. Acta 23, 1275-1280, (1978).

35. Gaskell, D.R., McLean, A. and Ward, R.G., Density and structure of ternary silicate melts, Trans. Faraday Soc. 65, 1498-1508, (1969).

36. Aksay, I.A. and Pask, J.A., Density of $SiO_2-Al_2O_3$ melts, J. Am. Ceram. Soc. 62, 332-336, (1979).

37. Bottinga, Y. and Weill, D.F., Density of liquid silicate systems calculated from partial molar volumes of oxide components, Am. J. Sci. 269, 169-182, (1970).

38. Bottinga, Y., Weill, D. and Richet, P., Density calculations for silicate liquids. I. Revised method for aluminosilicate compositions, Geochim. Cosmochim. Acta 46, 909-919, (1982).

39. King, T.B., Anomalies in surface tension of silicates, in: The Physical Chemistry of Melts, Institution of Mining and Metallurgy, London (1953), pp. 35-45.

40. Dietzel, A., Relations between surface tension and structure of glass melts, Kolloidzeitschrift 100, 368-380, (1942).

41. Carmichael, I.S.E., Nicholls, J., Spera, E.J., Wood, B.J. and Nelson, S.A., High-temperature properties of silicate liquids: application to equilibrium and ascent of basic magma, Phil. Trans. R. Soc. A286, 372-431, (1977).

42. Fujii, T. and Kushiro, I., Density, viscosity and compressibility of basaltic liquid at high pressure, Carnegie Inst. Wash. Yearb. 76, 419-424, (1976-77).

43. Nelson, S.A. and Carmichael, I.S.E., Partial molar volumes of oxide components in silicate liquids, Contrib. Mineral. Petrol. 71, 117-124, (1979).

44. Murase, T. and M^{c}Birney, A.R., Properties of some common igneous rocks and their melts at high temperatures, Bull. Geol. Soc. Am. 84, 3563-3592, (1973).

45. Walker, D. and Mullins, O., Surface tension of natural silicate melts from 1200-1500^{o}C and implications for melt structure, Contrib. Mineral. Petrol. 76, 455-462, (1981).

46. Epel'baum, M.B., Babashov, I.V. and Salova, T.P., Surface tension of felsic magmatic melts at high temperatures and pressures, Geochem. Int. 10, 343-345, (1973).

47. Helz, R.T., Phase relations of basalts in their melting range at P_{H_2O} = 5 kbar as a function of oxygen fugacity, J. Petrology 14, 249-302, (1973).

48. Hamilton, D.L., Burnham, C.W. and Osborn, E.F., Solubility of water and effects of oxygen fugacity and water content on crystallisation in mafic magmas, J. Petrology 5, 21-39, (1964).

49. Brey, G., CO_2 solubility and solubility mechanisms in silicate melts at high pressures, Contrib. Mineral. Petrol. 57, 215-221, (1976).

50. Eggler, D.H., Carbon dioxide in silicate melts: II. Solubilities of CO_2 and H_2O in $CaOMgSi_2O_6$ (diopside) liquids and vapours at pressures to 40 kb., Am. J. Sci. 278, 64-69, (1978).

51. Kennedy, G.C., Wasserburg, G.J., Heard, H.C. and Newton, R.C., The upper three-phase region in the system SiO_2-H_2O, Am. J. Sci. 260, 501-521, (1962).

52. Tuttle, O.F. and England, J.L., Preliminary report on the system SiO_2-H_2O, Bull. Geol. Soc. Am. 66, 149-152, (1955).

53. Bedford, R.G., The solubility of water in molten silicates, Glass Technol. 16, 20-24, (1975).

54. Tomlinson, J.W., A note on the solubility of water in molten sodium silicate, J. Soc. Glass Technol. 40, 25-31T, (1956).

55. Kurkjian, C.R. and Russell, L.E., Solubility of water in molten alkali silicates, J. Soc. Glass Technol. 42, 130-144, (1958).

56. Shimada, M., Melting of albite at high pressures in the presence of water, Earth Planet. Sci. Lett. 6, 447-450, (1969).

57. Orlova, G.P., The solubility of water in albite melts, Int. Geol. Rev. 6, 254-258, (1964).

58. Kadik, A.A. and Lebedev, Y.B., Temperature dependence of the solubility of water in an albite melt at high pressures, Geochem. Int. 5, 1172-1181, (1968).

59. Walsh, J.H., Chipman, J., King, T.B. and Grant, N.J., Hydrogen in steel making slags, J. Metals 8, Trans. A.I.M.E. 206, 1568-1576, (1956).

60. Russell, L.E., Solubility of water in molten glass, J. Soc. Glass Technol. 41, 304-317, (1957).

61. Moulson, A.E. and Roberts, J.P., Water in silica glass, Trans. Faraday Soc. 57, 1208-1216, (1961).

62. Uys, J.M. and King, T.B., The effect of basicity on the solubility of water in silicate melts, Trans. Metall. Soc. A.I.M.E. 227, 492-500, (1963).

63. Mysen, B.O., The solubility of H_2O and CO_2 under predicted magma genesis conditions and some petrological and geophysical implications, Rev. Geophys. and Space Phys., 15, 351-361, (1977).

64. Mysen, B.O., Solubility of volatiles in silicate melts under the pressure and temperature conditions of partial melting in the upper mantle, Bull. Dept. Geol. Mineral. Inds., Oregon 96, 1-14, (1977).

65. Burnham, C.W. and Davis, N.F., The role of H_2O in silicate melts: I. P-V-T relation in the system $NaAlSi_3O_8$-H_2O to 10 kb and 1000°C, Am. J. Sci. 270, 54-79, (1971).

66. Burnham, C.W. and Davis, N.F., The role of H_2O in silicate melts: II. Thermodynamic and phase relations in the system $NaAlSi_3O_8$-H_2O to 10 kb, 700-1100°C, Am. J. Sci. 274, 902-940, (1974).

67. Bowen, N.L. and Tuttle, O.F., The system $NaAlSi_3O_8$-$KAlSi_3O_8$-H_2O, J. Geol. 58, 489-511, (1950).

68. Kadik, A.A. and Khitarov, N.I., Thermodynamic conditions of melting of silicates at high water vapour pressures, Geochem. Int. 6, 465-475, (1969).

69. Wyllie, P.J., Experimental studies in 'granitic' systems with volatile components, Indian Mineralogist 10, 116-139, (1969).

70. Kadik, A.A., Influence of water on melting of silicates at high pressures, Phys. Earth Planet. Interiors 3, 343-347, (1970).

71. Hill, R.E.T. and Boettcher, A.L., Water in the earth's mantle: melting curves of basalt-water and basalt-water-carbon dioxide, Science 167, 980-982, (1970).

72. Holloway, J.R. and Burnham, C.W., Melting relation of basalt with equilibrium water pressures less than total pressure, J. Petrology 13, 1-29, (1972).

73. Mysen, B.O., Melting in a hydrous mantle: phase relations of mantle peridotite with controlled water and oxygen fugacity, Carnegie Inst. Wash. Yearb. 72, 467-478, (1972-1973).

74. Khitarov, N.I., About water and basaltic magma, Bull. Volcan. 24, 101-108, (1962).

75. Shaw, H.R., Theoretical solubility of H_2O in silicate melts: quasicrystalline models, J. Geol. 72, 601-617, (1964).

76. Khitarov, N.I., Kadik, A.A. and Lebedev, Y.B., Solubility of water in a basalt melt, Geochem. Int. 5, 667-674, (1968).

77. Scarfe, C.M., Water solubility in basic and ultrabasic magmas, Nature, Phys. Sci. 246, 9-10, (1973).

78. Hodges, F.N., The solubility of H_2O in silicate melts, Carnegie Inst. Wash. Yearb. 73, 251-255, (1974).

79. Mysen, B.O., The role of volatiles in silicate melts: solubility of CO_2 and H_2O in feldspar, pyroxene and feldspathoid melts to 30 kb and 1625°C, Am. J. Sci. 276, 969-996, (1976).

80. Kushiro, I., Density and viscosity of hydrous calc-alkali andesite magma at high pressure, Carnegie Inst. Wash. Yearb. 77, 675-678, (1977-1978).

81. Stopler, E., Water in silicate glasses: an infrared spectroscopic study, Contrib. Mineral. Petrol. 81, 1-17, (1982).

82. Stopler, E., The speciation of water in silicate melts, Geochim. Cosmochim. Acta 46, 2609-2629, (1982).

83. Janz, G.J. and Tomkins, R.P.T., Conductance cell calibrations: current practices, J. Electrochem. Soc. 124, 55-59C, (1977).

84. Barthel, J., Feuerlein, F., Neueder, R. and Wachter, R., Calibration of conductance cells at various temperatures, J. Solution Chem. 9, 209-219, (1980).

85. Juhasz, E. and Marsh, K.N., Electrolytic conductivity, Pure Appl. Chem. 53, 1841-1845, (1981).

86. Fuoss, R.M., Review of the theory of electrolytic conductance, J. Solution Chem. 7, 771-782, (1978).

87. Robbins, G.D. and Braunstein, J., Electrical conductivity measurement in molten fluoride mixtures, and some general considerations on frequency dispersion, in: Molten Salts: Characterization and Analysis, (Mamantov, G., ed.), Marcel Dekker, New York (1969), pp. 443-478.

88. Cohen, M.H. and Turnbull, D.J., Molecular transport in liquid and glasses, J. Chem. Phys. 31, 1164-1169, (1959).

Adam, G. and Gibbs, J.H., On the temperature dependence of cooperative relaxation properties in glass-forming liquids, J. Chem. Phys. 42, 139-146, (1965).

Glasstone, S.N., Laidler, K.J. and Eyring, H., The Theory of Rate Processes, McGraw Hill, New York (1941).

91. Bockris, J.O'M., Kitchener, J.A., Ignatowicz, S. and Tomlinson, J.W., Electric conductance in liquid silicates, Trans. Faraday Soc. 48, 75-91, (1952).

92. Bockris, J.O'M. and Lowe, D.C., Viscosity and structure of molten silicates, Proc. R. Soc. A226, 423-435, (1954).

93. Macedo, P.B. and Litovitz, T.A., On the relative roles of free volume and activation energy in viscosity of liquids, J. Chem. Phys. 42, 245-256, (1965).

94. (a) Tickle, R.E., The electrical conductance of molten alkali silicates, I, Experiments and results, Physics Chem. Glasses 8, 101-113, (1967); (b) Tickle, R.E., The electrical conductance of molten alkali silicates, II, Theoretical discussion, Physics Chem. Glasses 8, 113-124, (1967).

95. Smedley, S.I., The Interpretation of Ionic Conductivity in Liquids, Plenum Press, New York (1980) p. 163.

96. Hofman, A.W., Diffusion in natural silicate melts, in: Physics of Magmatic Processes, (Hargraves, R.B. ed.), Princeton University Press, Princeton (1980), pp. 385-417.

97. Kumar, S., Viscosity and free volume of fused borates and silicates, Physics Chem. Glasses 4, 106-111, (1963).

98. Kumar, S., The flow units in glass, Physics Chem. Glasses 6. 147-148 (1965).

99. Musikhin, V.I., Esin, O.A., Lepinskileh, B.M. and Cernyaev, V.G., Structural units in the viscous flow of molten silicates, Izvest. Akad. Nauk S.S.S.R., Neorg. Mater. 10, 332-337, (1974).

100. Sasek, L., The viscosity of silicate glass melts, Silikaty 21, 291-305, (1977).

101. Cranmer, D. and Uhlmann, D.R., Viscosities in the system albite-anorthite, J. Geophys. Res. 86, 7951-7956, (1981).

102. Cohen, M.H. and Grest, G.S., Liquid-glass transition, a free volume approach, Phys. Rev. B 20, 1077-1078, (1979).

103. Douglas, R. and Isard, J., Density of fused silica, J. Soc. Glass Technol. 35, 206-225, (1951).

104. Brummer, S.B., On the relative roles of free volume and activation energy in transport processes in liquids: A comment on the paper of Macedo and Litovitz, J. Chem, Phys. 42, 4317, (1965).

105. Jobling, A. and Lawerence, A.S.C., Viscosities of some lower aliphatic alcohols at constant volume, J. Chem. Phys. 20, 1296-1298, (1952).

106. (a) Brummer, S.B. and Hills, G.J., Kinetics of ionic conductance, part 1, Energies of activation and the constant volume principle. Trans. Faraday Soc. 57, 1816-1822, (1961); (b) Brummer, S.B. and Hills, G.J., Kinetics of ionic conductance, part 2, Temperature and pressure coefficients of conductance, Trans. Faraday Soc. 57, 1823-1837, (1961).

107. Brummer, S.B., Temperature and pressure coefficients of ionic conductance in N,N-Dimethylforamide, J. Chem. Phys. 42, 1636-1646, (1965).

108. Goldstein, M., Viscous liquids and the glass transition: a potential energy barrier picture, J. Chem. Phys. 51, 3728-3739, (1969).

109. Marcus, Y. Introduction to Liquid State Chemistry, Whiley, London (1977).

110. Bockris, J.O'M., Richards, S.R. and Nanis, L., Self-diffusion and structure in molten group II chlorides, J. Phys. Chem. 69, 1627-1637, (1965).

111. Ketelaar, J.A.A. and Maenaut, P.P.E., Conductivité électrique du chlorure de sodium fondu et son emploi comme sel de référence à 1000°C, Electrochim. Acta 17, 2195-2203, (1972).

112. Brockner, W., Grjotheim, K., Oheta, T. Øye, H.A., High-temperature viscometer for fluid liquids, part II: Viscosities of alkali chlorides, Ber. Bunsenges. Phys. Chem. 79, 344-347, (1975).

113. Bowen, D.W. and Taylor, R.W., Silica viscosity from 2300-2600K, Bull. Am. Ceram. Soc. 59, 818-819, (1978).

114. Urbain, G., Bottinga, Y. and Richet, P., Viscosity of liquid silica, silicates and alumino-silicates, Geochim. Cosmochim. Acta 46, 1061-1072, (1982).

115. Panish, M.B., The electrical conductivity of molten silica, J. Phys. Chem. 63, 1337, (1959).

116. Sharma, S.K., Virgo, D. and Kushiro, I., Relationship between density, viscosity and structure of GeO_2 melts at low and high pressures, J. Non-cryst. solids 33, 235-248, (1979).

117. Sperry, L.L. and Mackenzie, J.D., Pressure dependence of viscosity of boron trioxide, Physics Chem. Glasses 9, 91-95, (1968).

118. Mackenzie, J.D., Viscous flow of liquids at constant volume and constant pressure, J. Chem. Phys. 28, 1037-1039, (1958).

119. Bockris, J.O'M., Kitchener, J.A., Ignatowicz, S. and Tomlinson, J.W., The electrical conductivity of silicates melts: samples containing Ca, Mn, and Al, Discuss. Faraday Soc. 4, 265-281, (1948).

120. Bockris, J.O'M., Kitchener, J.A. and Davis, A.E., Ionic transport in liquid silicates, J. Chem. Phys. 19, 255, (1951).

121. Bockris, J.O'M., Kitchener, J.A. and Davis, A.E., Electric transport in liquid silicates, Trans. Faraday Soc. 48, 536-548, (1952).

122. Bockris, J.O'M. and Mellors, G.W., Electric conductance in liquid lead silicates and borates, J. Phys. Chem. 60, 1321-1328, (1956).

123. See references (2), (3) and (4) in reference (119).

124. Barus, C. and Iddings, J.P., Note on the change of electric conductivity in rock magmas of different composition on passing from liquid to solid, Am. J. Sci. 44, 242-249, (1892).

125. Mackenzie, J.D., The physical chemistry of simple molten glasses, Chem. Rev. 56, 455-470, (1956).

126. Bockris, J.O'M. and Mackenzie, J.D., Développement actuel des travaux sur la structure des silicates fondus, Rev. Metall., Paris 51, 658-664, (1954).

127. Doremus, R.H., Glass Science, Whiley, New York (1973)

128. Esin, O.A. and Kir'yanov, A.K., The calcium-ion transference number in the simplest fused slags, Izvest. Akad. Nauk S.S.S.R., Otdel. Tekh. Nauk 12, 28-34, (1955).

129. Simnad, M.T., Derge, G. and George, I., Ionic nature of liquid iron-silicate slags, J. Metals 6, Trans. A.I.M.E. 200, 1386-1390, (1954).

130. Baak, T., Studies on the electrochemistry of silicate melts, Acta Chem. Scand. 8, 166-174, (1954).

131. Mackenzie, J.D., The discrete ion theory and viscous flow in liquid silicates, Trans. Faraday Soc. 53, 1485-1493, (1957).

132. Kou, T.,Mizoguchi, K. and Suginohara, Y., The effect of aluminium oxide on the viscosity of silicate melts, Nippon Kink. Gakk. 42, 775-781, (1978).

133. Waff, H.S., Pressure-induced coordination changes in magmatic liquids, Geophys. Res. Lett. 2, 193-196, (1975).

134. Mysen, B.O., The structure of silicate Melts, Ann. Rev. Earth Planet. Sci. 11, 75-97, (1983).

135. Henderson, J., Yang, L. and Derge, G., Self-diffusion of aluminium in $CaO-SiO_2-Al_2O_3$ melts, Trans. Metall. Soc. A.I.M.E. 221, 56-60, (1961).

136. Henderson, J., Structure and transport in lime-silica-alumina melts, Trans. Metall. Soc. A.I.M.E. 227, 534-535, (1963).

137. Langanke, B. and Schmalzried, H., Ionic transport in $PbO-SiO_2$ melts (I). Tracer diffusion and chemical interdiffusion, Ber. Bunsenges. Phys. Chem. 83, 59-64, (1979).

138. Waff, H.S., Relations of electrical conductivity of physical conditions within the asthenosphere, Geophys. Surveys 4, 31-41, (1980).

139. Shankland. T.J., Physical properties of minerals and melts, Rev. Geophys. and Space Phys. 17, 792-802, (1979).

140. Waff, H.S., Theoretical considerations of electrical conductivity in a partially molten mantle and implications for geothermometry, J. Geophys. Res. 79, 4003-4010, (1974).

141. Waff, H.S. and Weill, D.F., Electrical conductivity of magmatic liquids: effects of temperature, oxygen fugacity and composition, Earth Planet. Sci. Lett. 28, 254-260, (1975).

142. Rai, C.S. and Manghnani, M.H., Electrical conductivity of ultramafic rocks to 1820 kelvin, Phys. Earth Planet. Interiors 17, 6-13, (1978).

143. Khitarov, N.I., Slutsky, A.B. and Pugin, V.A., Electrical conductivity of basalts at high T-P and phase transitions under upper mantle conditions, Phys. Earth Planet. Interiors 3, 334-342, (1979).

144. Watanabe, H., Measurements of electrical conductivity of basalts at temperatures up to 1500°C and pressures to about 20 kb, Spec. Contrib. Geophys. Inst., Kyoto Univ. 10, 159-170, (1970).

145. Tyburczy, J.A. and Waff, H.S., Electrical conductivity of molten basalt and andesite to 25 kilobars pressure: geophysical significance and implications for charge transport and melt structure, J. Geophys. Res. 88, 2413-2430, (1983).

146. Pilz, P. and Todheide, K., Electrical conductance of molten alkali nitrates at high pressure: pressures up to 55 kbars, Ber. Bunsenges. Phys. Chem. 77, 29-36, (1973).

147. Turkdogan, E.T. and Bills, P.M., A critical review of viscosity of CaO-MgO-Al_2O_3-SiO_2 melts, Bull. Am. Ceram. Soc. 39, 682-687, (1960).

148. Kozakevitch, P., Tension surperficielle et viscosité des scories synthetiques, Rev. Metall., Paris 46, 572-582, (1949).

149. Kozakevitch, P., Sur la viscosité des laitiers de hauts fournaux, Rev. Metall., Paris 51, 569-587, (1954).

150. Machin, J.S. and Hanna, D.L., Viscosity studies of system CaO-MgO-Al_2O_3-SiO_2. I. 40% SiO_2, J. Am. Ceram. Soc. 28, 310-316, (1945).

151. Machin, J.S., Yee, T.B. and Hanna, D.L., Viscosity studies of system CaO-MgO-Al_2O_3-SiO_2. III. 35, 45 and 50% SiO_2, J. Am. Ceram. Soc. 35, 322-325, (1952).

152. Bills, P.M., Viscosity in silicate slag systems, J. Iron Steel Inst. 201, 133-140, (1963).

153. Shaw, H.R., Comments on viscosity, crystal settling and convection in granite magmas, Am. J. Sci. 263, 120-152, (1965).

154. Shaw, H.R., Rheology of basalt in melting range, J. Petrology 10, 510-535, (1969).

155. Murase, T., Viscosity and related properties of volcanic rocks at 800°-1400°C, J. Fac. Sci., Hokkaido Univ. Ser. 7, 1, 489-584, (1962).

156. Kushiro, I., Yoder, H.S. and Mysen B.O., Viscosities of basalt and andesite melts at high pressures, J. Geophys. Res. 81, 6351-6356, (1976).

157. Kushiro, I., Changes in viscosity and structure of melt of $NaAlSi_2O_6$ composition at high pressures, J. Geophys. Res. 81, 6347-6350, (1976).

158. Kushiro, I., Viscosity and structural changes of albite ($NaAlSi_3O_8$) melt at high pressures, Earth Planet. Sci. Lett. 41, 87-90, (1978).

159. Angell, C.A., Cheeseman, P.A. and Tammadon, S., Pressure enhancement of ion mobilities in liquid silicates from computer simulation studies to 800 kilobars, Science 218, 885-887, (1982).

160. Angell, C.A., Cheeseman, P.A. and Tammadon, S., Computer simulation studies of migration mechanisms in ionic glasses and liquids, J. Phys. Colloq. C9, 381-385, (1982).

161. Carron, J., Chemical composition and viscosity of volcanic glasses: an attempted correlation, C. R. Somm. Seanc. Soc. Geol. Fr. 7, 246-248, (1964).

162. Bottinga, Y. and Weill, D.F., The viscosity of magmatic silicate liquids: a model for calculation, Am. J. Sci. 272, 438-475, (1972).

163. Shaw, H.R., Viscosities of magmatic silicate liquids: an empirical method of prediction, Am. J. Sci. 272, 870-893, (1972).

164. Bowen, N.L., Diffusion in silicate melts, J. Geol. 29, 295-317, (1921).

Alarède, F and Bottinga, Y.,
165. Kinetic disequilibrium in trace-element partitioning between phenocrysts and host lava, Geochim. Cosmochim. Acta 36, 141-156, (1972).

166. Shankland, T.J., Physical properties of minerals and melts, Rev. Geophys. and Space Phys. 17, 792-802, (1979).

167. Watson, E.B., Diffusion in magmas at depth in the earth: the effect of pressure and dissolved H_2O, Earth Planet. Sci. Lett. 52, 291-301, (1981).

168. Jambon, A., Tracer diffusion in granitic melts: experimental results for Na, K, Rb, Cs, Ca, Sr, Ba, Ce, Eu to 1300°C and a model of calculation, J. Geophys. Res. 87, 10,797-10,810, (1982).

169. Watson, E.B., Calcium diffusion in a simple silicate melt to 30 kbar, Geochim. Cosmochim. Acta 43, 313-322, (1979).

170. Lebedev, E.B. and Khitarov, N.I., Influence of water on the electrical conductivity of silicate melts at high pressures, in: Int. Corros. Conf. Series 1973 (Pub. 1976) NACE-4 (High Temp. High Press. Electrochemistry Aqueous Solutions, Conf.) pp. 182-187.

171. Khitarov, N.I., Lebedev, Y.B. and Dorfman, A.M., Physical properties of the silica-water system at high temperatures and pressures, Geochem. Int. 13, 129-133, (1976).

172. Lebedev, E.B. and Khitarov, N.I., Dependence of the beginning of melting of granite and the electrical conductivity of its melt on high water vapour pressure, Geochem. Int. 1, 193-197, (1964).

173. Khitarov, N.I., Lebedev, Y.B., Slutskii, A.B., Dorfman, A.M., Soldatov, I.A. and Revin, N.I., The pressure dependence of the viscosity of basalt melts, Geochem. Int. 13, 126-133, (1976).

174. Shaw, H.R., Obsidian-H_2O viscosity at 1000 and 2000 bars in the temperature range 700-900$_o$C, J. Geophys. Res. 68, 6337-6343, (1963).

175. Friedman. I., Long, W. and Smith, R.L., Viscosity and water content of rhyolite glass, J. Geophys. Res. 68, 6523-6535, (1963).

176. Scarfe, C.M., Viscosity of basic magmas at varying pressure, Nature, Phys. Sect. 241, 101-102, (1973).

177. Khitarov, N.I., Lebedev, E.B., Dorfman, A.M. and Slutskii, A.B., Viscosity of dry and water-containing basalt melts under pressure, Geokhimiya 6, 900-905, (1978).

178. Jambon, A., Carron, J.P. and Delbove, F., Données préliminaires sur la diffusion dans les magmas hydrates: le césium dans un liquide granitique à 3 kbar, C. R. Hebd. Seanc. Acad. Sci., Paris, Ser. D 287, 404-406, (1978).

179. Watson, E.B., Diffusion of cesium ions in H_2O-saturated granitic melt, Science 205, 1259-1260, (1979).

180. Karsten, J.L., Holloway, J.R. and Delaney, J.R., Ion microprobe studies of water in silicate melts: temperature-dependent diffusion in obsidian, Earth Planet. Sci. Lett. 59, 420-428, (1982).

181. Shaw, H.R., Diffusion of water in granitic melts: I. Experimental data; II. Mass transfer in magma chambers, in: Geochemical Transport Kinetics, (Hofmann, A.W., et al. eds.), Carnegie Institute of Washington Publishing, Washington (1974), vol. 634, pp. 139-170.

182. Watson. E.B., Sneeinger, M.A. and Ross, A., Diffusion of dissolved carbonate in magma: experimental results and applications, Earth Planet. Sci. Lett. 61, 346-358, (1982).

183. Wong, J. and Angell, C.A., Glass. Structure by spectroscopy, Marcell Dekker Inc., New York, (1976).

184. Sweet, J.R. and White, W.B., Study of sodium silicate glasses and liquids by infrared spectroscopy, Physics Chem. Glasses 10, 246-251, (1969).

185. Seifert, F., Mysen, B.O. and Virgo, D., Three-dimensional network structure of quenched melts (glass) in the systems SiO_2-$NaAlO_2$, SiO_2-$CaAlO_4$ and SiO_2-$MgAl_2O_4$, Am. Miner. 67, 696-717, (1982).

186. Taylor, N., Brown, G.E. and Fenn, P.M., Structure of mineral glasses. III. Sodium aluminosilicate supercooled liquid at 850°C and effects of thermal history, Geochim. Cosmochim. Acta 44, 109-117, (1980).

187. Nukui, A., Tagai, H., Morikawa, H. and Lwai, S., Structural study of molten silica by an x-ray radial distribution analysis, J. Am. Ceram. Soc. 61, 174-176, (1978).

188. Mackenzie, J.D. and White, J.L., The Si-O-Si angle and the structure of vitreous silica, J. Am. Ceram. Soc. 43, 170-171, (1960).

189. Bartholomew, R.F. and Schreurs, J.W.H., Wide-line NMR study of the protons in hydrosilicate glasses of different water content, J. Non-Cryst. Solids 38 & 39, 679-684, (1980).

190. Takata, M., Acocella, J., Tomozawa, M. and Watson, E.B., Effect of water content on the electrical conductivity of $Na_2O.3SiO_2$ glass, J. Am. Ceram. Soc. 64, 719-724, (1981).

191. Zachariasen, W.H., The atomic arrangement in glass, J. Am. Chem. Soc. 54, 3841-3851, (1932).

192. Zachariasen, W.H., The vitreous state, J. Chem. Phys. 3, 162-163, (1935).

193. Bell, R.J. and Dean, P., The structure of vitreous silica: validity of random network theory, Phil. Mag. 25, 1381-1398, (1972).

194. Gaskell, P.H. and Tarrant, I.D., Refinement of a random network model for vitreous silicon dioxide, Phil. Mag. B42, 265-286, (1980).

195. Bottinga, Y., Weill, D.F. and Richet, P., Thermodynamic modelling of silicate melts, in: Thermodynamics of Minerals and Melts, (Newton, R.C. et al. eds.), Springer-Verlag, New York (1981), pp. 207-245.

196. Evans, D.L. and King, S.V., Random network model of vitreous silica, Nature 212, 1352-1354, (1966).

197. Ordway, F., (a) A study of random network models, Tech. Rept. No. 1 Melpar No. 6353.00100, (Melpar Inc., Falls Church, Va.) (1967); (b) A study of random network models, Final Tech. Rept. Melpar No. 6363.00200, (Melpar Inc., Falls Church, Va.) (1967).

198. Lebedev, A.A., Polymerisation and tempering glass. Preliminary communication, J. Russ. Chem. Soc., Phys. Sect. 50, 57, (1921),

199. Endell, K. and Hellbrugge, J., The effect of ionic radius and the valence of the cations on the electrical conductivity of silicate melts between 1250-1450°C, Naturwissenschaften 30, 421-422, (1942).

200. Bloom, H. and Bockris, J.O'M., Molten electrolytes, in: Modern Aspects of Electrochemistry, (Bockris, J.O'M., ed.), Butterworths, London (1959), No. 2, pp. 219-261.

201. Easteal, A.J. and Angell, C.A., Phase equilibria, electrical conductance and density in the glass-forming system zinc chloride + pyridinum chloride. A detailed low-temperature analog of the silicon dioxide-sodium oxide system, J. Phys. Chem. 74, 3987-3999, (1970).

202. Goodman, C.H.L., Strained mixed-cluster model for glass structure, Nature, 257, 370-372, (1975).

203. Flory, P.J., Principles of Polymer Chemistry, Cornell University Press, New York (1953).

204. Toop, G.W. and Samis, C.S., Activities of ions in silicate melts, Trans. Metall. Soc. A.I.M.E. 224, 878-887, (1962).

205. Hess, P.C., Polymer model of silicate melts, Geochim. Cosmochim. Acta 35, 289-306, (1971).

206. Masson, C.R., Ionic equilibria in liquid silicates, J. Am. Ceram. Soc. 52, 134-143, (1968).

207. Masson, C.R., An approach to the problem of ionic distribution in liquid silicates, Proc. R. Soc. A287, 201-221, (1965).

208. Baes, C.F., A polymer model for BeF_2 and SiO_2 melts, J. Solid State Chem. 1, 159-169, (1970).

209. Lin, P.L. and Pelton, A.D., A structural model for binary silicate systems, Metall. Trans. 10B, 667-676, (1979).

210. Dron, R., Acid-base reactions in molten silicates, J. Non-cryst. solids 53, 267-278, (1982).

211. Lentz, C.W., Silicate minerals as sources of trimethlysilyl silicates and silicate structure analysis of sodium silicate Solutions, Inorg. Chem. 3, 574-579, (1964).

212. Wasserburg, G.J., The effects of H_2O in silicate systems, J. Geol. 65, 15-23, (1957).

213. Nichols, J. A simple thermodynamic model for estimating the solubility of H_2O in magmas, Contrib. Mineral. Petrol. 74, 211-220, (1980).

214. Bottinga, Y. and Richet, P., Thermodynamics of liquid silicates, a preliminary report, Earth Planet. Sci. Lett. 40, 382-400, (1978).

215. Burnham, C.W., Water and magmas; a mixing model, Geochim. Cosmochim. Acta 39, 1077-1084, (1975).

216. Holloway, J.R., Internally heated pressure vessels, in: Research techniques for high temperature and pressure, (Ulmer, G.C., ed.), Springer-Verlag, New York (1971), pp. 217-257.

217. Edgar, A.D., Internally heated pressure vessels, in: Experimental Petrology, Basic Principles and Techniques, Clarendon Press, Oxford, (1973), Chap. 6.

218. Burnham, C.W., Holloway, J.R. and Davis, N.F., The specific volume of water in the range 1000 to 8900 bars, 20° to 900°C, Am. J. Sci. 276, 79-95, (1969).

219. Edgar, A.D. and Platt, R.G., High temperature - high pressure: its application to geological science (a review), High Temperatures - High Pressures 3, 1-43, (1971).

220. Mason, W.P., Measurement of the viscosity and shear elasticity of liquids by means of a torsionally vibrating crystal, Trans. Am. Soc. Mech. Engrs. 69, 359-370, (1949).

221. Kroeger, K. and Heckmann, H., Electrical conductivity of soda-lime-silica melts, Glastech. Ber. 39, 479-483, (1966).

222. Urnes, S., Electrical conductivity in molten alkali silicates, Glass Ind. 40, 237-239, (1959).

223. Cleaver, B. and Smedley, S.I., Pressure dependence on electrical conductivity for fused mercuric halides, Trans. Faraday Soc. 67, 1115-1127, (1971).

224. Cleaver, B., Spencer, P.N. and Quddus, M.A., Effect of pressure on the electrical conductivities of some molten B group metal iodides and iodine, J. Chem. Soc. Faraday I, 3, 686-696, (1978).

225. Ingram, M.D., Moynihan, C.T. and Lesikar, A.V., Ionic conductivity and the weak electrolyte theory of glass, J. Non-Cryst. Solids 38 & 39, 371-376, (1980).

226. Moynihan, C.T., Mixed alkali effect in hydrate melts, J. Electrochem. Soc. 126, 2144-2149, (1979).

227. Isard, J.O., The mixed alkali effect in glass, J. Non-Cryst. Solids 1, 235-261, (1969),

228. Shelby, J.E. and McVay, G.L., Influence of water on the viscosity and thermal expansion of sodium trisilicate glasses, J. Non-Cryst. Solids 20, 439-449, (1976).

229. Schaeffer, J.A., Mecha, J. and Steinmann, J., Mobility of sodium ions in silica glass of different OH content, J. Am. Ceram. Soc. 62, 343-346, (1979).

230. Ass, H.M.J.M. and Stevels, J.M., (a) Internal friction of mixed alkali metaphosphate glasses (II). Discussion, J. Non-Cryst. Solids 16, 27-45, (1974); (b) The influence of dissolved heavy water on the internal friction of lithium metaphosphate glasses containing 1% potassium metaphosphate, J. Non-Cryst. Solids 16, 161-170, (1974).

231. Bray, P.J. and Henderson, J.R., Dependence of the mixed alkali effect on ion mass, J. Non-Cryst. Solids 21, 297-299, (1976).

232. Moynihan, C.T. et al., Thermodynamic and transport properties of liquids near the glass transition temperature, structural relaxation in vitreous materials, Ann. N. Y. Acad. Sci. 279, 15-35, (1976).

233. Moynihan, C.T., Mass transport in fused salts, in: Ionic Interactions, (Petrucci, S. ed.), Academic Press, New York (1971), chap. 5.

234. Moynihan, C.T. and Lesikar, A.V., Weak-electrolyte models for the mixed-alkali effect in glass, J. Am. Ceram. Soc. 64, 40-45, (1981).

235. Day, D.E. and Stevels, J.M., Internal friction of $NaPO_3$ glasses containing H_2O, J. Non-Cryst. Solids 11, 459-470, (1973).

236. Abe, Y., Shimakawa, H. and Heneh, L.L., Protonic conduction in alkaline earth metaphosphate glasses containing water, J. Non-Cryst. Solids 51, 357-366, (1982).

237. Smit, W., Modelling of interdiffusion of hydrogen and alkali ions in glass surfaces: electrical resistivity, J. Non-Cryst. Solids 50, 183-187, (1982).

238. Doremus, R.H., Interdiffusion of alkali and hydronium ions in glass: partial ionisation, J. Non-Cryst. Solids 48, 431-436, (1982).

239. Smit, W., Comments on "Interdiffusion of alkali and hydronium ions in glass: partial ionisation" by R.H. Doremus, J. Non-Cryst. Solids 48, 437-440, (1982).

240. Grigorovich, S.L., Kiselev, A.V. and Lygin, V.I., Study of surface dehydroxylation and water adsorption by microporous silica by the method of ir spectroscopy, Kolliod. Zh. 38, 139-144, (1976).

241. Bauche, F.G.K., Investigation of surface layers, formed on glass electrode membranes in aqueous solutions, by means of an ion sputtering method, J. Non-Cryst. Solids 14, 13-21, (1974).

242. Scholze, H., Helmreich, D. and Bakardzhiev, I., Investigation on the behaviour of soda-lime-silica glasses in dilute acid, Glastech. Ber. 48, 237-247, (1975).

243. Bauche, F.G.K., in: Mass Transport Phenomena in Ceramics, (Cooper, A.R. and Heuer, A.R. eds.), Plenum Press, New York (1975), p. 337.

244. Hensel, F. Electrical properties of unusual ionic melts, Adv. Phys. 28, 555-594, (1979).

245. Hwang, J.U., Ludmann, H.D. and Hartmann, D., Die elektrische Leitfahigkeit konzentrierter wässriger Alkalihalogenidlösungen bei hohen Drucken und Temperaturen, High Temperatures - High Pressures 2, 651-669, (1970).

246. Fellows, S.K., Conductance measurements on aqueous solutions over extended ranges of concentration and temperature, Ph.D. thesis, Victoria University of Wellington, Wellington, New Zealand (1971).

247. Lown, D.A. and Thirsk, H.R., Proton transfer conductance in aqueous solution, Trans. Faraday Soc. 67, 132-152, (1971).

248. Grantham, L.F. and Yosim, S.J., Negative temperature coefficients of electrical conductance in molten salts, J. Chem. Phys. 45, 1192-1198, (1966).

249. Treiber, G. von and Tödheide, K., Der kontinuierliche Übergang vom Isolator zum Ionenleiter am Beispiel des Wismutchlorids, Ber. Bunsenges. Phys. Chem. 77, 541-547, (1973).

250. Pickston, L., Smedley, S.I. and Woodall, G., The compressibility and electrical conductivity of concentrated aqueous calcium nitrate solutions to 6 kbar and 150°C, J. Phys. Chem. 81, 581-586, (1977).

251. Angell, C.A., Pollard, L.J. and Strauss, W., Transport in ionic liquids under pressure, I: Concentrated calcium nitrate-water and magnesium chloride-water solutions, J. Solution Chem. 1, 517-530, (1972).